SYNTHESIS OF BIO-INSPIRED BLOCK POLYELECTROLYTES FOR THE FORMATION OF COACERVATES

BY

MOUHEDDIN TAHSEEN ALHAFFAR

A Dissertation Presented to the
DEANSHIP OF GRADUATE STUDIES

KING FAHD UNIVERSITY OF PETROLEUM & MINERALS

DHAHRAN, SAUDI ARABIA

In Partial Fulfillment of the
Requirements for the Degree of

DOCTOR OF PHILOSOPHY

In

CHEMISTRY

DECEMBER 2017

KING FAHD UNIVERSITY OF PETROLEUM & MINERALS
DHAHRAN- 31261, SAUDI ARABIA
DEANSHIP OF GRADUATE STUDIES

This thesis, written by **MOUHEDDIN TAHSEEN ALHAFFAR** under the direction his thesis advisor and approved by his thesis committee, has been presented and accepted by the Dean of Graduate Studies, in partial fulfillment of the requirements for the degree of **DOCTOR OF PHILOSOPHY IN CHEMISTRY**.

23/1/2018

Dr. Abdulaziz A. Al-Saadi

Department Chairman

Dr. Salam A. Zummo
Dean of Graduate Studies

28/1/18
Date

Sk. Asrof Ali

Dr . Shaikh Asrof Ali
(Advisor)

Dr. Muhammad Naseem Akhtar
(Member)

Dr. Nisar Ullah
(Member)

Dr. Bassam El Ali
(Member)

Dr. Hasan Ali Al-Muallem

(Member)

Dedicated to my parent, my wife and my sons

ACKNOWLEDGMENTS

First, I give thanks to Allah, the generally merciful and the especially merciful, for His favors on me by aiding the successful completion of my PhD study. Indeed, all praises are due to Allah.

I would like to express my profound indebtedness and sincere appreciation to my advisor Professor Shaikh Asrof Ali for his tremendous support in carrying out the work. He shall be long remembered. Also, it gives me great pleasure to thank my committee members Dr. Muhammad Naseem Akhtar, Prof. Nisar Ullah, Prof. Bassam El Ali and Dr. Hasan Ali Al-Muallem. I am also grateful to Dr. Saviour Umoren and Dr. Ime Obot (KFUPM – Research Institute). for their help in electrochemical and computational study.

Furthermore, I would like to express my special appreciation to my family for their prayers, patience and moral support that permit me to indulge my passion for the long task of completing this work. My appreciation also goes to my friends, and also my laboratory mates Dr. Mohammad Mazumder, Dr. Abdulkareem Zakariyah, Dr. Mohammad Manshaa, Mr. Ibrahim Yaagoob, Mr. Abdulwaheed Abdulhameed and Mr. Lipiar Khan

Finally, this work was funded by the National Plan for Science, Technology and Innovation (MAARIFAH)-King Abdulaziz City for Science and Technology-through the Science & Technology Unit at King Fahd University of Petroleum & Minerals (KFUPM), Kingdom of Saudi Arabia (Award Number 12-ADV2397-04). I gratefully acknowledge the facilities provided by KFUPM.

TABLE OF CONTENTS

LIST OF TABLES

LIST OF FIGURES

LIST OF SCHEMES

LIST OF ABBREVIATIONS

EIS	: Electrochemical Impedance Spectroscopy
MMA	: Methyl methacrylate
IMO	: International Maritime Organization
IUPAC	: International Union of Pure and Applied Chemistry
DOPA	: L-3,4-Dihydroxyphenylalanine
LPR	: Linear Polarization Resistance
NMR	: Nuclear Magnetic Resonance
IR	: Infra Red
TGA	: Thermo Gravimetric Analysis
GPC	: Gel Permeation Chromatography
RTV silicone	: Room-Temperature-Vulcanization silicone
PDMS	: Polydimethylsiloxane
PDP	: Potentiodynamic polarization
TBT	: Tributyltin
SPC	: Self-polishing copolymer

ABSTRACT

Full Name : Mouheddin T. Alhaffar

Thesis Title : Synthesis of Bio-inspired Block Polyelectrolytes for the Formation of Coacervates

Major Field : Chemistry

Date of Degree : December 2017

Safrole oxide **2** obtained by epoxidation of naturally occurring safrole (**1**) has been polymerized for the first time using Lewis acid initiator/catalyst comprising of triphenylmethylphosphonium bromide/triisobutylaluminum to obtain polyether **6** in excellent yields. Epoxy monomer **2** and allyl glycidyl ether **7** in various proportions have been randomly copolymerized to obtain random copolymer **16**. The deprotection of methylene acetal of **16** has been achieved successfully to obtain **17**.

The pendant allyl groups in **17** have been elaborated via thiol-ene reaction using cysteamine hydrochloride and thioglycollic acid to obtain polymers **18** and **19** containing *Mussel*-inspired Dopa-based catechol moiety and anionic/cationic groups required for the formation of coacervate. The cationic **18** and anionic **19** polymers are also obtained via an alternate route using epoxide **14** of 3,4-di-tert-butyldimethylsilyloxyallylbenzene **13**. Monomer **14** was homo- as well as copolymerized with **7** using Lewis acid initiator/catalyst system to obtain homopolymer **15** and copolymer **20**. Copolymer **20** was then elaborated using thiol-ene reaction followed by F^- catalysed silyl deprotection to obtain Mussel inspired polymers **18** and **19**.

Naturally occurring sesamol **26** has been converted to epoxy monomer **27** by reacting with epibromohydrin **25**. Monomer **27** has been polymerized for the first time using a variety of basic tetrabutylammonium hydroxide and tetrabutylammonium fluoride as well as by Lewis acid initiator/catalyst comprising of triphenylmethylphosphonium bromide/triisobutylaluminum to obtain polyether **28** in excellent yields. Epoxy monomer **27** and allyl glycidyl ether **7** in various proportions have been randomly copolymerized to obtain random copolymer **29** in which the methylene acetal was activated by placing an acetoxy group acetal carbon to obtain **31** in which the pendant allyl groups have been elaborated via thiol-ene reaction using cysteamine hydrochloride to obtain cationic copolymer **32** required for formation of coacervate.

Pyrogallol **32,** usually obtained by heating induced decarboxylation of naturally occurring gallic acid, has been protected as methylene acetal **33**. The free hydroxyl group in **33** is converted to epoxy monomer **34** by reacting with epibromohydrin **25**. Monomer **34** has been polymerized for the first time using Lewis acid initiator/catalyst comprising of triphenylmethylphosphonium bromide/triisobutylaluminum to obtain polyether **35** in excellent yields.

Paramagnetic Manganese oxide MnO nanoparticles have been synthesized. This metal oxide nano-particles was chelated by catechol moieties of the polymer **18** to be a hydrophilic ligand for potential application in MRI as a contrast agent. The results were analyzed by SEM and showed a nice basket of the polymer-MnO nanoparticles with diameter size 200 -500 nm.

Many isoxazolidine derivatives from natural compounds base such as safrole and eugenol were synthesized and characterized. Two of them: 5-(benzo[d][1,3]dioxol-5-ylmethyl)-2-tetradecyl isoxazolidine (BDMTI) and 5-((4-hydroxy-3-methoxybenzyl)-2-tetradecyl isoxazolidine (HMBTI) were evaluated as corrosion inhibitors for API 5L X60 steel in 1 M HCl at the temperature range of 25 – 60 ºC. Experimental results showed that the two compounds inhibited the corrosion of carbon steel in the acid environment with HMBTI showing superior performance. Corrosion inhibition effect was found to be dependent on the inhibitors' concentration and temperature. Addition of iodide ions improves the inhibition efficiency considerably. Surface which was competitive in nature as confirmed from synergistic parameter (S_1) which was less than unity at higher temperature.

Initial polymerization reactions were carried out to obtain block copolymers having block of polyethylene glycol (PEG) **49** in the middle were prepared by using potassium naphthalenide **50**. PEG was converted into its alkoxide at both ends of the polymer which was then subjected to undergo block or semi-block polymerization with allyl glycidyl ether **7;** safrole oxide **2;** and both allyl glycidyl ether **7**, and safrole oxide **2** in presence of $^{i}Bu_3Al$ to get block copolymers **51**, **52** and **53** respectively.

ملخص الرسالة

الاســـم الكامل: محي الدين تحسين الحفار

عنوان الرسالة: اصطناع بوليميرات مستوحاة من الطبيعية تحتوي على ايونات لتشكيل قواصر

التخصـــــــص: الكيميـــاء

تاريخ الدرجة العلمية: ديسمبر (كانون الأول) 2017

حُضِر إيبوكسيد السافرول **2** من المركب الطبيعي السافرول **1** ثم بُلمر للمرة الأولى باستخدام حمض لويس (البادئ /محفز) تتالف من (triphenylmethylphosphonium bromide /triisobutylaluminum) للحصول على المبلمر **6** بمردود ممتاز. أجريت البلمرة المشتركة بشكل عشوائي بين ايبوكسي مونومر **2** والمونومر **7** (allyl glycidyl ether) بنسب مختلفة للحصول على بوليمر مشترك عشوائي **16** وأُزيلت مجموعة الحماية بواسطة استلة المثيلين للحصول على البوليمر **17** بنجاح.

عُولجت زمر الأليل المتدلية من البوليمر **17** بواسطة تفاعل ثيول – رابطة ثنائية باستخدام (cysteamine hydrochloride) و ايضا (thiglycollic acid) للحصول على البوليمر **18** و **19** التي تحتوي على زمرة الكاتيكول دوبا المستوحاة من بلح البحر و مجموعات شوارد الموجبة/ السالبة اللازمة لتشكل قوصرة.

البوليمر المشحون موجب **18** والبوليمر المشحون سالب **19** تم الحصول عليهما أيضا بواسطة طريقة بديلة باستخدام أكسدة المركب **13** (dit-butyldimethylsilyloxyallylbenzene-3,4) للحصول على المونومر إيبوكسي **14** والذي بدوره بُلمر لوحدة وأيضا مع المونومر **7** (allyl glycidyl ether) باستخدام نظام حمض لويس (البادئ /محفز) للحصول على البوليمر المتجانس **15** والبوليمر المشترك **20** ثم عولجت زمر الأليل باستخدام تفاعل ثيول – رابطة ثنائية تلتها عملية إزالة لمجموعة الحماية بواسطة محفز للحصول على البوليمرات المستوحاة من بلح البحر **18** و**19**.

حُوِّل المركب الطبيعي سيسامول **26** إلى المونومر الإيبوكسي **27** بواسطة تفاعلة مع المركب **25** (epibromohydrin) ثم بُلمر للمرة الأولى باستخدام مجموعة متنوعة من الاسس (tetrabutylammonium hydroxide) و(tetrabutylammoniumfluride) فضلا عن حمض لويس (البادئ /محفز) تتالف من

(triphenylmethylphosphonium bromide /triisobutylaluminum) للحصول على البوليمر **28** بمردود ممتاز. تمت البلمرة المشتركة العشوائية للمونومر **27** والمونومر **7** (glycidyl ether allyl) بنسب مختلفة للحصول على بوليمر مشترك عشوائي **29** ونُشِطت زمرة أستال الميثيلين عن طريق وضع زمرة أسيتوكسي للحصول على البوليمر **31** والذي بدوره تعرض لتفاعل ثيول – رابطة ثنائية لزمر الاليل المتدلية باستخدام (cysteamine hydrochlorid) للحصول على بوليمر مشترك مشحون موجبا **32** لتشكيل قوصرة.

تمت عملية حماية للبيروغالول -الذي حُصل عليه بواسطة التسخين ونزع الكربوكسيل من المركب الطبيعي حمض الغاليك – على شكل المثيلين أسيتال للحصول على **33**. حُوِّلت زمرة الهيدروكسل الحرة في **33** إلى الإبوكسي المونومر **34** عن طريق التفاعلى مع المركب **25** (epibromohydrin). بُلمر المونومر **34** للمرة الأولى باستخدام حمض لويس (البادئ /محفز) تتالف من (triphenylmethylphosphonium bromide /triisobutylaluminum) للحصول على البوليمر **35** بمردود ممتاز.

صُنعَت جسيمات أكسيد المنغنيز النانوية ذو الخواص البارامغناطيسية. غُلِف اكسيد المنغنيز بالبوليمر **18** بواسطة تمخلب مجموعات الكاتيكول على أكسيد المعدن ليصبح محبة للماء ليكون من المحتمل استخدامه في التصوير الرنين المغناطيسي كعامل تباين. تم تحليل النتائج بواسطة المجهر الإلكتروني الماسح (SEM) وأظهرت الصورة تجمع البوليمر مع الجسيمات النانوية لأكسيد المنغنيز على شكل سلل جميلة ذات قطر 200-500 نانومتر.

تم توليف العديد من مشتقات ايزكزازوليدين (isoxazolidine) من مركبات طبيعية مثل السافرول والإوجينول. تم توليف العديد من مشتقات ايزكزازوليدين من مركبات طبيعية مثل السافرول والإوجينول. اثنان منهم (-5 (benzo[d][1,3]dioxol-5-ylmethyl)-2-tetradecyl isoxazolidine) (BDMTI) و (-5-((4-hydroxy- (3-methoxybenzyl)-2-tetradecyl isoxazolidine) (HMBTI) قُيّما كمثبطات تآكل للفولاذ (API 5L X60) في حمض كلور الماء ١ مولار عند مجال من درجات الحراة من ٢٥ - ٦٠ درجة مئوية. أظهرت النتائج التجريبية أن المركبين ثبطا تآكل الفولاذ في البيئة الحمضية وأن المركب (HMBTI) أظهر أداء أفضل. وَوُجد أنَّ تأثير تثبيط التآكل يعتمد على تركيز المثبطات ودرجة الحرارة. كما أنه إضافة شوارد اليود يحسن من كفاءة المثبط بشكل كبير. السطح كان تنافسيا في الطبيعة كما أكدت المعايير (S_1) الذي كان أقل من وحدة في درجات الحرارة العالية.

أُجريت تفاعلات أولية للحصول على بوليميرات مشتركة كتلية تحتوي على بولي اثيلين جليكول في المنتصف . حيث حُول بولي اثيلين جليكول بواسطة البوتاسيوم نفثالينايد إلى ألكوكسيد في كِلا طرفي البوليمر، والذي بدوره أُستخدِم كبادئ لبلمرة كتلية أو شبه كتلية مع المونومير **7** (allyl glycidyl ether) أو المنومير **2** (إيبوكسيد السافرول) أو المنومير **7** والمنومير **2** سوية بحضور المحفز (triisobutylaluminum) للحصول على البوليميرات المشتركة **51** و **52** و **53** على التوالي.

CHAPTER 1

INTRODUCTION

Efficacy of coatings for the aqueous environment depends on its ability to form engineering durable adhesive bonds and generate controlled surfaces which resist biofouling. The development of advanced materials as components of coatings must address those two challenges. The majority of synthetic adhesive systems deteriorate significantly or even fail completely owing to surface hydration because of immersion in body fluids or sea water. In addition, most surfaces undergo biofouling in an aqueous environment or when exposed to biological fluids. There is a great demand to develop coatings that allow very low bio-fouling for use in water purification, marine environments, and biomedical applications. In this research, a novel bio-mimicked polymer was prepared by an innovative synthesis method for adhesive applications in wet conditions.

1.1 Copolymers:

When two or more species of different monomers react to form a polymer, this polymer is called copolymer. Copolymers are classified according to the arrangement of the monomers. Therefore, the copolymer may be random, block, alternating, periodic, graft, gradient or aperiodic copolymer (Figure 1.1). When the repeating units in the two monomers are distributed randomly along the chain, a random copolymer is formed. However, in the periodic copolymer, the repeating units have a sequence along the polymer chain, when this sequence becomes an alternating between the two monomer units an alternating copolymer is obtained. In the block copolymer, the block of the different monomer has a linear arrangement while the grafted copolymer happens when one polymer forms a backbone of the copolymer and the second polymer chains are grafted [1].

Gradient copolymers vary their monomer composition gradually along molecular chains

Structures, and can be defined as copolymers in which monomer sequence distribution is not regular but follows the same arrangement in all chains[2].

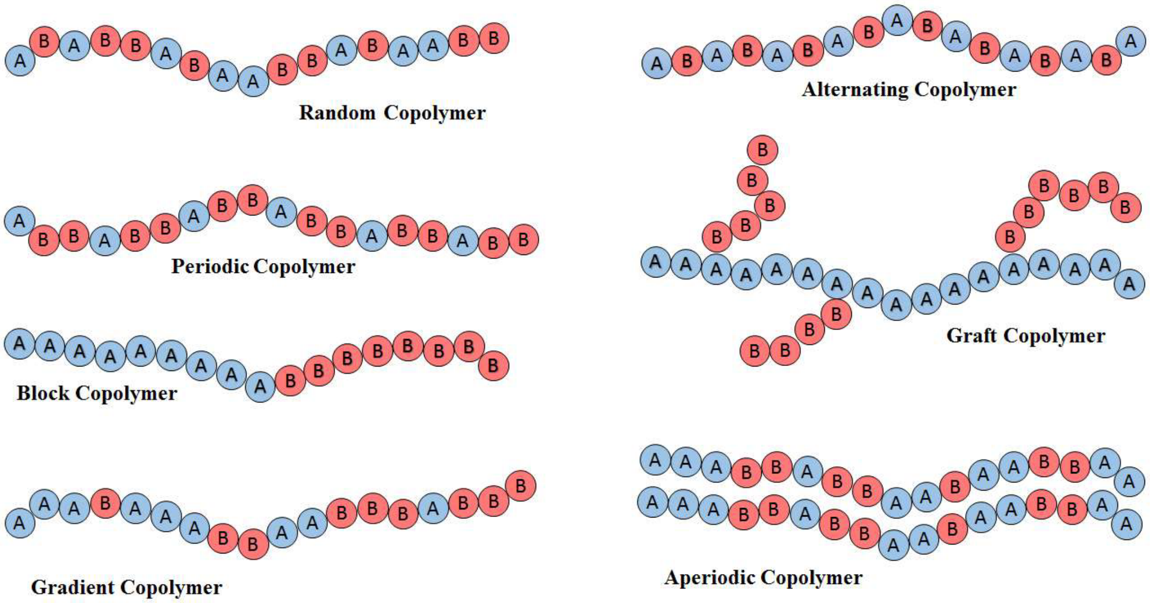

Figure 1.1 Types of the polymer

1.1.1 Polyelectrolyte

The polyelectrolyte is a polymer whose repeating units carry an ionic charge which helps the polymer to be soluble in water. When the ion charge is positive, a cationic polyelectrolyte is formed, while in the case of negative charge an anionic polyelectrolyte is formed [3].

Disolving in a suitable dilute solution, hydrophobic polymers are arranged as random coils Figure 1.2a. On the other hand, polyelectrolytes are expanded (Figure 1.2b). However, adding an electrolyte salt such as NaCl leads to a rapid decrease in the viscosity. Furthermore, the effective charge of the polymer will be decreased, and the hydrodynamic volume will also be decreased. Those effects are due to coiling up of the polyelectrolyte molecule by opposite charge ions (Figure 1.2c) [3].

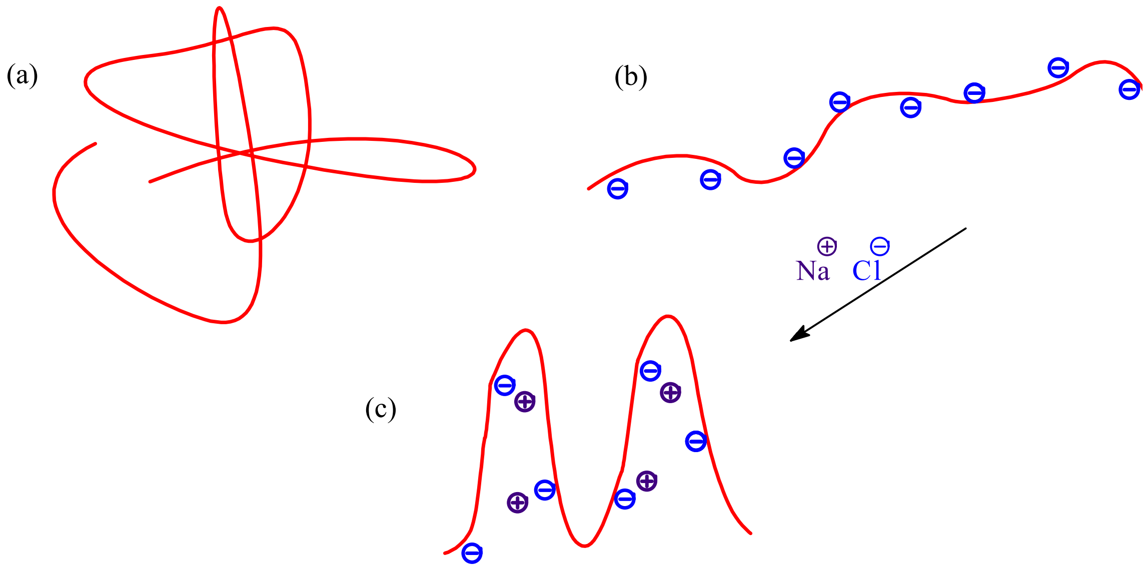

Figure 1.2 (a) Randomly coiled, (b) expanded polyelectrolyte, (c) the salt effect on a polyelectrolyte

1.2 Coating Material

A **coating material** is a covering that is applied to the surface of an object, usually referred to as the **substrate**. The purpose of applying the coating may be decorative, functional, or both. There are wide purposes of the coating material including, adhesion, anti-corrosion, anti-fouling, insulation, etc. Wet adhesive and antifouling properties are targeted in this research as applications of the synthesized polymers.

1.2.1 Adhesive Materials

1.2.1.1 Definition

The meaning of adhesive is any material that can be applied to one or more surfaces of separate items that binds them together. The solid materials or the surfaces joint are identified as the adherents. The adhesion is the phenomenon that refers to the tendency of the adhesive to be attached to the adherent [4].

1.2.1.2 Theories of the Adhesion

There are several theories for adhesion phenomenon that have been proposed, which together are complementary and contradictory at the same time [4].

- **Mechanical interlocking**

The effects of both mechanical interlocking and thermodynamic interfacial interactions could be taken into account as multiplying factors for estimating the joint strength G:

G = (constant) × (mechanical keying component) × (interfacial interactions component)

So, according to the previous equation, the adhesion level will be achieved by improving the properties of physicochemical surface and surface morphology [5].

- **Electronic Theory**

The Coulomb's law that describes the force interacting between static electrically charged particles is:

$$F = K_e \frac{q_1\, q_2}{r^2}$$

where K_e is a constant ($K_e = \frac{1}{4\pi\varepsilon}$), ε is the permittivity of free space in $C^2\ m^{-2}\ N^{-1}$, q_1 and q_2 are the signed magnitudes of the charges, and the r is the distance between the charges.

- **Theory of boundary layers and interphases**

Bikerman's theory describes the theory involving boundary layers and interphases. The theory is based on observation of adhesion failure; rarely seen to occur at the interface, but typically is a cohesive failure of the adherend [6].

- **Adsorption thermodynamic theory**

This theory is based on the belief that the adhesive will adhere to the substrate because of interatomic and intermolecular forces established at the interface, provided that an intimate contact is achieved. The most common interfacial forces result from van der Waals and Lewis acid-base interactions [5].

- **Diffusion theory**

This theory suggests that there is an interdiffusion between the adhesive material and the adherend surface across the interface.

- **Chemical bonding theory**

The adhesion phenomenon arises when chemical bonds formed between the adhesive material and the adhered surface across the interface .

1.2.2 Antifouling Materials

1.2.2.1 Definition

The biofouling can be defined as the undesirable accumulation of bacteria, microalgae, and macro-organism on surfaces of ships when immersed in sea water. This biofouling material causes a lot of problems such as increasing the corrosion of the surfaces, thereby requiring high energy to move the ship [7].

1.2.2.2 Classification

There are three major classes of antifouling: chemical, biological and physical methods [8].

- **Chemical Methods**

Organic tin compounds and its derivatives have been wildly used in the last three decades because of its powerful action as fungicides, and ability to inhibit the growth of most fouling organisms even at a very low concentration. The traditional method could be in the soluble matrix or insoluble matrix and each one has advantages and disadvantages. Figure 1.3 shows the method of releasing of insoluble and soluble matrix paints [9].

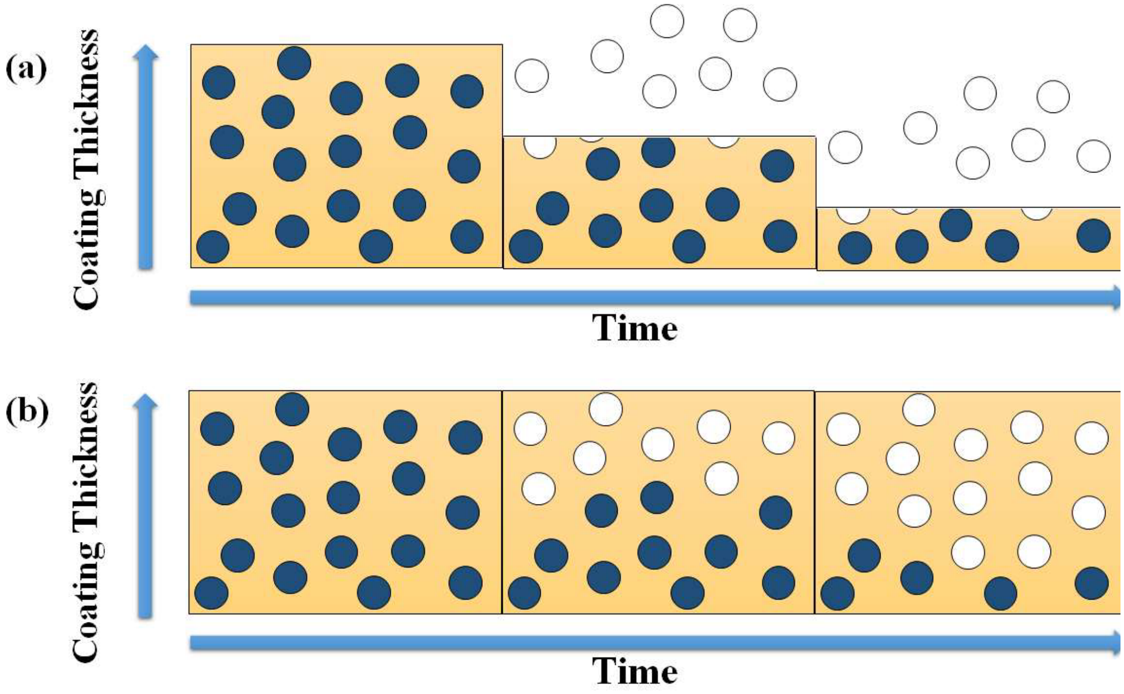

Figure 1.3 Method of release biocide of traditional soluble (a) and insoluble (b) matrix paints by the time

A revolution on antifouling happened the early 1970s when a TBT self-polishing copolymer (TBT-SPC) technique was used. This paint is based on an acrylic copolymer with TBT groups bonded to the polymer backbone by an ester linkage (Figure 1.4). This technique provides a new coating surface during the sailing. Moreover, it has a low cost of maintenance and high stability with fast drying. However, the side effect of TBT on the environment such as malformations of organisms was established and International Maritime Organization (IMO) banned TBT in 2008. This has led to the synthesis and development of tin-free antifouling coating [8].

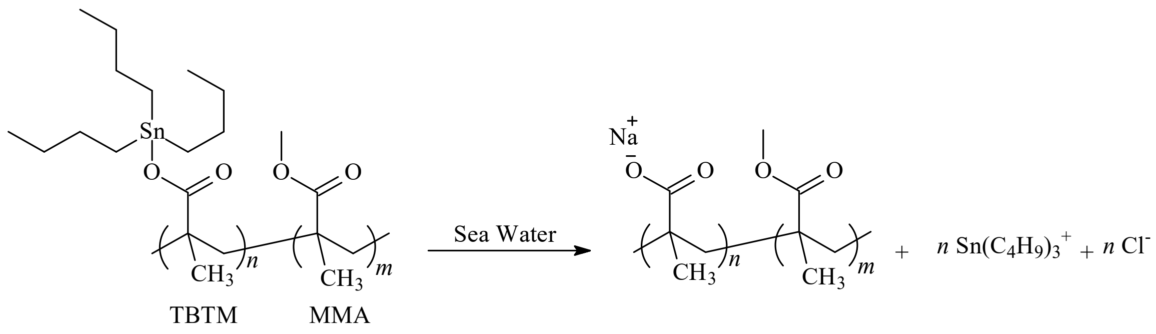

Figure 1.4 Hydrolysis of TBTM-co-MMA polymer by sea water (Na^+ and Cl^- ion present)

- **Biological Methods**

Some enzymes and metabolites excreted from organisms were found to prevent biofouling [8].

- **Physical Methods**

Research is also focused on the surface modification and physical properties using radiation and charge potential methods to prevent biofouling [8].

1.3 Coacervation

The International Union of Pure and Applied Chemistry (IUPAC) defines in the IUPAC goldbook 2014 that coacervation is the separation into two liquid phases in colloidal systems. The phase more concentrated in the colloid component is the coacervate, and the other phase is the equilibrium solution, and the complex coacervation is coacervation caused by the interaction of two oppositely charged colloids. The first phenomenon of complex coacervation is reported on the gelatin and gum arabic system by Bungenberg de Jong and Kruyt in 1929 [10], [11].

1.4 Biomimicked Polymers

It is vital to learn how a marine organism like mussels does generate wet marine bioadhesives and a non-fouling surface. It requires a fundamental understanding of the following three prominent features: i) the role of surface-active polyelectrolyte fluids having polymer backbone of opposite algebraic signs that remain phase-separated from water and undergo triggered solidification (coacervates), ii) the presence of polymer functionalities (e.g. DOPA) that provide energetic wet surface bonding, and iii) the nanoscale morphology/domain size of the natural systems.

The *mussels* store the anionic and cationic peptides in separate body cavities and mix them in a special organ right before application (Scheme 1.1). The unique ability of these marine adhesives to resist bio-fouling will be exploited to design novel coatings for a variety of applications.

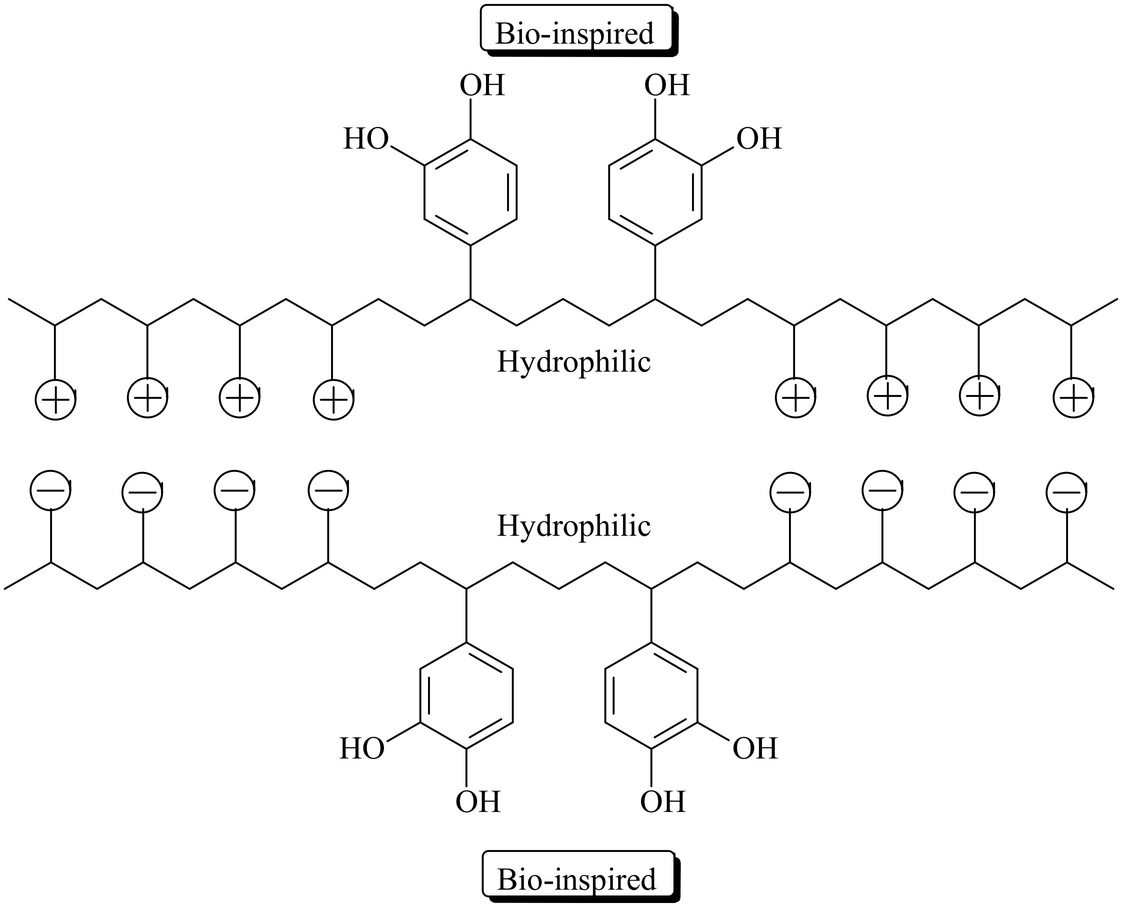

Scheme 1.1 The anionic and cationic polymer containing catechol moity in separate body and mix them

By developing bio-inspired novel advanced materials, new nanostructured films and coatings can be obtained which have direct relevance to water purification, marine, and biomedical applications. The power of this new approach to exploiting biological inspiration in the design of advanced material systems is the opening up of new research fields and directions, which will significantly increase both industrial exploitation of these findings as well as the impact of this research worldwide.

1.5 Importance of the Proposed Research

One of the key advantages of this bio-inspired approach to designing new hydrogel materials is that new functionality, structure, and properties can be designed into the synthetic system that is not present or possible with the natural system.

To illustrate the power of this approach we propose to develop a full understanding of the role of balanced ionic bonding, termed coacervation. Coacervation is widely used by marine organisms due to their unique ability to employ water-soluble, highly charged anionic and cationic polymeric materials which on mixing, phase separate from aqueous solution and form a distinct, water-insoluble fluid phase (termed a coacervate). Once formed, these coacervates have exceptional properties such as shear thinning and low interfacial energy[12]–[14]. Major advances are anticipated in the production of surfaces that resist fouling caused by organisms and biomolecules in the marine environment, water purification as well as medical systems.

1.6 Grand Challenge

Two fundamental challenges in the development of advanced materials are engineering durable adhesive bonds in a wet environment and the generation of controlled surfaces which resist biofouling. From a molecular level, we propose that these two areas are related and major advances are possible through new design paradigms which are inspired by natural systems. For example, most synthetic adhesive systems suffer significant deterioration, even complete failure, in the presence of moisture, which in its broadest sense ranges from surface hydration to immersion in body fluids or seawater. Similarly, most surfaces undergo biofouling when exposed to aqueous systems and biological fluids. The high-risk, future study is to discover new strategies for controlling surface chemistry and adhesion, achieve translation to synthetic systems, and by tuning physical properties by incorporating non-natural building blocks, realize superior performance and application when compared to natural systems. An anticipated outcome of this work will be to develop coatings that have very low bio-fouling for use in water purification, marine environments and biomedical applications which will further increase the impact of these fundamental studies.

1.7 Innovation

The working hypothesis of this thesis is that formulating a practical wet adhesive or a non-fouling surface requires the creative translation and fundamental understanding of three prominent features of marine bio-adhesives: i) the role of dense surface-active polyelectrolyte fluids (coacervates) that remain phase-separated from water and undergo triggered solidification, ii) the presence of polymer functionalities (e.g. Dopa) that provide energetic wet surface bonding and iii) the nanoscale morphology/domain size of the natural systems. In particular, the unique ability of these marine adhesives to resist bio-fouling, a feature not traditionally appreciated, will be exploited to design novel coatings for a variety of applications. Key issues to be addressed include the optimization of coacervate formation – coacervation is the unique ability of water-soluble anionic and cationic polymers to phase separate from water when mixed in aqueous solution – and the role of naturally occurring crosslinking systems – such as DOPA which is based on the redox chemistry of diphenolic/catechol-based systems, coupled with the resulting chemically distinct nanoscale environments created by these coacervate systems.

1.8 Relationship to the Priority Areas

Key components of this dissertation clearly and fully address priority areas such as water and nanotechnology. By developing these novel advanced materials, new nanostructured films and coatings can be obtained which have direct relevance to water purification, marine, and biomedical applications. The power of this new approach to exploiting biological inspiration in the design of advanced material systems is the opening up of new research fields and directions which will significantly increase both industrial exploitation of these findings as well as the impact of this research worldwide.

1.9 Objectives and Work Plan

A new, hierarchical strategy for the formation of hydrogel coatings based on design principles originating from marine organisms is described. The inspiration is provided by marine organisms for the design of new materials for the formation of the coating and adhesive. We propose to transition the adhesive concepts present in marine organisms such as mussels into the bio-inspired practical wet adhesive, coating systems, and non-biofouling surfaces.

1.9.1 Objectives

The proposed study will have the following objectives:

I. Synthesis of epoxides containing catechol motifs.
II. Polymerization of epoxides containing catechol motifs.
III. Copolymerization of epoxides containing catechol motifs with allyl glycidyl ether to block and/or random copolymer.
IV. Synthesis of bio-inspired, water-soluble cationic and anionic polyelectrolytes from the copolymers described under objective III.
V. Characterization of polymers using NMR, IR, TGA, and GPC analysis for determination molar masses.
VI. Investigation on the formation of coatings from coacervate precursors.

CHAPTER 2

LITERATURE REVIEW

2.1 Introduction

The ability of a modern technological society to control their interactions with as common a substance as water is becoming a defining issue for the 21st century. These interactions range from the coating of ships that navigate waters for global trade, to understanding and controlling biofouling and adhesion in medical implants which are increasingly necessary as the population ages, and to the purification of the sea and contaminated water through membrane technology in order to satisfy global clean water challenges. At the heart of all of these critical issues is the dynamic nature of the interface between the synthetic coating/adhesive/membrane and the surrounding aqueous solution. In order to tackle these significant universal challenges, major technological breakthroughs are needed in many areas of membrane and coating technology. These include fouling assessment and control, pre- and post-treatment, cleaning, improved mechanical properties, etc. We propose to examine a new materials platform, inspired by marine organisms, in two major areas – low biofouling coatings for underwater paints/adhesives as well as bulk hydrogels that may have application as nanoscale structures for water purification.

2.2 Coatings as Antifouling Materials

Fouling constitutes the buildup of nonliving material and/or living organisms on a solid surface. The accumulation of living organisms, referred to as biofouling, is observed on a variety of surfaces ranging from ship hulls [15] to human teeth [16]. This undesired accumulation affects numerous material systems including water purification membranes [17], [18] and biomedical implants and has proven to be an exceedingly difficult problem to solve using traditional materials [19], [20]. An excellent example of this difficulty is the biofouling on the surface of ship hulls which is well known for its undesirable consequences such as decreasing the fuel efficiency and speed of marine vessels [21]. A number of strategies have been developed to cope with this problem with self-polishing coatings which release toxic tributyltin (TBT) once appearing to be an ideal solution. However, due to the toxicity of TBT in the environment, its use is now globally prohibited. Environmental concerns about copper as an ingredient of antifouling paint are also well documented [8], [22], [23]. Of all the vessel-related coatings, antifouling bottom paints are amongst the largest source of trace metals, in particular, copper and for environmentally sensitive areas such as the Red Sea, these strategies are not acceptable.

With increasingly stringent regulations on antifouling coatings, a need has been identified for new, robust, environmentally friendly materials to be developed that inhibit attachment and prevent biofouling. Presently, a number of strategies are emerging to produce metal-free, non-toxic, fouling resistant coatings. The most successful commercial, metal-free coatings continue to be the Intersleek series of paints by International Paints based on RTV-based silicone elastomers. The fouling release behavior of these materials is moderate and poorly understood due to the combination of the rubbery character of the polymer and the many surface components including amphiphilic and charged structures. More recently, several new strategies have emerged based on the observation that coatings with complex, "ambiguous" surfaces show promise in fouling release. Surfaces such as microstructured PDMS (Polydimethylsiloxane) with variations in topography modeled after shark skin features have been explored [24]. Crosslinked polymers with different functional groups including silicone, perfluoroalkyl segments and PEG (Polyethylene glycol) chains were also tested by different groups [25]–[27]. Simple amphiphilic polymer phase separation was also used as a tool to inhibit biofouling [28], while surfaces containing zwitterionic groups have also shown promise [29]–[34]. Patterned surfaces in which both polar and non-polar materials are combined at very small length scales were developed and studied against Ulva spores to develop a better understanding of feature size against the size of the fouling organisms [35], [36]. While these strategies are successful to a degree, all of these materials still do not perform as well as surfaces and adhesive structures formed by marine organisms, such as the *mussel*. It is therefore proposed to build on this work, especially the concept of nanoscale patterned – *ambiguous* – surfaces to develop hierarchical coatings which are initially formed by dynamic coacervation of block copolymers to give surfaces that have nanoscale morphology (hydrophobic coacervate domains surrounded by a hydrophilic matrix), are amphiphilic on the nanoscale and have the potential for secondary crosslinking and adhesion through covalent bonding.

2.3 Bulk Hydrogels

The synthetic and modular nature of our proposed approach to bio-inspired coatings and adhesives allows these strategies to become a broad platform for the development of other advanced materials that benefit from controlled fouling, adhesion, and mechanical properties. To further demonstrate the robustness of this coacervate driven strategy it is proposed to examine the modular preparation of bulk hydrogels. The need for robust and responsive hydrogels for use in several biomedical, industrial and pharmaceutical applications has motivated great research efforts in these important polymeric materials [37]–[41]. The main feature that makes hydrogels distinctive is that most of their mass consists of water, however they still show solid-like mechanical properties due to the presence of a 3D network structure that is created through *in situ* covalent bond formation between multifunctional, reactive precursors [42]. Many chemistries have been utilized for covalent crosslinking of hydrogel-forming materials, e.g. Michael addition, free radical polymerization, and thiol-ene coupling, with the resulting hydrogels that have good mechanical properties due to the strong covalently-bonded framework [42]–[45]. The covalent approach has few limitations e.g., the hydrogels have limited responsiveness to external stimuli, are not re-moldable once formed, and may require organic co-solvents/reagents during their formation. In order to overcome these limitations, hydrogels formed through non-covalent, physical associations arising from intermolecular interactions, in lieu of covalent crosslinks, have attracted significant interest recently, particularly as responsive materials and injectable gels. Typically, a drawback of such physically-associated hydrogels is their poor mechanical properties due to generally weak intermolecular interactions [46], [47]. On the other hand, recent works by Yasuda et al.

[48] and Gong et al. [49] on double network gels and Wang et al. [50] on the development of "aquamaterials" have demonstrated that significant improvement in hydrogel mechanical properties is possible through careful design of the intermolecular interactions and length-scales between physical associations.

In addressing new strategies to yield high performance, physically-associated hydrogels, the role of dynamic materials formed via electrostatic (coacervate) interactions serves as a powerful model. While block copolyelectrolytes are widely used in the construction of hydrogel materials, the majority of these systems are based on block or random copolymers where the ionic blocks serve as the water-soluble component and neutral, hydrophobic blocks lead to network formation [51]–[55]. In these examples, hydrogel formation requires the hydrophobic collapse of the neutral blocks into discrete domains with the ionic mid-block forming the solvated matrix and connection between discrete, hydrophobic crosslinking domains. In direct contrast, charge driven assembly based solely on ionic interactions has received only minor attention with recent studies led by Stuart [52], Aida [50], and Lemmers [55] demonstrating the responsive nature and significant potential of hydrogels based on ionic interactions.

2.4 Literature Review

A polystyrene-block-poly[(ethylene oxide)-stat-(allyl glycidyl ether)] [PS-b-P(EO-stat-AGE)] statistical diblock terpolymer was synthesized with varying incorporations of allyl glycidyl ether (AGE) in the poly(ethylene oxide) block from 0 to 17 mol% [56]. The pendant alkenes of the AGE repeat units were subsequently functionalized by thiol-ene chemistry to incorporate perfluorinated chemical moieties to control the surface properties Figure 2.1. The material has been shown to have the potential as fouling-release coatings.

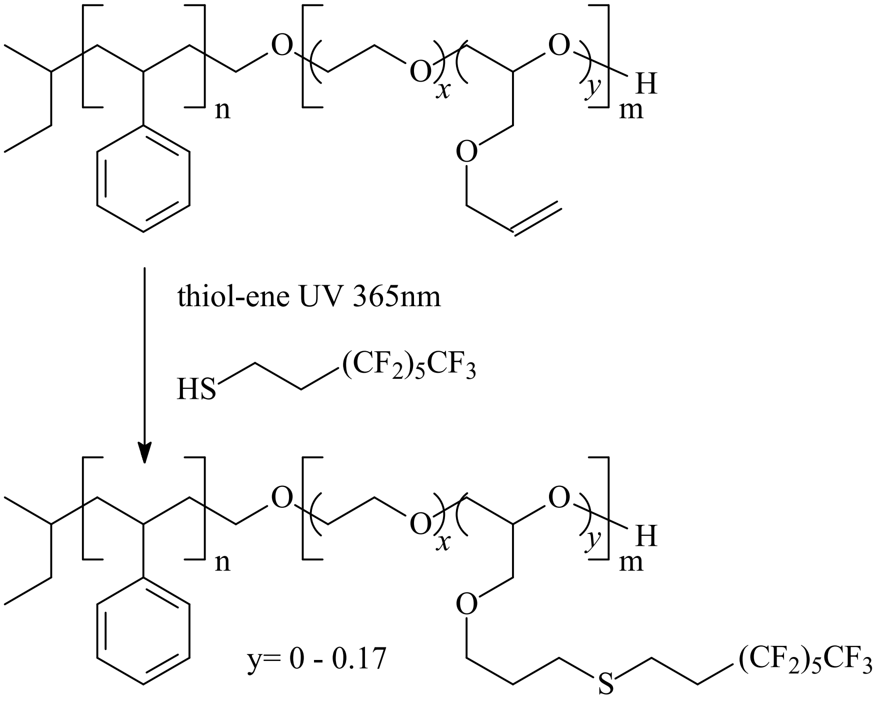

Figure 2.1 Synthesis of perfluorinated terpolymers

Protein-based catechol repeating units contained within the adhesive secretions of mussels help them survive by strongly attaching to a variety of different surfaces, primarily rock surfaces composed of metal oxides via formation of complexes with metal ions or metal oxides. In this respect, catechol-functionalized tri(ethylene oxide) has been synthesized as a removable and recoverable self-assembled monolayer for use on oxides surfaces Figure 2.2 [57]. This tunable assembly based on catechol binding to metal oxides represents a new concept for reformable antifouling coatings.

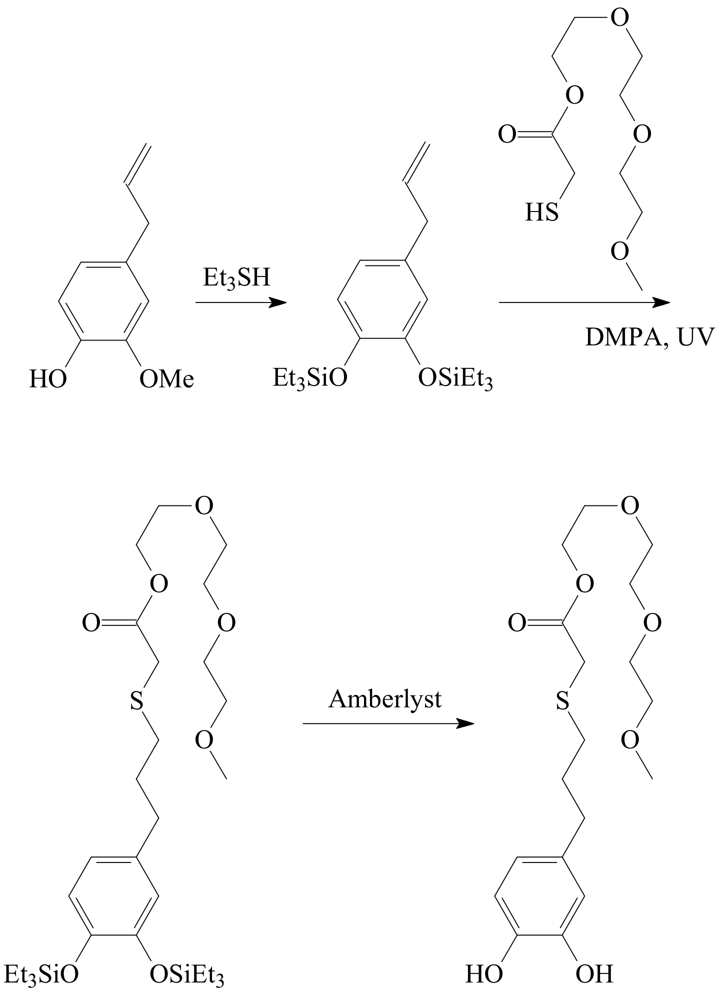

Figure 2.2 Synthesis of catechol-functionalized tri(ethylene oxide)

A catechol-functionalized polyacrylamide binder in combination with inorganic nanoparticles has been developed as shown in Figure 2.3 [58]. The composite has been used for the fabrication of robust composite coatings via a layer-by-layer process.

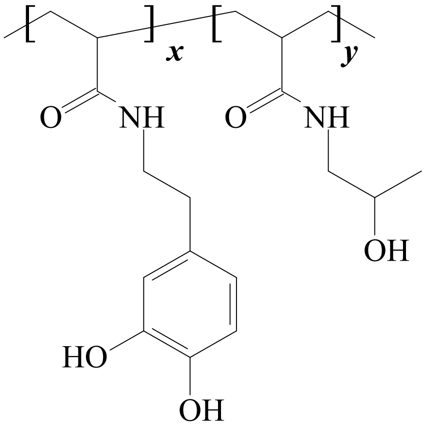

Figure 2.3 Synthesis of a catechol-functionalized polyacrylamide binder

The chemical basis for mussels' ability to adhere to both inorganic and organic surfaces has never been fully explained. The detailed binding mechanisms of unusual amino acid 3,4-dihydroxy-L-phenylalanine (dopa) has been investigated [59]. A new picture of the interfacial adhesive role of dopa emerges from these studies.

An article describes the synthesis of polyacrylate and polymethacrylate materials that are surface-functionalized with mussel-inspired catechols Figure 2.4 [60]. Polymeric materials that intrinsically heal at damage sites under wet or moist conditions are needed for biomedical and environmental applications. It is shown that the triggering of complete self-healing is enabled underwater by the formation of extensive catechol-mediated interfacial hydrogen bonds.

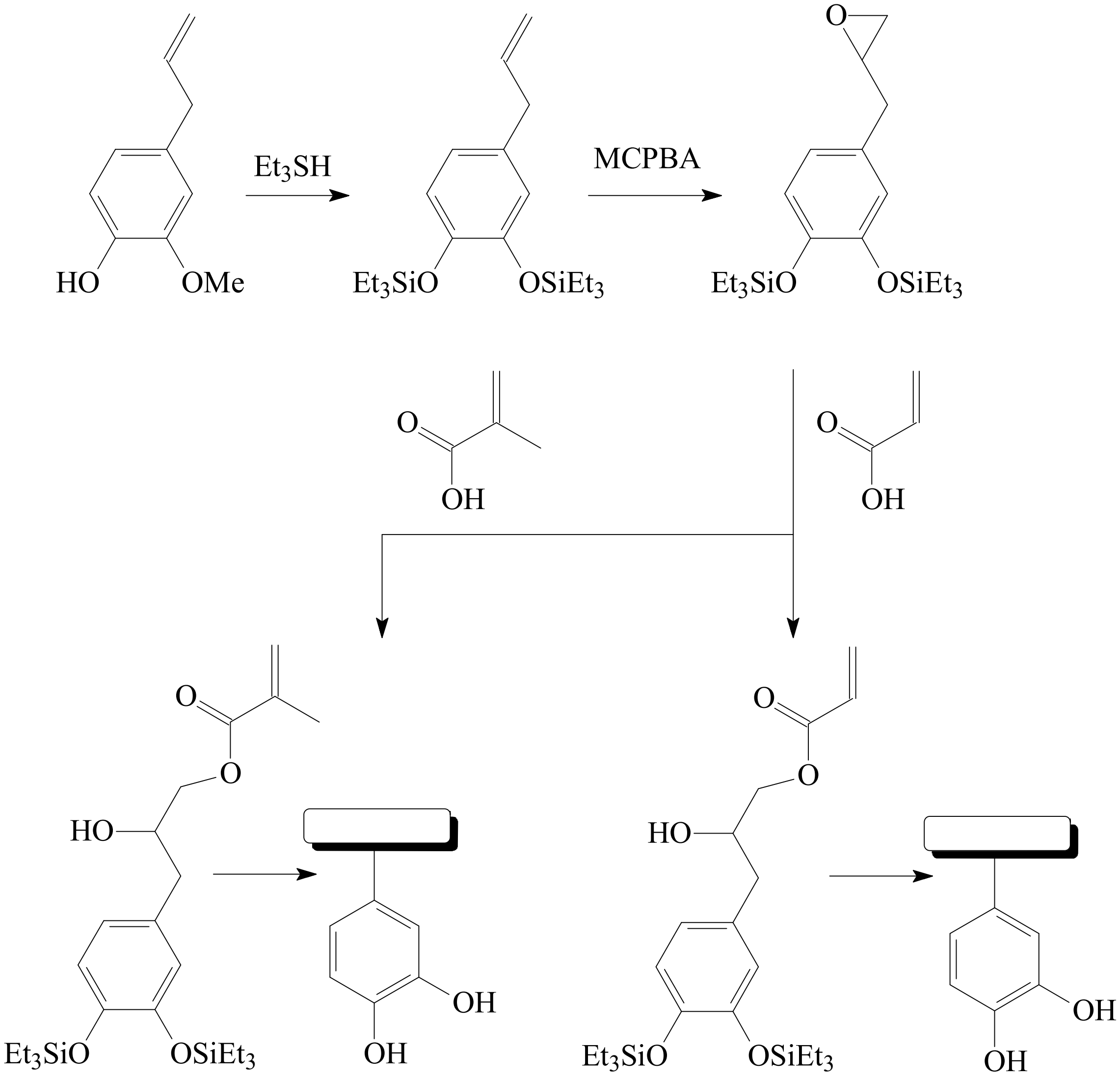

Figure 2.4 Synthesis of catechol-functionalized polyacrylates

A novel injectable thermosensitive self-healing hydrogel DNODN based on self-assembly of a mussel-inspired tri-block copolymer with anti-biofouling property has been developed Figure 2.5 [61]. The self-mending DNODN hydrogel can withstand high strain and repeated deformation and quickly recover its mechanical properties and structure through the catechol-mediated reconstruction of hydrogen bonding and aromatic interactions. The novel DNODN hydrogel materials exhibited great potential in various bioengineering applications (e.g., drug delivery).

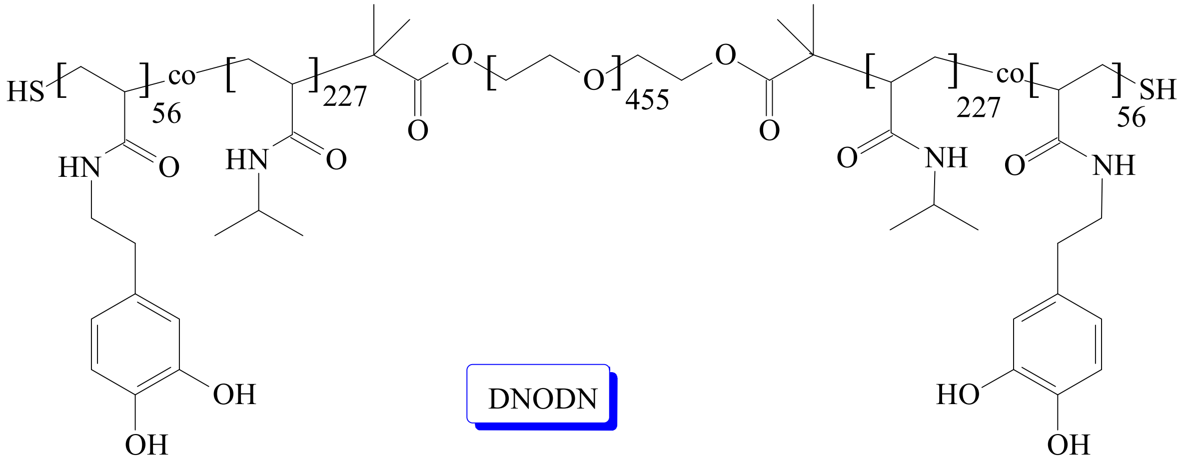

Figure 2.5 Synthesis of a thermosensitive self-healing hydrogel DNODN

A facile synthetic strategy or the functionalization of well-defined polyether copolymers with control over the number and location of catechol groups has been reported Figure 2.6 [62]. The effects of polymer architecture, molecular weight, and catechol incorporation on the adhesive properties of surface-anchored PEO has been studied [63].

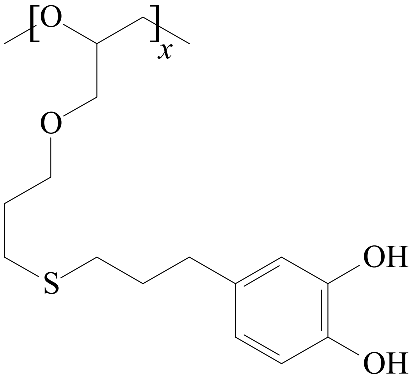

Figure 2.6 Synthesis of a polyethylene oxide (PEO)-based polymers with catechols

Allyl glycidyl ether, polymerized from potassium alkoxide/naphthalenide initiators under both neat and solution conditions, was shown to be a highly-controlled process Figure 2.7 [63].

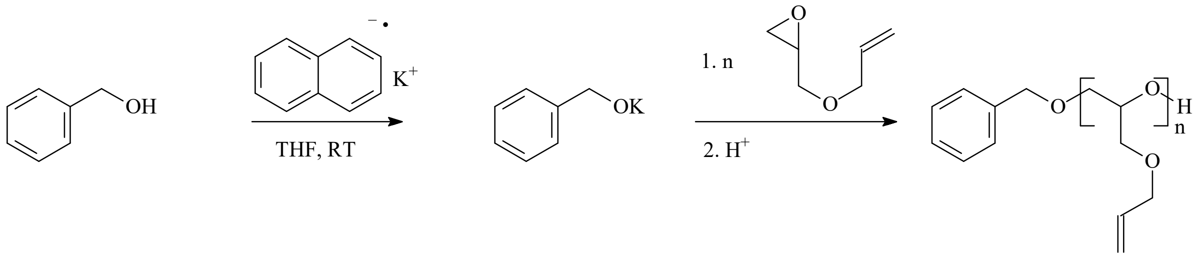

Figure 2.7 Synthesis of allyl glycidyl ether based polymers

A new family of polymer electrolytes based on a poly(allyl glycidyl ether) platform has been developed for battery electrolyte applications Figure 2.8 [64].

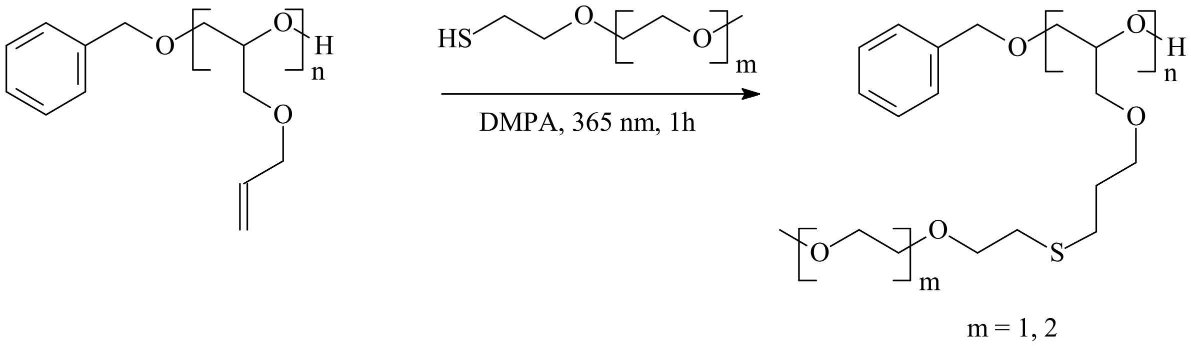

Figure 2.8 Synthesis of a poly(allyl glycidyl ether) platform for battery electrolyte applications

A series of linear poly glycidol copolymers, tethering with both alkene and hydroxyl groups, has been prepared by a combination of anionic ring-opening polymerization (ROP) [65]. The final copolymers have abundant double bonds and hydroxyl as side groups Figure 2.9.

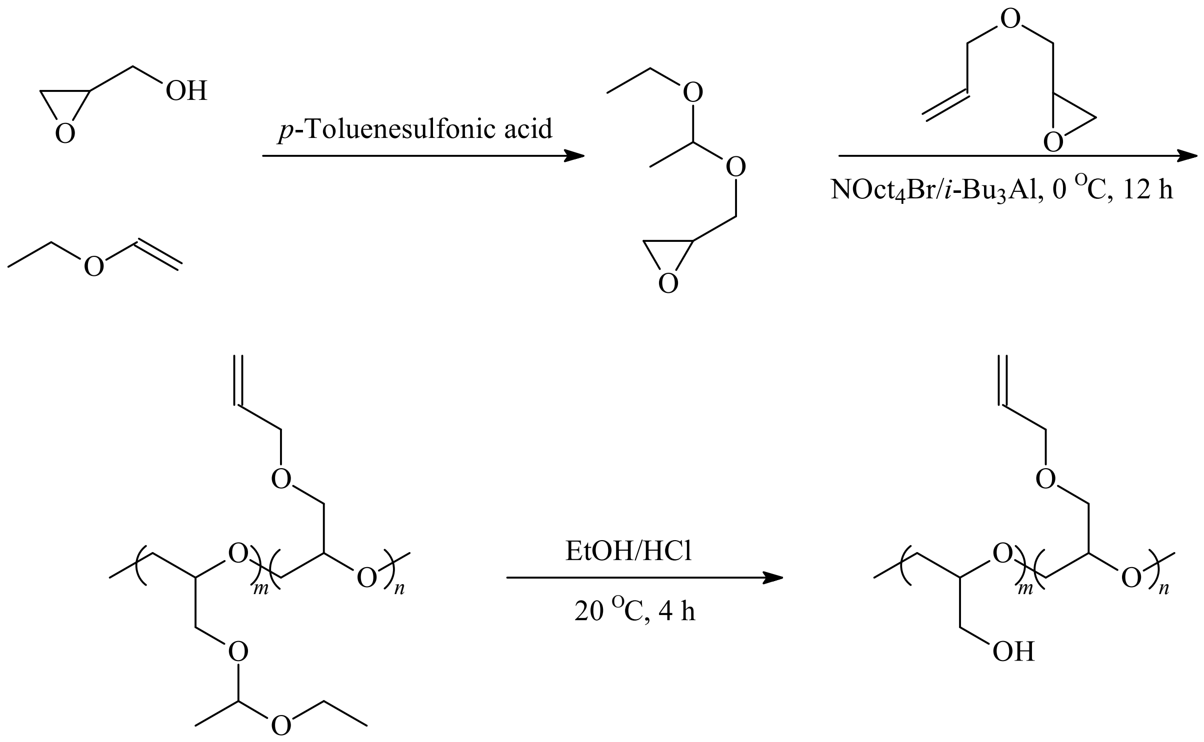

Figure 2.9 Synthesis of a series of linear poly glycidol copolymers, tethering with both alkene and hydroxyl groups

Catechol containing pH-sensitive polymeric carriers are designed for delivery of the anticancer drug bortezomib (BTZ) to cancer cells [66]. The polymer used as a building block in this study was poly(ethylene glycol) incorporated with a catechol moiety. The catechol moiety was exploited for its ability to bind and release borate-containing therapeutics such as BTZ in a pH-dependent manner.

A facile synthetic strategy for introducing catechol moieties into polymeric materials based on a readily available precursor (eugenol) and efficient chemistries [tris-(pentafluorophenyl)borane-catalyzed silation and thiol−ene coupling] is reported as shown in Figure 2.10 [67]. The advantage of silyl protection for catechol-functionalized polysiloxanes is demonstrated, and represents a promising and versatile new platform for underwater surface treatments.

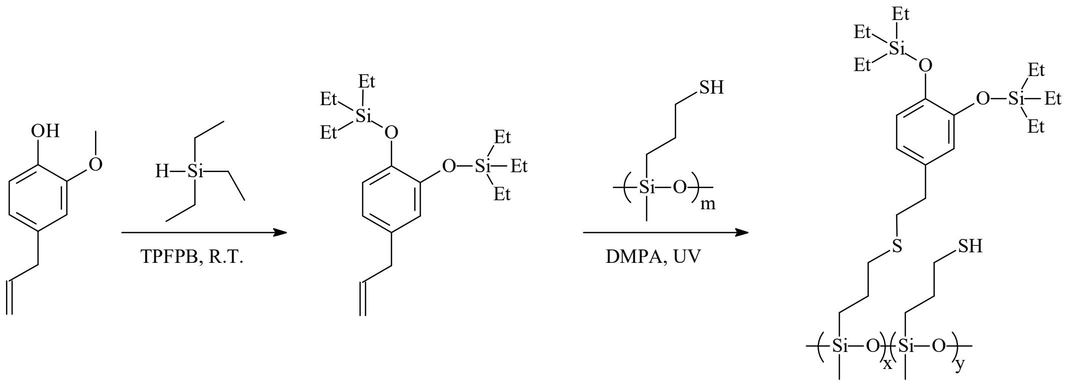

Figure 2.10 Synthesis catechol-functionalized polysiloxanes

A bifunctional CA-PEG (catechol-poly(ethylene glycol)) and multifunctional CA-PEG-PGA/PEVGE (poly- (glycidyl amine)/poly(ethylene glycol vinyl glycidyl ether)) ligands for the functionalization and solubilization of MnO nanoparticles has been reported Figure 2.11 [68]. The functional PEG ligands were synthesized starting from the acetonide-protected catechol initiator 2,2-dimethyl-1,3-benzodioxole-5-propanol (CA-OH) for oxyanionic polymerization. CA-OH was used both for homopolymerization of ethylene oxide (EO) as well as copolymerization with functional epoxides *N,N*-diallyl glycidyl amine (DAGA), releasing primary amino groups and ethylene glycol vinyl glycidyl ether (EVGE), exhibiting a double bond for click-type reactions, to generate CA-PEG and CA-PEG-PGA/ PEVGE. Coupling with fluorescein isothiocyanate (FITC) allows for optical monitoring of the nanoparticle fate in biological systems.

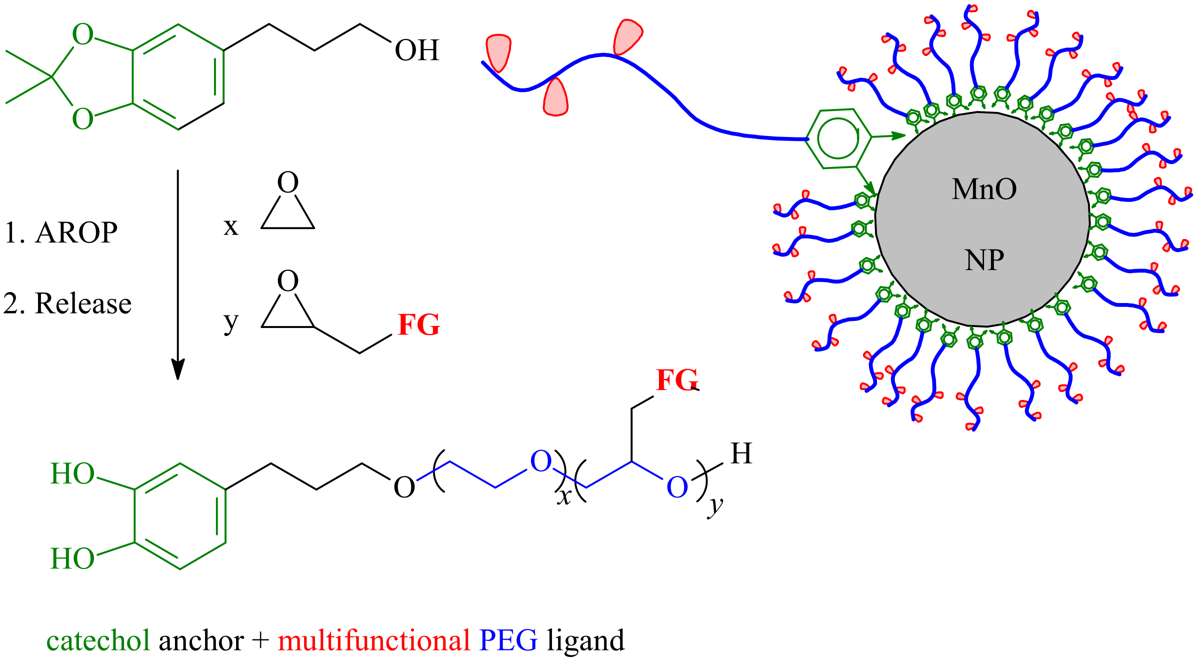

Figure 2.11 Synthesis of multifunctional CA-PEG-PGA/PEVGE (poly- (glycidyl amine)/poly(ethylene glycol vinyl glycidyl ether)) ligands for the solubilization of MnO nanoparticles

Diblock copolymers consisting of hydrophobic poly(allyl glycidyl ether) and hydrophilic poly(ethylene oxide), were prepared for the preparation of micellar drug delivery systems, and their self-assembly into micellar structures was studied Figure 2.12 [69]. The pendant double bonds to the hydrophobic part of the chain upon was further modified via thio-ene reaction.

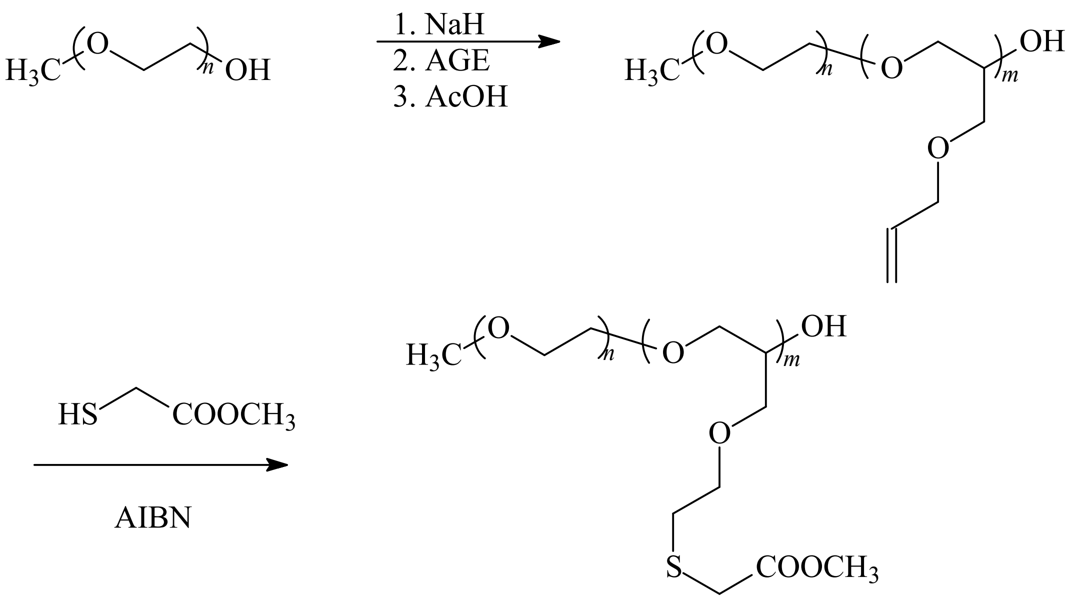

Figure 2.12 Synthesis of Diblock copolymers consisting of hydrophobic poly(allyl glycidyl ether) (PAGE) and hydrophilic poly(ethylene oxide) (PEO)

A series of random copolymers comprising ethylene oxide (EO) and 0-100% allyl glycidyl ether (AGE) has been prepared by anionic ring-opening polymerization. Poly(EO-co-AGE)s were conjugated with cysteine or the tripeptide glutathione (GSH) via thiol-ene coupling, resulting in well-defined hybrid materials with multiple peptide units conjugated to the PEG backbone Figure 2.13 [70].

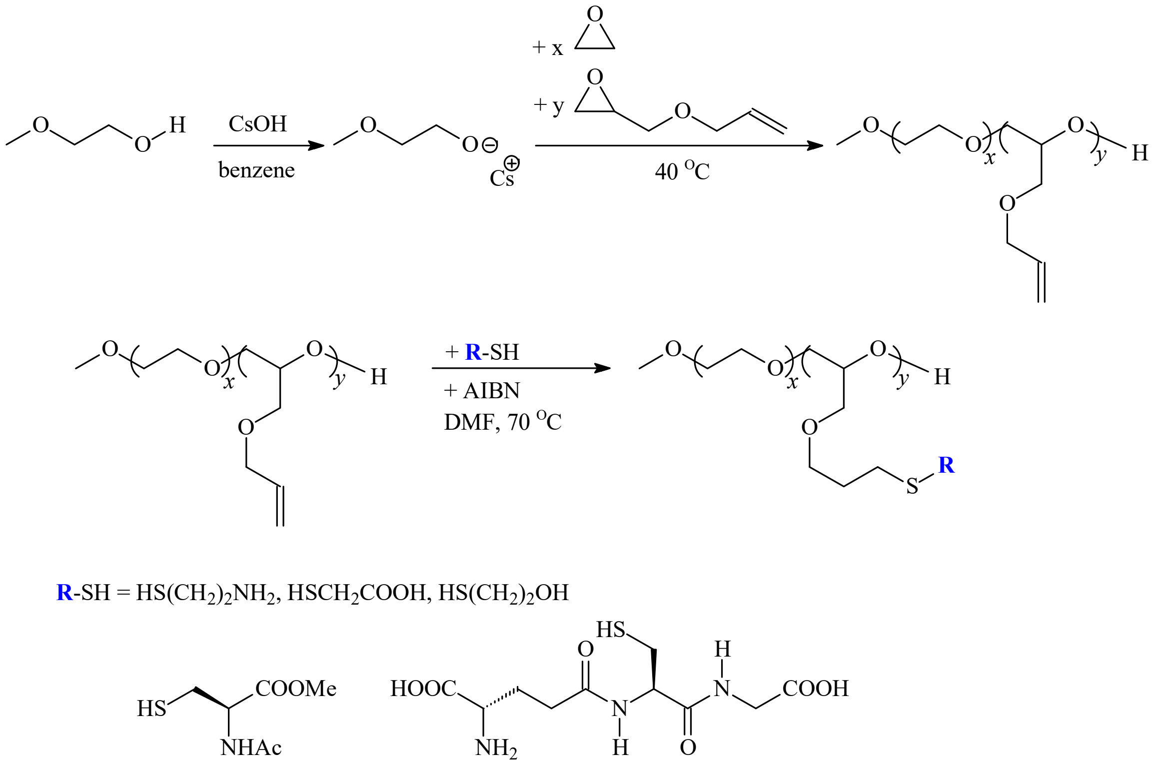

Figure 2.13 Synthesis of Poly(ethylene glycol-co-allyl glycidyl ether)s for multiple bioconjugation

New amphiphilic graft copolymers with hydrophilic poly(ethylene oxide-co-allyl glycidyl ether) (PEAG) as the backbone and hydrophobic poly(3-caprolactone) (PCL) as the side chains (PEAG-gPCL) were synthesized using techniques of anionic copolymerization, radical-mediated thiol–ene reaction and ring-opening polymerization Figure 2.14 [71]. The polymers had the capacity to encapsulate protein molecules (like hemoglobin, Hb) through a modified lyophilization–rehydration method as analyzed by TEM and SDS-PAGE.

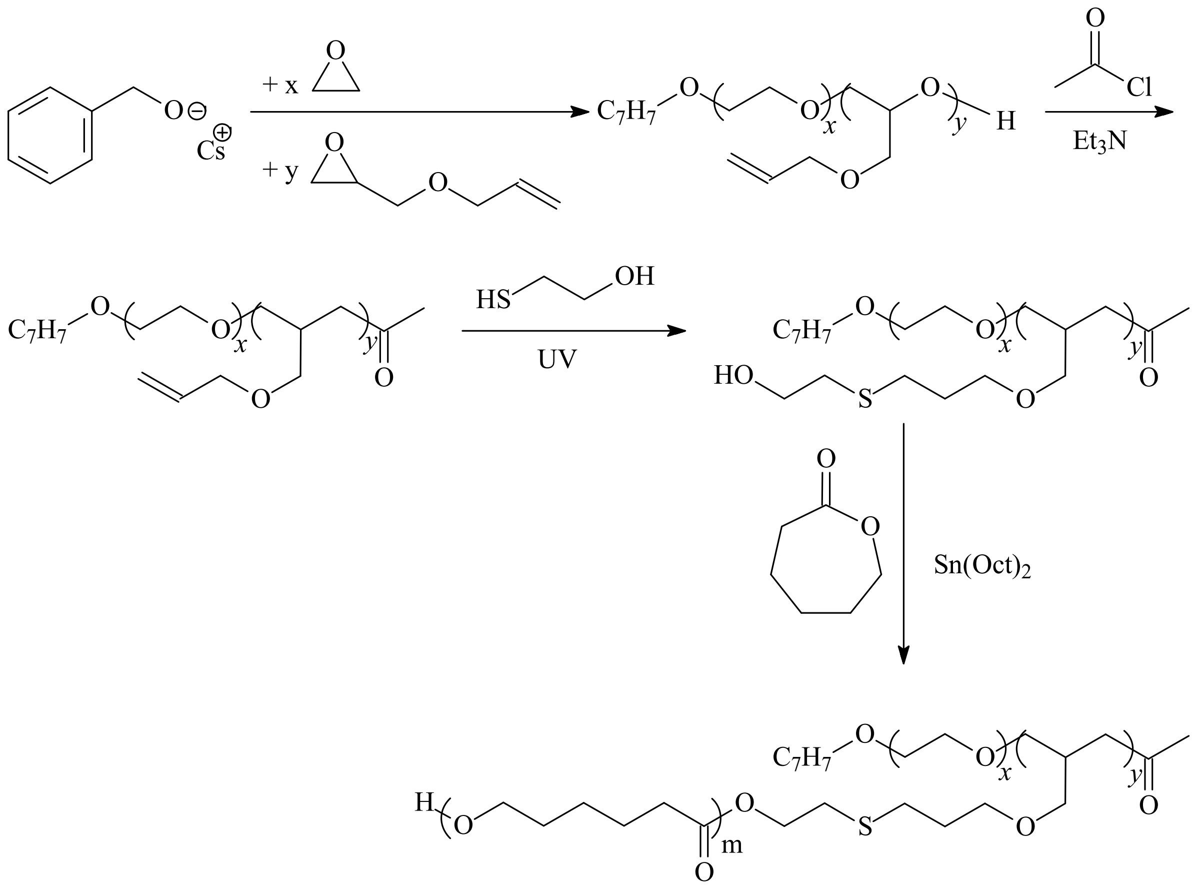

Figure 2.14 Synthesis of amphiphilic copolymer poly(ethylene oxide-co-allyl glycidyl ether)-graft-poly(3-caprolactone)

A novel epoxide monomer with a methyl-thioether moiety, 2-(methylthio)ethyl glycidyl ether (MTEGE) has enabled the synthesis of well-defined thioether functional poly(ethylene glycol) Figure 2.15 [72]. The thioether moieties of MTEGE can be selectively oxidized into sulfoxide units, leading to full disassembly of the micelles. Oxidation responsive release of encapsulated Nile Red demonstrates the potential of these micelles as redox-responsive nanocarriers. Further, sulfonium PEG polyelectrolytes can be obtained via alkylation or alkoxylation of MTEGE, providing access to a large variety of functional groups at the charged sulfur atom.

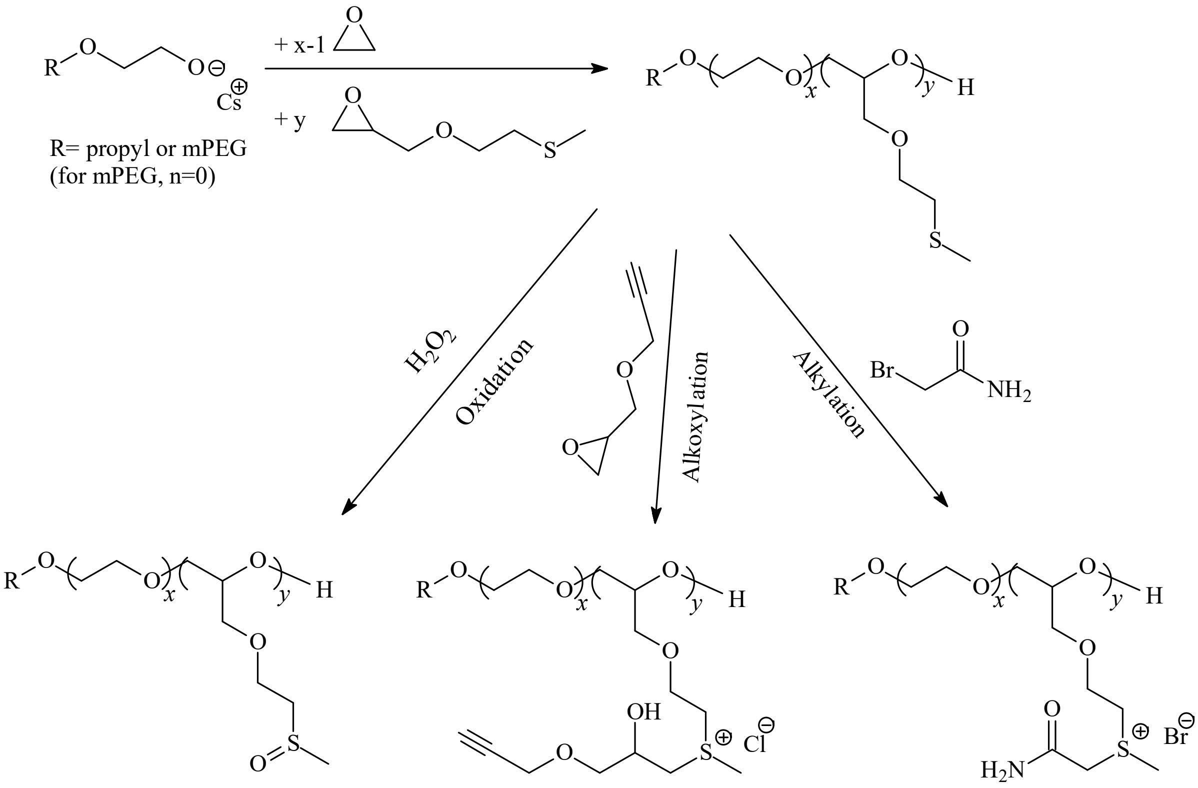

Figure 2.15 Synthesis of thioether functional poly(ethylene glycol)

In situ ^{1}H NMR spectroscopy was utilized to monitor the monomer-activated anionic ring opening copolymerization (AROP) of ethylene oxide (EO) with ethoxy ethyl glycidyl ether (EEGE) Figure 2.16 [73]. The results highlight the importance of understanding reactivity ratios of comonomer pairs under certain polymerization conditions.

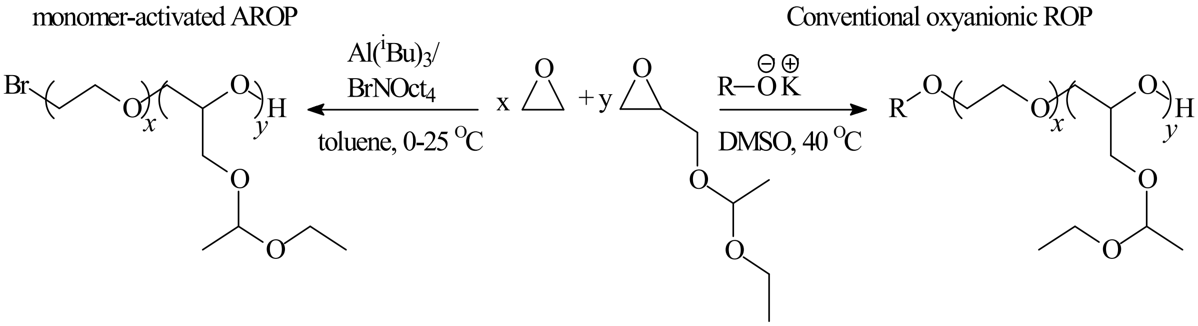

Figure 2.16 Monomer-activated anionic ring opening copolymerization (AROP) of ethylene oxide (EO) with ethoxy ethyl glycidyl ether (EEGE)

Charged triblock copolymers were synthesized by functionalizing poly[(allyl glycidyl ether)-b-(ethylene oxide)-b-(allyl glycidyl ether)] with either guanidinium (**a**) or sulfonate (**b**) functional groups Figure 2.17 [74]. When aqueous solutions (ca. 5−40 wt %) of these oppositely charged polymers were mixed, the electrostatic interactions of the functionalized blocks led to the association of the oppositely charged end-blocks into phase-separated complex coacervate domains bridged by the uncharged, hydrophilic PEO midblock. The viscoelastic properties and the physical nature of the cross-links have important implications for the applicability of these gels as injectable drug delivery systems.

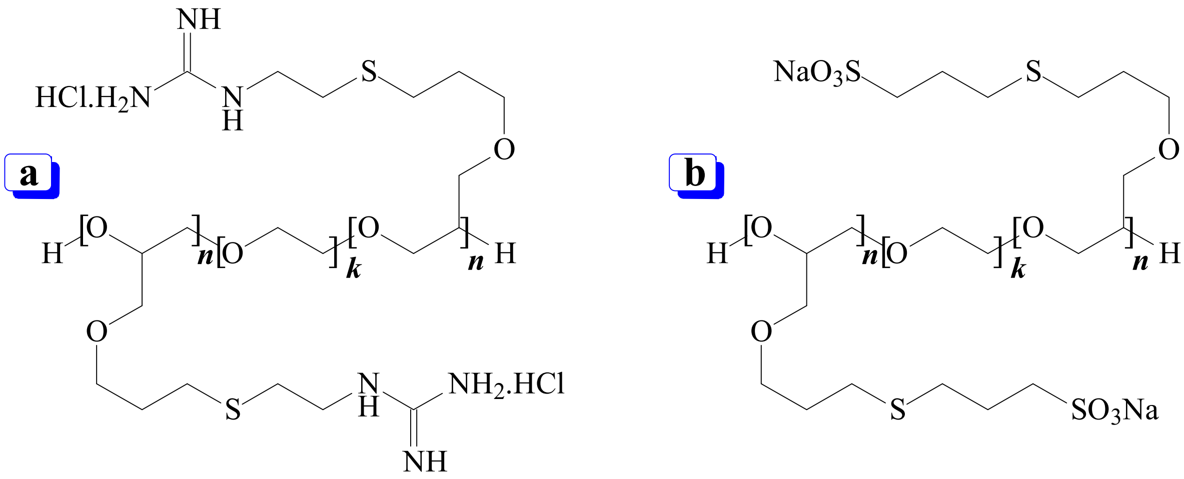

Figure 2.17 Synthesis of Triblock Copolymer Coacervate Hydrogels

Synthesis of high performance, physically associated hydrogels, dynamic materials formed through electrostatic interactions can serve as a powerful model. A convenient strategy led to the formation of biodegradable hydrogels from ABA triblock ionic polypeptides formed by mixing poly(L-glutamic acid)–block-poly(ethylene glycol)–block-poly(L-glutamic acid) (PGA–PEG–PGA) with poly(L-lysine)–block-poly(ethylene glycol)–block-poly(L-lysine) (PLL–PEG– PLL) Figure 2.18 [75]. The synthetic accessibility of the copolymer, makes this cross-linking system a flexible and powerful new tool for the development of injectable hydrogels for biomedical applications.

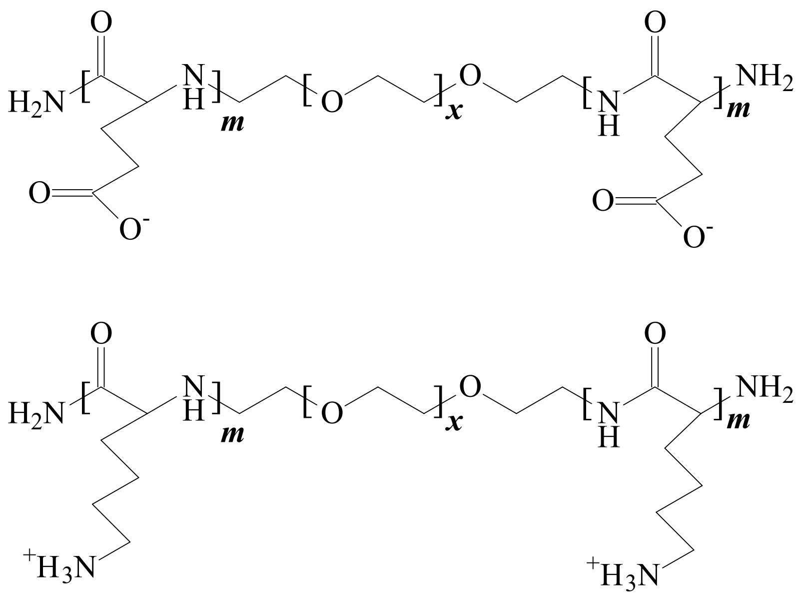

Figure 2.18 Synthesis of reversible ionic polypeptide hydrogel

Inspired by the chemical features of the cement proteins of the sandcastle worm, it was reported that a versatile and strong wet-contact microporous adhesive resulting from polyelectrolyte complexation triggered by solvent exchange. After premixing a catechol-functionalized weak polyanion Figure 2.19 with a polycation in dimethyl sulphoxide (DMSO), the solution was applied underwater to various substrates whereupon electrostatic complexation, phase inversion, and rapid setting were simultaneously actuated by water–DMSO solvent exchange [76].

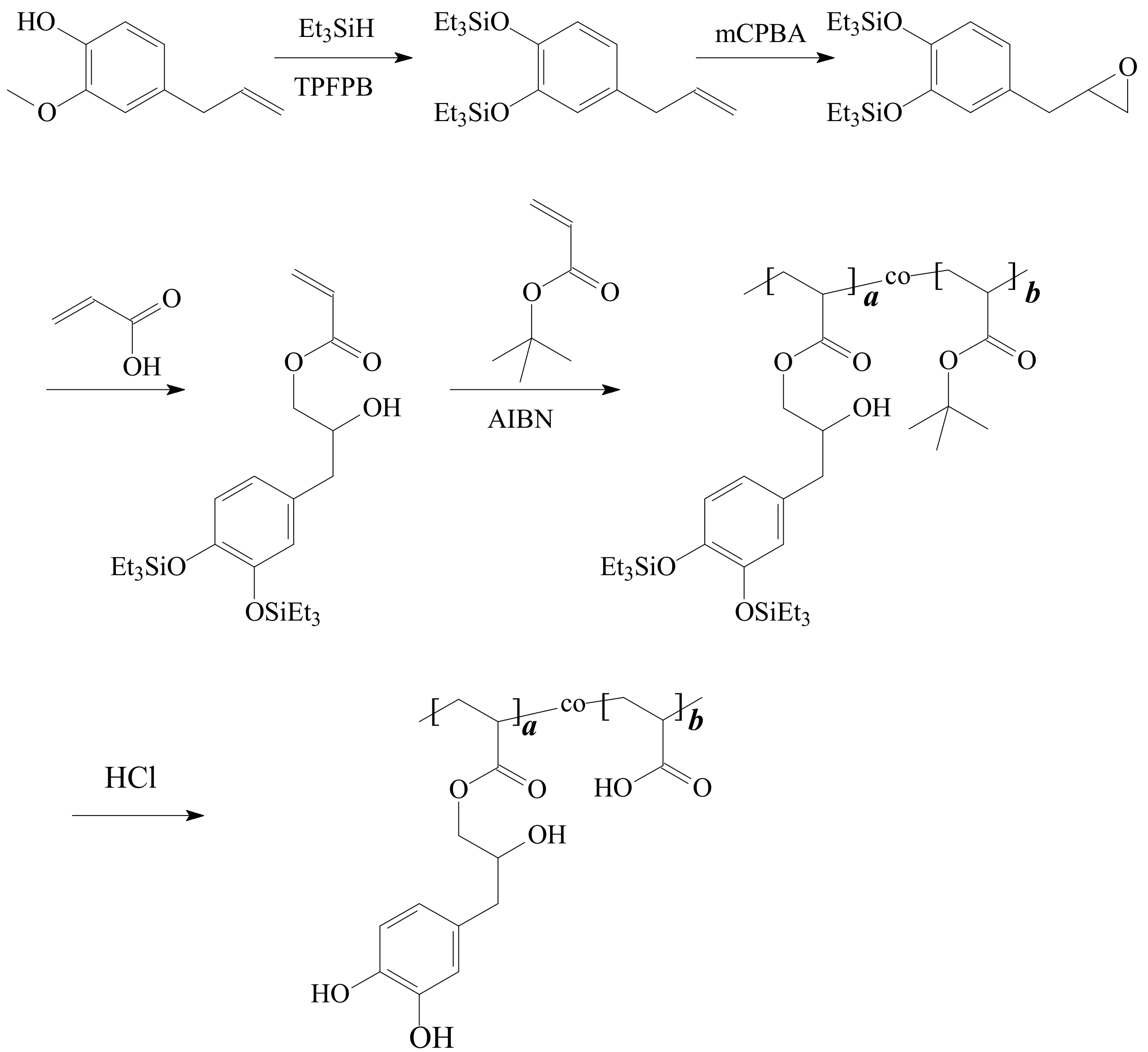

Figure 2.19 Synthesis of a catechol-functionalized weak polyanion

In a recent review, the unique features and the key functionalities of Mussel foot proteins (Mfps), catechol chemistry, and strategies for preparing catechol-functionalized polymers have been reviewed [77]. Recent findings on the contributions of various features of Mfps on the interfacial binding, which include coacervate formation, surface drying properties, control of the oxidation state of catechol, among other features have been highlighted. The applications of catechol-functionalized materials for the use as biomedical adhesives, therapeutic applications, and antifouling coatings have been discussed.

In a recent study, copolyampholytes, which combine the catechol functionality with amphiphilic and ionic features of mussel foot protein 3 slow (mfp-3s), were synthesized and formulated as coacervates for adhesive deposition on surfaces Figure 2.20 [78]. The ratio of hydrophilic/hydrophobic, as well as cationic/anionic units, was varied in order to enhance the coacervate formation and wet adhesion properties. The mfp-3s-mimetic copolymer was stable to oxidation, formed coacervates that spread evenly over mica, and strongly bonded to mica surfaces.

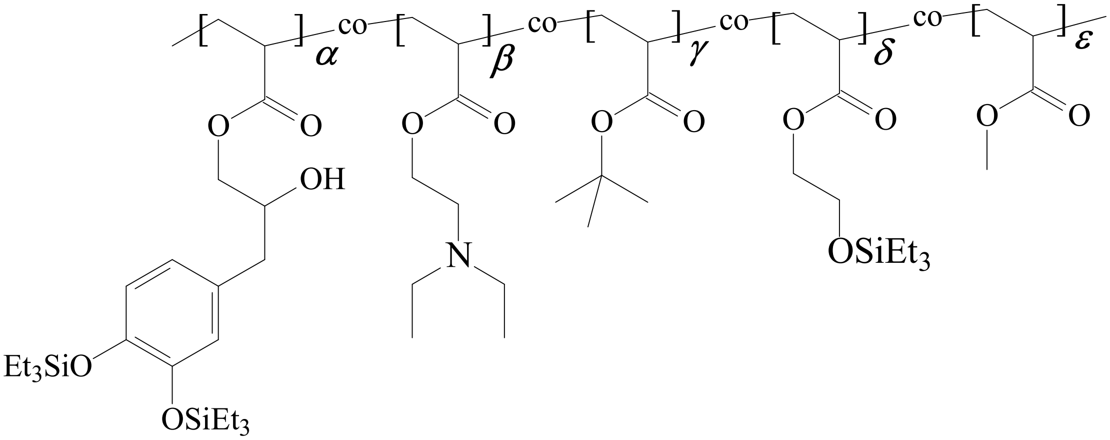

Figure 2.20 Synthesis of a copolyampholytes, which combine the catechol functionality with amphiphilic and ionic features of mussel foot protein 3 slow

Structure of complex coacervate core micelles in an aqueous solution formed by oppositely charged polyelectrolytes based on poly(ethylene oxide-b-allyl glycidyl ether) diblock copolymer was investigated using dynamic light scattering (DLS) and small-angle neutron scattering (SANS) Figure 2.21 [79].

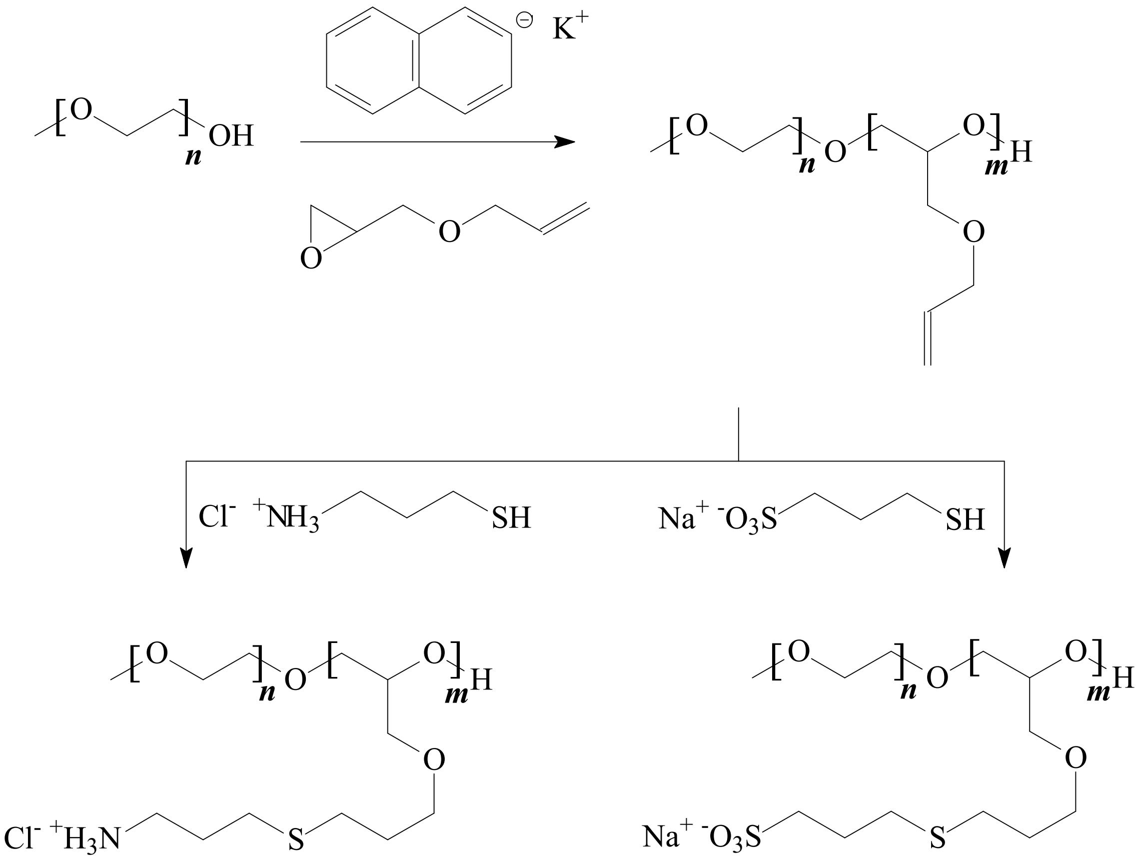

Figure 2.21 Synthesis polyelectrolytes based on poly(ethylene oxide-b-allyl glycidyl ether)

Recently, an anchored triblock copolymers that adopt loop conformations on surfaces and endow them with unprecedented lubricating and antifouling properties have been synthesized Figure 2.22 [80]. The triblocks have two end blocks with catechol-anchoring groups and a looping poly(ethylene oxide) (PEO) midblock.

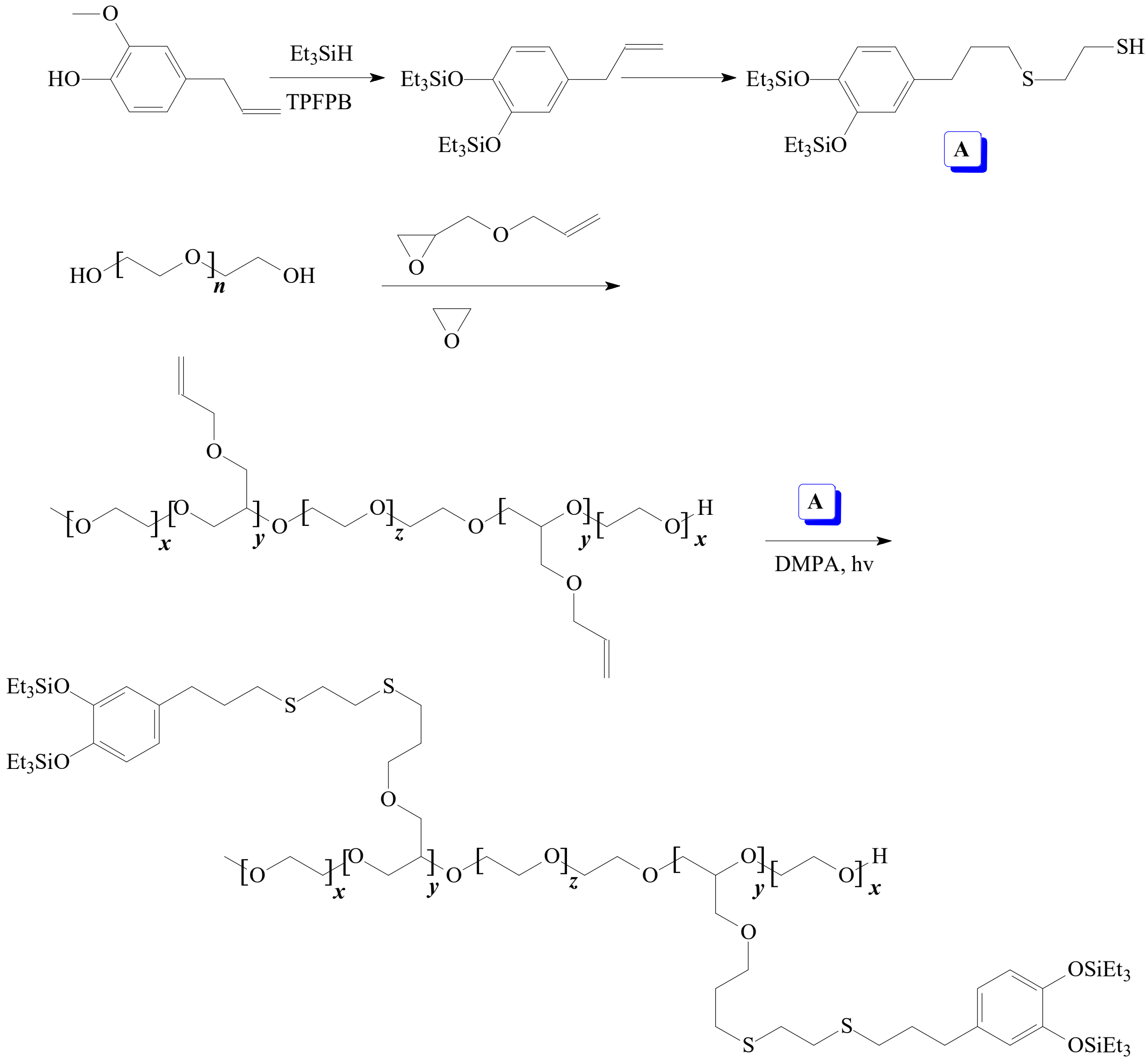

Figure 2.22 Synthetic strategy of catechol functionalized polyethylene glycol

Mussels have a remarkable ability to bond to solid surfaces under water. From a microscopic perspective, the first step of this process is the adsorption of dopa molecules to the solid surface. The nature of the competitive absorption by atomic-scale modeling of water and catechol adsorbed at the silica surface has been investigated using density functional theory calculations. It is found that catechol molecules displace preadsorbed water molecules and bond directly on the silica surface [81].

The synthesis of photocurable, ternary polymer networks prepared by incorporating dopamine acrylamide (DAm) into a cross-linked thiol–ene network based on pentaerythritol triallyl ether (APE) and pentaerythritol tetra(3-mercaptopropionate) (PETMP) has been reported Figure 2.23 [82]. The effect of DAm, in the nonoxidized catechol form, on photopolymerization kinetics and thermal, thermomechanical, and mechanical properties of the modified thiol–ene networks has been evaluated. The polymer demonstrated improved macroscopic adhesion of DAm–APE–PETMP coatings to a range of substrates.

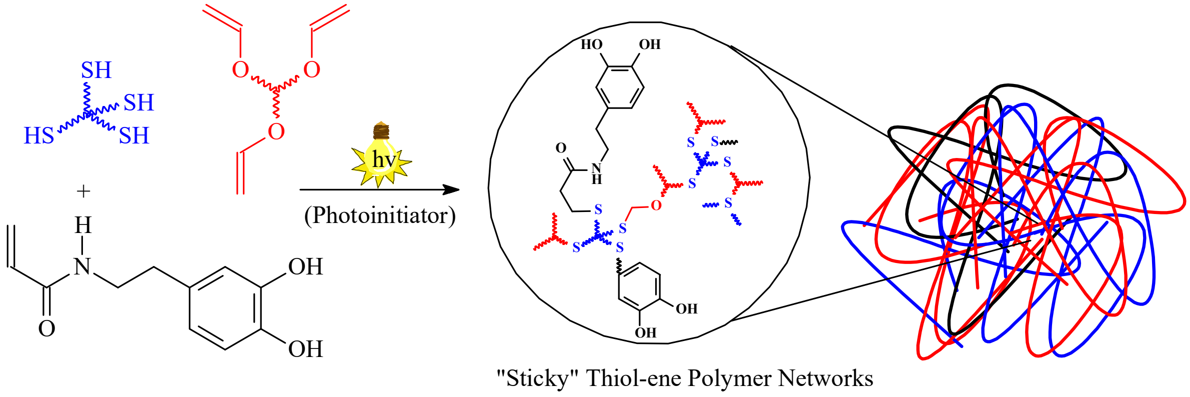

Figure 2.23 Synthetic strategy of catechol functionalized sticky thiol-ene networks

Sandcastle worms secrete a water-resistant proteinaceous glue that is used to bind mineral particulates into their protective tubing. the constitutive proteins of the glue are oppositely charged co-polypeptides that form a complex coacervate precursor phase, which is critical for stable underwater delivery of the adhesive. A synthesis strategy enabled the incorporation of non-standard phosphoserine (pSer) and 3,4-Dihydroxyphenylalanine (Dopa) amino acids in the co-polypeptides, thereby duplicating chemical functionalities of the native glue that are key for electrostatic complexation and adhesion Figure 2.24 [83].

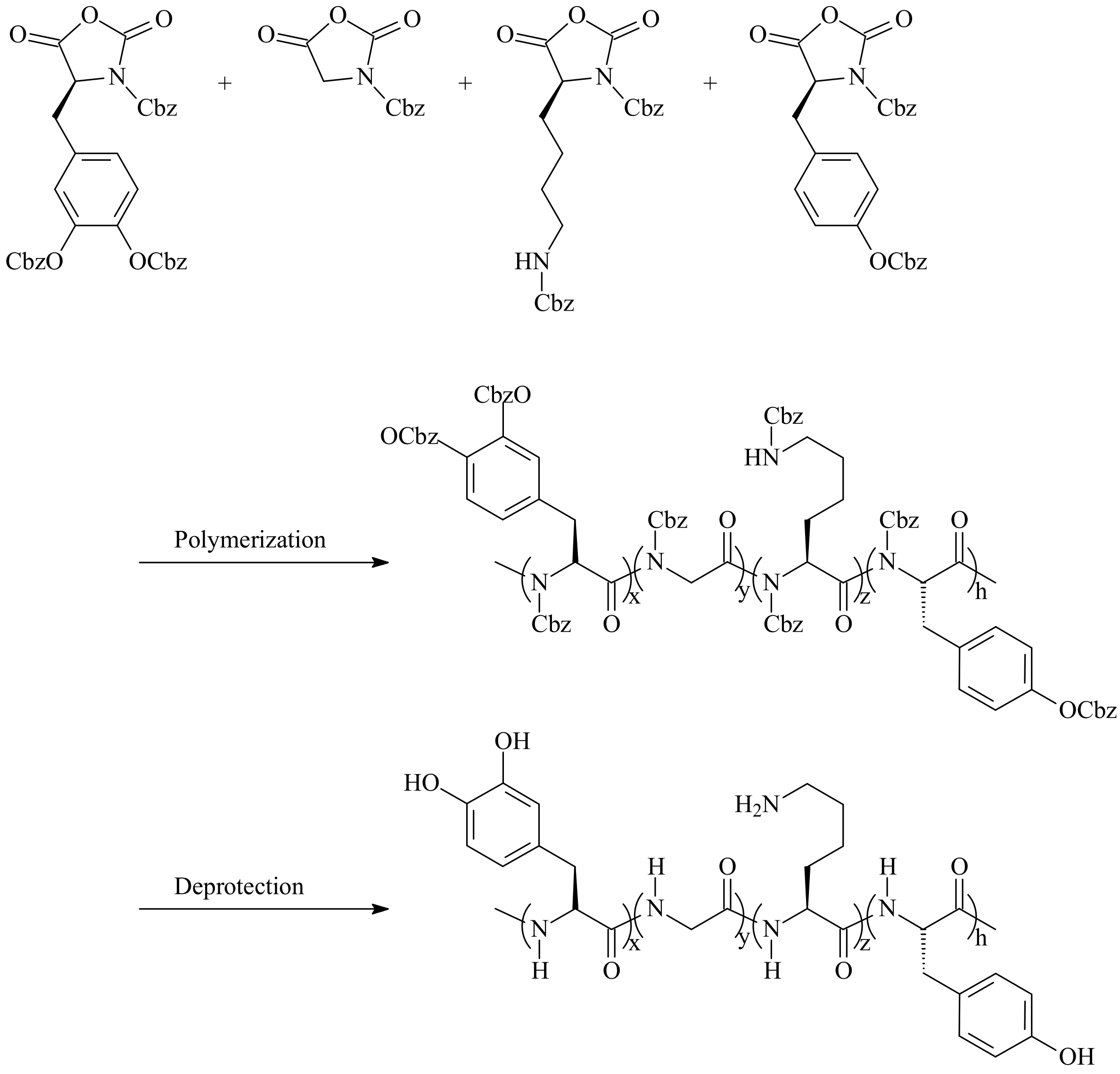

Figure 2.24 Synthetic route of the positively charged polypeptide

Amino acid-based poly(ester urea) (PEU) copolymers functionalized with pendant catechol groups that address the need for strongly adhesive yet degradable biomaterials have been developed Figure 2.25 [84]. The adhesive strength on porcine skin adherends was found to be comparable with commercial fibrin glue.

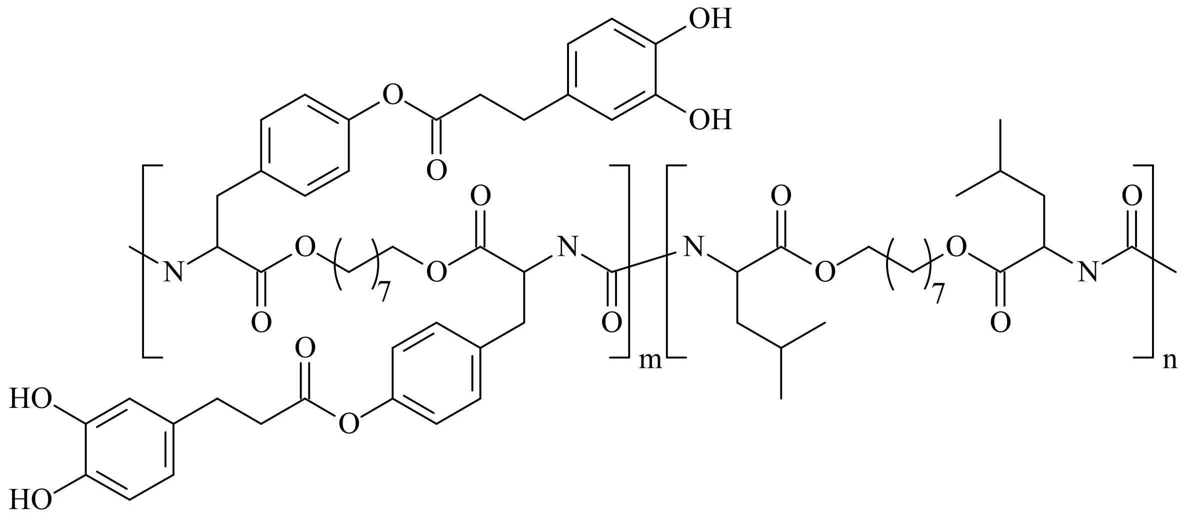

Figure 2.25 Synthetic of Amino acid-based poly(ester urea) (PEU) copolymers functionalized with pendant catechol groups

Inspired by mussels and sandcastle worms, a water-soluble adhesive is prepared by grafting catechol and phosphoric acid functionalities to the polyoxetane backbone, which achieves improved adhesion in a humid environment Figure 2.26 [85].

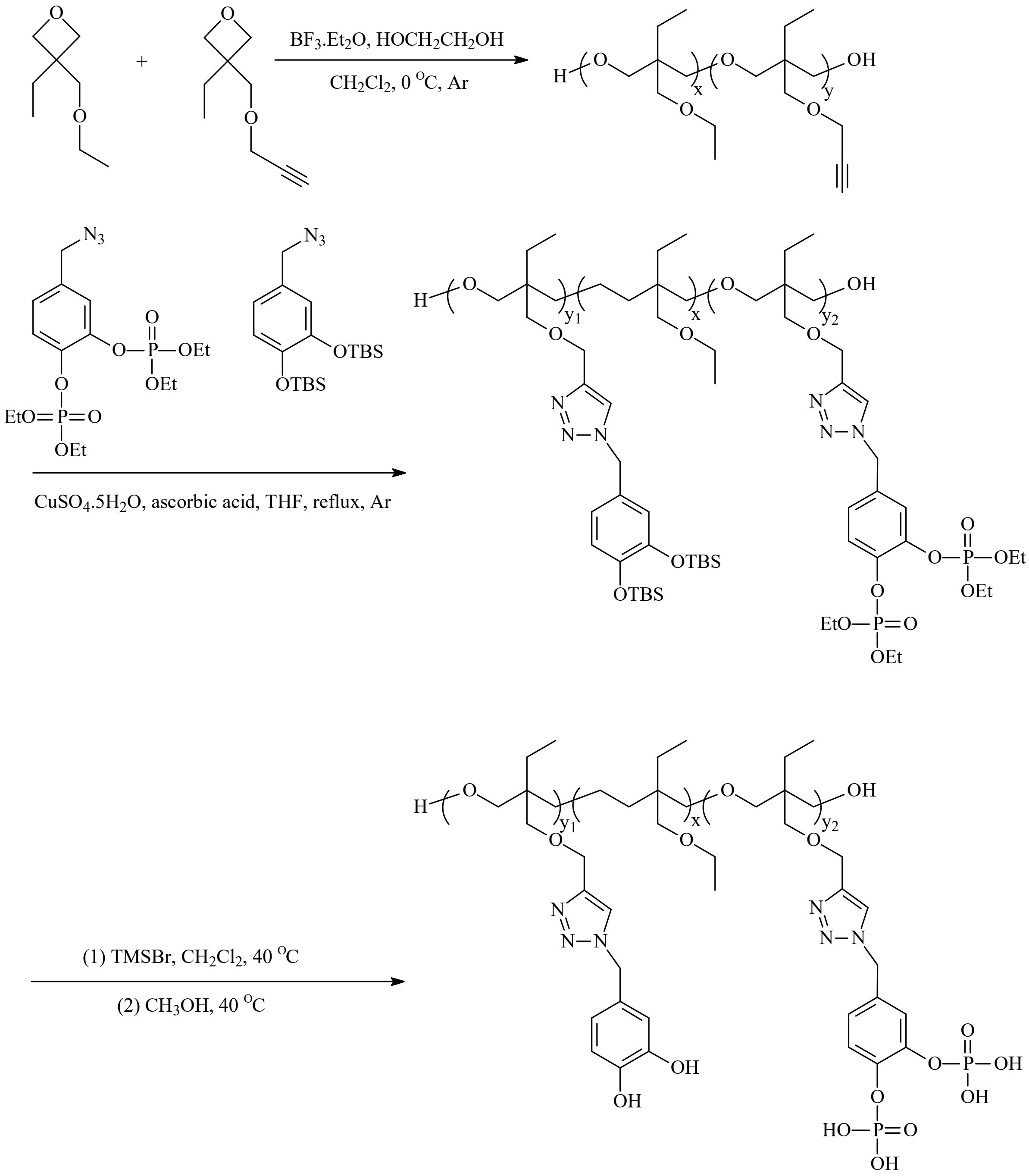

Figure 2.26 Synthetic of polyethylene glycol with pendant catechol groups

2.5 Approach

To achieve the overall and specific objectives, the proposed dissertation will be divided into the following tasks:

2.5.1 Synthesis of Bio-inspired Copolyelectrolytes:

This will be one of the major tasks of the proposed dissertation. It is planned to synthesize precisely tailored polymers with position-defined anionic, cationic and catecholic functionalities, e.g. catechol-terminated dendrimers and block polyelectrolytes with variable catechol mole% and co-monomer sequence length, polarity, and distribution. The proposed synthetic approach will be modular in nature and includes tailoring of the flexibility and amphiphilicity of the polymer backbone, control of the architecture of the polymer chain with regard to comonomer sequence (random, segmented, block), spacer and end group effects. The optimal balance between ionic interactions/coacervation versus the critical number of acid-base interactions needed for bio-adhesion will be explored by the synthesis and analysis of model copolyelectrolytes of variable mole fraction of acid and/or base units.

2.5.2 Characterization of Copolymer Systems

The synthesized block copolymer will be subjected to a range of characterization tools (i.e. NMR and GPC) and property tests in order to determine their nanostructure, rheological and mechanical performance. It is anticipated that detailed characterization will provide valuable information about the fundamental chemical/physical insights into the mechanisms and molecular processes involved in wet bioadhesion and biofouling.

2.6 Research Methodology

The proposed dissertation is aimed at the development of a complete, molecular-based understanding of the hierarchical nature of wet adhesion process (by mussels) – initial coacervation followed by chemical crosslinking - and its translation to synthetic systems for use in various applications.

The description of the proposed dissertation is detailed in the following sections. Included are procedures and techniques to be used with an explanation why these are considered the most suitable to the research in question; detailed description of the experiments and measurements; as well as methods to be used in data collection, analysis, and interpretation.

The research activities of this proposal will develop molecular insights and design principles to exploit initial, primary coacervation assembly of well-defined ionic polymer pairs followed by covalent crosslinking (initially utilizing DOPA or catechol groups) in the design of new materials. Outcomes will include the synthesis of precisely tailored polymers with position-defined anionic, cationic and catecholic functionalities, *e.g.* catechol-terminated copolyelectrolytes with variable catechol mol% and co-monomer sequence length, polarity, and distribution. A proposed new strategy for the incorporation of a catechol building block into the backbone of poly(ethylene glycol) is shown in Figure 2.27 and demonstrates the wide variety of structures that are proposed – all starting from readily available starting materials – eugenol (clove oil) in this case.

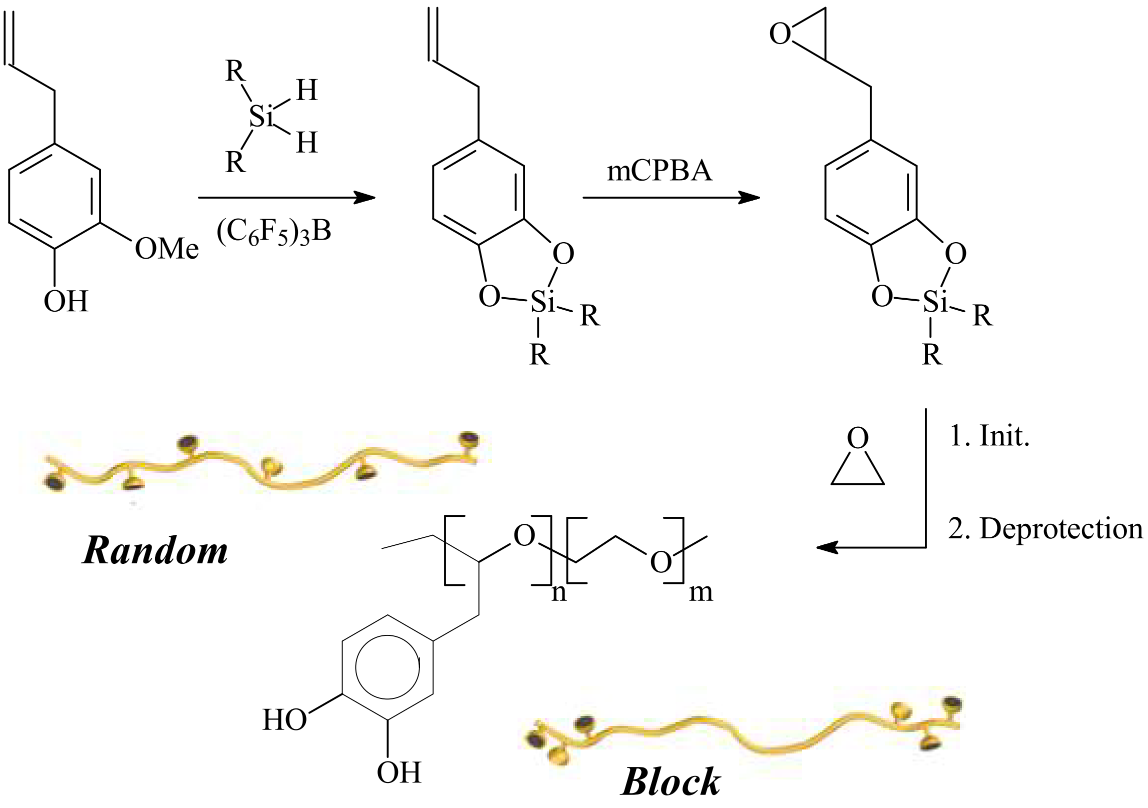

Figure 2.27 Synthesis of catechol functionalized poly(ethylene glycol) based random/block copolymers from eugenol

It should be noted that the catechol unit is specifically chosen based on analysis of the proteins used by marine organisms as it affords both adhesion to a variety of surfaces through the ortho-phenolic groups as well as potential crosslinking through oxidative addition chemistry. It is proposed that the utilization of these groups in a similar fashion to how they are used in natural systems – i.e. *mussel* adhesion – will lead to outstanding properties such as improved adhesion and/or tough, non-fouling coatings. From these initial studies, we will translate these fundamental structure-property relationships into the design of broad material platforms with the final result being the evaluation of these systems as novel nanostructured hydrogels, high-performance adhesives for aqueous applications, and unique coating systems.

Mussel-inspired polymer design must include optimization of both the Dopa-based catechol moiety and anionic/cationic groups (coacervate formation) - both key elements of the bio-adhesive systems. The proposed synthetic approach will be modular in nature and includes tailoring of the flexibility and amphiphilicity of the polymer backbone, control of the architecture of the polymer chain with regard to comonomer sequence (random, segmented, block), spacer and end group effects. The optimal balance between ionic interactions/coacervation versus the critical number of acid-base interactions needed for bio-adhesion will be explored by the synthesis and analysis of model copolyelectrolytes of variable mole fraction of acid and/or base units. The performance of these synthetic materials will then be studied theoretically. In view of the superstructure and/or network formation, position-specific incorporation of functionalities capable of ionic and/or hydrogen bond formation, as well as polarity-based interactions is envisaged. The choice of comonomers with regard to steric requirements, polarity, and H-bond forming potential, as well as type of ionic groups and their mole ratio, will be examined in detail.

A key requirement in this area will be the development of Dopa-mimetic monomeric units based on catechol derivatives. Preliminary work has shown that safrole (5-allylbenzo[d][1,3]dioxole) and eugenol (4-allyl-2-methoxyphenol) are an inexpensive and readily available natural product for the synthesis of a wide variety of catechol-based building blocks through orthogonal reactivity of the terminal alkene group and catechol moiety. As an illustrative example, the reaction of eugenol with a series of different disubstituted silanes in the presence of tris(pentafluorophenyl)borane followed by epoxidation of the terminal double bond gives the silyl-protected epoxy monomer, in near-quantitative yield over both steps. Either block or random copolymerization with ethylene oxide and subsequent deprotection then gives the desired catechol functionalized synthetic polymers in which the distribution of the reactive catechol units along the backbone can be accurately controlled Figure 2.27. Similarly, preliminary work has shown that a wide variety of anionic (carboxylate, sulfonate) and cationic (amino, guanidinium) groups can be introduced into well-defined polymeric structures through thiol-ene and thiol-yne chemistry without the need for protection/deprotection strategies. Initial studies of coacervate gels by Hawker revealed that the simple mixing of guanidinium and sulfonate functional triblockcopolyelectrolytes form strong hydrogel coatings. Gelation, which results from the nano-phase separation between charged (coacervate) and neutral domains, occurs rapidly upon mixing. It is thus necessary to mix the components only at the moment of application. Further experimentation may reveal that gelation of the polyelectrolytes occurs too rapidly to allow for an efficient coating process and needs to be delayed. This delayed-onset gelation could be achieved by protecting the ionic groups in one of the polyelectrolyte components and loading the deprotection trigger in solution with the other component. Both the sulfonate groups and the guanidinium groups can be protected using well-established chemical modifications. Protection of the amines in the guanadinium generally results in relatively stable compounds that require harsh deprotection conditions, e.g. aqueous solutions of very low pH (pH<1) or very high pH (pH>12) [86]. However, sulfonates can be protected through the formation of sulfonic esters which are known to be hydrolytically unstable. In addition, the stability can be tailored by the choice of alcohol used to form the sulfonic ester. Synthetically, sulfonic acids can be converted to sulfonic esters using a wide variety of transformations. Either by converting the sulfonic acid to an acid chloride, followed by reaction with an alcohol, or by direct reaction using any of a wide variety of different reagents, some of which are shown in Figure 2.28b. Thus, a multi-component coating formulation with delayed gelation could be formulated wherein one component contains a solution of sulfonic ester-functionalized triblock copolymers. The other component, a solution of guanadinium functionalized triblock copolymer, could be stored in a weakly acidic solution. Upon mixing – exposing the protected sulfonate groups to the weakly acidic guanadinium-component solution – triggered deprotection should occur, revealing to the sulfonate group and leading to onset of gel formation albeit delayed relative to the unprotected guanadinium/sulfonate system. Alternatively, a one-pot system could be developed based on an external trigger such as heat or light. In this case, a solution of guanidinium functionalized triblock copolymer is mixed with the protected sulfonatetriblock copolymer to give a room temperature stable solution. This stable mixture can then be spin-coated or spray coated to give a thin film and on heating the sulfonate esters undergo deprotection to generate in-situ the desired anionic sulfonate groups leading to coacervate formation. Again, the wide range of sulfonate groups known in the literature with different thermal profiles allows a wide range of annealing conditions to be examined. Alternatively, a small molecule photoacid generator can be incorporated into the mixture which would allow a strong acid to be generated by exposure to light, again by correct choice of the sulfonatester,deprotection can occur leading to in-situ coacervate formation. One attractive feature of the final photochemical strategy is that spatial and temporal control of the light source allows for patterning of the thin film/coating.

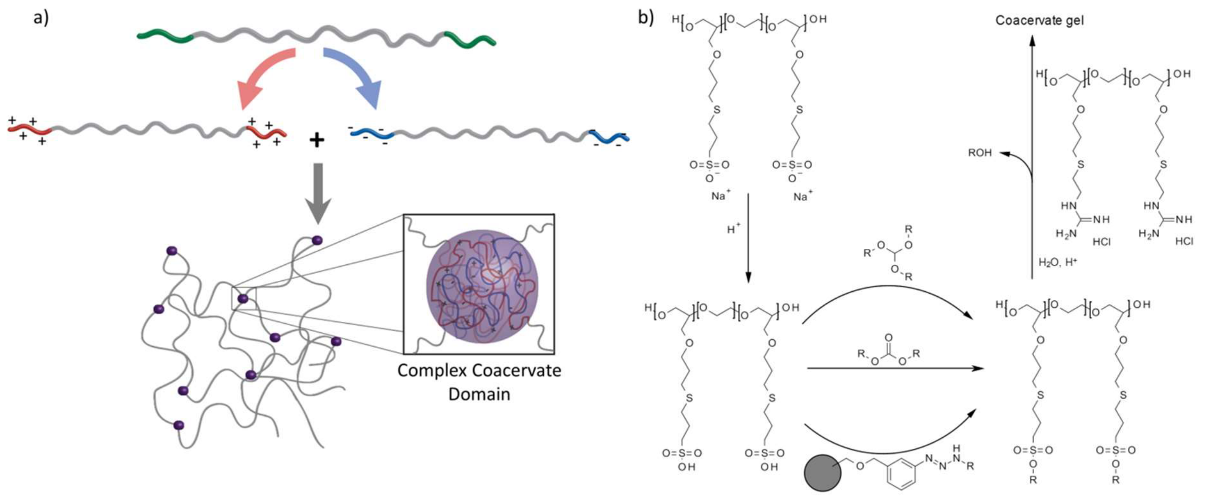

Figure 2.28 a) General macromolecular design for coacervate-driven hydrogel formation. b) Three possible reaction pathways for the synthesis of a sulfonic ester from a sulfonic acid followed by deprotection mixing with guanidinium functional polymer in acidic aqueous solution: reaction with a trialkylorthoformate [87] (top), reaction with an alkyl carbonate [88] (middle), and reaction with a resin bound triazene [89] (bottom)

As mentioned above, the individual anionic and cationic coacervate components should be stored separately before application to avoid premature gelation or deprotection. The natural marine organisms – *mussels* – solve this problem by storing the anionic and cationic peptides in separate body cavities, only mixing them in a special organ right before application. We propose to investigate a close mimic of this strategy through synthesis cationic and anionic polymer with catechol moieties which have a potential application as coacervate components.

CHAPTER 3

COPOLYMERIZATION OF SAFROLE OXIDE AND ALLYL GLYCIDYL ETHER AND ELABORATION OF PENDANT ALKENE USING THIOL-ENE REACTION

3.1 Abstract

Safrole oxide **2**, obtained by epoxydization of naturally occurring safrole **1**, has been polymerized for the first time using Lewis acid initiator/catalyst comprising of triphenylmethylphosphonium bromide as initiator and triisobutylaluminum as catalyst to obtain polyether **6** in excellent yields. Epoxy monomer **2** and allyl glycidyl ether **7** in various proportions have been randomly copolymerized to obtain random copolymer **16**. The deprotection of methylene acetal of **16** has been successfully achieved to obtain **17**.

The pendant allyl groups in **17** have been elaborated via thiol-ene reaction using cysteamine hydrochloride and thiglycollic acid to obtain polymers **18** and **19** containing *Mussel*-inspired Dopa-based catechol moiety and anionic/cationic groups required for the formation of coacervate. The cationic **18** and anionic **19** are also obtained via an alternate route using epoxide **14** of 3,4-ditert-butyldimethylsilyloxyallylbenzene **13**. Monomer **14** was homo- as well as copolymerized with **7** using Lewis acid initiator/catalyst system to

obtain homopolymer **15** and copolymer **20**. Coplymer **20** was then elaborated using thiol-ene reaction followed by F^- catalysed silyl deprotection to obtain Mussel inspired polymers **18** and **19**.

3.2 Introduction

Performance of synthetic adhesive polymers in aquatic environment is most often frustrating because of various adverse effects of water or moisture in inducing hydrolysis of polymers, swelling, interfacial wicking, etc. [90], [91]. Rapid, strong and tough moisture-resistant adhesion to solid surfaces in the sea by the holdfast of marine mussels have lured many a researcher to mimick the essential features of the adhesive chemistry practiced by the mussels roughly 25–30 different adhesive proteins of varying molar masses proteins used by the mussels contained a considerable proportion of randomly placed 3,4-dihydroxyphenyl-L-alanine (L-DOPA)(≈1 -28 mol%) and 4-hydroxyarginine resulting from a posttranslational modification of amino acid tyrosineand arginine, respectively [90]. To be an effective adhesive, it must exert more favourable interaction with the wet polar surfaces than a layer of water is able to offer. Formation of covalent bonds into the interfaces may mitigate the deleterious effects of moisture, but it is a costly process [92]. As such the situation demanded a closer look at the way mussels adhesive chemistry works. The byssus, a bundle of filaments of Dopa decorated proteins secreted by mussels that function to attach the mussels to a solid surface whereby the catecholic functionalities provide bidentate or covalent interfacial interactions. The proteins themselves gain cohesiveness through metal chelation, and covalent coupling.

Hydrogen bonding by phenolic hydroxyls of bidentate DOPA leads to its bridging adhesion to the polysiloxane surface of mica [93]. The mussel adhesives may also be dispensed as complex coacervates[94]–[96]. Complex coacervation, a process in which aqueous solutions of polyanions (e.g.Dopa-containing proteins having phophoserine residues) and polycations (e.g.Dopa-containing proteins having 4-hydroxyarginine residues) with charge symmetry undergo phase separation, has considerable potential for wet adhesion.

The cohesive and adhesive roles played by the catechol functionality of Dopa in byssal proteins and their exceptional adhesive performance in wet and turbulent environments have now been firmly established. As such the mussel byssal proteins have attractive targets for biomimetic efforts. The earliest examples of synthesis of mussel mimetic polymers include Dopapolypeptides [97]–[99] and Dopa and lysine polypeptide copolymers [100]–[102]. Synthesis of mussel mimetic polymers have been achieved through polymerization of catechol-based monomers [103]–[106].

Polymerization of Dopamine methacrylamide (DMAm) with 2-methoxyethyl acrylate (MEA) or poly(ethylene glycol) methyl ether methacrylate (mPEG-MA) gave adhesive polymers having divergent physical properties [107]. Homo- and copolymers of catecholic monomer 3,4-dihydroxystyrene with styrene or styrene sulfonate have been reported to polymers having a wide range of physical properties [105]–[109]. A complex coacervates adhesive has been formed from a mixture of catechol containing synthetic polyanion and a synthetic polycation [94], [110]. Coating of PEG containing Dopa as an anchor has been demonstrated to be effective at preventing bacterial adhesion and biofilm formation on a titanium and a variety of other surfaces [111], [112].

One of the serious drawbacks of mussel proteins is the oxidation of Dopa at or above neutral pH to Dopaquinone which is significantly less sticky than Dopa on many surfaces. While the mussels have the talents [113], [114] to control the deleterious oxidation, it remains a challenge to the researchers to safeguard the integrity of the catecholic functionality in Dopa for facile bidentate surface binding. Even in the more adverse pH of 8.2 of seawater, the mussels secret their proteins at a low pH of 5-6 in the confined space of a reducing environment where the redox balance is provided by the thiol functionalities of a cysteine-rich protein.

Herein, we report the use of readily available naturally occurring safrole or eugenol to synthesize epoxy functionalized monomers and their ring opening homo- and copolymerization with allyl glycidyl ether. The allyl pendants of the mussel mimicking polymers decorated with catechol functionalities would offer the latitude of transformation to ionic polymer backbones of both algebraic signs. The work would thus pave the way to study this polymer from the perspective of coacervate adhesive.

3.3 Experimental

3.3.1 Materials

m-Chloroperbenzoic acid (MCPBA), LiCl, tert-butylammonium fluoride (TBAF.3H_2O), tert-butylammonium hydroxide (TBAH), 4-dimethylaminopyridine (DMAP), $^{i}Bu_3Al$ solution (25% in Toluene), eugenol, 2-butanone, Allyl alcohol, 2,2-dimethoxy-2-

phenylacetophenone (DMPA), tert-butyldimethylsilyl chloride (TBDMSCl), cysteamine-HCl, thioglycolic acid and safrole purchased from Aldrich Chemical, $MePPh_3Br$, imidazole and CaH_2 purchased from Fluka. 1 M tert-butylammonium fluoride (TBAF) solution in THF purchased from ChemCruz, and diphenylsilane and $B(C_6F_5)_3$ purchased from Alfa Aesar were used as received. 4-Allylcatechol was prepared by reacting eugenol with LiCl in dimethyl formamide (DMF) as described [115]. Allyl glycidyl ether **7** from Aldrich was dried over CaH_2 and distilled. All solvents were of reagent grade. Lead tetra acetate $Pb(AcO)_4$ was freshly prepared as described [116]. For dialysis, membrane (Spectra/Por) with a MWCO of 6000-8000 was purchase from Spectrum Laboratories, Inc.

3.3.2 Physical Methods

A Perkin Elmer (Series II Model 2400) Elemental Analyzer and a Fourier transform infrared (FTIR) spectrometer (Perkin Elmer 16F PC) were utilized for elemental analyses and IR spectroscopy, respectively. The nuclear magnetic resonance (NMR) spectra were recorded using a 500-MHz JEOL LA spectrometer. Tetramethylsilane (TMS) in $CDCl_3$ and residual H in D_2O at δ4.65 ppm were used as internal standards. The ^{13}C chemical shifts in D_2O were referenced against ^{13}C peak of external standard dioxane at δ 67.4 ppm. The TGA was carried out under O_2 by using a SDT analyser (Q600: TA Instruments).

3.3.3 Synthesis of safrole oxide (2) from safrole (1)

Safrole was converted to safrole oxide using a modified procedure [117], [118]. To a solution of m-chloroperbenzoic acid (54 g, 0.22 mol, 70%) dissolved in 400 ml chloroform was added safrole **1** (32.4 g, 0.20) and stirred at room temperature for 24 h. After adding additional portions of m-chloroperbenzoic acid (20 g, 0.082 mol), the reaction mixture was stirred at room temperature for a total of 48 h. The reaction mixture was washed with aqueous 10% sodium hydroxide solution (3×100 mL), then washed with water (2×30 mL). The chloroform layer was dried over anhydrous magnesium sulfate, filtered and concentrated. The residual liquid was purified by silica gel chromatography using hexane/ether as eluent to give safrole oxide (**2**) as a colorless oil (25.3 g, 59%). The oil was then distilled over calcium hydride to exclude any moisture. b.p. $_{0.8\ \mathrm{mbarHg}}$ 92°C. δ_H ($CDCl_3$): 2.52 (1H, m), 2.83 -3.73 (3H, m), 3.10 (1H, m), 5.91 (2H, s), 6.69 (1H, d, *J* 7.6 Hz), 6.74 (1H, s), 6.75 (1H, d, *J* 7.9 Hz); δ_C ($CDCl_3$): 28.39, 46.77, 52.53, 100.87, 108.26, 109.43, 121.85, 130.79, 146.28, 147.66 ($CDCl_3$ middle carbon: 77.00).

3.3.4 Base catalyzed polymerization of safrole oxide (2) (Table 3.1) and (Scheme 3.1)

3.3.4.1 Polymerization using TBAF catalyst

Bu_4NF (0.1 mol) was added as $Bu_4NF.3H_2O$ or as 1 M solution in THF to a solution of safrole oxide **(2)** (1 mmol) in Toluene (2.0 mL). The solvent was carefully removed under vacuum to remove moisture. The reaction mixture was heated at 70 °C for 24 h. After that methanol/water was added and then the polymer **5** was extracted with ether. The ether layer dried over anhydrous sodium sulfate and concentrated.

3.3.4.2 Polymerization using TBAH catalyst

Safrole oxide **2** (237 mg, 1.33 mmol), TBAH 40% in water (28 mg, 0.0432 mmol) and toluene (2×3.0 mL) were mixed and allowed the solvent to evaporate under N_2 so as to remove water. The mixture was heated at 70 °C for 15 h. Methanol/water was added and then polymer **5** was extracted with ether. The ether layer dried over anhydrous sodium sulfate and the solvent was removed under N_2.

3.3.5 Polymerization of safrole oxide (2) using $^{i}Bu_3Al$ as Lewis acid catalyst [118], [119] (Table 3.2) and (Scheme 3.2)

As described in entry 13 (Table 3.2), methyltriphenylphosphonium bromide was put in a round bottom flask and closed with rubber septum, safrole oxide (**2**) (445 mg, 2.5 mmol) and anhydrous toluene were added by syringe under Ar. The mixture was allowed to cool to 0 ºC, then 1 M triisobutylaluminium solution (25 wt. % in toluene) was added by syringe under Ar in one portion. The polymerization was stopped after specified time by adding 4:1 (v/v) MeOH/H_2O, and the solvent was removed by rotary evaporator. Then the residue was dissolved in CH_2Cl_2 and filtered over celite 545. The filtrate was dried (Na_2SO_4) and evaporated under vacuum to obtained polymer **6** (Scheme 3.2).

For purification, polymer **6** was dissolved in dichloromethane then methanol was added to precipitate the polymer which was separated by centrifuge. This process was repeated three times to get rid of initiator and unreacted monomer. $\nu_{max.}$ (KBr): 3444, 3066, 2899, 2772, 1608, 1475, 1435, 1248, 1090, 1026, 742, and 693 cm^{-1}.

3.3.6 Polymerization of allylglycidyl ether (7) (Scheme 3.2). [63], [120]

Allyl glycidyl ether (**7**) (296 mg, 2.60 mmol) and methyltriphenylphosphonium bromide (8.2 mg, 0.023 mmol) were dissolved in toluene (1.6 mL) under Ar. Triisobutylaluminium (0.24 mL, 0.26 mmol of 25 wt. % in toluene) was added to the mixture at 0 °C by a syringe under Ar in one portion. The polymerization was stopped after 2 h by adding 4:1 (v/v) MeOH/H_2O (10 mL), and the solvent was then removed by rotary evaporator. Then the residue was dissolved in CH_2Cl_2 and filtered over celite 545. The filtrate was dried (Na_2SO_4) and evaporated under vacuum to obtain polymer **8**.

3.3.7 Deprotection of methylene acetal of safrole (1) as a model case [121], [122] (Scheme 3.2).

A solution of safrole (**1**) (1.05 g, 6.48 mmol) and benzene (35 mL) were mixed and heated to 75 ºC with condenser attached to oil trap. Then, $Pb(OAc)_4$ (4.23 g, 9.5 mmol) was added under N_2. The reaction mixture was stirred at 75 ºC for 3 h. The reaction mixture was diluted with EtOAc (30 mL) and washed with H_2O (3×25 mL). The EtOAc layer was dried over anhydrous sodium sulfate, filtered and concentrated. The residual liquid was purified by silica gel chromatography using 1:2 EtOAc/Hexane as eluent to give **9** as a faint yellow oil (1.08 g, 82%).

δ_H ($CDCl_3$): 2.09 (3H, s), 3.34 (2H, d, *J* 6.7 Hz), 5.05-5.09 (2H, m), 5.89-5.96 (1H, m), 6.77 (1H, dd, *J* 7.9 Hz, *J* 1.6 Hz), 6.83 (1H, d, *J* 1.6 Hz), 6.88 (1H, d, *J* 7.9 Hz), 7.66 (1H, s); δC ($CDCl_3$): 20.92, 39.80, 108.85, 109.64, 112.64, 115.92, 122.30, 134.88, 134.92, 137.16, 143.05, 144.83, 168.99, ($CDCl_3$ middle carbon: 77.00). ν_{max}. (KBr): 3079, 3005, 2979, 2914, 1838, 1768, 1639, 1495, 1445, 1376, 1255, 1216, 1181, 1100, 1009, 963, and 760 cm^{-1}.

3.3.8 Attempted synthesis of diphenylsilyl protected 4-allylcatechol (11) [67]

Eugenol (871 mg, 5.3 mmol), diphenylsilane (1.11 g, 6.0 mmol, 1.1 equiv) and 5 mL of dichloromethane were added to a 50 mL round bottomed flask with condenser under nitrogen. Tris(pentafluorophenyl)borane (5.6 mg, 0.01 mmol) was added as a catalyst into the reaction mixture. The reaction mixture was stirred at room temperature, a fast and exothermic reaction ensued with evolution of gas. The reaction mixture was passed through silica gel chromatography using hexane/ether as eluent to obtain pure compound, but the product was unstable during purification to give 4-allylcatechol (**12**) (77%): δ_H ($CDCl_3$): 3.27 (2H, d, *J* 6.7 Hz), 5.03 - 5.07 (2H, m), 5.88 – 5.96 (1H, m), 6.62 (1H, dd, *J* 2.2 Hz, *J* 7.9 Hz), 6.71 (1H, d, *J* 2.2 Hz), 6.79 (1H, d, *J* 7.9 Hz); δ_C ($CDCl_3$): 39.51, 115.37, 115.59, 115.72, 121.02, 133.25, 137.64, 141.70, 143.48 ($CDCl_3$ middle carbon: 77.04), $\nu_{max.}$ (KBr): 3422, 3078, 3005, 2978, 2904, 1697, 1639, 1605, 1520, 1444, 1413, 1356, 1281, 1192, 1147, 1112, 995, 964, 916, 814, and 789 cm^{-1}.

3.3.9 ((4-allyl-1,2-phenylene)bis(oxy))bis(tert-butyldimethylsilane) (13) [123]

A mixture of allylcatechol (**12**) (10.86 g, 72.4 mmol), DMF (130 mL), imidazole (23.6 g, 347 mmol), TBSCl (25.0 g, 166 mmol), and DMAP (2.11 g, 17 mmol) were added at 0 ºC under N_2. The reaction mixture was allowed to warm to room temperature and stirred for 16 h. The reaction mixture was taken up in water (300 mL) and extracted with of ether (2×100 mL). Then the ether layer was washed with water (4×200 mL) and dried (Na_2SO_4). The residue obtained could be used to the next step without further purification or distilled (b.p. $_{0.2\ mbarHg}$122ºC) to obtain **13** as a colorless oil (20.5 g, 75%). δ_H ($CDCl_3$): 0.17 (12H, s), 0.97 (18H, s), 3.24 (2H, d, *J* 6.7 Hz), 4.99–5.03 (2H, m), 4.99–5.03 (1H, m), 6.59 (1H, dd, *J* 1.8 Hz, *J* 8.3 Hz), 6.64 (1H, d, *J* 1.8 Hz), 6.72 (1H, d, *J* 8.3 Hz). δ_C ($CDCl_3$): (-) 4.10, 18.44, 25.97, 39.45, 115.33, 120.83, 121.31, 121.47, 133.07, 137.83, 145.02, 146.59 ($CDCl_3$ middle carbon: 77.01). ν_{max}. (KBr): 2957, 2930, 2896, 2859, 1640, 1606, 1577, 1510, 1473, 1463, 1421, 1294, 1254, 1228, 1155, 1125, 986, 912, 839, and 781 cm^{-1}.

3.3.10 ((4-(oxiran-2-ylmethyl)-1,2-phenylene)bis(oxy))bis(tert-butyldimethylsilane) (14) [60]

A solution of *m*-chloroperbenzoic acid (mCPBA) (19.8 g, 70% purity, 80 mmol) in 150 ml CH_2Cl_2 was separated in a separatory funnel from water present in the mCPBA. Silyl derivative **13** (16.3 g, 43 mmol) was then added to the solution of mCPBA and the reaction mixture was stirred at room temperature for 12 h. The reaction mixture was washed with 10% sodium hydroxide solution (3×22 mL), and then washed with water (2×25 mL). The CH_2Cl_2 layer was dried over anhydrous sodium sulfate, filtered and concentrated. The product was distilled (b.p. $_{0.2\ mbarHg}$127-130 ºC) to obtain **14** (6.7 g, 40%).

δ_H ($CDCl_3$): 0.17 (6H, s), 0.18 (6H, s), 0.966 (9H, s), 0.971 (9H, s), 2.49 (1H, q), 2.66 (1H, dd, *J* 14.7 Hz, *J* 5.5 Hz), 2.74 – 2.68 (2H, m), 3.06 – 3.09 (1H, m), 6.65 (1H, dd, *J* 8.3 Hz, *J* 2.2 Hz), 6.71 (1H, d, *J* 2.2 Hz), 6.74 (1H, d, *J* 8.3 Hz). δC ($CDCl_3$): -4.11, 18.43, 25.94, 37.99, 46.72, 52.57, 120.93, 121.82, 121.89, 130.14, 145.56, 146.65, ($CDCl_3$ middle carbon: 77.02). ν_{max}. (KBr): 3044, 2930, 2897, 2859, 1765, 1727, 1701, 1607, 1577, 1514, 1473, 1464, 1423, 1292, 1256, 1224, 1159, 1127, 988, 907, 842, and 783 cm^{-1}.

3.3.11 Lewis acid catalyzed polymerization of((4-(oxiran-2-ylmethyl)-1,2-phenylene)bis(oxy))bis(tert-butyldimethylsilane) (14) (Table 3.3)

3.3.11.1 General Procedure

As described in (Table 3.3), methyltriphenylphosphonium bromide was placed in a round bottom flask under Ar and closed with rubber septum. Epoxidized silyl derivative **14** and anhydrous toluene were added by syringe under Ar. The mixture was allowed to cool to 0 ºC, then triisobutylaluminium solution (25 wt. % in toluene) was added by syringe under Ar as one portion. The polymerization was stopped after complete polymerization by adding 4:1 (v/v) MeOH/H_2O, and extracted with CH_2Cl_2. The organic layer was dried over anhydrous $MgSO_4$, filtered over celite 545, and concentrated to obtain polymer **15a**. The polymer was purified by dissolving in ether and precipitating in MeOH. This process was repeated three times. ν_{max}. (KBr): 2930, 2896, 2859, 1607, 1578, 1518, 1473, 14273, 1422, 1362, 1305, 1254, 1224, 1160, 1128, 983, 852, 778, and 666 cm^{-1}.

3.3.12 Random copolymerization of safrole oxide (2) and allyl glycidyl ether (7) (Table 3.4) and (Scheme 3.6)

3.3.12.1 General procedure for attempted block copoymerization

Block copolymerization of **2** and **7** was unsuccessful. After completion of polymerization of monomer **2**, the second monomer **7** was added. However, the sequence led to the formation of two homopolymers.

When 1 M $^{i}Bu_3Al$ solution in hexane was used for polymerization a two-phase system developed in which the homopolymer **2** remained in the more viscous phase, while that of **7** remained in the less viscous layer.

When $Al^{i}Bu_3$ solution (25% in toluene) was used for polymerization, the system remained in one phase. But after work up, the material separated into two phases with the upper phase having the homopolymer of allyl glycidyl ether **7,** while the lower phase contained the homopolymer of safrole oxide **2.**

3.3.12.2 General procedure for random copoymerization

As described in (Table 3.4), methyltriphenylphosphonium bromide was placed in a round bottom flask under Ar and closed with rubber septum. Safrole oxide (**2**), allyl glycidyl ether (**7**) and anhydrous toluene were added by syringe under Ar. The mixture was allowed to cool to 0 ºC, and then triisobutylaluminium solution (25 wt. % in toluene) was added by syringe under Ar in one portion. The polymerization was stopped after complete polymerization (as indicated by ^{1}H NMR spectrum) by adding 4/1 (v/v) $MeOH/H_2O$ (10 mL), extracted with CH_2Cl_2 and dried over anhydrous ($MgSO_4$) filtrated over celite 545 followed by evaporation to afford random copolymer **16**. The following IR data belong to a 1:1 copolymer of **2** and **7**. ν_{max}. (KBr): 3076, 2869, 2773, 1646, 1608, 1500, 1443, 1353, 1249, 1121, 928, 808, and 774 cm^{-1}.

3.3.13 Conversion of 16 using lead tetraacetate to 17 (Scheme 3.6)

The procedure as described under Section 3.3.7 was followed [121], [122]. A solution of polymer **16** (containing 15 mol% safrole oxide **2** repeating unit) (1.1 g, 8.9 mmol of total repeating units and 1.33 mmol of safrole oxide units) in benzene (25 mL) was heated to 75 ºC in a round bottom flask with a condenser attached to oil trap. Then $Pb(OAc)_4$ (0.90 g, 2.0 mmol) was added under N_2. The reaction mixture was stirred at 75 ºC for 4 h. Then, it was cooled, diluted with EtOAc (30 mL) and washed with H_2O (3×25 mL). The EtOAc layer was dried over anhydrous sodium sulfate, filtered and concentrated to give **17**. For a copolymer having 1:1 ratio of the monomer unts: ν_{max}. (KBr): 3080, 30113, 2919, 2867, 1763, 1645, 1496, 1446, 1352, 1215, 1105, 923, 786, 758 cm^{-1}.

3.3.14 Synthesis of 18 via thiol-ene reaction (Scheme 3.6)

The copolymer **17** (Entry 5, Table 3.4) (containing 85 mol% repeating unit of allyl glycidyl ether **7**) (274 mg, 2.2 mmol, containing 1.9 mmol of alkene motifs) was dissolved in tetrahydrofuran (2 mL) and methanol (1.5 mL). Cysteamine.HCl (1.4 g, 12 mmol) and a photoinitiator 2,2-dimethoxy-2-phenylacetophenone (DMPA) (227 mg, 0.9 mmol) were added. The mixture was purged with N_2 for 10 min, then irradiated with a 365 nm UV lamp until the reaction was complete as indicated by ^1H NMR spectrum. After removal of the solvent, the residue was taken up in 1:1 MeOH/0.1 M HCl (5 mL) and dialyzed against water. The polymer solution was freeze-dried to obtain deprotected polymer **18** (394 mg, 86%). (15 mol% catechol units) ν_{max}. (KBr): 3469, 2960, 2923, 2857, 1624, 1494, 1384, 1259, 1105, 808, and 587 cm^{-1}.

3.3.15 Synthesis of 19 via thiol-ene reaction (Scheme 3.6)

The copolymer **17** (containing 85 mol% repeating unit of allyl glycidyl ether **7**) (240 mg, 1.9 mmol, contaning 1.6 mmol akene motifs) was dissolved in THF (3 mL). Thioglycolic acid (1.00, 11 mmol) and photoinitiator 2,2-Dimethoxy-2-phenylacetophenone (DMPA) (200 mg, 0.8 mmol) were added. The mixture was purged with N_2 for 10 min, then irradiated with a 365 nm UV lamp until the reaction was complete as indicated by ^{1}H NMR spectrum. The product was dissolved in methanol and precipitated by addition of chloroform. The process was repeated three times to obtain **19** (292 mg, 81%). The polymer was found to be soluble in methanol but insoluble in water. (15 mol% catechol units) ν_{max}. (KBr): 3500 (br), 2916, 2869, 1734, 1601, 1520, 1471, 1111, 682, and 523 cm^{-1}.

3.3.16 Copolymerization of ((4-(oxiran-2-ylmethyl)-1,2-phenylene)bis(oxy))-bis(tert-butyldimethylsilane) and allyl glycidyl ether (Table 3.5) (Scheme 3.8)

3.3.16.1 General procedure

As described in (Table 3.5), methyltriphenylphosphonium bromide was placed in a round bottom flask under Ar and closed with rubber septum. Silyl protected monomer **14**, allyl glycidyl ether **7** and anhydrous toluene were added by syringe under Ar. The mixture was allowed to cool to 0 ºC, then triisobutylaluminium solution (25 wt. % in toluene) was added by syringe under Ar in one portion. The polymerization was stopped (after its completion as indicated by ^{1}H NMR spectrum) by adding 4/1 (v/v) MeOH/H_2O (10 mL), and extracted with CH_2Cl_2 (25 mL). The organic layer was dried over anhydrous ($MgSO_4$), filtered over celite 545, and concentrated to obtain **20**.

The polymer was dissolved in diethyl ether, precipitated in methanol and separated by centrifuge. This process was repeated three times to obtain pure **20.**

(25 mo% silyl unites, entry 3, Table 3.5): ν_{max}. (KBr) 3081, 3014, 2855, 1646, 1605, 1576, 1512, 1469, 1422, 1358, 1298, 1255, 1224, 1160, 984, 839, 782, 696, and 667 cm^{-1}.

3.3.17 Silyl deprotection of polymer 15a [123], [124]

Tetra-n-butylammonium fluoride TBAF (1.0 M in THF) (1.26 mL, 1.26 mmol) was added to a solution of polymer **15a** (entry 4, Table 3.3) (227 mg, 0.575 mmol) in THF (4 mL) under N_2 at 0 °C. The reaction mixture was stirred at 0 °C for 1 h. A 1:1 mixture of H_2O/acetic acid (2 mL) was added to the reaction mixture. The solvent was evaporated using a gentle stream of N_2, and the residue was dissolved in methanol and precipitated in water. The process was repeated three times to wash out extra TBAF remaining and thus to obtain deprotected polymer **15b**, (Yield: 72 mg, 75%). The fluoride ion could chelate with catechol moiety according to literature [123], [124]. The polymer was soluble in methanol but insoluble in H_2O, Et_2O and CH_2Cl_2. ν_{max}. (KBr): 3445, 2921, 2921, 2870, 1608, 1521, 1446, 1363, 1285, 1190, 1113, 1052, 958, 871, 811, 788, and 754. cm^{-1}.

3.3.18 Thiol–ene reaction of cysteamine and 20 [125].

3.3.18.1 General procedure

Copolymer **20** was dissolved in minimum amount of THF/MeOH. Cysteamine.HCl (5-7 equiv to vinyl double bonds) and a photoinitiator 2,2-dimethoxy-2-phenylacetophenone (DMPA) (0.5 eq to vinyl double bonds) were added. The mixture was purged with N_2 for 10 min, then irradiated with a 365 nm UV lamp until completion of the reaction.

3.3.19 Synthesis of 21 via thiol-ene reaction (10 mol% catechol units)

The copolymer **20** (entry 7, Table 3.5) (230 mg, 1.60 mmol, containing 1.44 mmol of alkene motifs) was dissolved in tetrahydrofuran (6 mL) and methanol (1.5 mL). Cysteamine.HCl (1.2 g, 11 mmol) and photoinitiator 2,2-dimethoxy-2-

phenylacetophenone (DMPA) (194 mg, 0.8 mmol) were added. The mixture was purged with N_2 for 10 min, and then irradiated with a 365 nm UV lamp at room temperature until completion of the reaction. The reaction mixture was dialyzed against MeOH (to remove DMAP) for 30 min and then against deionized water (1 h). The resultant polymer solution was freeze-dried to obtain polymer **21** (370 mg, 90%). (50% silyl) ν_{max}. (KBr): 3430, 2962, 2927, 2857, 1637, 1511, 1467, 1422, 1385, 1301, 1256, 1221, 1162, 1100, 981, 910, 840, 778, 664, and 614 cm^{-1}.

3.3.20 Thiol−ene reaction of thioglycolic acid to vinyl double bonds in copolymer 20

3.3.20.1 General procedure:

This click reaction was done by using UV light in dark room. The product was purified but also can be used for subsequent step without purification. This reaction was done for polymer samples **20** having SP **14** and AGE **7** repeating units in mole ratios of 50:50 and 10:90 to obtain polymer **22**.

3.3.21 Synthesis of 22 containing 10 mol % catechol units (Scheme 3.8)

Thioglycolic acid (627 mg, 6.8 mmol) and photoinitiator DMPA (174 mg, 0.7 mmol) were added to a solution of copolymer **20** (entry 7, Table 3.5) (206 mg, 1.5 mmol containing 1.35 mmol akene motifs) in THF (4 mL). The mixture was purged with N_2 for 10 min, and then irradiated with a 365 nm UV lamp at room temperature until completion of the reaction. The THF-soluble product was precipitated with the addition of ether to the reaction mixture. The process of dissolving in THF followed by precipitation in ether was repeated three times to obtain **22** (295 mg, 84%). IR for a 50:50 copolymer **22** is given: (50% silyl) ν_{max}. (KBr): 3458, 2931, 2858, 2511, 1727, 1632, 1511, 1467, 1421, 1385, 1301, 1255, 1223, 1122, 983, 910, 841, 790, 669, and 552 cm^{-1}.

3.3.22 Synthesis of 18 from 21 (catechol 10 mol%) (Scheme 3.8)

The crude copolymer **21** as obtained from **20** (1.0 mmol) (entry 7, Table 3.5) using procedure described under Section 3.3.19, was dissolved in MeOH/0.5M HCl (6 mL) and stirred at room temperature for 18 h. The reaction mixture was dialyzed against water, then freeze-dried. The polymer solution was centrifuged to get rid of insoluble material and it was freeze dried to obtain polymer **18** in (90 %).

IR and NMR spectra of **18** (10 mol% silyl) were found to be similar to the one prepared earlier from safrole-oxide under Section 3.3.14.

3.3.23 Synthesis of 19 from 22 (catechol 10 mol%)

Tetra-n-butylammonium fluoride TBAF (1.0 M in THF) (0.25 ml, 0.25 mmol) was added to a solution of polymer **22** (50 mg, 0.22 mmol) under N_2 at 0 °C. After stirring the reaction mixture for 12 h, a 2:1 mixture of H_2O/acetic acid (2 mL) was added. The crude polymer was soluble in methanol but insoluble in H_2O. Therefore, it was purified by dissolving in methanol and precipitating in water. The process was repeated two times to obtain polymer **19** (Yield: 90% mg,)

Removal of protecting group of copolymer **22** containing higher mol% silylated motifs could not be achieved owing to the solubility problem.

IR and NMR spectra of **19** (10 mol% silyl) were found to be similar to the one prepared earlier from safrole-oxide under Section 3.3.15.

3.4 Results and Discussion

Natural safrole (**1**) was converted into its epoxide **2** (Scheme 3.1). Figure 3.1a displays its ^{1}H NMR spectrum. Numerous attempts were made to polymerize safrole oxide **2** using various basic catalyst. The results are given in (Table 3.1). The ring opening polymerization of epoxide **2** as neat or in solvent THF was carried out under argon using tert-butylammonium fluoride (TBAF) (1-6 mol%) or tert-butylammonium hydroxide (TBAH) (2-5 mol%) or NaO^{t}Bu as initiators at 50-100 °C for 2-72 h. However, we were unable to obtain the expected polymer **5**; under the reaction conditions, the monomer **2** was recovered unreacted in the case of initiator NaO^{t}Bu. TBAF failed to give any polymer, however extensive base catalyzed elimination reaction occurred. Use of TBAH as the initiator led to the formation of polymer in high yields in the temperature range 70-100 °C; however, the proton NMR analysis revealed the presence of alkene motifs (≈10 mol%) on the polymer terminal (Figure 3.1b). Here, the F^{-} or OH^{-} or the ring opened alkoxide ion (RO^{-}) is involved in a competing reaction between nucleophilic ring opening and base catalyzed elimination reaction via abstraction of labile benzylic protons as depicted in Scheme 3.1. The elimination process was very extensive with F^{-} as confirmed by appearance of ^{1}H signal at δ6.2, 6.5 and 4.1 ppm attributed to the $–CH=CH-CH_2-O$ motifs (Figure 3.1b). For the sake of comparison, the ^{1}H NMR spectrum of cinnamyl alcohol is shown in Figure 3.1c. The signals for the protons marked ‘a’, ‘b’ and ‘c’ are readily identifiable for comparison thereby confirming base catalysed chain transfer to monomer

2 by abstraction of benzylic protons leading to alkene motifs akin to the motifs of cinnamyl alcohol. With TBAH, ring opening polymerization happened accompanied by chain transfer via elimination process as depicted by **A** (Scheme 3.1). This extensive chain transfer to monomer led us to pursue this important polymerization using other protocols with the objective of minimizing the chain transfer reaction, which puts a limit on the maximum molar mass possible for this polymerization.

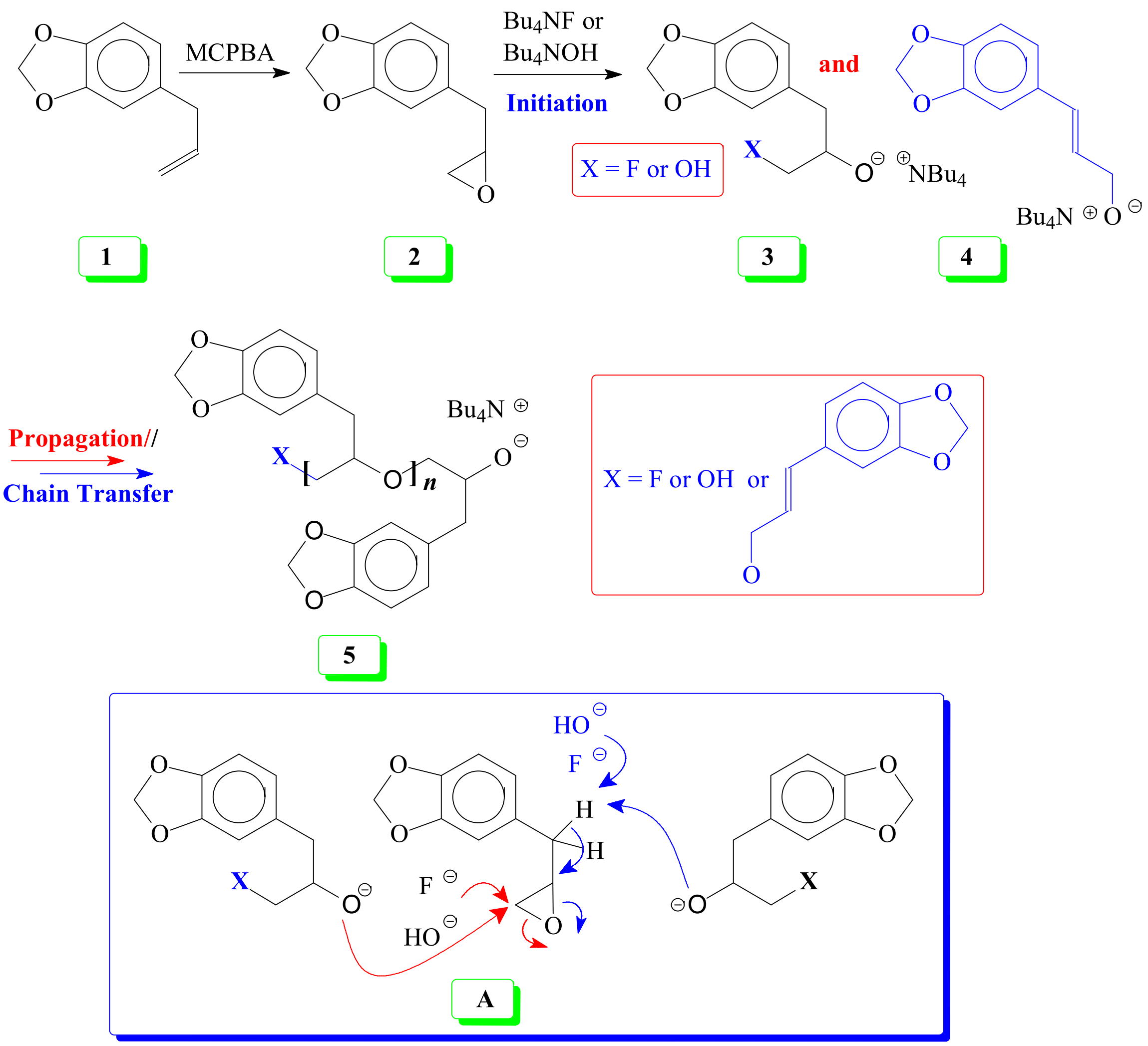

Scheme 3.1 Base catalyzed polymerization of safrole oxide using Bu$_4$NF and Bu$_4$NOH

Table 3-1 Polymerization of safrole oxide **2**[a]

Entry	Solvent	Catalyst (mmol)	Temp (^{o}C)	Time (h)	Yield (%)
1	Neat[b]	TBAF.3H_2O (0.06)	85	18	Trace
2	Neat[b]	TBAF.3H_2O (0.06)	90	18	Trace
3	Neat[b]	TBAH 40% H_2O (0.05)	85	18	≈100
4	Neat[c]	TBAH 40% H_2O (0.03)	50	24	45
5	Neat[c]	TBAH 40% H_2O (0.03)	50	66	55
6	THF[d]	TBAH 40% H_2O (0.03)	50	24	Trace
7	THF[d]	TBAH 40% H_2O(0.03)	50	66	Trace
8	Neat[b]	TBAH 40% H_2O (0.05)	70	18	78
9	Neat[b]	TBAH 40% H_2O (0.02)	90	2	≈100
10	Neat[b]	TBAH 40% H_2O(0.02)	100	18	≈100
11	Neat[b]	TBAH 40% H_2O (0.04)	100	2	77
12	Neat[b]	TBAH 40% H_2O (0.04)	100	4	86
13	Neat[b]	TBAH 40% H_2O (0.04)	100	24	94
14	Neat[b]	NaO^{t}Bu (0.05)	100	18	0

[a] 1 mmol; [b] Toluene was added and removed under N_2; [c] Toluene was added and removed under N_2, then by vacuum; [d] THF was added and removed under N_2, then by vacuum.

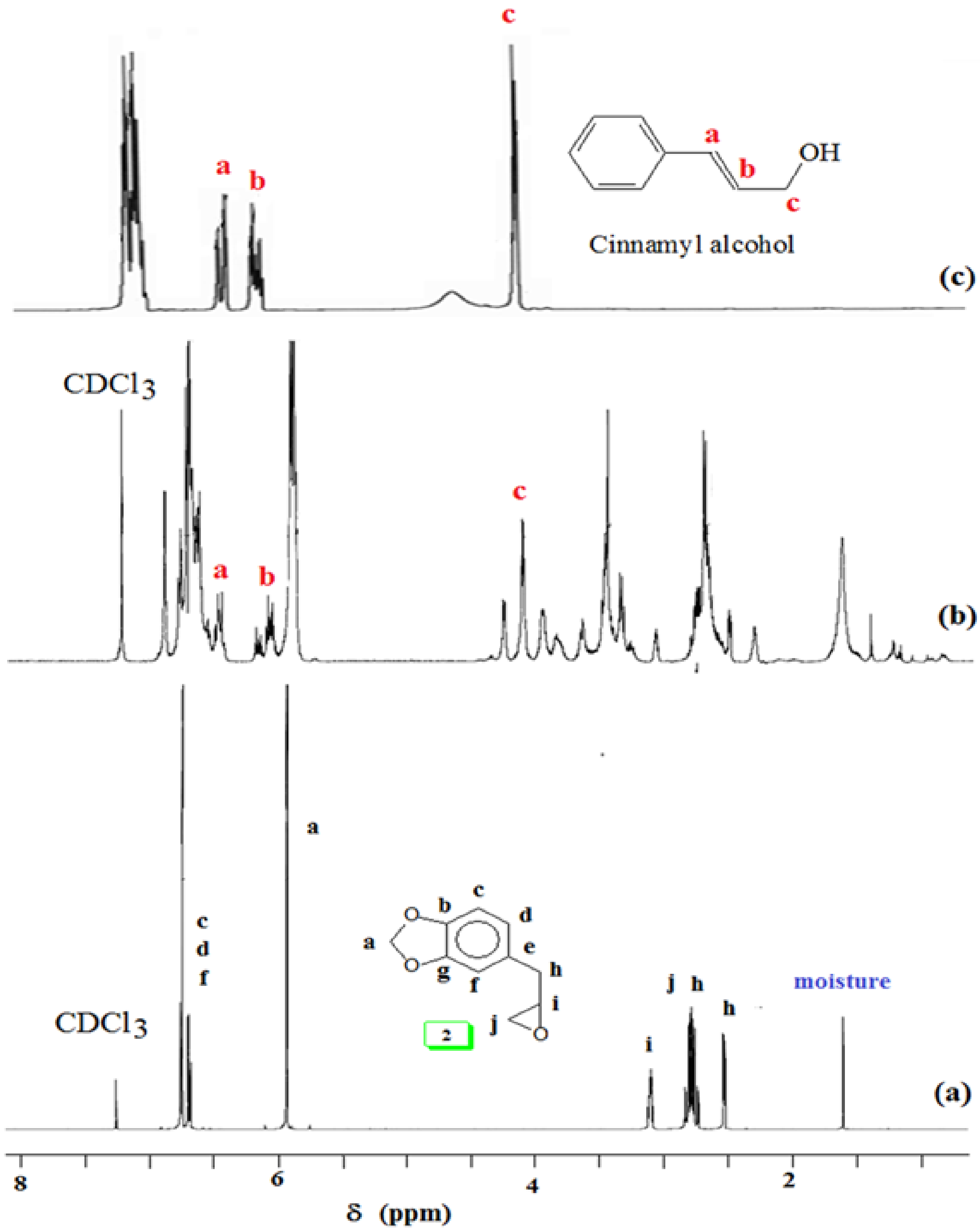

Figure 3.1 ^{1}H NMR spectra of (a) safrole epoxide **2**, (b) base catalyzed polymerized product from **2** and (c) cinnamyl alcohol

There have been considerable efforts exerted on the polymerization of propylene oxide (PO) and on methods to control its living character. In most cases, alkali metal alkoxides and hydroxides are widely used as anionic polymerization initiators [126]–[128]. The high basicity of propagating species leads to proton abstraction from the PO methyl group, thereby constituting a transfer reaction to monomer. This side process is also observed in the current work involving the base catalysed polymerization of safrole oxide (SO) **2,** thereby resulting in the exclusive formation of SO oligomers with a large fraction possessing a terminal cinnamylic unsaturation (Scheme 3.1). One significant problem inherent in SO is the much higher acidity of the benzylic protons than that of CH_3 protons in PO; the labile H in SO is, therefore, much more prone to base catalysed abstraction than the methyl protons in PO.

Polymerization reaction of **2** using Lewis acid triisobutylaluminium as a catalyst and methyltriphenyphosphonium bromide as an initiator [118], [119] gave ring opened polymer **6** in excellent yields (Scheme 3.2). The conditions of polymerization are given in (Table 3.2). The NMR spectra (Figures 3.2 and 3.3) revealed the formation of ring opened polymer without any indication of chain transfer reaction via abstraction of allylic proton.

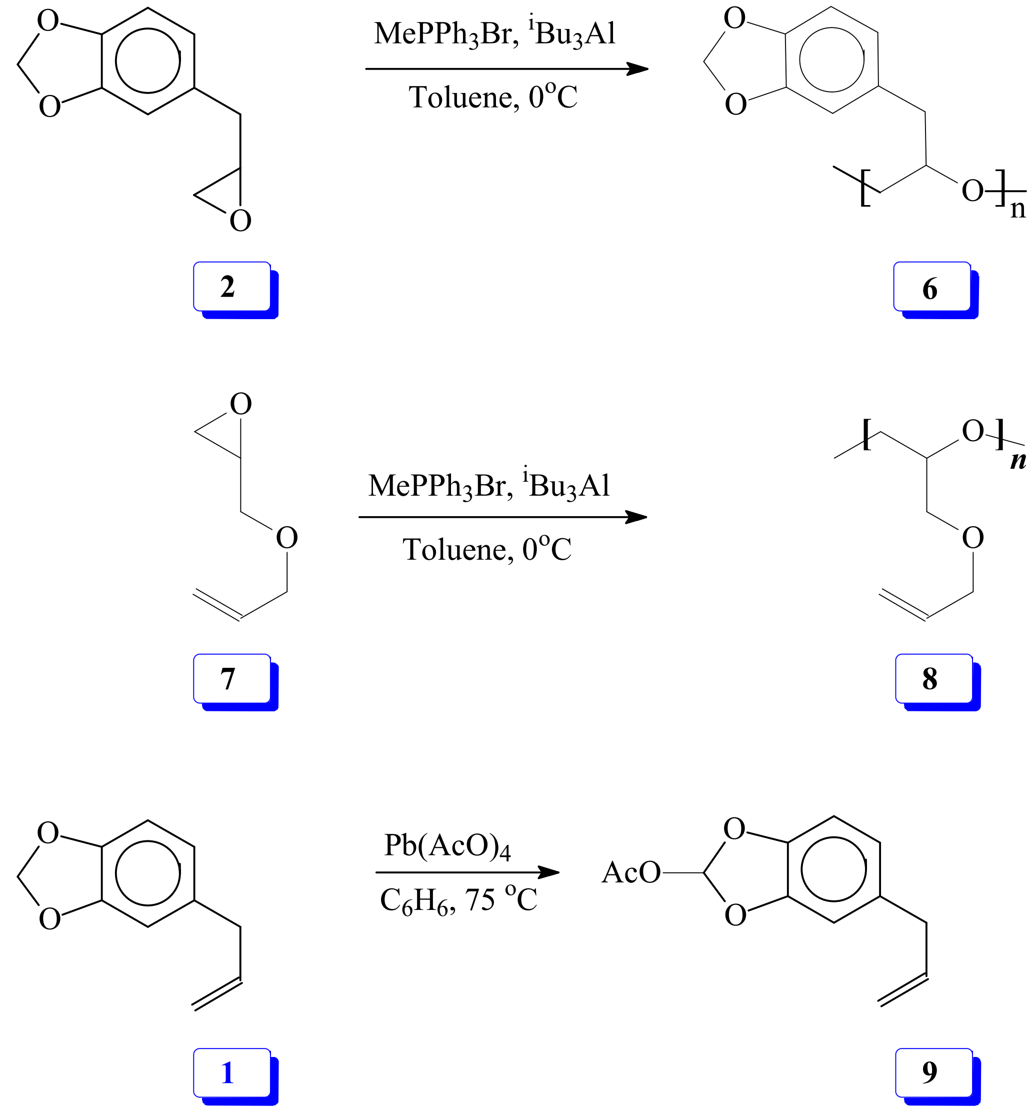

Scheme 3.2 Lewis acid catalyzed polymerization of safrole oxide, allyl glycidyl ether and deprotection of methylene acetal of safrole

Table 3-2 Polymerization[a] of Safrole Oxide (**SO**) (**2**) initiated with $MePPh_3Br$ (**I**) and catalyzed by $^{i}Bu_3Al$ (**C**)[b]

Entry	**I** (mmol)	**C** (mmol)	[**SO**]/[**I**]	[**C**]/[**I**]	Time (h)	Yield[c] (%)	$M_{n,Theor}$	$M_{n,Exp}$[d]	PDI
1	0.0256	0.263	98	10.3	3	94	17,500		
2	0.0116	0.261	216	22.5	3	91	38,500	14,450	1.38
3	0.0458	0.264	55	5.76	6	95	9,800	7,500	1.45
4	0.0220	0.239	114	10.9	2	93	20,300	11,150	1.23
5	0	0.418	–	–	2	0			
6[e]	0	0.418	–	–	24	0			
8[f]	0.0331	0.416	76	12.6	3	69			
11	0.0227	0.725	110	31.9	12	70			
12	0.0222	0.235	113	10.6	12	65			
13	0.0328	0.403	76	12.3	2	99	17,000	9,970	1.32

[a] Polymerization was carried out at 0 °C using 2.5 mmol of monomer **2** with 1.8 ml of additional toluene except in entry 4 where no additional toluene was added.

[b] 25 wt. % solution in toluene (≈ 1 M $^{i}Bu_3Al$).

[c] NMR indicates complete conversion to polymer where isolated yields are over 90%.

[d] GPC using light scattering detector

[e] Carried out at 20 °C.

[f] 1 M $^{i}Bu_3Al$ solution in hexane.

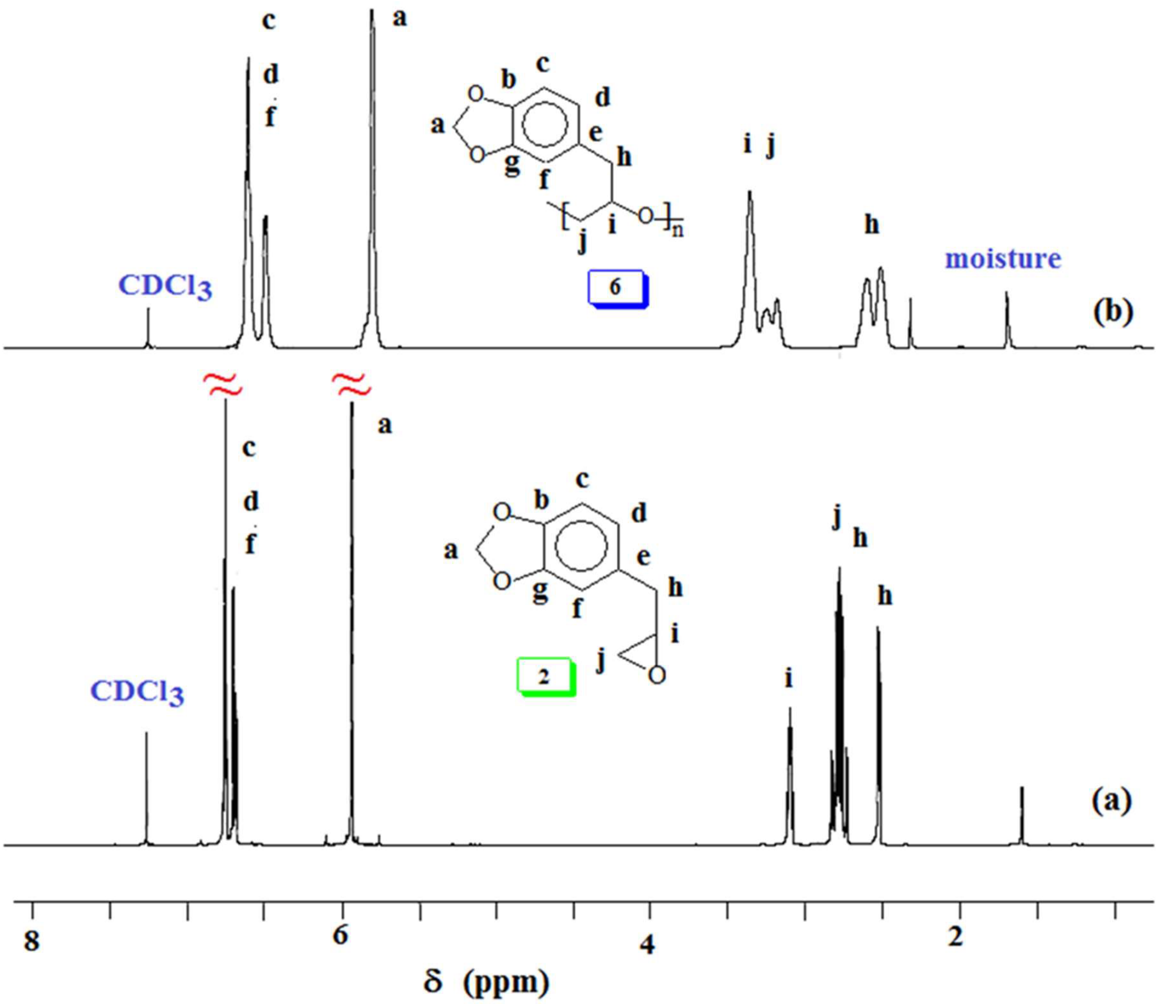

Figure 3.2 ^{1}H NMR spectra in $CDCl_3$ of (a) safrole oxide **2** and (b) polymer **6**

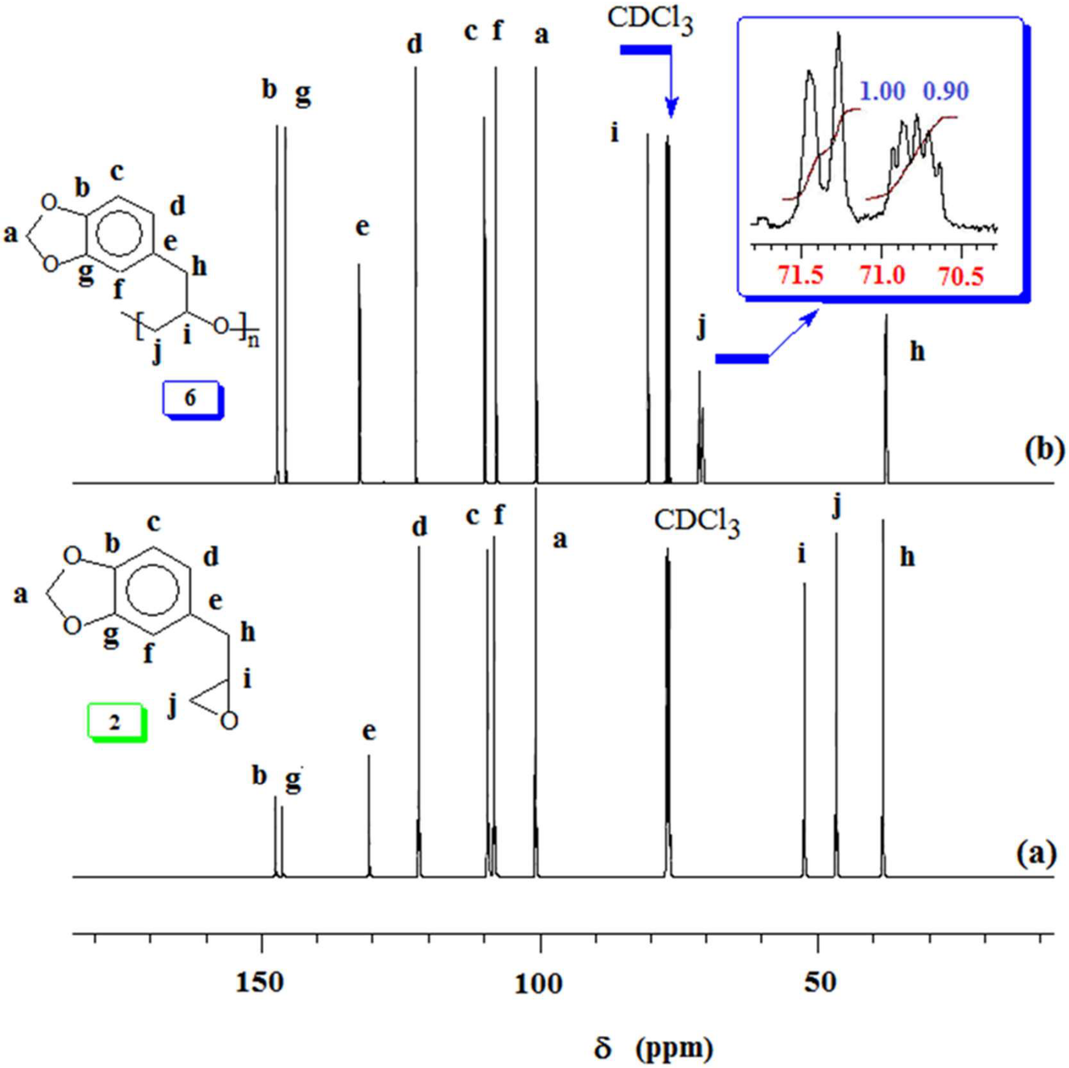

Figure 3.3 ^{13}C NMR spectra in $CDCl_3$ of (a) safrole oxide **2** and polymer **6**

The use of new widespread initiating systems for the "controlled" high-speed anionic polymerization of propylene oxide, based on the combination of alkali metal alkoxides (initiator, I) and trialkylaluminum (catalyst) has been reported [118]. However, this catalyst-initiator system did not work in oxides containing perfluorinated alkyl chain, instead a new system of trialkylaluminum (catalyst) and methyltriphenyphosphonium bromide (initiator) has been developed [119], [129].

Experimental evidence suggests the requirement of $[AlR_3]/[I] \geq 1$ for successful polymerization. Trialkylaluminum is completely involved in the formation of an aluminate complex as depicted by '**A**' (Scheme 3.3). The complex is unable to initiate and/or propagate the SO polymerization. In the presence of an excess of $^iBu_3Al$ (with respect to $Ph_3MeP^+Br^-$), a fast polymerization of SO takes place and reaches completion in a few hours at 0 °C, suggesting an important activating effect of the "free" triisobutylaluminum derivative as depicted by **B**. At 0 °C, in the whole molar mass range examined, the experimental poly(safrole oxide) PSO molar masses are not close to theoretical values calculated assuming the formation of one polymer chain per $Ph_3MeP^+Br^-$ (see Table 3.2)..

This does not suggest the living-like polymerization of SO. There is a significant contribution of the monomer transfer process, which is not observed with pure alkali metal alkoxide initiators. It has been reported that the number of PPO chains is independent of the initial R_3Al concentration but is only determined by the $Ph_3MeP^+Br^-$concentration [118].

These results are in agreement with a reaction mechanism in which the monomer is activated by the electrophilic aluminum compound **B**, prior to its insertion into the poly(safrole oxide) triisobutyl aluminate methyltriphenyphosphonium (**C, D**) growing chain end (Scheme 3.3). The important transfer reaction to SO, which characterizes alkali metal alkoxide initiators, is also strongly reduced. The much larger electron-withdrawing effect of R_3Al complexation imparts greater positive charges on the methylene and methine ring-carbons, the two potential active sites in the ring opening process, than on the benzyl hydrogens involved in the transfer process to monomer (Scheme 3.1). Also, note that reduction of the basicity of alkali metal alkoxide species in alkoxy aluminate complexes (as compared to alkali metal alkoxide species) may also contribute to the reduction of the proton abstraction reaction yielding transfer to monomer.

It was reported that the initiation process involved the attack by not only bromide but also the isobutyl group and hydride as shown in Scheme 3.3 [119], [129]. Three series of polymers were detected corresponding to bromide, isobutyl, and hydride end groups corresponding to bromide, isobutyl, and hydride end groups as supported by MALDI-TOF mass spectrometry [129]. $^{i}Bu_3Al$ can work as both a hydride and an isobutyl anion source in the ring-opening reaction of various epoxides [130], [131].

It has been reported that aggregation of $^{i}PrONa–Al^{i}Bu_3$ might be responsible for the catalyst deactivation in some cases of epoxide polymerization [129]. However, the use of organic salts containing non-coordinating cations such as ammonium and phosphonium were expected to prevent aggregation [132], [133].

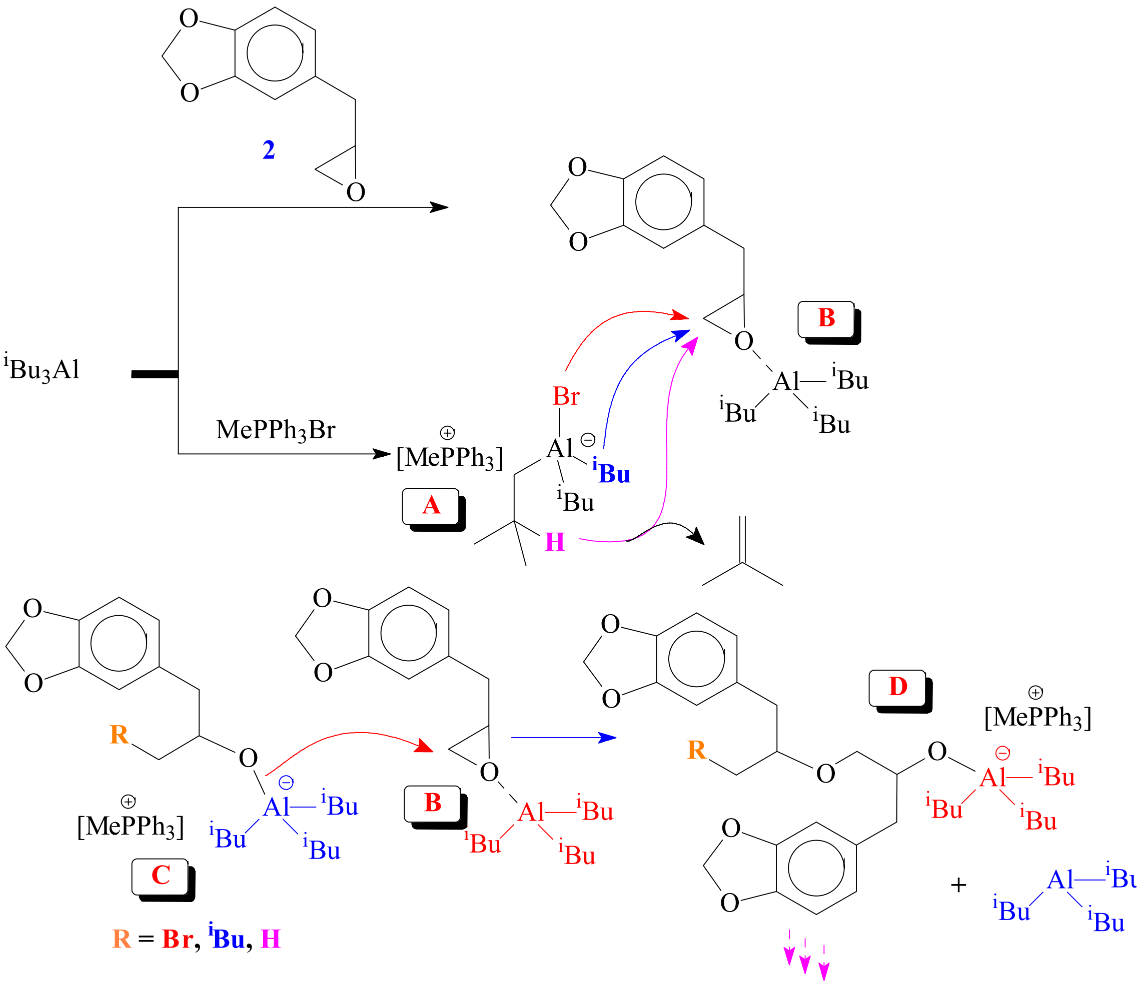

Scheme 3.3 Triphenylmethylphosphonium bromide initiated triisobutylaluminum catalysed polymerization of safrole oxide

Generally, regioregular ring-opening polymerization of epoxides proceeds through successive nucleophilic attacks on the less hindered methylene carbon rather than the methine carbon [134], [135]. Optically pure (i.e. enantiopure) epoxides are thus expected to provide an easy access to isotactic polymers since the methine carbon retains its configuration (Scheme 3.4). However, for a racemic epoxide, formation of an atactic polymer is expected with equal percentages of mm, mr, rm and rr triads (Scheme 3.4).

The regioregularity and stereospecificity of monomer insertion have been investigated before by ^{13}C NMR. The observed methine and methylene carbon signals can be unambiguously attributed to exclusive head-to-tail (HT) enchainments [136]. In the current work, while the methine carbon marked 'i' appeared as single signal, the methylene carbon marked 'j'resolved into triads and diads (splitted into higher stereosequences) (Figure 3.3). The ^{13}C NMR spectrum thus showed the current polymer **6** as atactic (Scheme 3.2) [118], [136], [137].

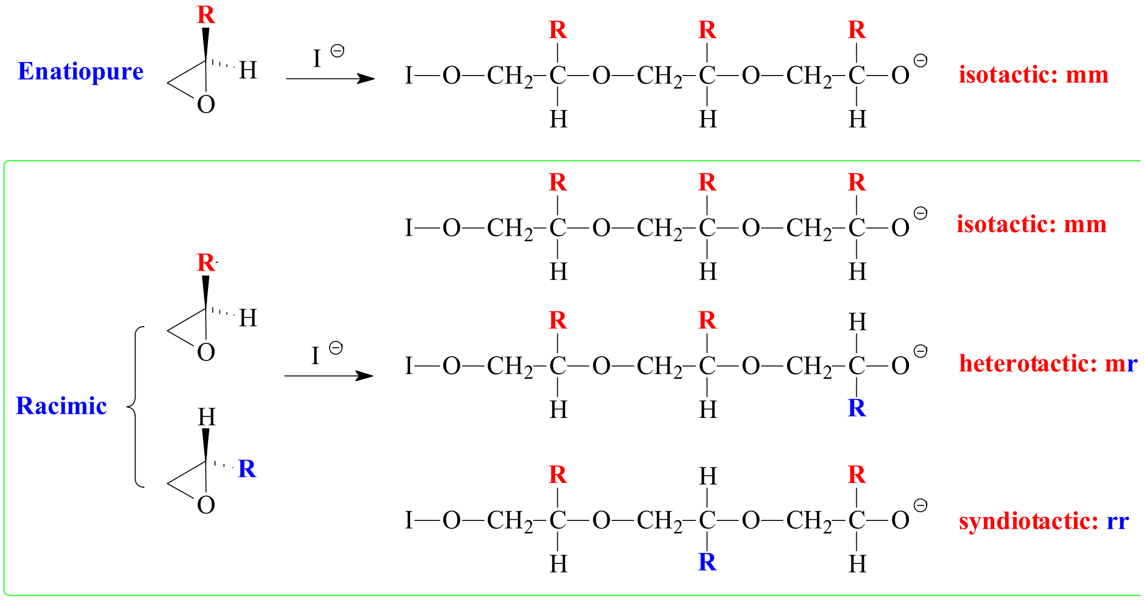

Scheme 3.4 Regioregular ring opening polymerization of enantiopure and racemic epoxide

Our research plans demands the formation of copolymers of monomers safrole oxide **2** and allyl glycidyl ether **7** (Scheme 3.2). In this context, triisobutylaluminium-methyltriphenyphosphonium bromide catalyst-initiator system was used to homopolymerize **7** to obtain polymer **8** (Scheme 3.2). The ^{1}H and ^{13}C NMR spectra of **7** and **8** are shown in Figures 3.4 and 3.5, respectively. The spectral data is consistent with the regioregular ring opening to give **8**. As in the case of safrole oxide polymer **6**, the splitting of carbon marked ‘a’ in the ^{13}C NMR spectrum (Figure3.5b) pointed toward the formation of an atactic microstructure.

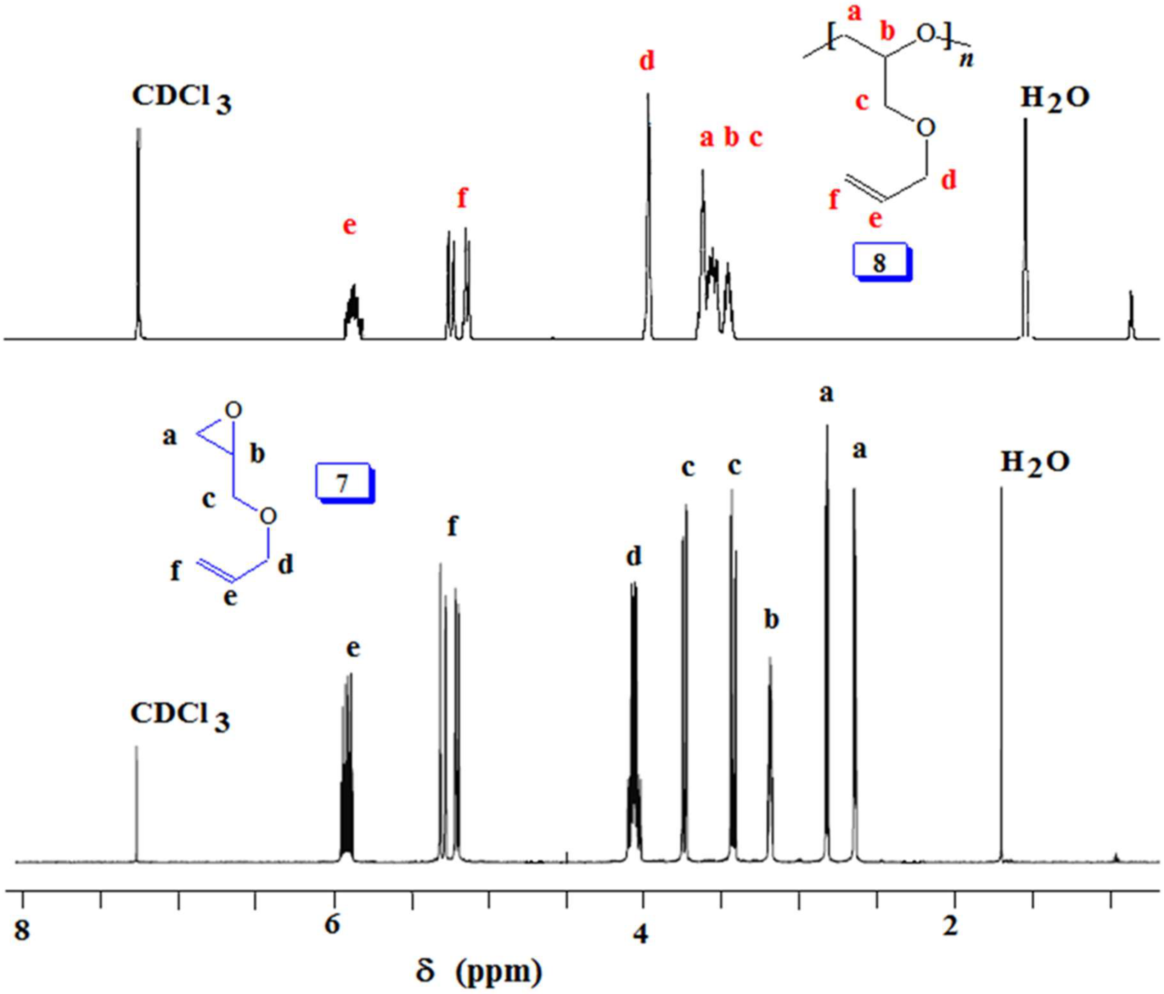

Figure 3.4 ^{1}H NMR spectra in $CDCl_3$ of (a) allyl glycidyl ether **7** and (b) polymer **8**

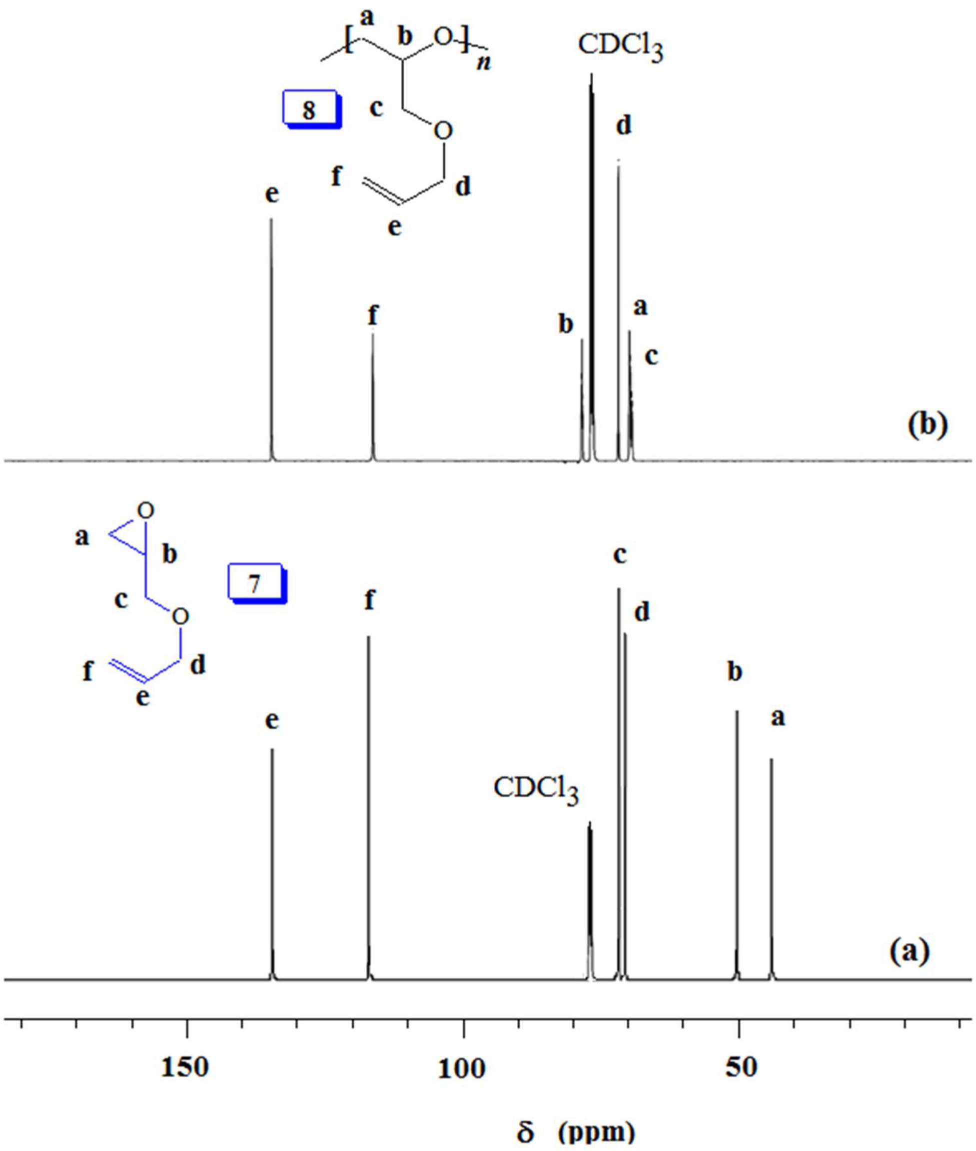

Figure 3.5 ^{13}C NMR spectra in CDCl$_3$ of (a) allyl glycidyl ether **7** and (b) polymer **8**

At this stage, we were apprehensive about the deprotection of methylene acetal protecting group in PSO **6**. Methylene acetal is indeed a robust protective group which does not respond to acid catalyzed deprotection. As a model case, safrole **1** was used for examining the deprotection aspect using lead tetraacetate [121], [122]. To our great relief, safrole **1** on treatment with the oxidizing agent afforded **9** having labile acetoxy group (Scheme 3.2). In fact, the similar acetoxy derivatives are usually removed during aqueous work up leading to catechol motifs. The ^{1}H and ^{13}C NMR spectra of **1** and **9** are displayed in Figures 3.6 and 3.7, respectively. The methylene protons of **1** marked 'a' (Figure 3.6a) is shifted downfield in the spectrum of **9** (Figure 3.6b) owing to the presence of electron withdrawing AcO substituent. Similar downfield shift is observed for the carbon marked 'j' in the ^{13}C NMR spectrum (Figure 3.7).

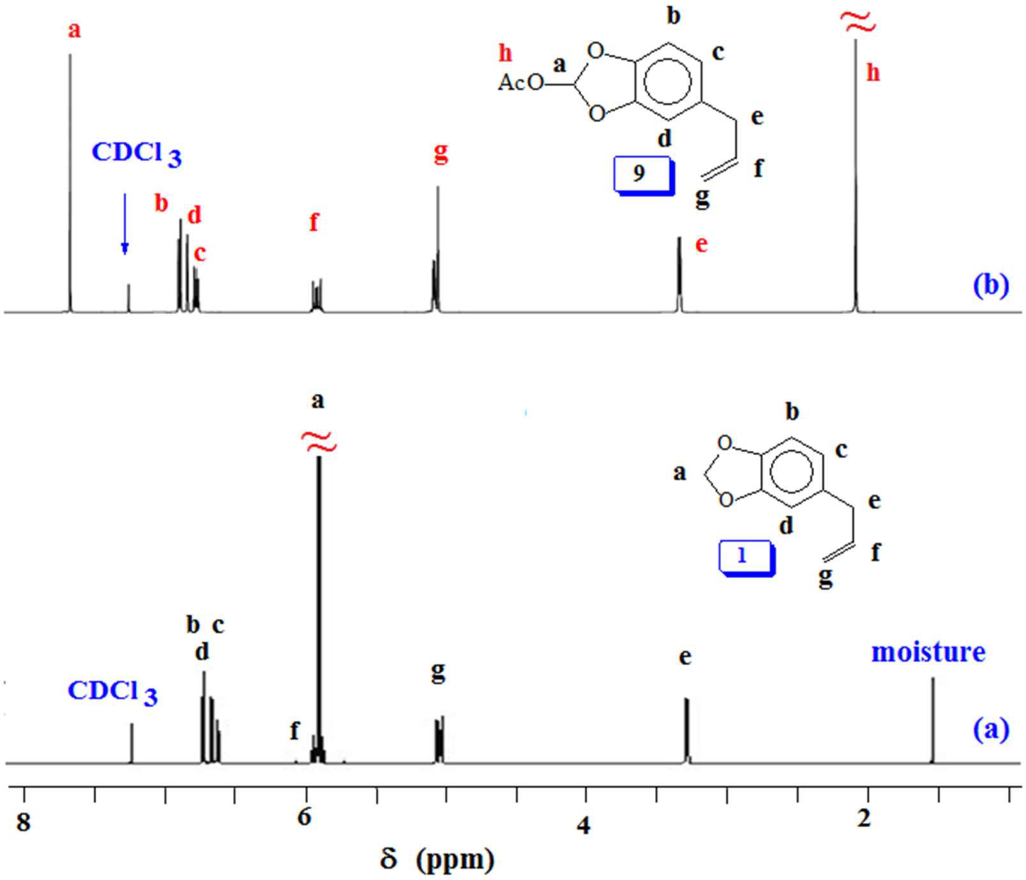

Figure 3.6 ^{1}H NMR spectra in $CDCl_3$ of (a) safrole **1** and (b) acetoxysafrole **9**

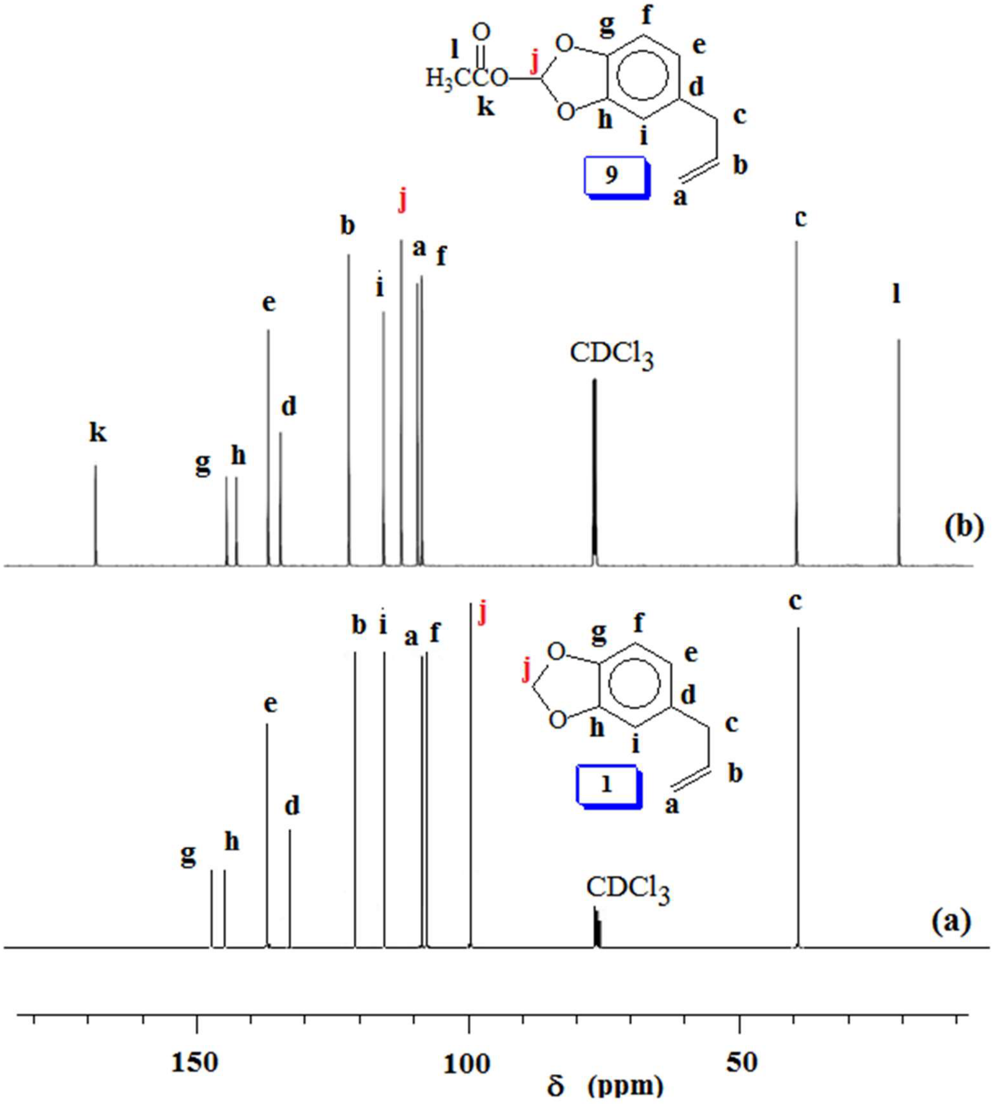

Figure 3.7 ^{13}C NMR spectra in CDCl$_3$ of (a) safrole **1** and (b) acetoxysafrole **9**

Unaware of the AcO group's ability in **9** (Scheme 3.2) to survive during subsequent chemical transformation, we set out to explore the related chemistry using silyl protecting group. In this context, natural product eugenol **10** was demethylated and protected by reacting with diphenylsilane in the presence of catalyst tris-pentafluorotriphenylborane to give **11** (Scheme 3.5). To our dismay, silyl protected **11** was found to be extremely moisture sensitive; it broke down during silica gel chromatography to give allylcatechol **12** quatitatively. Thereafter, we decided to prepare **12** via demethylation using LiCl. The 'OH' groups in **12** were then protected to give **13** by reacting with tert-butyldimethylsilyl chloride in the presence of imidazole. Epoxidation using m-chloroperbenzoic acid transformed **13** to **14** which was then subjected to Lewis acid catalysed ring opening polymerization to afford **15a**. The results of the polymerization reaction are given in (Table 3.3). The tert-Butyldimethylsilyl groups in **15a** were then deprotected using tetrabutylammonium fluoride to obtain **15b** containing the catechol motifs.

Table 3-3 Polymerization[a] of silyl protected (**SP**) monomer **14** initiated with $MePPh_3Br$ (**I**) and catalyzed by $^iBu_3Al$ (**C**)[b]

Entry	**I** (mmol)	**C** (mmol)	[**SP**]/[**I**]	[**C**]/[**I**]	Time (h)	Yield (%)[c]	$M_{n,Theor}$[d]	$M_{n,Exp}$[e]	PDI
1	0.0213	0.24	117	11.3	1	0	–	–	
2	0.0213	0.70	117	32.9	2	60	27,700	16,300	1.8
3	0.0495	0.53	50	10.7	20	90	17,700	12,900	1.5
4	0.0092	0.53	272	57.6	40	75	80,200	11,500	1.6
5	0.0370	0.53	68	14.3	18	85	22,800	10,300	1.8

[a] Polymerization was carried out at 0°C for 6 h using 2.5 mmol of monomer **14** with 1.8 mL of additional toluene except in entry 4 where no additional toluene was used.

[b] 25 wt.% solution in toluene (≈ 1 M $^iBu_3Al$).

[c] isolated and NMR yields are similar within 2%.

[d] M_n is calculated by multiplying the molar mass by a conversion factor of Percent yield/100.

[e] GPC using light scattering detector.

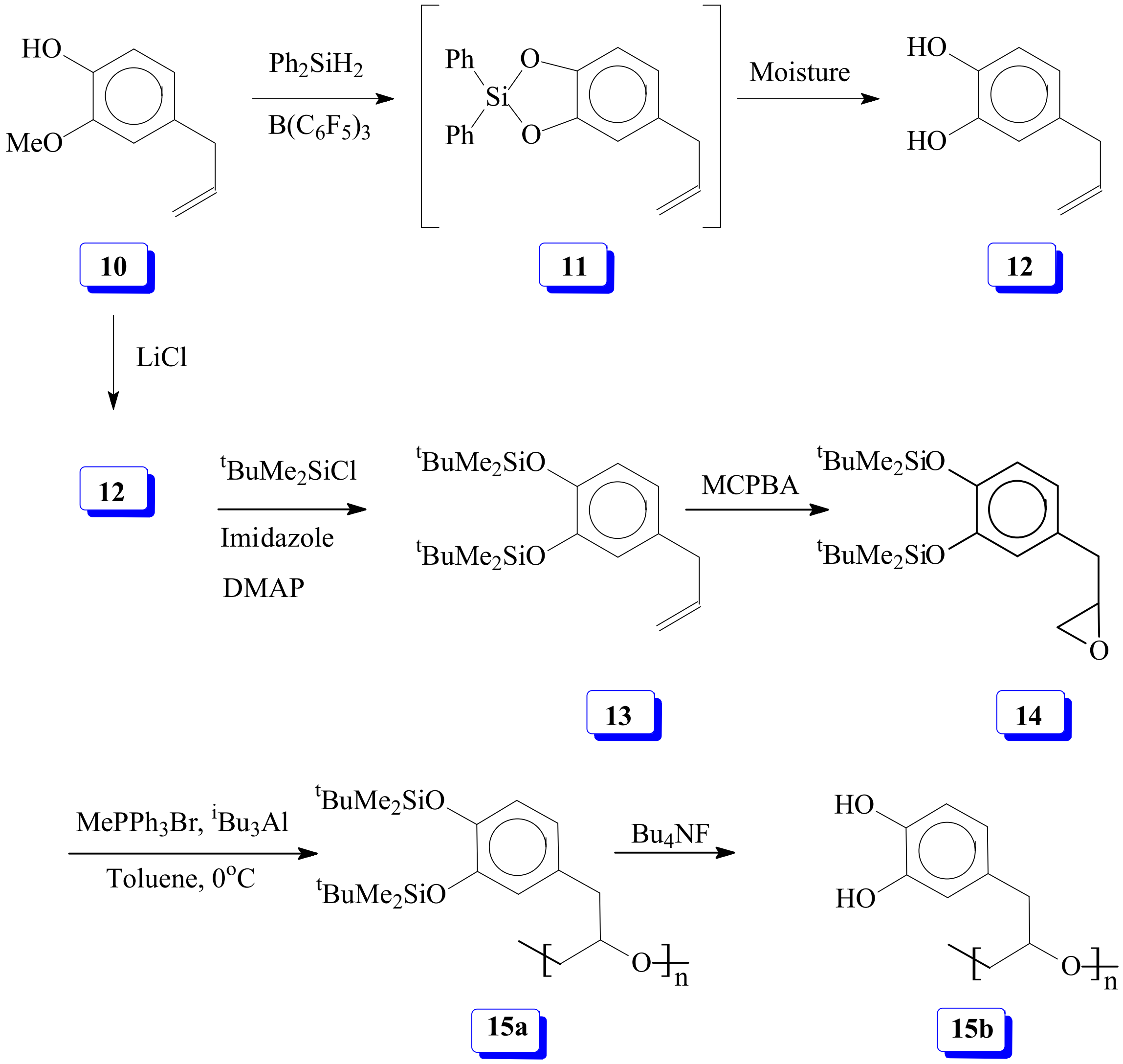

Scheme 3.5 Lewis acid catalyzed polymerization of silylated epoxide

The ^{1}H and ^{13}C NMR spectra of **14, 15a** and **15b** are displayed in Figures 3.8 and 3.9, respectively. The spectra confirmed the structures of the monomer and polymers. The silyl protons and carbons marked 'a' and 'c' in Figures 3.8a,b and 3.9a,b disappeared upon deprotection of the silyl groups as indicated by the absence of the corresponding signals in Figure 3.8c and Figure 3.9c. However, it was very difficult to remove the F^- as it is known to bind strongly with catechol motifs via H-bonding [124], [138]. In such a scenario, the ammonium counterion remained with the polymer sample as can be seen as minor peaks in the region around δ 1 ppm (Figure 3.8c). Minor carbon signals are also observed in Figure 3.9c.

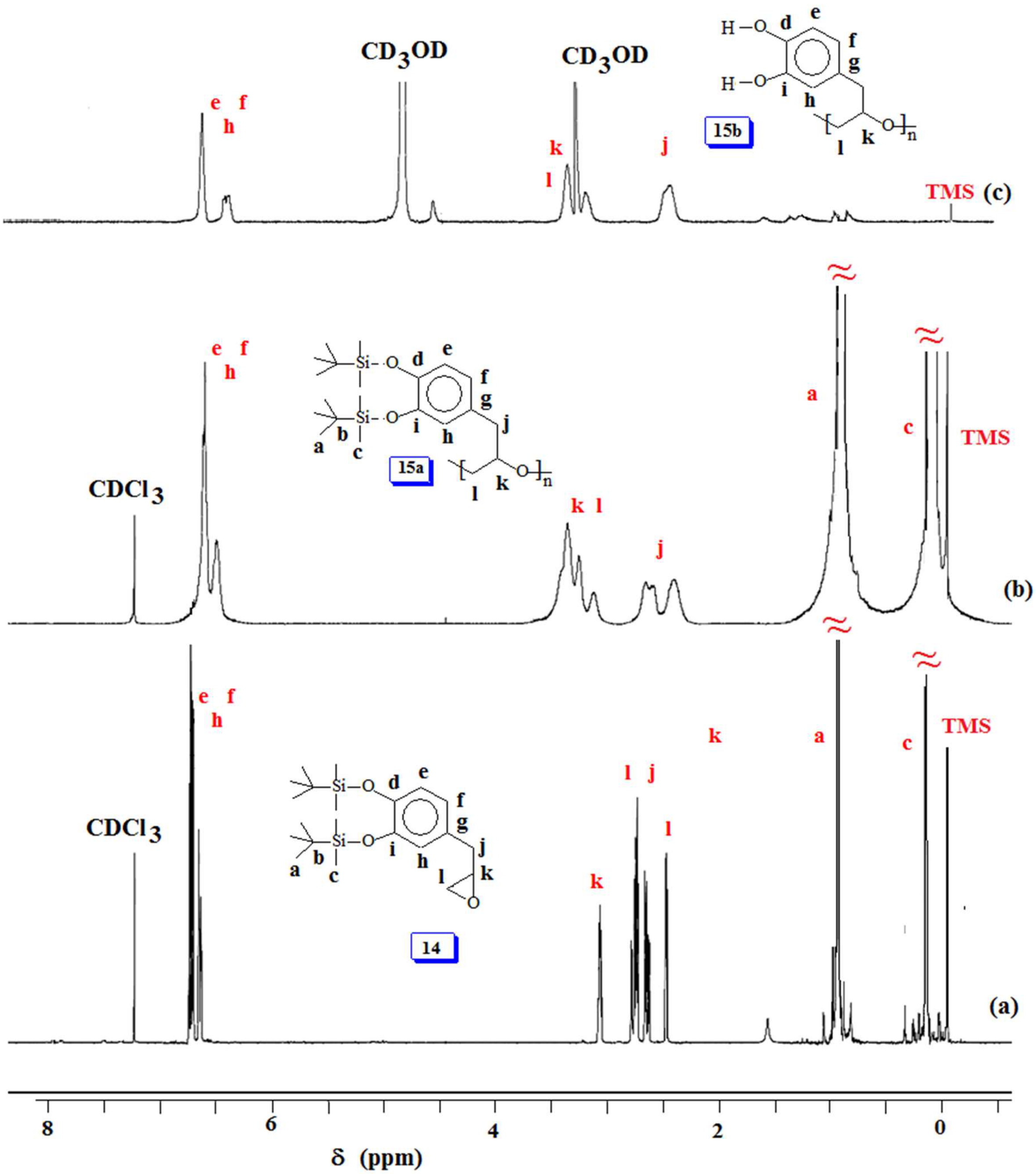

Figure 3.8 ^{1}H NMR spectra of (a) SP **14** in CDCl$_3$ (b) polymer **15a** in CDCl$_3$ and (c) **15b** in CD$_3$OD.

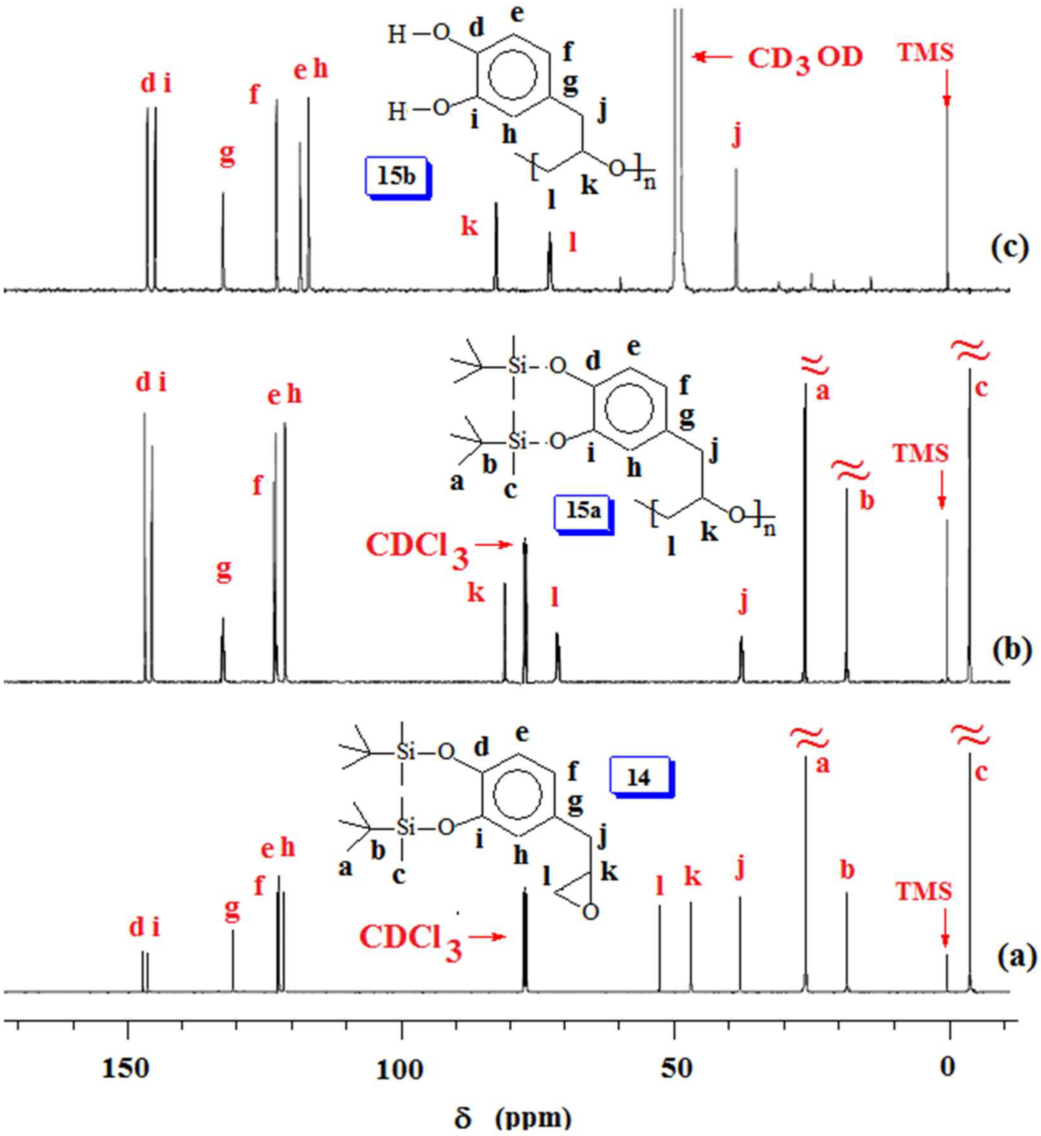

Figure 3.9 ^{13}C NMR spectra of (a) SP **14** in $CDCl_3$ (b) polymer **15a** in $CDCl_3$ and (c) **15b** in CD_3OD

Next, we focussed our attention to Lewis acid catalysed copolymerization reaction of SO (**2**) and allyl glycidyl ether (**7**) as outlined in Scheme 3.6. Numerous attempts to obtain block copolymers by sequential addition of the monomers resulted in failures. At every instance, the reaction resulted in the formation of a mixture of homopolymers which were separated as explained in the Experimental section. A plausible rationale is illustrated in

Scheme 3.7 where the hydride or butyl transfer to the second monomer might be able to initiate new chain thereby resulting in the formation of two homopolymers.

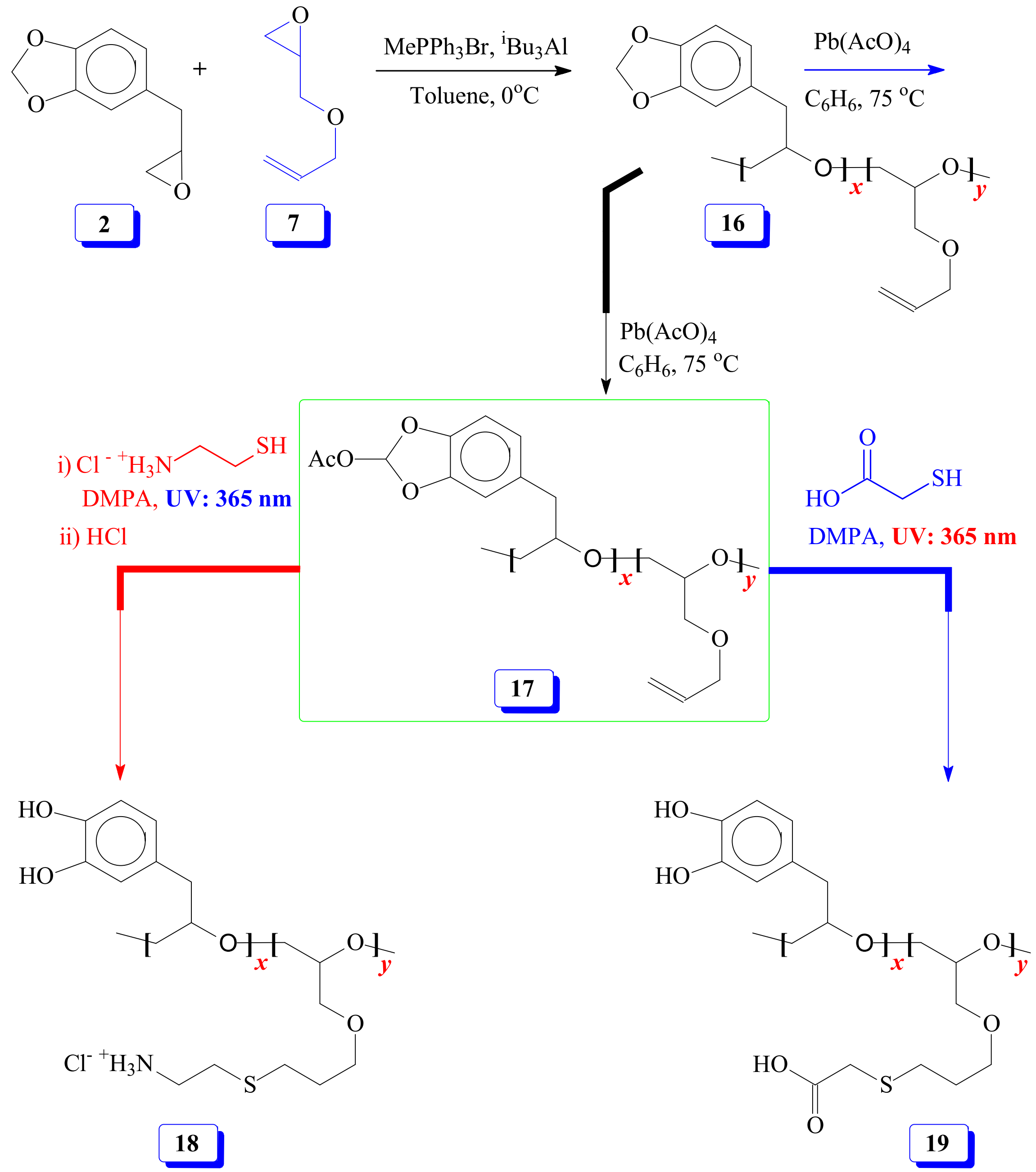

Scheme 3.6 Lewis acid catalyzed copolymerization of epoxides and thiol-ene reaction

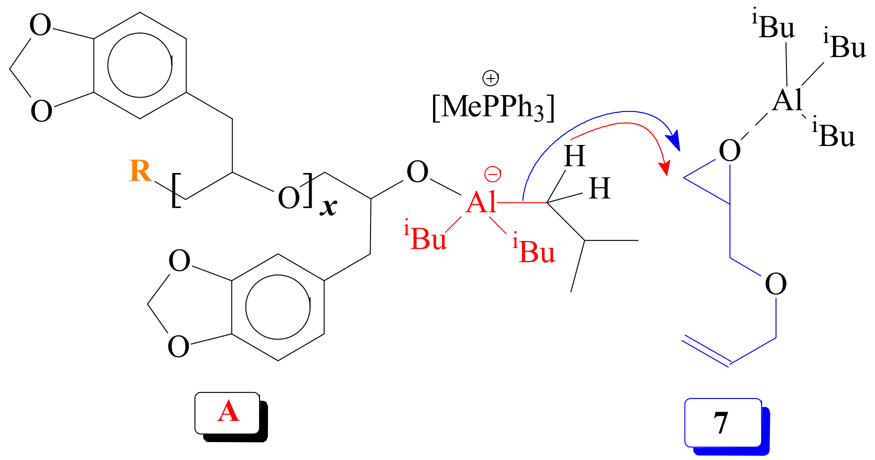

Scheme 3.7 A plausible hydride or isobutyl transfer to activated monomer **7**

We, therefore, shifted our attention to obtain the random copolymer from monomers **2** and **7** as shown in Scheme 3.6. Lewis acid catalysed polymerization of **2** and **7** afforded random copolymer **16** in excellent yields. The results are given in (Table 3.4).

Table 3-4 Random copolymerization[a] of Safrole Oxide (**SO**) **2** and allyl glycidyl ether **7** initiated/catalyzed by $MePPh_3Br$ /$^iBu_3Al$[b]

Entry	**SO** (mol%)[c]	$MePPh_3Br$ (mmol))	Toluene (ml)	$^iBu_3Al$ (mmol)	Temp (°C)	Time (h)	Yield (%)
1	50	0.063	2.5	0.835	20	20	91
2	50	0.065.	2.0	0.860	20	24	93
3	50	0.025	1.0	0.484	0	2	89
4[d]	50	0.042	3.0	0.513	0	18	92
5[e]	15	0.040	2.5	0.534	0	20	93

[a] Polymerization was carried out using a total of 5.0 mmol of monomer **2** and **7**.
[b] 25 wt. % solution in toluene (≈ 1 M $^iBu_3Al$).
[c] mol% of the monomer in the mixture of the two monomers.
[d] This reaction was run using a total of 35 mmol of **2** and **7,** however, calculations are shown for the total of 5.0 mmol.
[e] This reaction was run using a total of 50 mmol of **2** and **7,** however, calculations are shown for the total of 5.0 mmol.
.

The ^1H spectra of homopolymers **6** and **8** and their random copolymer **16** are displayed in Figure 3.10. The feed ratio of the monomers matched with incorporated ratio of the corresponding repeating units as determined by integration of several non-overlapping proton signals Figure 3.10c. The finding thus implies that the two monomers have equal reactivity ratio. The NMR presented in Figure 3.10c represents a polymer with 1:1 ratio of the monomer units.

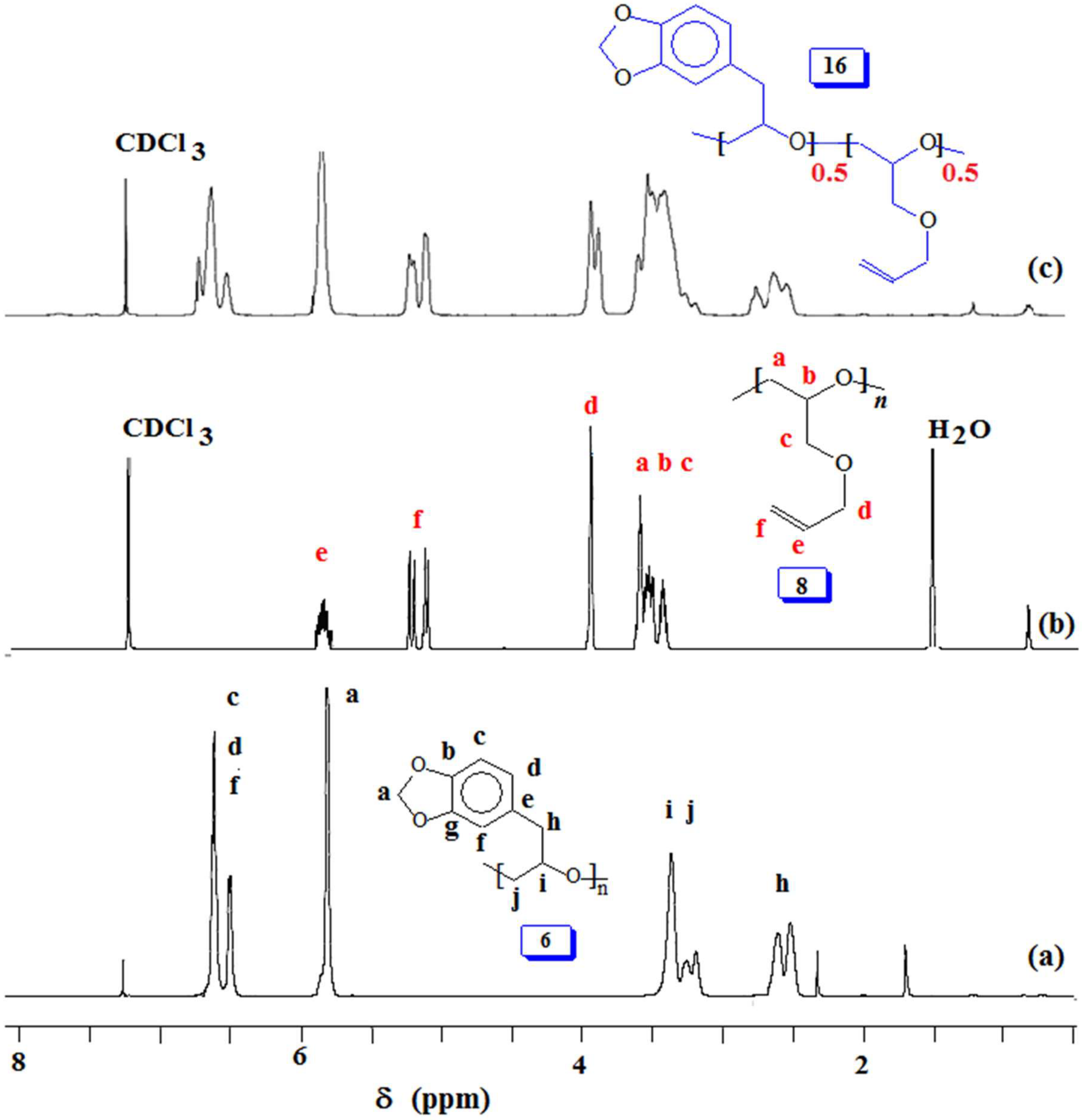

Figure 3.10 ^{1}H NMR spectra in CDCl$_3$ of (a) polymer **6**, (b) polymer **8** and (c) 1:1 random copolymer **16**

The 1:1 random copolymer **16** was then subjected to lead tetraacetate oxidation thereby giving copolymer **17** containing acetoxy group (*vide supra*, Scheme 3.6). The ^{1}H and ^{13}C NMR spectra of **16** and **17** are displayed in Figures 3.11 and 3.12, respectively. The proton marked 'a' (Figure 3.11a) is shifted downfield at 'a′' (Figure 3.11b) and the new CH_3CO protons marked 'd′' appeared at δ2 ppm as expected (Figure 3.11b). The ^{13}C NMR spectrum (Figure 3.12) also revealed the formation of acetoxy derivative **17**. The acetoxy carbons marked 'r′' and 'q′') appeared at δ20.5 and 170.3 ppm, respectively (Figure 3.12b). Also note that carbon marked 'a′' in **17** is shifted downfield as compared to 'a' of **16**.

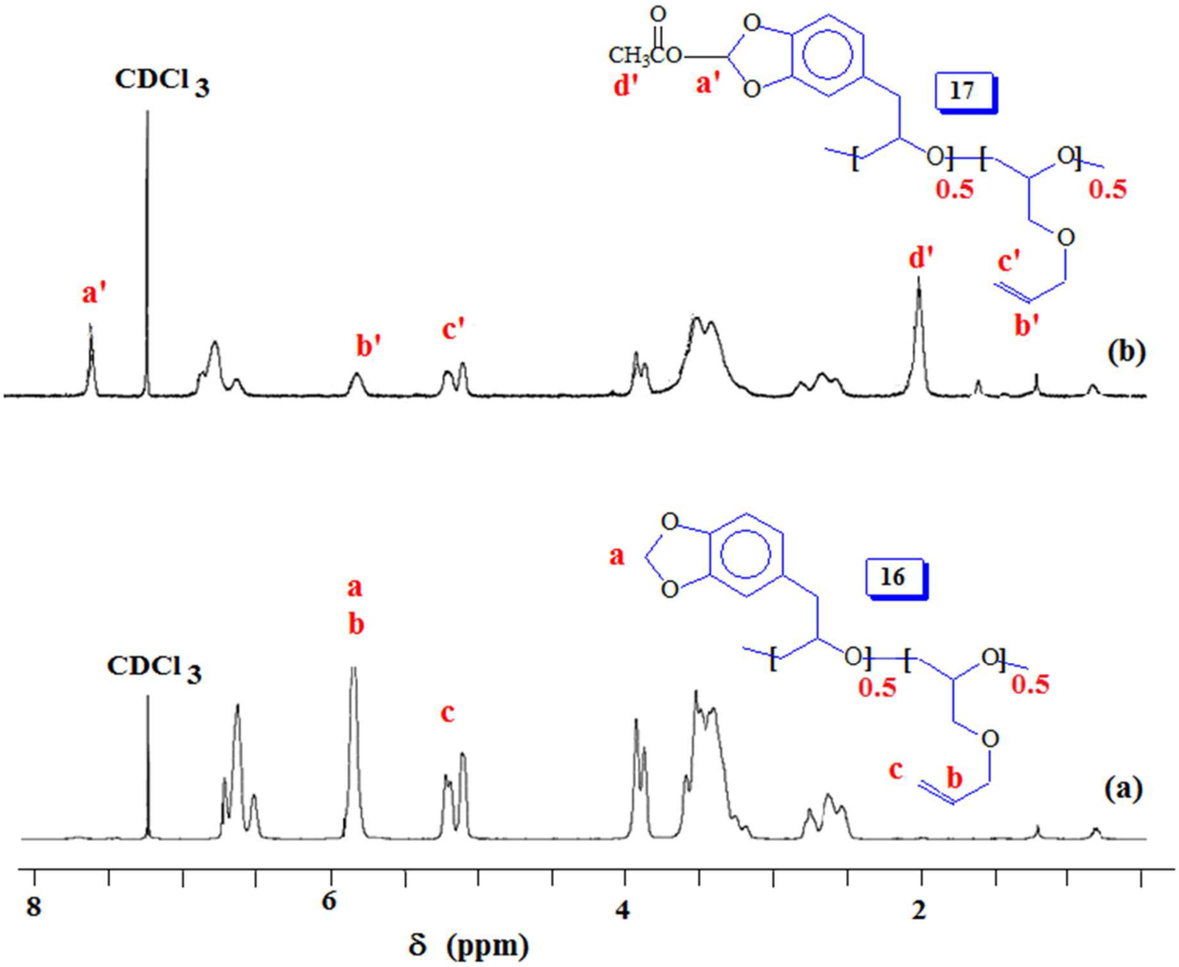

Figure 3.11 ^{1}H NMR spectra in $CDCl_3$ of (a) 1:1 random copolymer **16** and (b) 1:1 random copolymer **17**

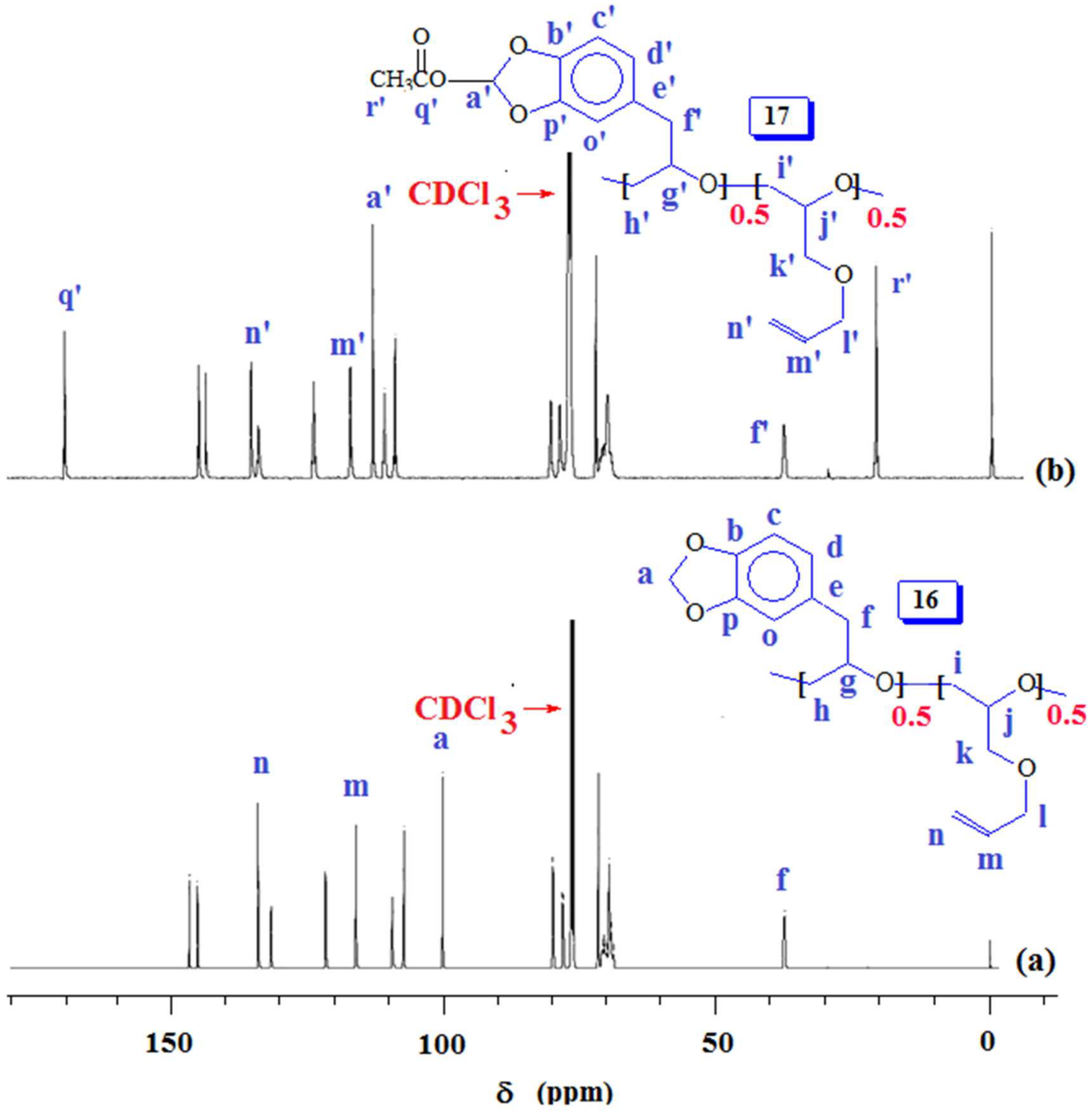

Figure 3.12 ^{1}H NMR spectra in CDCl$_3$ of (a) 1:1 random copolymer **16** and (b) 1:1 random copolymer **17**

The acetoxy derivative **17** was subjected to thio-ene reaction using photoinitiator 4-dimethylaminopyridine (DMAP) using UV light (λ = 365 nm). The addition of cystemine.HCl ($H_3N^+CH_2CH_2SH\ Cl^-$) and thioglycollic acid (HO_2CCH_2SH) to **17** with a 15:85 ratio of SO **2**/AGE **7** repeating units converted **17** to **18** and **19**, respectively (Scheme

3.6, *vide supra*). The ^{1}H NMR spectra of **17, 18** and **17**, displayed in Figure 3.13 confirms the successful transformation. The acetoxy proton signal (marked ‘d’, Figure 3.13a) disappeared in the spectra of **18** and **19** (Figure 3.13b and c) as a result of hydrolysis of the functional motifs during aqueous workup under mild acidic condition. This is further confirmed by the absence of the signal (for proton marked ‘c’, Figure 3.13a) in the spectra of **18** and **19**. The spectra are consistent with the addition of the thiol motifs into the alkene double bond as confirmed the absence of alkene proton signals in Figure 3.13b, and c. The aromatic protons are visible; chemical shifts of some of the readily identifiable protons are assigned. The work presented in the previous paragraph are repeated using silyl protected epoxide **14** which was copolymerized with allyl glycidyl ether **7** (Scheme 3.8) to give copolymer **20** having various proportions of the *x/y* units. The results of the polymerization are given in (Table 3.5). The silyl protected copolymer was then elaborated using thiol-ene reaction as discussed before to give **21** and **22**, which on treatment with HCl and Bu_4NF respectively afforded **18** and **19** after deprotection of the silyl groups. The spectra analysis revealed the identical nature of the polymers to the polymers derived *via* acetoxy protective groups (*vide supra*). The ^{1}H NMR spectra of random copolymer **20** with SP/AGE ratio of 1:1 and 0.15:0.85 are shown in Figure 3.14a and b, respectively. Figure 3.14c and d display the spectra for **21** and **22**; the absence of alkene protons in the range δ5-6 ppm clearly confirms the addition of the thio group onto the double bonds.

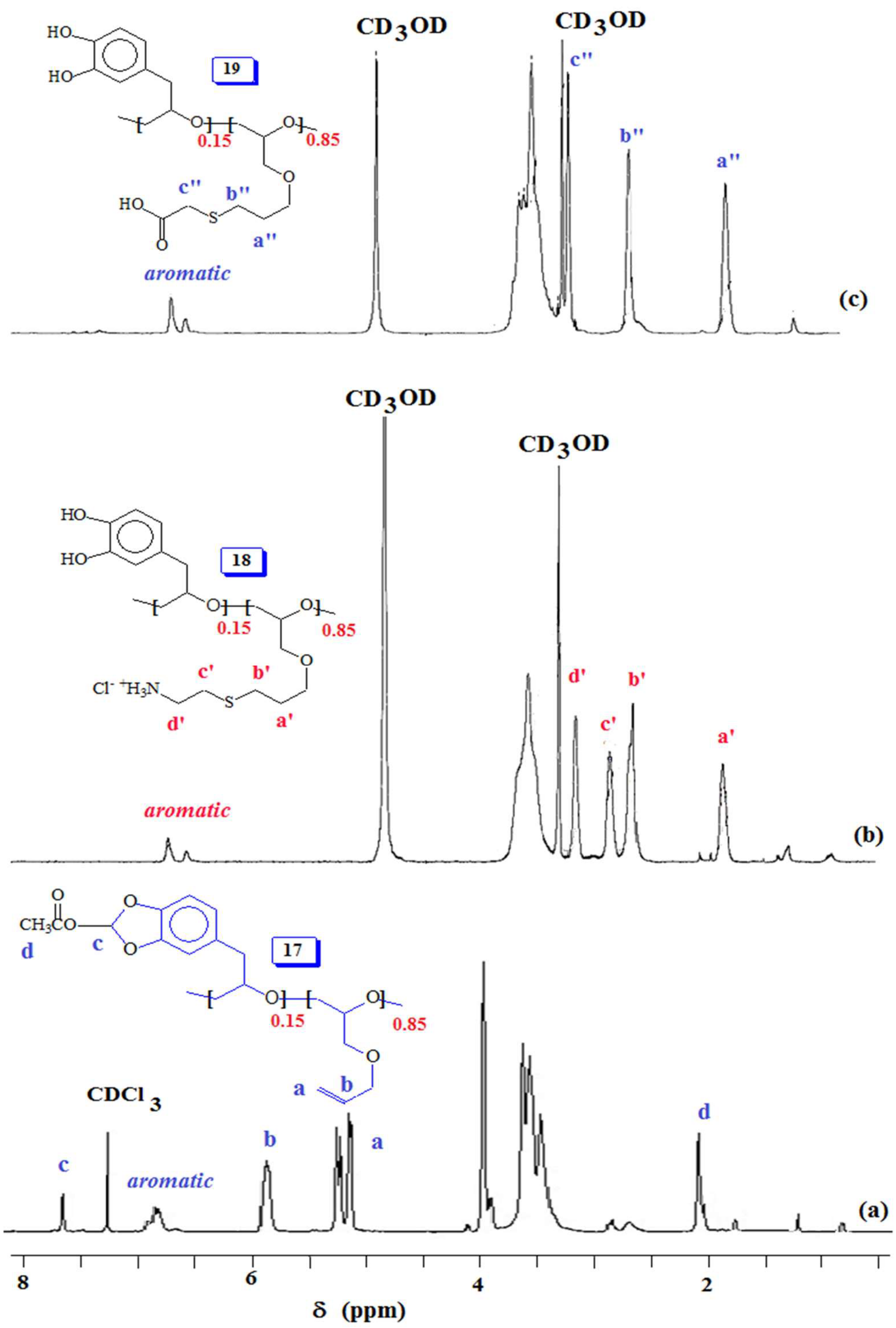

Figure 3.13 ^{1}H NMR spectra of 15:85 random copolymer (a) **17** in $CDCl_3$, (b) **18** in CD_3OD and (c) **19** in CD_3OD.

The thermogravimetric analysis (TGA) curve of copolymer **20** is shown in Figure 3.15. The first weight loss 11 % up to 281 °C is accounted for the removal of trapped solvent and moisture. The second loss of about 62 % in the range 281-418 °C. The third loss 21 % in the range 418-600 °C. At 394 °C the residual mass was found to be 4.8 %.

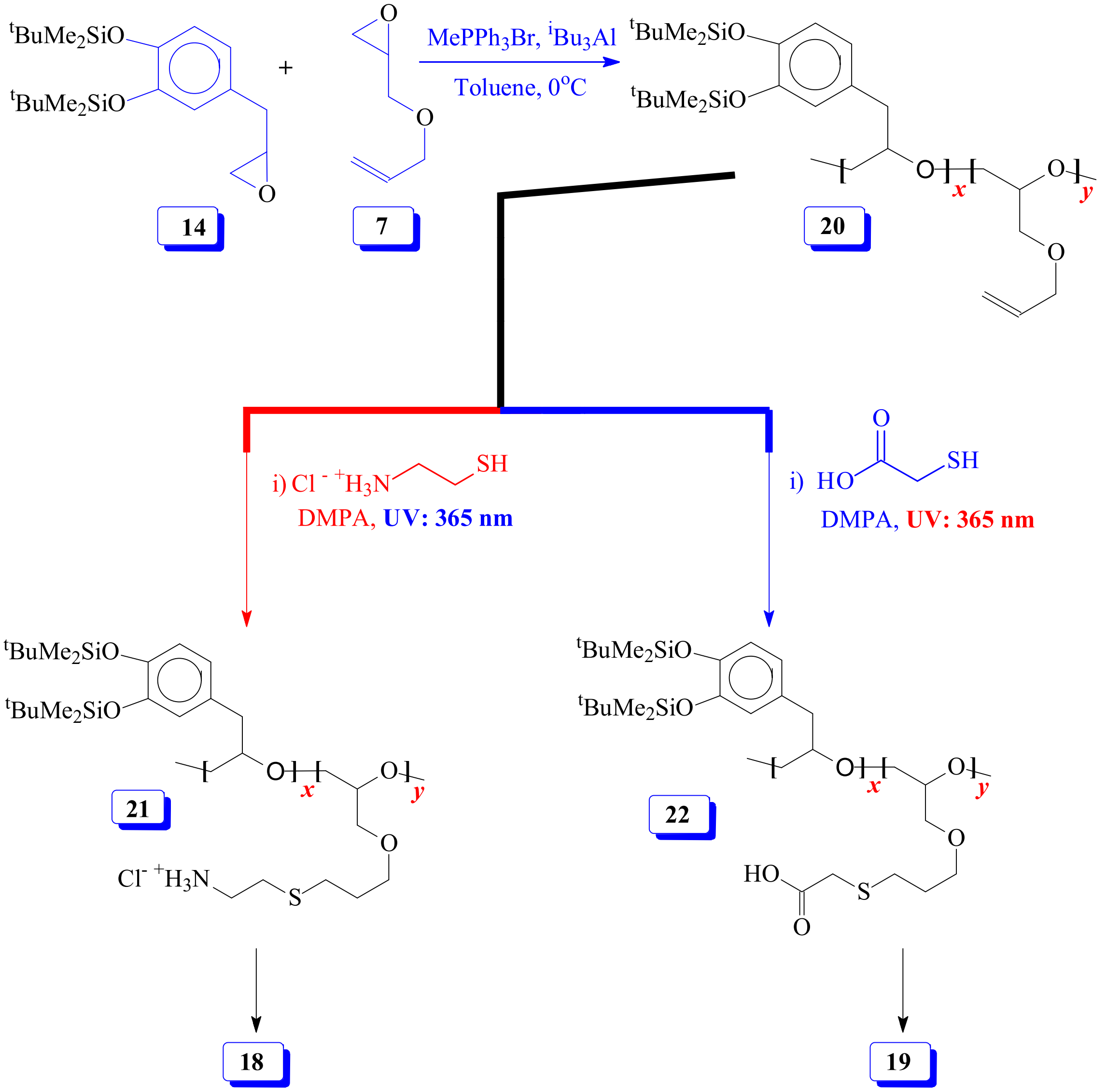

Scheme 3.8 Lewis acid catalyzed copolymerization of silylated epoxides and thio-ene reaction

Table 3-5 Random copolymerization[a] of silyl protected oxide (**SP**) **14** and allyl glycidyl ether **7** initiated with $MePPh_3Br$ (**I**) and catalyzed by $^iBu_3Al$ (**C**)[b]

Entry	**SP** (mol%)[c]	**I** (mmol)	[**M**][d] /[**I**]	**C** (mmol)	[**C**]/ [**I**]	Time (h)	Conv.[e,f] (%)	$M_{n,Theor}$	$M_{n,Exp}$[g]	PDI
1	50	0.045	111	0.76	17	3	88 (88)			
2	50	0.053	94	0.76	14	5	95 (99)	22600	14300	1.5
3	25	0.045	111	0.50	11	12	99 (99)	20500	12700	1.3
4	10	0.045	111	0.50	11	12	96 (99)	15800	6100	2
5	10	0.092	54	0.50	5	3	84 (99)			
6	10	0.012	417	0.50	42	15	78 (93)			
7[h]	10	0.032	156	0.50	16	17	99 (99)			
8	5	0.045	111	0.50	11	12	98 (99)	14200	5900	2.1

[a] Polymerization was carried out at 0 °C using a total of 5.0 mmol of monomer **14** and **7** with an additional amount toluene added (3.5 mL) .

[b] 25 wt. % solution in toluene (≈ 1 M $^iBu_3Al$).

[c] mol% of the monomer in the mixture of the two monomers.

[d] Total monomers of silyl protected oxide **14** and allyl glycidyl ether **7** is 5 mmol.

[e] % conversion monomer **14** as determined by ^1H NMR, the number in parentheses belongs to % conversion of AGE **7**.

[f] Isolated yield was in the range 85-95%

[g] GPC with a light scattering detector

[h] This reaction was run using a total of 30 mmol of **2** and **7;** however calculation are based on a total of 5.0 mmol of monomers **2** and **7**.

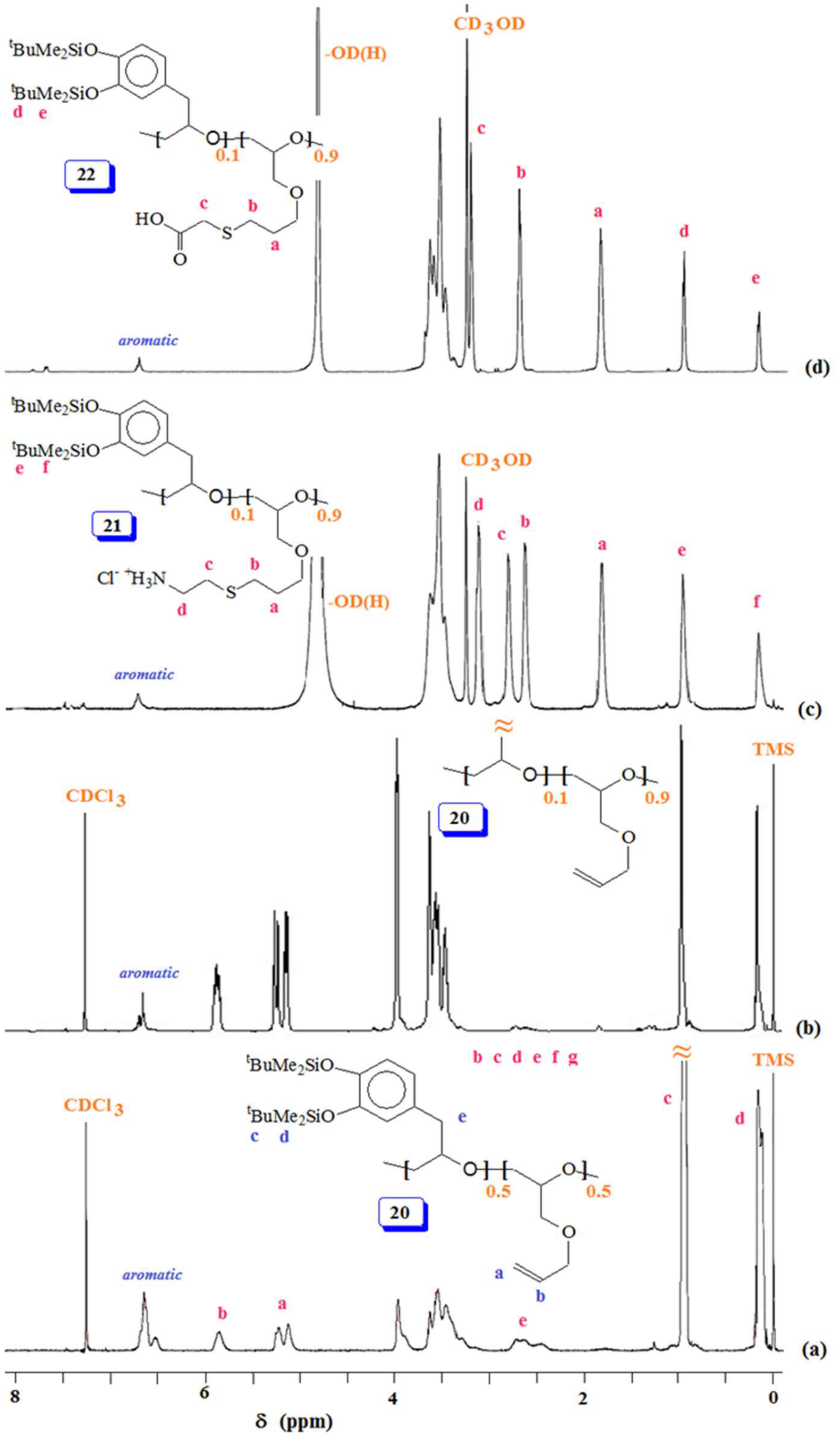

tBuMe2SiO
tBuMe2SiO
d e
0.1
0.9
22
HO
O
S
c
b
a
-OD(H)
CD3OD
c
b
a
d
e
aromatic
(d)
tBuMe2SiO
tBuMe2SiO
e f
0.1
0.9
21
Cl- +H3N
S
d
c
b
a
CD3OD
d
c
b
a
e
f
-OD(H)
aromatic
(c)
CDCl3
20
0.1
0.9
TMS
aromatic
(b)
b c d e f g
tBuMe2SiO
tBuMe2SiO
c d
e
0.5
0.5
20
a
b
CDCl3
TMS
c
d
aromatic
b
a
e
(a)
8
6
4
2
0
δ (ppm)

Figure 3.14 ^{1}H NMR spectra of (a) 50:50 copolymer **20** in $CDCl_3$, (b) 10:90 copolymer **20**.in $CDCl_3$, (c) 10:90 copolymer **21** in CD_3OD and (d) 10:90 copolymer **22** in CD_3OD

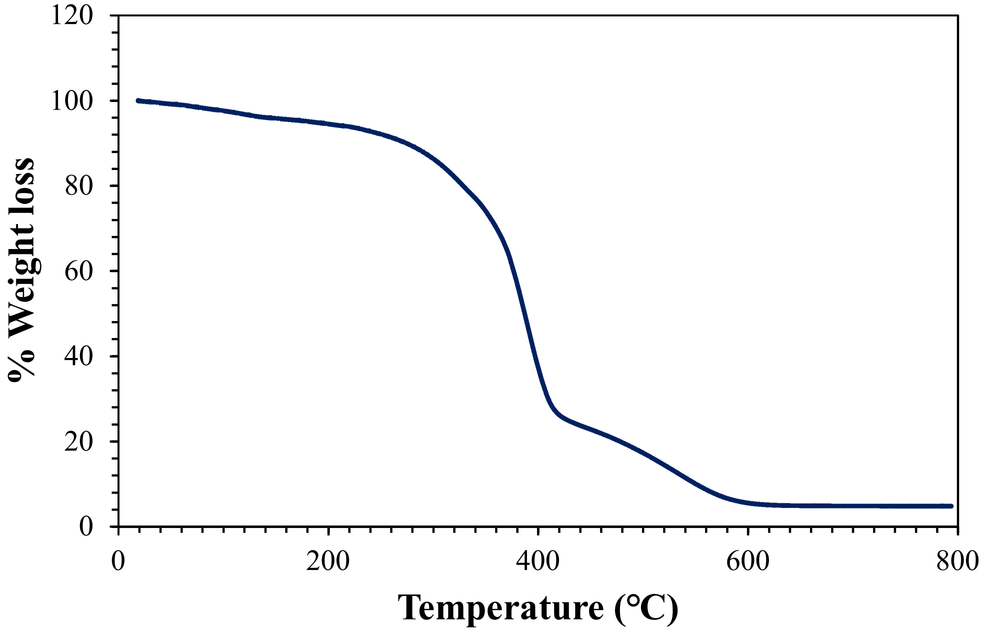

Figure 3.15 TGA Analysis for copolymer **20**

3.5 Conclusions

To the best of our knowledge, safrole oxide **2,** derived from naturally occurring safrole **1** has been homo- as well as copolymerized with allyl glycidyl ether **7** for the first time. The random polymers thus obtained were elaborated by incorporating anionic (CO_2^-) and cationic (NH_3^+) group on the terminal of the pendants by thiol-ene reaction. The polymer backbones having charges of either algebraic signs could be used for the formation of complex coacervate by electrostatic attraction. Such complex is expected to be adsorbed on a surface where the catechol motifs would stabilize the adhesion. A way has been found to remove the acetal protective group under mild conditions using lead tetracetate to generate catechol moieties on the polymer backbone. Use of tert-butyldimethyl groups as a protective group for the catechol motifs has also been explored.

CHAPTER 4

COPOLYMERIZATION OF SESAMOL-BASED OXIDE AND ALLYL GLYCIDYL ETHER AND ELABORATION OF ALKENE PENDANTS

4.1 Abstract

Naturally occurring sesamol (**26**) has been converted to epoxy monomer **27** by reacting with epibromohydrin **25**. Monomer **27** has been polymerized for the first time using a variety of basic tetrabutylammonium hydroxide and tetrabutylammonium fluride as well as by Lewis acid initiator/catalyst comprising of triphenylmethylphosphonium bromide/triisobutylaluminum to obtain polyether **28** in excellent yields. Epoxy monomer **27** and allyl glycidyl ether **7** in various proportions have been randomly copolymerized to obtain random copolymer **29.** The methylene acetal was activated by placing an acetoxy group to obtain **31**. **T**he pendant allyl groups have been elaborated via thiol-ene reaction using cysteamine hydrochloride to obtain cationic copolymer **32** required for formation of coacervate.

4.2 Introduction

Sesamol **(26)** is a component of sesame seeds and sesame oil. Sesamol has been found to be an antioxidant [139], [140] and can act as an antifungal [141]. Sesamol is used as a precursor in the industrial synthesis of the pharmaceutical drug paroxetine (Paxil) [142]. Sesame oil is used in Ayurvedic Medicine [143]. Chelation therapy is administered for the management of heavy metal-induced toxicity; however, it usually causes adverse effects. Sesame oil (a natural edible oil) and sesamol (an active antioxidant) are potently beneficial for treating lead- and iron-induced hepatic and renal toxicity and have no adverse effects. A review article deals with the possible use and beneficial effects of sesame oil and sesamol during heavy metal toxicity treatment [144].

It is our objective to use sesamol **26** as part of an epoxide **27** which could be used to obtain ring opened homo and copolymers (Scheme 4.8). The polymers are expected to have metal chelating properties. Also, it can serve as a bio-mimic of mussel adhesives discussed in earlier chapters.

4.3 Experimental

4.3.1 Materials

tert-Butylammonium fluoride (TBAF.3H_2O), tert-butylammonium hydroxide (TBAH), 4-dimethylaminopyridine (DMAP), $^{i}Bu_3Al$ solution (25 wt% in Toluene, 1 M), 2-butanone, allyl alcohol, 2,2-dimethoxy-2-phenylacetophenone (DMPA), t-butyldimethylsilyl chloride (TBDMSCl), cysteamine-HCl, thioglycolic acid and safrole purchased from Aldrich Chemical, $MePPh_3Br$, imidazole and CaH_2 purchased from Fluka, 1M tert-butylammonium fluoride (TBAF) solution in THF purchased from ChemCruz, and diphenylsilane and $B(C_6F_5)_3$ purchased from Alfa Aesar were used as received. Allyl glycidyl ether from Aldrich was dried over CaH_2 and distilled. All solvents were of HPLC grade. Lead tetra acetate $Pb(AcO)_4$ was freshly prepared as described [116]. For dialysis, membrane (Spectra/Por) with a MWCO of 6000-8000 was purchase from Spectrum Laboratories, Inc.

4.3.2 Physical Methods

A Perkin Elmer (Series II Model 2400) Elemental Analyzer and a Fourier transform infrared (FTIR) spectrometer (Perkin Elmer 16F PC) were utilized for elemental analyses and IR spectroscopy, respectively. The nuclear magnetic resonance (NMR) spectra were recorded using a 500-MHz JEOL LA spectrometer. Tetramethylsilane (TMS) in $CDCl_3$ and residual H in D_2O at δ4.65 ppm were used as internal standards. The ^{13}C chemical shifts in D_2O were referenced against ^{13}C peak of external standard dioxane at δ 67.4 ppm. The TGA was carried out under O_2 by using a SDT analyser (Q600: TA Instruments).

4.3.3 Synthesis of 2,3-dibromo-1-propanol 24 [145]

To an ice-cooled stirred solution of allyl alcohol **23** (24.39 g, 0.42 mol) in CCl_4 (70 mL) was added dropwise for 30 min a solution of liquid bromine (67.9 g, 0.42 mol) in CCl_4 (70 mL). After complete addition, the reaction was stirred at room temperature for 15 min. The reaction mixture was concentrated under nitrogen, and then it was distilled under vacuum to give pure product **24** (B.P. 94-95 °C at 9 mm Hg) 71.5 g (78% yield), δ_H ($CDCl_3$): 3.78-3.84 (2H, m), 4.03 (2H, d, *J* 3.8 Hz), 4.30-4.35 (1H, m).

4.3.4 Synthesis of epibromohydrin 25 [146], [147].

A solution of 2,3-dibromopropanol **24** (71 g, 0.33 mol) in ether (600 ml) was stirred with 30% NaOH solution (260 g) for 2 h at 40 °C. The ether layer was separated, dried (Na_2SO_4) and concentrated. The residual liquid obtained was purified by distillation under vacuum to obtain **25** (30 g, 66%). δ_H ($CDCl_3$): 2.67-2.68 (1H, m), 2.94-2.96 (1H, m), 3.26-3.45 (3H, m). δ_C ($CDCl_3$): 32.6, 48.6, 51.3.

The low yield could be attributed to the hydrolysis of epibromohydrin in the presence of NaOH to give glycerol [148].

4.3.5 Synthesis of 3,4-methylenedioxy-1-oxyranylmethoxybenzene 27 [149]–[151].

The solution of sesamol **26** (10.4 g, 75 mmol), epibromohydrin **25** (17.8 g, 130 mmol), 2-butanone (90 mL) and potassium carbonate (40.0 g, 290 mmol) was refluxed overnight. The reaction mixture was cooled to room temperature, filtered and washed with ether to remove inorganic salts. The filtrate was concentrated, dissolved in CH_2Cl_2 (100 mL) and washed with 1% NaOH (2×40 mL) and H_2O (20 mL), dried with Na_2SO_4, and concentrated. The residual liquid was distilled to get product **27** ($bp_{0.1mm\ Hg}$ 103 °C) (10.4 g, 71%). δ_H ($CDCl_3$): 2.72-2.74 (1H, m), 2.88-2.89 (1H, m), 3.30-3.33 (1H, m), 3.87 (1H, dd, *J* 5.5 Hz, *J* 11.0 Hz), 4.22 (1H, dd, *J* 3.2 Hz, *J* 11.1 Hz), 5.91 (2H, s), 6.33 (1H, dd, *J* 2.5 Hz, *J* 8.5 Hz), 6.52 (1H,d, *J* 2.5 Hz), 6.69 (1H, d, *J* 8.5). δ_C ($CDCl_3$): 44.6, 50.1, 69.8, 98.4, 101.2, 105.9, 107.9, 142.1, 148.3, 154.0.

4.3.6 Polymerization of 27 using tetrabutylammonium derivatives [152]–[155]

4.3.6.1 General procedure

TBAF (1 M in THF) was placed in a flask, and the THF was removed under N_2. Monomer **27** was added and stirred at 50 °C until the reaction was complete as indicated by ^1H NMR spectrum. The reaction mixture was dissolved in CH_2Cl_2 and washed with water three times. The organic layer was dried (Na_2SO_4) and concentrated to obtain polymer **28**.

4.3.6.2 Time versus percent conversion of monomer 27 to polymer 28

A specific reaction involved the use of TBAF (0.125 mmol from 1 M in THF). The TBAF in THF was taken in a flask and the solvent was removed under N_2 followed by vacuum. Monomer **27** (2.5 mmol) was then added and stirred at 50 °C. ^1H NMR spectra were recorded at several intervals and the results are given in Figure 4.1. The present conversion was determined using area integration of severeal proton signals of the polymer and the monomer.

4.3.7 Polymerization of 27 using $MePPh_3Br$ and $^iBu_3Al$

General Procedure

Methyltriphenylphosphonium bromide (12.0 mg, 0.033 mmol) was placed in a round bottom flask under Ar and closed with rubber septum. Monomer **27** (550 mg, 2.83 mmol), and anhydrous toluene (1.5 ml) were added by a syringe under Ar. The mixture was cooled to 0 ºC, then triisobutylaluminium solution (25 wt % in toluene) (0.4 mL) was added by syringe under Ar as one portion. The polymerization was stopped after 2 h by adding 4/1 v/v MeOH/H_2O (5 mL). The reaction mixture was extracted with CH_2Cl_2, dried over anhydrous (Na_2SO_4), filtered over celite 545.and evaporated to obtain **28** as a solid **(**530 mg, 96%). $\nu_{max.}$ KBr: 3527, 3086, 2879, 2778, 1633, 1510, 1287, 986, 922, 787, 738, 703, and 610 cm^{-1}.

4.3.8 Random copolymerization of 27 and allyl glycidyl ether 7 by using MePPh$_3$Br and ^{i}Bu$_3$Al.

General Procedure

Methyltriphenylphosphonium bromide (100 mg, 0.28 mmol) was placed in a round bottom flask under Ar and closed with rubber septum. Monomer **27** (1.7 g, 8.6 mmol), allyl glycidyl ether **7** (3.9 g, 33.8 mmol) and anhydrous toluene were added by syringe under Ar. The mixture was allowed to cool to 0 ºC, and then triisobutylaluminium solution (25 wt. % in toluene) (4.2 mL, 4.2 mmol) was added by a syringe under Ar as one portion. The polymerization was terminated by adding 4:1 v/v MeOH/H_2O (50 mL). After removal of the solvents, the residual mixture was dissolved in CH_2Cl_2 (50 mL) and filtered over celite 545. The organic layer was dried ($MgSO_4$), filtered and evaporated to afford a 20:80 random polymer **29** (5.3 g, 96%). $\nu_{max.}$ KBr: 3485, 3081, 3017, 2919, 2866, 1635, 1496, 1355, 1255, 1192, 1134, 991, 925, 846, 738, 697, 614, and 561 cm^{-1}.

4.3.9 Lead tetraacetate oxidation to activate O-CH$_2$-O in the copolymer 29 [122], [156].

Pb(OAc)$_4$ (2.0 g, 4.5 mmol) was added under N_2 to a solution of copolymer **29** (1.90 g, 14.6 mmol) in benzene (25 mL), and stirred at 75 ºC under N_2 for 24 h. The reaction mixture was diluted with EtOAc (35 mL) and washed with H_2O (3×30 mL). The EtOAc layer was dried over anhydrous sodium sulfate and concentrated to give **31**. $\nu_{max.}$ KBr: 3503, 3080, 3015, 2927, 2869, 1841, 1759, 1645, 1613, 1497, 1367, 1224, 1189, 917, 844, 789, 758, 711, 669, 615, and 560 cm^{-1}.

4.3.10 Thiol−Ene reaction of cysteamine to vinyl double bonds in 29 [125].

To a solution of copolymer **29** (x = 0.2, y = 0.8) (625 mg, 4.8 mmol) in 2:1 THF/MeOH (4.5 mL) was added cysteamine.HCl (2.0 g, 19 mmol) and photoinitiator DMPA (0.488 g, 1.9 mmol). The mixture was purged with N_2 for 10 min, and then irradiated with a 365 nm UV lamp until completion of the reaction (5 h). The mixture was dialyzed against water and then freeze-dried to obtain polymer **30** (0.750 g, 66%). $\nu_{max.}$ KBr: 3585, 3414, 3083, 2963, 1490, 1406, 1260, 1189, 1099, 1017, 869, 798, and 677 cm^{-1}.

4.3.11 Thiol−Ene reaction of cysteamine to vinyl double bonds in 31 [125].

To a solution of copolymer **31** (x = 0.2, y = 0.8) (0.30 g, 2.1 mmol) in 2:1 THF/MeOH (3.5 mL) was added cysteamine.HCl (0.96 g, 8.4 mmol) and photoinitiator DMPA (0.215 g, 0.84 mmol). The mixture was purged with N_2 for 10 min, and then irradiated with a 365 nm UV lamp until completion of the reaction (6 h). The mixture was dialyzed against 0.1 M HCl and the resultant solution was freeze-dried to obtain polymer **32** (0.36 g, 75%). $\nu_{max.}$ KBr: 3471, 3424, 3081, 2917, 2869, 1622, 1488, 1354, 1257, 1189, 1101, 1029, 928, 801, 678, and 554 cm^{-1}.

4.4 Results and Discussion

Epibromohydrin **25** was prepared as described in Scheme 4.1. Sesamol **26** was alkylated using **25** to obtain epoxide monomer **27**. The polymerization reaction was carried out using base or acid catalysed ring opening process to obtain polyether **28** having the pendants of sesamol residues. Polymerization catalysed by Bu_4NOH is expected have ‘OH’ groups on the both terminals, while catalysis by Bu_4NF is expected to insert ‘F’ on one end of the chain. As discussed earlier, Lewis acid catalysed polymerization would place ^{i}Bu, H, and Br at one end of polymer **28**.

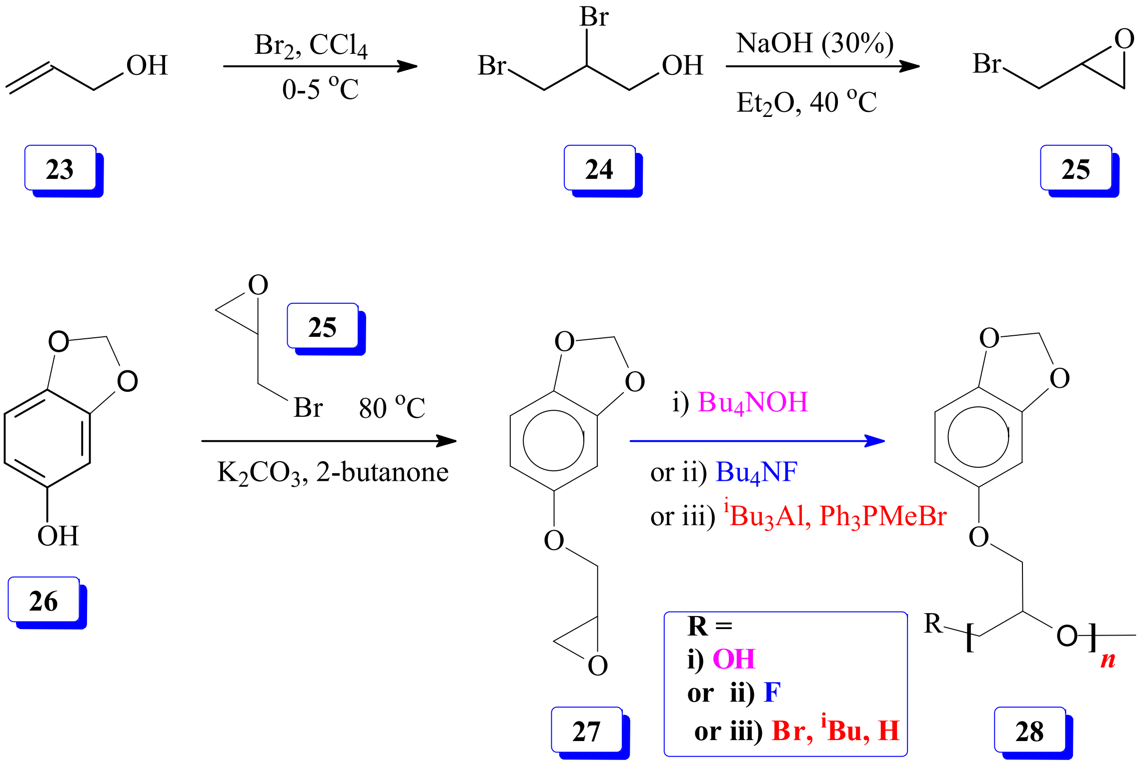

Scheme 4.1 Base as well as Lewis acid catalyzed polymerization of sisamol oxide

Conversion versus time profile for the polymerization reaction cried out under TBAF catalysis is shown in Figure 4.1. The percent conversion after a time interval was determined by ^{1}H NMR technique; at each interval, a small portion of the reaction mixture was withdrawn and quenched to terminate the propagation process. Figure 4.1 reveals that 50% conversion had occurred after 90 min.

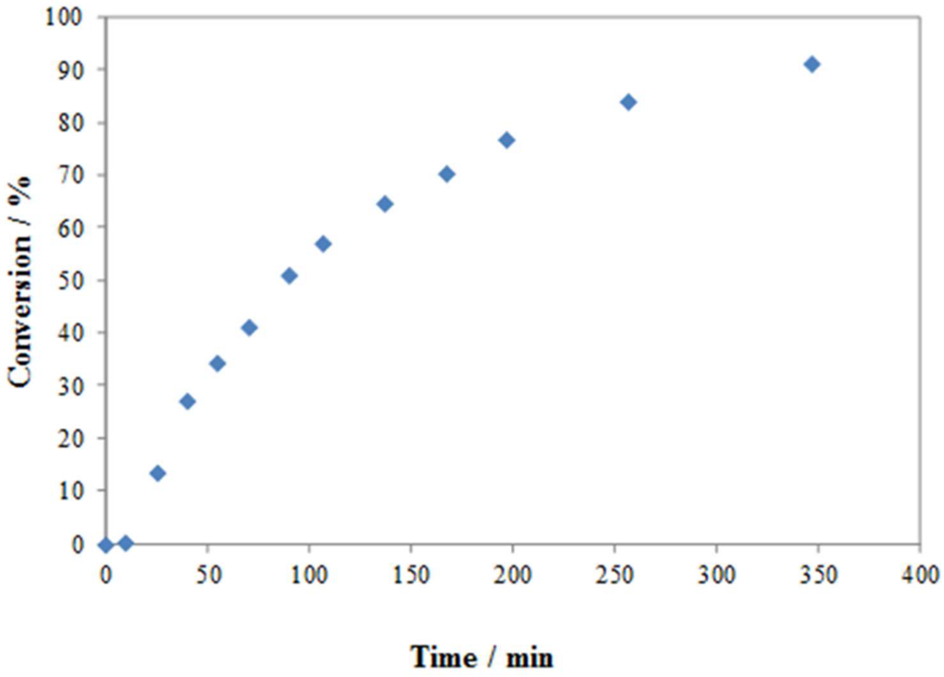

Figure 4.1 Percent conversion of sesamol-based oxide **27** to polymer **28** under TBAF cataysed polymerization

The results of the polymerizations are given in (Table 4.1). The Table includes PDI and molar masses. The M_n values are determined to be less than the theoretical values thereby suggesting chain transfer rection. The polymerization reactions afforded polymer in excellent yield (Table 4.1). The polymerization catalysed by TBOH (entry 6, Table 4.1) afforded polymer with a higher molar mass that the polymer obtained via catalysis of TBAF (entries 1-5).

Table 4-1 Polymerization[a] of sesamol derived monomer (**SD**) **27** initiated by TBAF (**I**)[b]

Entry	**I** (mmol)	[**SD**]/[**I**]	Time (h)	Conv.[c,d] (%)	$M_{n,Theor}$	$M_{n,Exp}$[e]	PDI
1	0.10	25	6	85			
			26	96	4,900	1532	1.2
2[e]	0.025	100	6	1			
			24	7			
			32	11			
			69	89			
			93	93			
			117	95			
			141	98	19,400	1230	2.6
3	0.075	33	6	80			
			24	94			
			46	98	6,400	1529	1.2
4	0.175	14	18	99	2,700	1264	1.2
5	0.225	11	6	98	2,100	1169	1.3
6[f]	0.10	25	6	98	4,900	2985	1.4

[a] Polymerization was carried out at 50 °C using 2.5 mmol of monomer **27**.

[b] 1M in THF

[c] Conversion as determined by ^{1}H NMR.

[d] Isolated yield of all the polymers were > 90% in each case.

[e] GPC with a light scattering detector

[f] TBOH (40 wt% in water) instead of TBAF

The ^{1}H and ^{13}C NMR spectra of monomer **27** and its corresponding polymers using different catalysts are shown in Figures 4.2 and 4.3, respectively. There are minor differences in the ^{1}H spectrum of **28** obtained by base and Lewis acid catalysed polymerization (cf. Figure 4.2b,c vs. d) in the region of δ3.5 ppm. Note that the CH_2F protons attached at one end of **28** is displayed at δ4.6 ppm as a minor signal (Figure 4.2c). While the signal pattern of the aromatic carbons remains similar in the monomer and polymer, there are some differences in the complexity of the carbons attached to oxygen as a result of differences in the microstructure of the polymers obtained via base or Lewis acid catalysed polymerization (Figure 4.3).

Assuming no chain transfer for polymerization catalysed by TBAF, the polymer sample **28** from entry 4 (Table 4.1) revealed its molar mass (Mn) of 5000 g mol^{-1} as determined by end group analysis involving area integration of CH_2F protons versus the aromatic proton signals Figure 4.2c. The experiment Mn value of 1260 therfore reveals the involvement of extensive chain transfer.

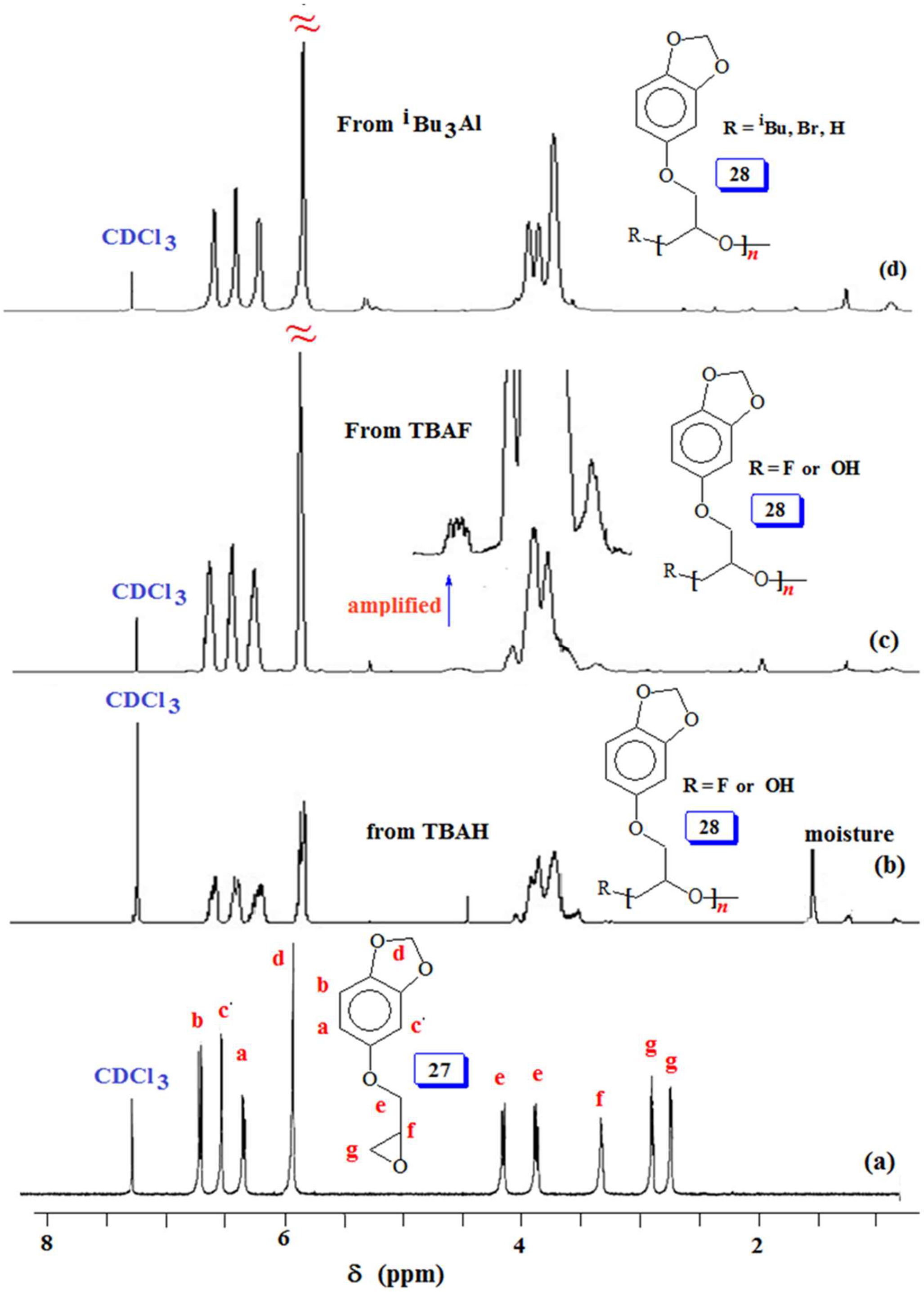

Figure 4.2 ^{1}H NMR spectra in CDC$_3$ of (a) sesamol-based oxide **27**; and polymer **28** obtained using initiator (b) TBAH, (c) TBAF and (d) Lewis acid

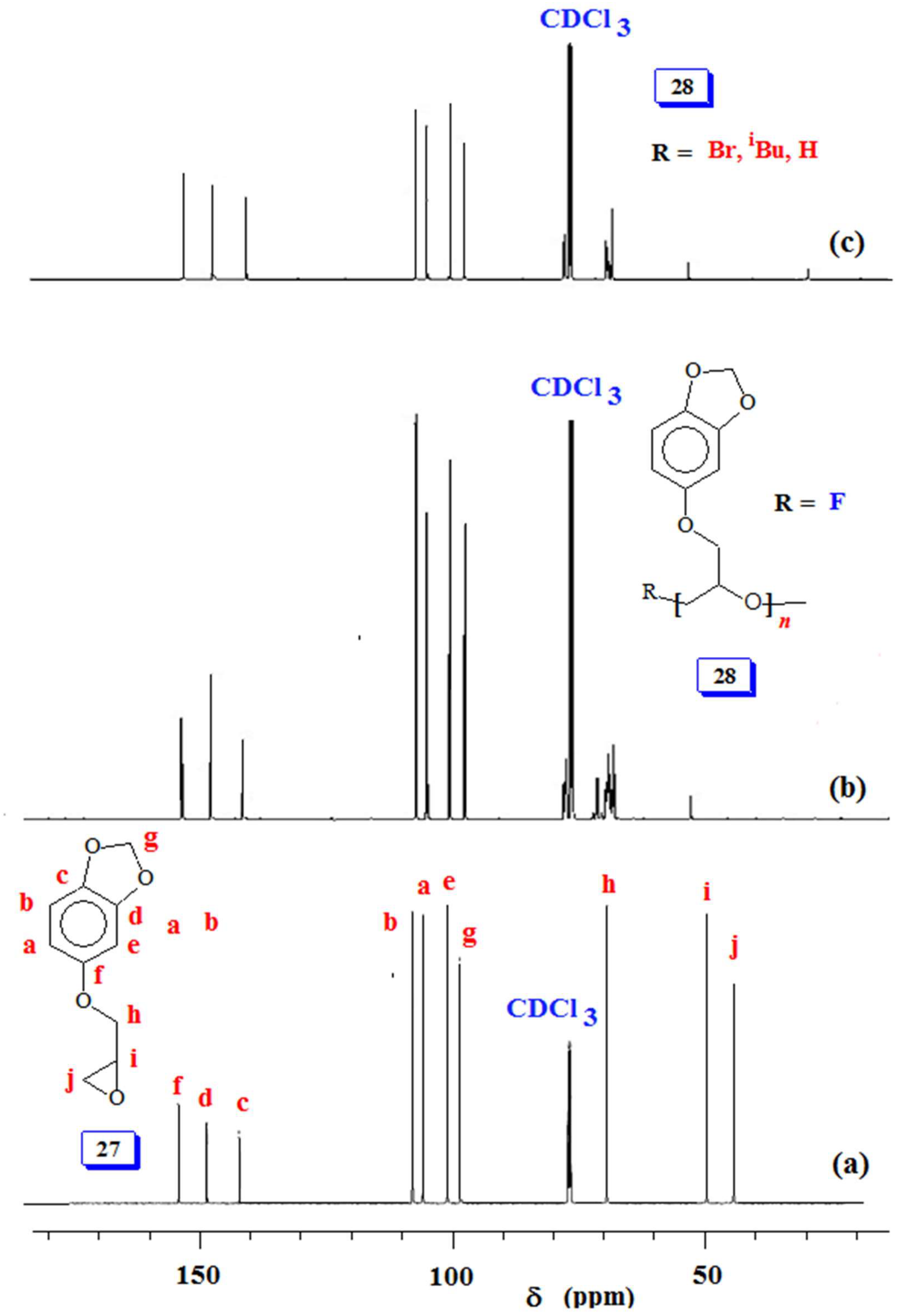

Figure 4.3 ^{13}C NMR spectra in $CDCCl_3$ of (a) sesamol-based oxide **27**; and polymer **28** obtained using initiator (b) TBAF and (c) Lewis acid

The thermogravimetric analysis (TGA) curve of polymer **28** is shown in Figure 4.2. The first weight loss 9% up to 350 is accounted for the removal of trapped solvent and moisture. The second loss of about 34% in the range 350-413. The third loss 56% is in the range 423-594. At 793, the residual mass was found to be 0.9%.

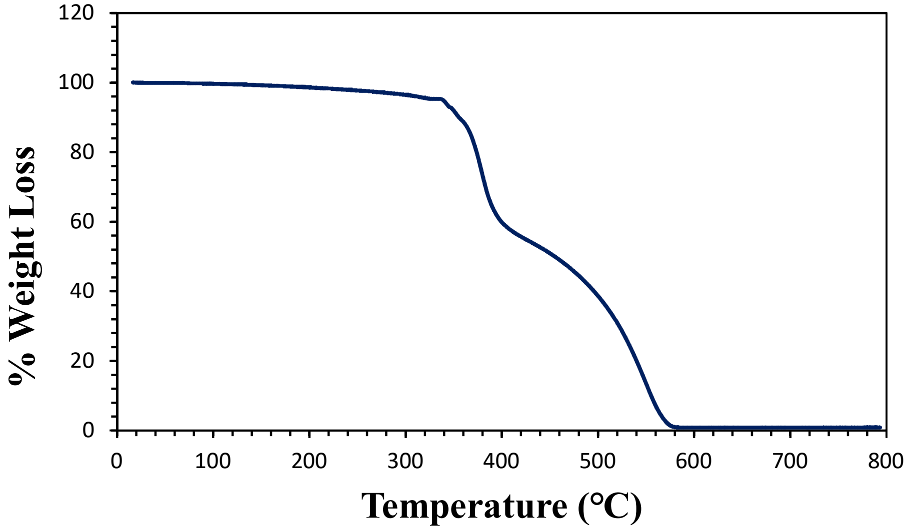

Figure 4.4 TGA curve of polymer **28**

Copolymerization of **27** and **7** under Lewis acid catalysis afforded copolymer **29** (x=0.2, y=0.8) which upon thiol-ene reaction [125] using cysteamine.HCl gave **30** (Scheme 4.2). As before, the O-CH_2-O motifs in **29** were activated using lead tetraacetate to obtain **31** containing the labile acetoxy substituent. Polyether **31** was then elaborated by thiol-ene reaction which converted it to **32**; during aqueous work up, the acetal group is deprotected.

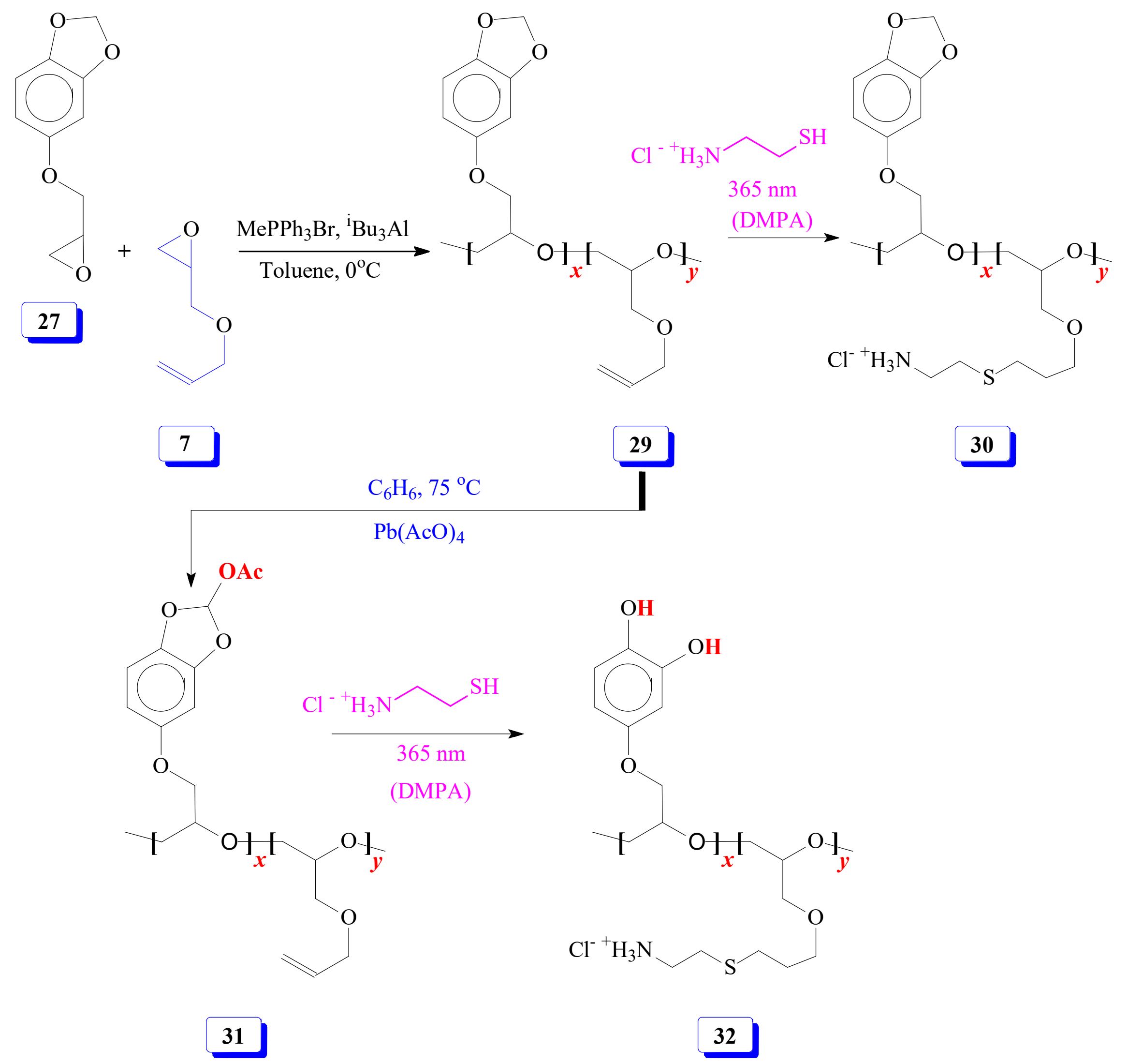

Scheme 4.2 Lewis acid catalyzed copolymerization of sisamol-based oxide **27** and allyl glycidyl ether **7**. thiolene and lead tetraacetate reaction of the copolymer.

The ^{1}H NMR spectra of **29-32** are shown in Figure 4.5. A sample of polymer **29** with a 20:80 ratio of repeating unit of sesamol derived monomer **27** and allyl glycidyl ether **7** was used for its conversion to **30-32**. The ratio of the repeating units was determined by area integration of several non overlapping signals such as 3 aromatic Hs versus 2 alkene Hs marked ‘c’ Figure 4.5a. The activation of methylene protons by acetoxy group is confirmed. The presence of acetyl proton is marked ‘d’ and acetal proton is marked ‘a’ in

Figure 4.5b. Alkenes protons disappeared after thiol-ene reaction in the spectra of **32** Figure 4.5c and **30** Figure 4.5d. The NMR spectra confirmed the incorporation cysteamine motifs.

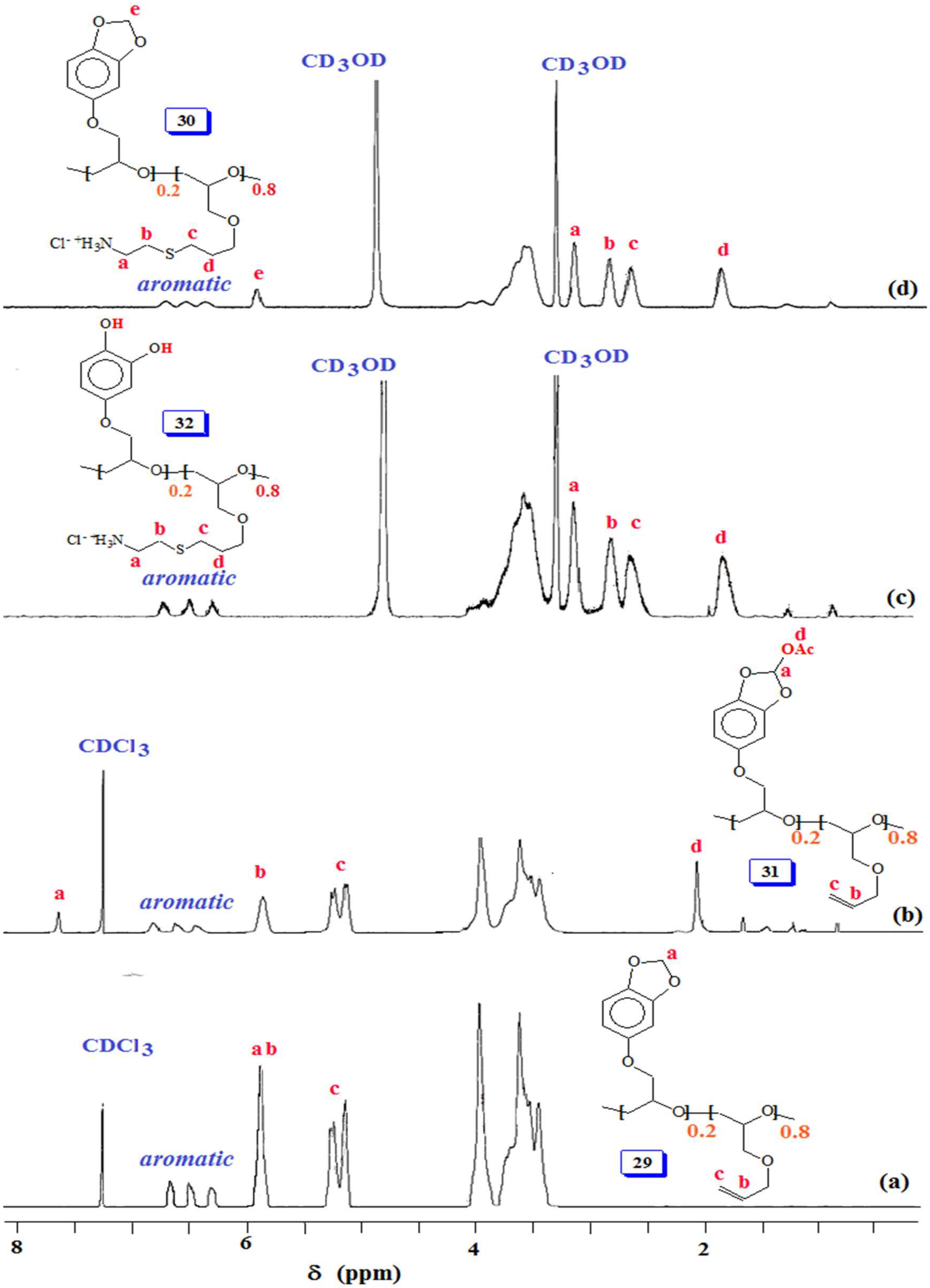

Figure 4.5 ^{1}H NMR spectra in $CDCl_3$ of copolymer (a) **29**, and (b) **31**; and in CD_3OD of copolymer (c) **32** and (d) **30**.

4.5 Conclusions

To our knowledge, oxide **27** derived from naturally occurring sesamol**,** has been homo- as well as copolymerized with allyl glycidyl ether **7** for the first time. The random polymers thus obtained were elaborated by incorporating cationic (NH_3^+) group on the terminal of the pendants by thiol-ene reaction. A way has been found to remove the acetal protective group under mild conditions using lead tetracetate to generate catechol moieties on the polymer backbone.

CHAPTER 5

POLYMERIZATION OF PYROGALLOL-DERIVED EPOXIDE

5.1 Abstract

Pyrogallol **32,** obtained by heating induced decarboxylation of naturally occurring gallic acid, has been protected as methylene acetal **33**. The free hydroxyl group in **33** is converted to epoxy monomer **34** by reacting with epibromohydrin **25**. Monomer **34** has been polymerized for the first time using Lewis acid initiator/catalyst comprising of triphenylmethylphosphonium bromide/triisobutylaluminum to obtain polyether **35** in excellent yields.

5.2 Introduction

Pyrogallol **32** is obtained by heating induced decarboxylation of naturally occurring gallic acid (3,4,5-trihydroxybenzoic acid) [157]. Pyrogallol is sensitive toward oxygen. In colorless alkaline solution, it absorbs oxygen from the air, as the solution turns brown. As such, it can be used in this way to calculate the amount of oxygen in air. Herein, we report the incorporation of pyrrogalol residue in the pendants in the polymer backbone of polyethers.

5.3 Experimental

5.3.1 Synthesis of methylene acetal of pyrogallol 33 [158]

A solution of pyrogallol **32** (42.9 g, 0.34 mol) in DMSO (500 mL) was stirred with $KHCO_3$ (66.8 g, 0.67 mol) and dibromomethane CH_2Br_2 (59.8 g, 0.34 mol) under nitrogen at 75 ºC for 70 h. Water (100 mL) was added to the mixture, and then it was extracted three times with ether (3×100 mL), and the combined organic layers was washed with water (50 mL), dried over Na_2SO_4 and concentrated. The residual liquid was purified by column chromatography (silica gel, 1:9 ether:hexane) to obtain compound **33** as a white solid (11 g, 23.4% yield), δ_H ($CDCl_3$): 5.48 (1H, s), 5.91 (2H, s), 6.46-6.50 (2H, m), 6.69-6.72 (1H, m). δC13 ($CDCl_3$): 101.1, 102.0, 111.0, 122.3, 134.0, 139.5, 148.6.

5.3.2 Conversion of acetal 33 to epoxide 34 [149]–[152]

To a solution of **33** (3.8 g, 32.6 mmol) in 2-butanone (40 mL) was added epibromohydrin **25** (7.0 g, 51 mmol), and potassium carbonate (16 g, 0.11 mol) and the mixture was refluxed. After 6 h, another portion of epibromohydrin (2 g, 14.5 mmol) was added and the reflux was continued for another 3 h. The reaction mixture was cooled to room temperature and the inorganic salts was filtered off and washed with ether. The filtrate was concentrated and the residual liquid was dissolved in CH_2Cl_2 (50 mL) and washed with 1% NaOH (2×20 mL) and H_2O (20 mL). The organic layer was dried (Na_2SO_4), concentrated and distilled to obtain **34** (bp $_{0.12\ mmHg}$ 103 °C), (4.5 g, 71%). δ_H ($CDCl_3$): 2.72-2.74 (1H, m), 2.87-2.89 (1H, m), 3.34-3.37 (1H, m), 4.09 (1H, dd, *J* 5.8 Hz, *J* 11.3 Hz), 4.32 (1H, dd, *J* 3.4 Hz, *J* 11.3 Hz), 5.95 (2H, s), 6.53-6.55 (2H, m), 6.74-6.77 (1H, m). δ_C ($CDCl_3$): 44.7, 50.1, 70.5, 101.1, 103.0, 109.7, 122.1, 135.5, 142.8, 149.0. IR KBr: 3052, 3002, 2892, 2775, 1639, 1604, 1502, 1462, 1356, 1290, 1255, 1184, 1087, 1057, 1026, 972, 927, 910, 834, 757, 712, 693, 539, 511 and 498 cm^{-1}.

5.3.3 Polymerization of 34 using $MePPh_3Br$ and $^{i}Bu_3Al$

Methyltriphenylphosphonium bromide (11.6 mg, 0.032 mmol) was placed in a round bottom flask under Ar and closed with rubber septum. Monomer **34** (472 mg, 2.43 mmol), and anhydrous toluene (1.5 ml) were added by syringe under Ar. The mixture was allowed to cool to 0 ºC, then triisobutylaluminium solution (25 wt. % in toluene) (0.4 ml) was added by syringe under Ar as one portion. The polymerization was stopped after 1.5 h by adding 4:1 $MeOH/H_2O$ (5 mL), and extracted with CH_2Cl_2, and dried over anhydrous (Na_2SO_4). The organic layer was then filtered over celite 545 and evaporated to obtain **35** (457 mg, 97%).

5.4 Results and Discussion

Pyrogallol **32** was protected as its methylene acetal thereby leaving one hydroxyl group in **33** unprotected for further elaboration (Scheme 5.1). Thus **33** upon reaction with epibromohydrin **25** was converted to epoxy monomer **34** which on Lewis acid catalysed polymerization afforded polyether **35**. Figures 5.1 and 5.2 display the ^{1}H and ^{13}C NMR spectra of **33-35**, respectively. Protected acetal **33** as well as epoxy monomer **34** were readily identified by its NMR spectra (Figures 5.1a,b and 5.2a,b). Epoxy motifs' ^{1}H and ^{13}C NMR signals are missing in the NMR of polether **35** (Figures 5.1c and 5.2c) thereby confirming the formation of the polyether containing the residue of pyrogallol for the first time.

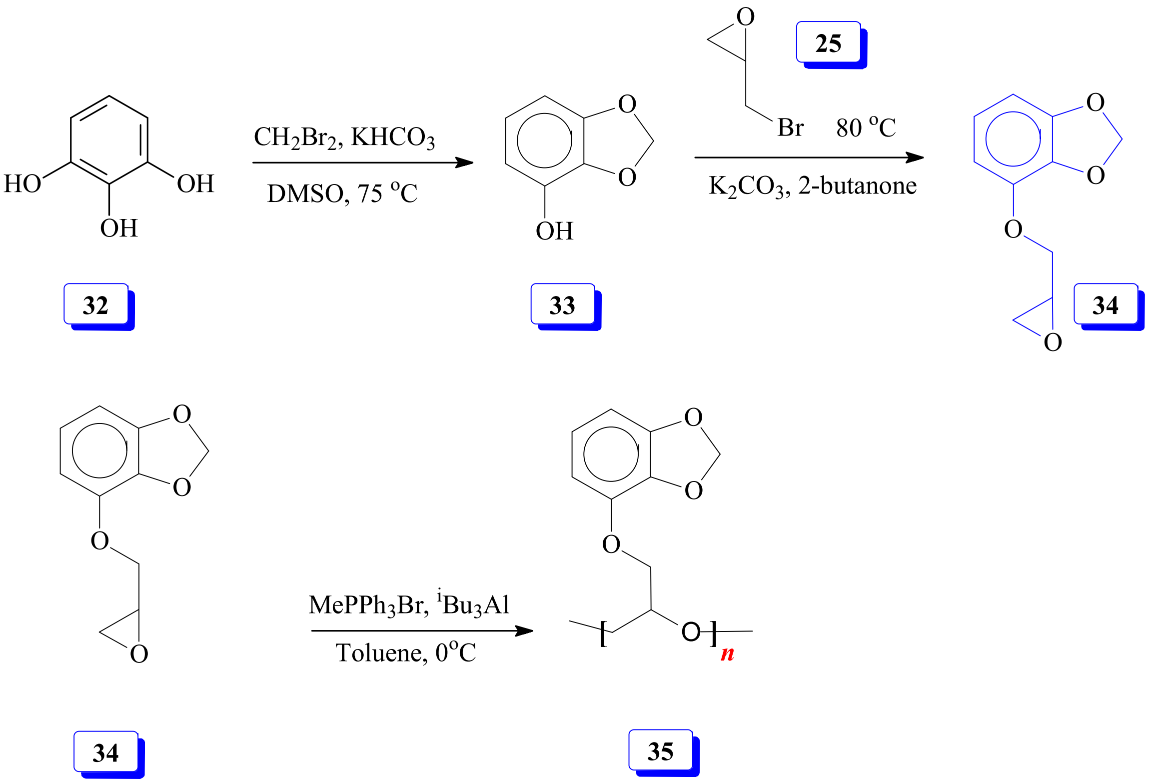

Scheme 5.1 Lewis acid catalyzed copolymerization of epoxide **34**

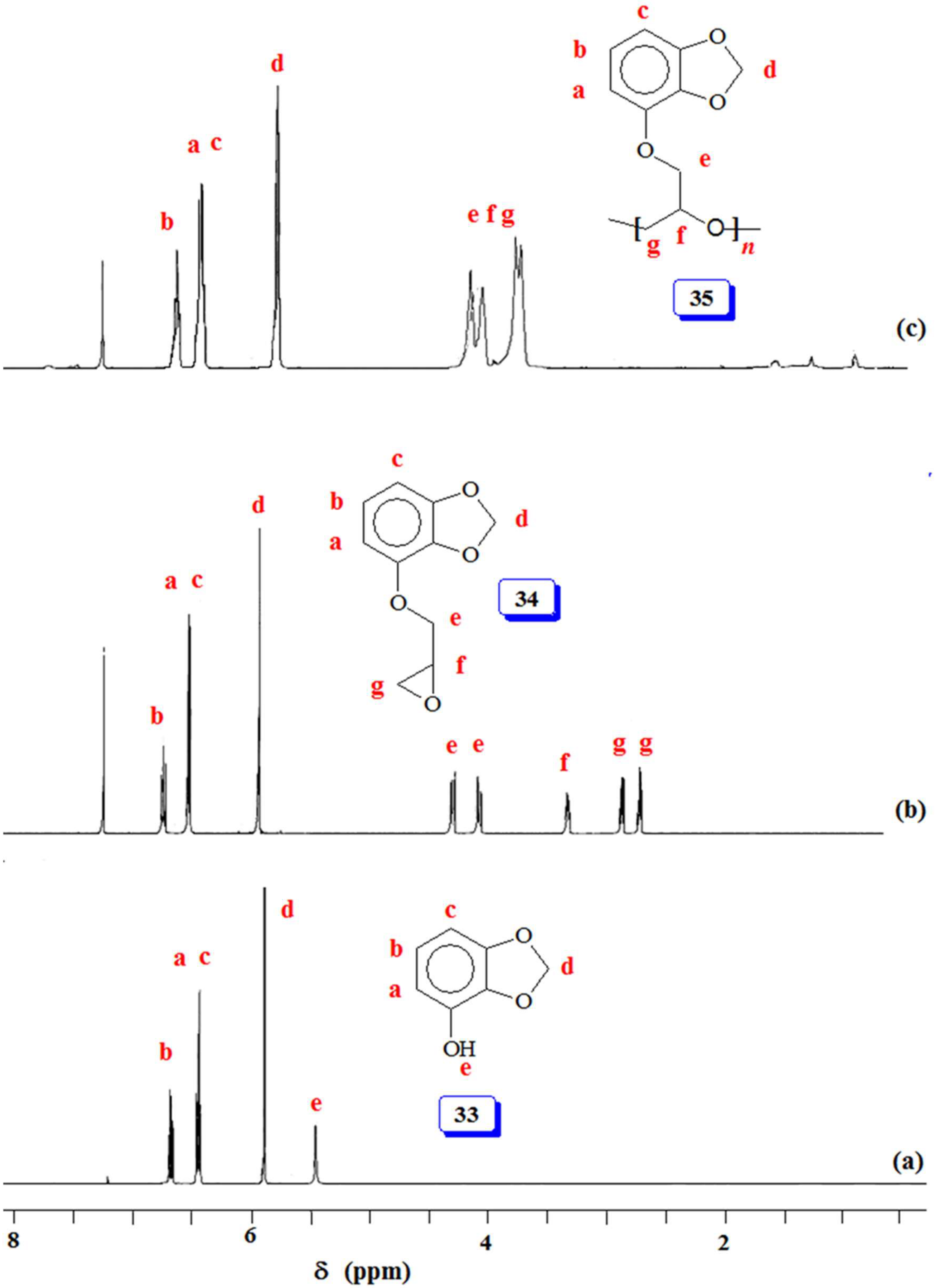

Figure 5.1 ^{1}H NMR spectra in $CDCl_3$ of (a) **33**, (b) epoxide **34**, and (c) homopolymer **35**

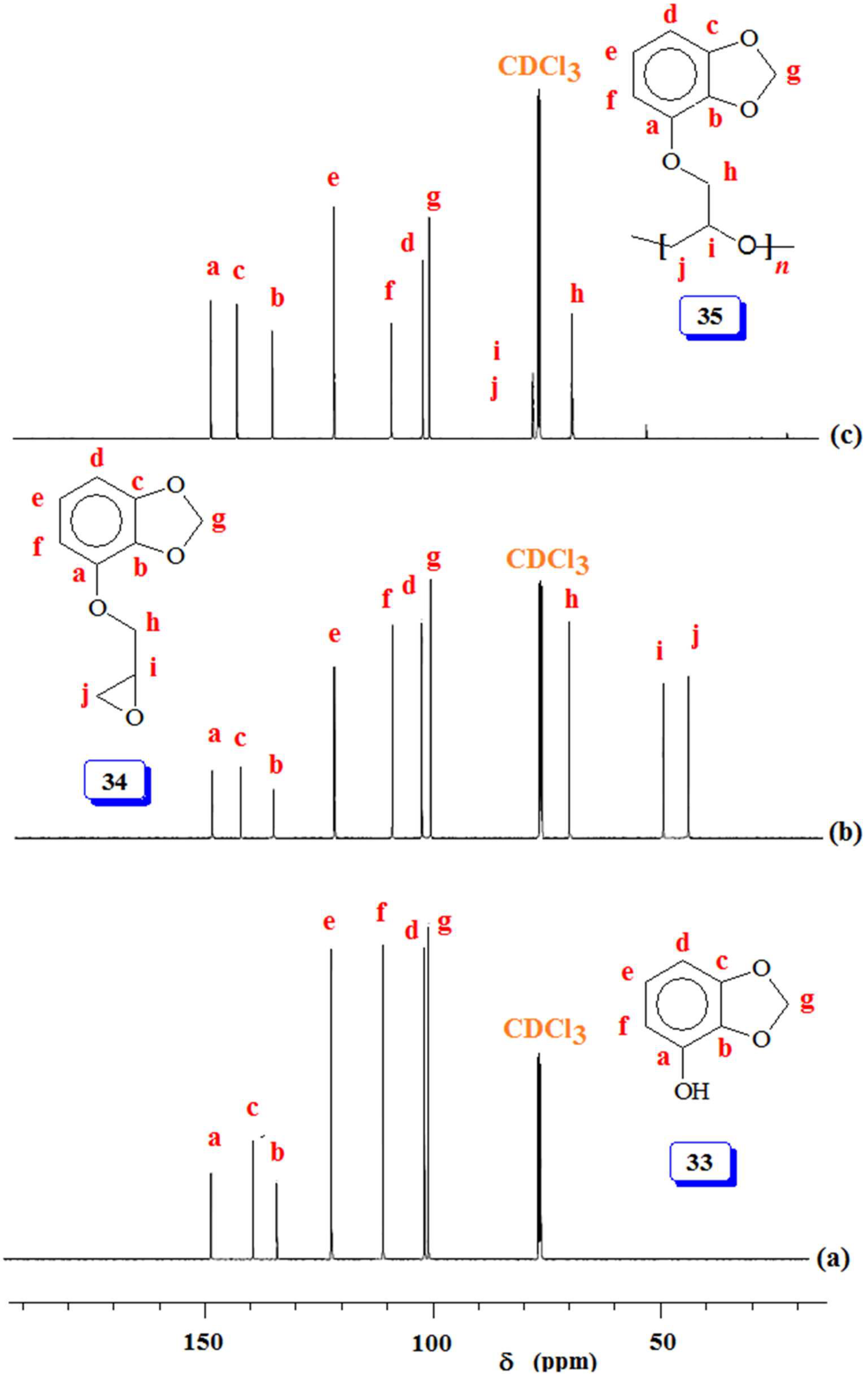

Figure 5.2 ^{13}C NMR spectra in $CDCl_3$ of (a) **33**, (b) epoxide **34**, and (c) homopolymer **35**

5.5 Conclusion

To the best of our knowledge, Pyrogallol **32,** usually obtained by heating induced decarboxylation of naturally occurring gallic acid, has been protected as methylene acetal **33** for the first time. The free hydroxyl group in **33** is converted to epoxy monomer **34**. Monomer **34** has been polymerized for the first time using Lewis acid initiator/catalyst comprising of triphenylmethylphosphonium bromide/triisobutylaluminum to obtain polyether **35** in excellent yields.

CHAPTER 6

BIO-INSPIRED ADVANCED POLYMERIC MATERIALS FOR FUNCTIONALIZATION OF MANGANESE OXIDE NANOPARTICLES

6.1 Abstract

Paramagnetic Manganese oxide (MnO) nanoparticles have been synthesized. This metal oxide nano-particles was chelated by catechol moieties of the polymer (Chapter 2) to be a hydrophilic ligand for potential application in MRI as a contrast agent. The results show a nice basket of the polymer-MnO nanoparticles with diameter size 200 -500 nm.

6.2 Introduction

Nanoparticles NPs of early transition metal oxide in the fifth period have a unique chemical and physical properties, and the functionalize of these nanoparticles have attracted enormous attention by researchers in the recent years [159]–[161]. The functionalize metal oxide NPs have a lot of potential applications e.g. protein separation, drug delivery, and magnetic resonance imaging (MRI) as contrast agent. Among them, MRI contrast agent application has become one of the most important applications in the clinical use [162],

[163]. Due to that the contrast agents in MRI enables whole-body imaging without the use of ionizing radiation e.g. X-ray and γ-ray imaging, at a near-microscopic resolution, and excellent soft-tissue contrast [163], [164]. Iron oxide NPs as contrast agent have been extensive studied in the last decade, which enhance T_2 relaxation. However, these NPs could damage the back-ground image and could confuse between NPs deposits and bleeding negative or dark signal. The other metals have been studied as contrast agent effected on T_1 relaxation spin-lattice relaxation. Gd^{+3} and Mn^{+2} base contrast agents have gained a numerous attention in the resent years, because of their paramagnetic behavior. Nevertheless, they still have a lot of restrictions because the toxicity of these metals especially Mn^{+2} which is still applied in animal studies only. MnO NPs could be a potential substitution and have less toxicity. The major problems in the use of the MnO NPs are the stability and solubility especially that MnO NPs have a hydrophobic surface behavior because they are prepared by thermal decomposition of manganese oleate precursor [68], [159]–[166]. The modification of the surface of MnO will be done by using the polymer **18** by chelating with catechol moieties (Scheme 6.1).

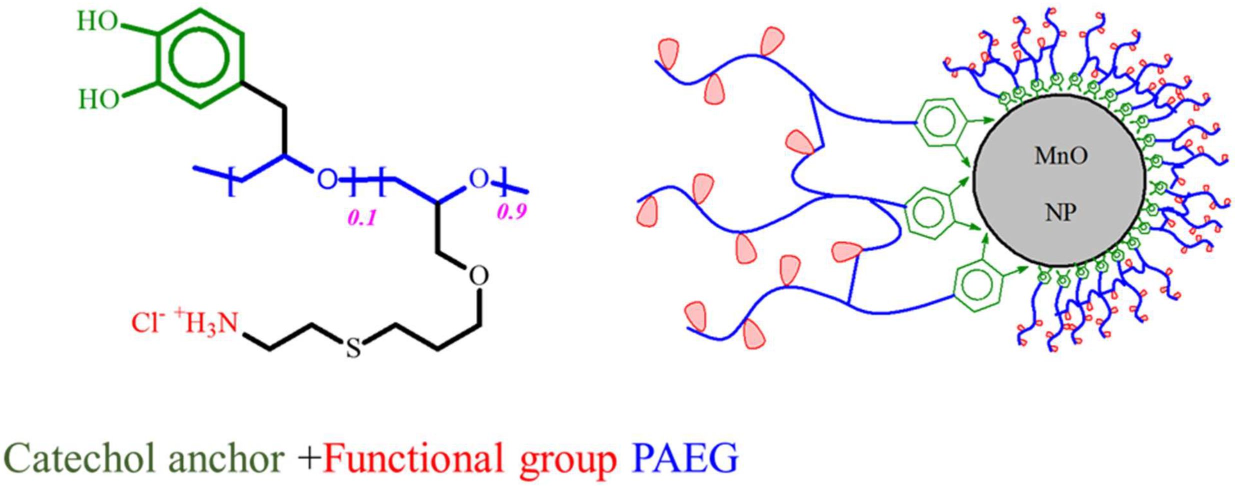

Scheme 6.1 Model of modification the surface of MnO NPs by polymer **18**

6.3 Experimental

6.3.1 Materials

Manganese(II) chloride tetrahydrate from fisher scientific company, octadecene from fluka company, oleic acid from lobachemie, and polymer **18** was synthesized as mention in Scheme 3.8.

6.3.2 Synthysis of MnO nanoparticles

MnO NPs were synthesized by thermal decomposition of Mn-oleat [167] [160]. A 1.0 g of Mn-oleat was dissolved in 10 g of octadecene in a round bottom flask, then it was heated at 70 ºC under vacuum for 2 h. The pressure was released under argon, and the reaction was gradually heated up to 318 ºC during 90 min, then it was held under reflux for 1 hour. The MnO NPs were washed 3 times with hexane, and precipitated by ethanol. Mn-oleat was synthesized as reported in the literature [160], [167] briefly to a mixture of manganese(II) chloride tetrahydrate (4.0 g, 20.0 mmol) and oleic acid (11.4 g, 40.0 mmol) in methanol (100 cm^3) was added dropwise for 1 h solution of sodium hydroxide (1.6 g in methanol 100 cm^3). After adding all sodium hydroxide solution, stirring was continued at room temperature for another 1 h. The oily precipitate was washed by water (2×50 cm^3), then by methanol (2×25cm^3), and at the end by acetone (2×25 cm^3). The residual was dissolved in hexane and dried over ($MgSO_4$) and concentrated. Then, it was dried under vacuum at 105 ºC for 2 h.

6.3.3 Nanoparticle functionalization

To a solution of polymer **18** (10 mg) was dissolved in water (2.5 cm^3), the solution of MnO NPs (30 mg) in hexane (2.5 cm^3) was added and stirred overnight. The water layer was freeze-dried to obtain our target structure (Scheme 6.1).

6.4 Results and Discussion

Surface morphology and chemical composition of Polymer **18,** MnO NPs, and MnONPs-B-P**18** were analyzed by FESEM equipped with EDX. Figure 6.1.

Figure 6.1a and 6.1b show that the morphology of polymer has a smooth surface with amorphous shape. Figure 6.1c shows that MnONPs are spherical in shape with smooth surface, some of it aggregated, and the size of the particles around 50-100 nm. The SEM images of Figure 6.1d, e and f show a rough surface because the MnONPs are bagged by the polymer with spherical shape, and it is clear that the size of each bag containing MnoNPs around 200-500 nm Figure 6.1f. The EDX spectra and the mapping images proof that the MnONP$_s$-B P**18** contain both the polymer **18** and MnONPs with well distribution Figure 6.2.

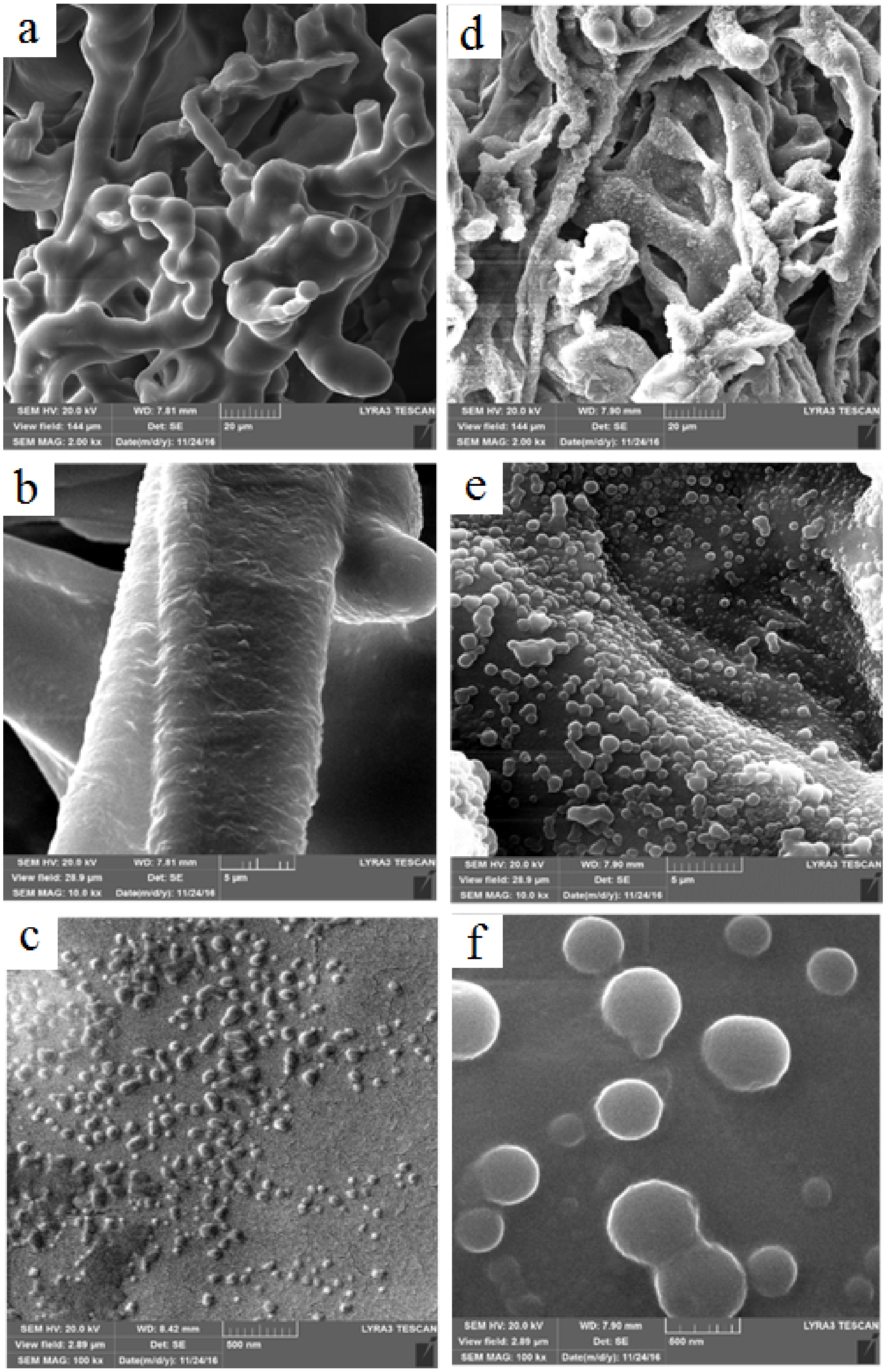

Figure 6.1 SEM images for (a) polymer **18** 20µm and (b) 5µm; (c) MnONPs 500nm; and MnONP$_s$-B P**18** (d) 20µm, (e) 5µm, and (f) 500 nm

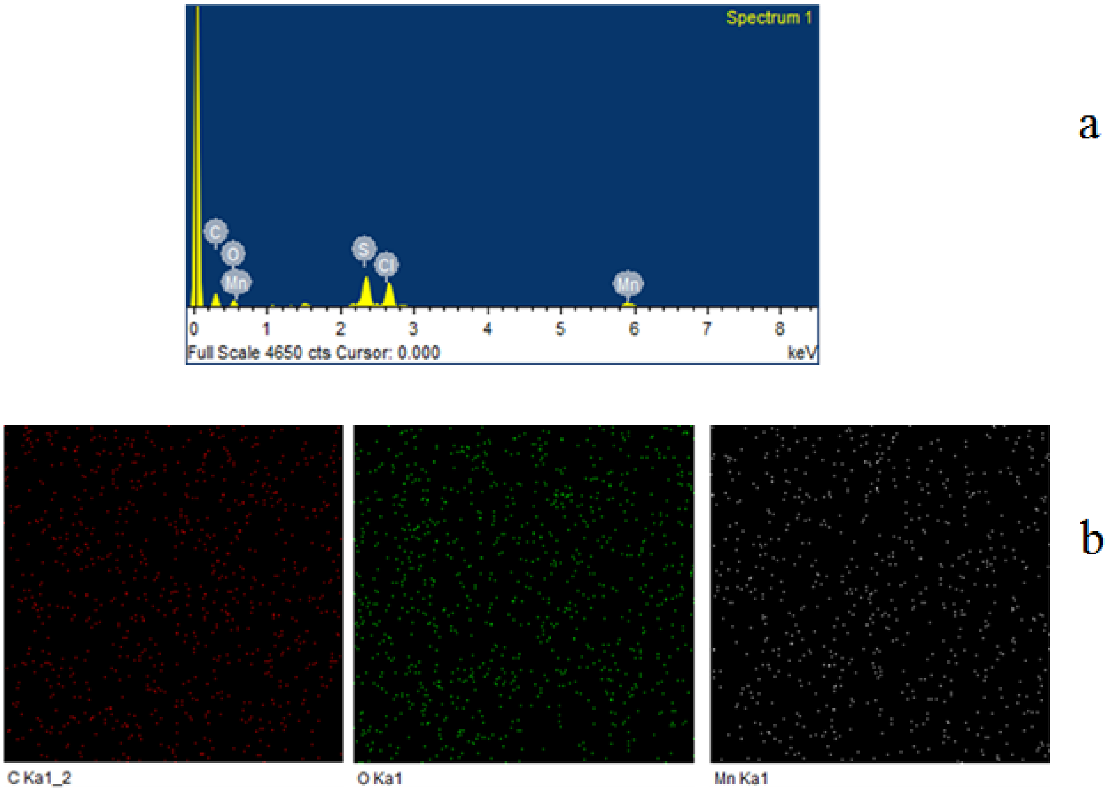

Figure 6.2 (a) EDX spectrum; (b) EDX mapping for carbon, oxygen, and manganese from left to right respectively.

6.5 Conclusion

This work presents an example to use the adhesive properties of DOPA moiety to activate the surface of MnONPs. The resulting full accessibility of the catechol anchor group could be used to change the properties of MnONPs, to result into a more hydrophilic particle or enhance water-solubility of the particles. So, it could be a good potential to use this formation as contrast agents in MRI.

CHAPTER 7

BIO-INSPIRED MATERIALS AS CORROSION INHIBITORS FOR LOW CARBON STEEL IN HCl SOLUTION

7.1 Abstract

Two isoxazolidine derivatives namely 5-(benzo[d][1,3]dioxol-5-ylmethyl)-2-tetradecyl isoxazolidine (BDMTI) and 5-((4-hydroxy-3-methoxybenzyl)-2-tetradecyl isoxazolidine (HMBTI) were synthesized and characterized using FTIR, C-NMR, H-NMR, and elemental analyzer. The synthesized compounds were evaluated as corrosion inhibitors for API 5L X60 steel in 1 M HCl at the temperature range of 25 – 60 °C using gravimetric and electrochemical (Electrochemical Impedance Spectroscopy (EIS), Potentiodynamic Polarization (PDP) and Linear Polarization Resistance (LPR) techniques. The effect of addition of a small amount of iodide ions on the corrosion inhibition performance of the compounds was also assessed. In addition, quantum chemical calculations and Monte Carlo simulations were employed to correlate the electronic properties of the compounds to the corrosion inhibition effect as well as the evaluation of the adsorption/binding of the inhibitor molecules on the steel surface. Experimental results showed that the two

compounds inhibited the corrosion of carbon steel in the acid environment with HMBTI showing superior performance. Corrosion inhibition effect was found to be dependent on the inhibitors' concentration and temperature. Addition of iodide ions improves the inhibition efficiency considerably due to co-adsorption of the iodide ions and the inhibitors on the steel surface which was competitive in nature as confirmed from synergistic parameter (S_1) which was less than unity at higher temperature.

7.2 Introduction

The effective strategy adopted by oil, gas and chemical industries in order to maximize profit and reduce cost is to use low carbon steel in place of expensive corrosion resistant alloys (CRAs) in their operations. However, the major problem associated with low carbon steel is its susceptibility to corrosion when it comes in contact with corrosive environment such as acids (HCl, H_2SO_4, H_3PO_4), chloride rich solution and aqueous hydrogen sulfide medium. The consequences of corrosion are enormous ranging from economic, health and safety as well as environmental standpoints amongst others.

Corrosion mitigation strategies adopted by some industries include materials selection, coatings and linings, cathodic protection and the use of corrosion inhibitors amongst others. The use of corrosion inhibitors is the most practical and cost-effective method in fighting corrosion. Corrosion inhibitors retard corrosion by adsorbing onto the low carbon steel surface and blocking one or more of the electrochemical reactions occurring at the solution/metal interface. Well known corrosion inhibitors are organic compounds, including imidazolines, amides, amines and their derived salts [168]–[170]. These organic compounds typically contain nitrogen, sulfur and oxygen, and hydrophobic hydrocarbon chains in their structures. However, inhibitors are usually effective only for a particular material in a certain environment [171], but the corrosion environments are highly variable; therefore, an inhibitor that works in one well may not work in another [172]. Thus, it is necessary to continuously develop new formulas for different environments [173], and numerous compounds are designed [174], [175]. Also, organic compounds alone are usually not effective enough, and a proper mixture containing additional intensifiers, surfactants and solvents is needed [176].

The functional groups in the organic molecules impart inhibition of corrosion [177]. Isoxazolidines, known for many decades [178]–[180], are widely used in the synthesis of various natural products of biological interest [181]. Relatively recently, the isoxazolidine functionality has been introduced to the corrosion literature for the first time [182], [183]. In the present work, we have synthesized two new isoxazolidines using cycloaddition reaction of nitrones and naturally occurring alkenes: eugenol and safrole, and studied their effects on the corrosion inhibition of mild steel in HCl solution using gravimetric and electrochemical techniques complemented by surface morphology characterization of the corroded steel samples without and with the synthesized inhibitors using SEM. Also, the influence of addition of a small amount of iodide ions on the corrosion inhibition performance of the isoxazolidines derivatives has been assessed. The corrosion inhibition efficacy of the two new isoxazolidines derivatives BDMTI and HMBTI are correlated with quantum chemical parameters and Monte Carlo simulations with a view of understanding how the electronic properties of the compounds can influence the corrosion inhibition effect as well as evaluating the adsorption/binding of the inhibitor molecules on the steel surface. The information derived from the computational studies will be highly useful in the design and synthesis of better performing corrosion inhibitors from this class of organic compound.

7.3 Experimental

7.3.1 Synthesis and characterization of isoxazolidines derivatives

7.3.1.1 Materials

1-Bromotetradecane, N-methylhydroxylamine hydrochloride, hydroxylamine hydrochloride, triethylamine, Silica gel 100, and paraformaldehyde (Fluka Chemie AG) and 1-tetraadecene were used as received. Safrole (**1**) and eugenol (**2**) were purchased from Aldrich Co.

7.3.1.2 Physical Methods

A Perkin Elmer Series II Model 2400 and a Perkin Elmer (16F PC) spectrometer were used for elemental analyses and recording FTIR spectra, respectively. The NMR spectra were taken in $CDCl_3$ on a 500-MHz JEOL LA spectrometer using TMS as standard.

7.3.2 Synthesis

7.3.2.1 N-Tetradecylhdroxylamine 37

To a mixture of hydroxylamine hydrochloride (35 g, 0.5 mol) in ethanol (250 cm^3), was added triethylamine (46 g, 0.45 mol). After stirring using a magnetic stir bar at 20 ºC for 10 min, 1-bromotetradecane **36** (20 g, 0.072 mol) was added in one portion, and the resulting mixture was heated in a closed vessel for 7 h at 90 ºC. The mixture was dumped onto water (600 cm^3), and the white solid was filtered and washed with liberal excess of water. The white solid was taken in hot (50 ºC) methanol and filtered, and the solid was washed with excess hot methanol. The white solid was crystallized from petroleum-ether to give the ditetratdecylhydroxylamine **38** (3.5 g, 22.8%). The filtrate (~700 cm^3) was concentrated and the residual solid was crystallized from petroleum ether to give the white crystal of the tetradecylhydroxylamine **37** (9.5 g, 57.5%). Mp 94-95 ºC; (Found: C, 73.1; H, 13.4; N, 6.0. $C_{14}H_{31}NO$ requires C, 73.30; H, 13.62; N, 6.11%); $\nu_{max.}$ (KBr) 3263, 3158, 2918, 2851, 1654, 1512, 1466, 1379, 1151, 1062, 998, 970, 891, and 721 cm^{-1}; δ_H ($CDCl_3$) 0.88 (3H, t, *J* 7.0 Hz), 1.28 (22H, m), 1.52 (2H, quint, *J* 7.0 Hz), 2.93 (2H, t, *J* 7.0 Hz), NHOH protons are not observed presumably as a result of very broad signal; δ_C ($CDCl_3$) 14.09, 22.70, 27.12, 27.21, 29.38, 29.60, 29.65, 29.69 (5C), 31.97, 54.12.

7.3.2.2 5-(benzo[d][1,3]dioxol-5-ylmethyl)-2-methylisoxazolidine 39

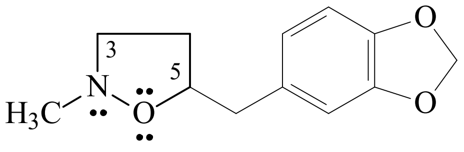

A mixture *N*-methylhydroxylamine hydrochloride (3.34 g, 40.0 mmol), sodium acetate trihydrate (5.85 g, 43 mmol), paraformaldehyde (1.80 g, 60 mmol) and safrole **1** (16.6 g, 50 mmol) in ethanol (35 cm^3) was strirred using a magnetic stir bar at 110˚C in a closed pressure vessel for 7 h. After removal of solvent, the mixture was basified using K_2CO_3 solution (50 mL), and extracted with ether (2×50 cm^3). The organic layer was dried (Na_2SO_4) and chromatographed over silica gel using 3:1 hexane/ether as eluant to give the yalow liquid **39** (7.6 g, 84.8%). $\nu_{max.}$ (KBr) 2956, 2886, 2778, 1855, 1609, 1495, 1446, 1357, 1243, 1194, 1097, 1038, 931, 864, 805, 601, and 529 cm^{-1}; δ_H ($CDCl_3$): 1.96 (1H, m), 2.29-2.42 (1H, m), 2.67-2.73 (5H, m), 2.90 (1H, m), 3.25 (1H, m), 4.21 (0.5H, m), 4.39 (0.5H, m), 5.95 (1H, s), 6.68-6.78 (3H, m); δ_C ($CDCl_3$): 33.3 (0.5C), 33.8 (0.5C), 40.5

(0.5C), 41.0 (0.5), 45.0 (0.5C), 45.5 (0.5C), 56.3 (0.5C), 57.1 (0.5C), 77.5 (0.5C), 78.6 (0.5C), 100.8, 108.1, 109.6, 122.0, 131.4 (0.5C), 131.8 (0.5C), 145.7, 147.2 ($CDCl_3$ middle carbon: 77.1)

7.3.2.3 2-Methoxy-4-((2-methylisoxazolidin-5-yl)methyl)phenol 40

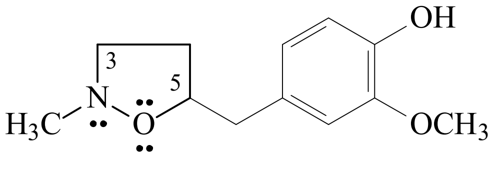

The cycloaddition reaction was repeated as described for the preparation of **39** (*vide supra*) except that eugenol **10** (8.21 g, 50.0 mmol) instead of safrole **1** was used. At the end of reaction, ethanol was removed, the mixture was basified using K_2CO_3 solution and extracted with ether (2×50 cm^3). The organic layer was dried (Na_2SO_4) and chromatographed over silica gel using 5% ether / methanol as eluant to give product **40** (5.7 g, 63.8%). $\nu_{max.}$ (KBr) 3511, 3953, 2916, 2849, 1602, 1519, 1449, 1369, 1277, 1128, 1029, 735, 861, 801, 738, and 565; δ_H ($CDCl_3$): 2.02 (1H, m), 2.31-2.79 (6H, m), 2.91(1H, m), 3.30-3.46 (2H, m), 3.83 (0.5×3H, s), 3.85 (0.5×3H,s), 4.31 (0.5H, m), 4.48 (0.5H, m), 6.65-6.85 (3H, m); δ_C ($CDCl_3$): 33.0 (0.5C), 33.3 (0.5C), 40.0 (0.5), 40.6 (0.5C), 44.7 (0.5C), 45.0 (0.5C), 55.4, 55.7 (0.5C), 56.4 (0.5C), 78.0 (0.5), 79.0 (0.5), 111.7, 114.7, 121.4, 128.6 (0.5C), 129.0 (0.5C), 144.4, 146.9 ($CDCl_3$ middle carbon: 77.2)

7.3.2.4 5-(3,4-Dimethoxybenzyl)-2-methylisoxazolidine 41

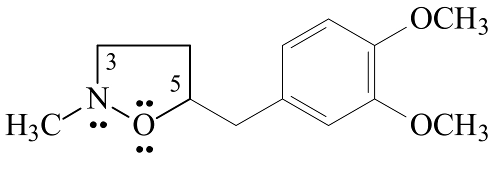

The cycloaddition reaction was repeated as described for the preparation of **39** (*vide supra*) except that eugenol methyl ether **42** (8.9 g, 50.0 mmol) instead of safrole **1** was used. At the end of reaction, ethanol was removed, the mixture was basified with K_2CO_3 solution and extracted with ether (2×50 cm^3). The organic layer was dried (Na_2SO_4) and chromatographed over silica gel using 5% ether / methanol as eluant to give product **41** (8.9 g, 93.8%). $\nu_{max.}$ (KBr) 3605, 2836, 1597, 1520, 1449, 1426, 1258, 1144, 1027, 938, 863, 807, 747, and 562; δ_H ($CDCl_3$): 2.00 (1H, m), 2.30-2.75 (6H, m), 2.93(1H, m), 3.27 (1H, m), 3.88-3.92 (6H, m), 4.28 (0.5H, m), 4.45 (0.5H, m), 6.81 (3H, m); δ_C (CDCl3): 33.2 (0.5C), 33.6 (0.5C), 40.2 (0.5), 40.8 (0.5C), 45.0 (0.5C), 45.3 (0.5C), 55.6, 56.1 (0.5C), 56.9 (0.5C), 78.6, 110.2 (0.5C), 110.3 (0.5C), 111.7, 120.9 (0.5C), 121.0 (0.5C), 129.9 (0.5C), 130.4 (0.5C), 146.9, 148.0 ($CDCl_3$ middle carbon: 77.3).

7.3.2.5 Sesamol allyl ether 43

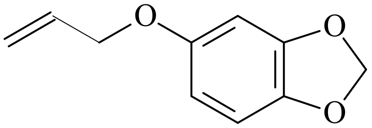

The solution of sesamol **26** (13.0 g, 94 mmol), allyl bromide **44** (12.5 g, 103.5 mmol), acetone (200 mL) and potassium carbonate (26 g, 188 mmol) was refluxed overnight. The reaction mixture was cooled to room temperature, and solvent was removed. Water (100 mL) was added, extracted by ether (2×50 mL), washed with 5% NaOH (2×50 mL) and H_2O (30 mL), dried with Na_2SO_4, and concentrated to get a yellow oil product **43** (15.9 g) which is used without more purification for the next step.

7.3.2.6 5-((Benzo[d][1,3]dioxol-5-yloxy)methyl)-2-methylisoxazolidine 45

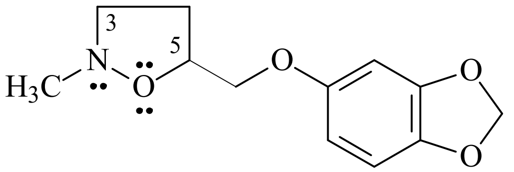

The cycloaddition reaction was repeated as described for the preparation of **39** (*vide supra*) except that sesamol allyl ether **43** (8.9 g, 50.0 mmol) instead of safrole **1** was used. At the end of reaction, ethanol was removed, the mixture was basified with K_2CO_3 solution and extracted with ether (2×50 cm^3). The organic layer was dried (Na_2SO_4) and chromatographed over silica gel using 5% ether / methanol as eluant to give product **45** (5.7 g, 60.1%). $\nu_{max.}$ (KBr) 3078, 2909, 2846, 2777, 1872, 1825, 1628, 1499, 1397, 1351, 1285, 1190, 1100, 1029, 943, 895, 848, 796, 621, and 509 cm^{-1}; δ_H ($CDCl_3$): 2.08 (1H, m), 2.54-2.80 (5H, m), 3.35 (1H, m), 3.80 (0.6H, m), 3.99 (1.4H, m), 4.44 (0.4H, m), 4.59 (0.6H, m), 5.95 (2H, s), 6.35 (1H, d, *J* 8.5 Hz), 6.55 (1H, s), 6.72 (1H, d, *J* 8.5 Hz); δ_C ($CDCl_3$): 31.1 (0.6C), 31.4 (0.4C), 44.9 (0.6C), 45.4 (0.4C), 56.4 (0.6C), 56.9 (0.4C), 69.9 (0.4C), 70.3 (0.6C), 75.0 (0.6C), 75.8 (0.4C), 97.9, 101.1, 104.8, 107.7, 141.3 (0.6C), 141.4 (0.4C), 147.9, 153.8 ($CDCl_3$ middle carbon: 77.1)

7.3.2.7 (Benzo[d][1,3]dioxol-5-ylmethyl)-2-tetradecylisoxazolidine (46)

A mixture of hydroxylamine **37** (1.50, 6.5 mmol), paraformaldehyde (0.36 g, 12 mmol), and safrol (alkene) **1** (1.95 g, 12 mmol) in toluene (6 mL) was strirred using a magnetic stir bar at 110 ˚C in an RB flask at 110 °C under N_2 for 7 h. After removal of solvent, the residual mixture was chromatographed over silica gel using 5:1 hexane/ether as eluant to give product **46** as a white solid (2.2 g, 84%). Mp 50-51 °C; (Found: C, 74.1; H, 10.1; N, 3.4. $C_{25}H_{41}NO_3$ requires C, 74.40; H, 10.24; N, 3.47%); $\nu_{max.}$ (KBr) 3027, 2918, 2846, 1863, 1608, 1496, 1451, 1367, 1250, 1186, 1110, 1041, 932, 861, 813, 763, 723 and 662 cm^{-1}; δ_H ($CDCl_3$, -30 °C): 0.88 (3H, t, *J* 6.1 Hz), 1.24 (22, m), 1.57 (2H, m), 1.90-3.30 (8H, m), 4.21 (0.5H, quint, *J* 7.0 Hz), 4.31 (0.5H, quint, *J* 7.0 Hz), 5.96 (2H, s), 6.70 (3H, m);δ_C ($CDCl_3$, -30 °C): 14.3, 22.8, 27.3, 27.5, 28.1, 29.5, 29.6, 29.7, 31.7, 31.9, 33.2, 40.5 (0.5), 40.9 (0.5 C), 54.7 (0.5 C), 55.2 (0.5 C), 57.9 (0.5 C), 59.1 (0.5 C), 78.1, 100.8, 108.1, 109.7, 122.1, 131.4 (0.5 C), 132.0 (0.5 C), 145.7 (0.5 C), 145.8 (0.5 C), 147.2 ($CDCl_3$ middle carbon: 77.1). The NMR signals indicated the presence of nitrogen invertomers in a 1:1 ratio equilibrating slowly on a NMR time scale.

7.3.2.8 5-(4-Hydroxy-3-methoxybenzyl)-2-tetradecylisoxazolidine (47)

A mixture of hydroxylamine **37** (1.50, 6.5 mmol), paraformaldehyde (0.36 g, 12 mmol), and eugenol (**10**) (1.97 g, 12 mmol) in toluene (6 mL) in an RB flask was strirred using a magnetic stir bar at 110 ˚C under N_2 for 7 h. After removal of solvent, the residual mixture was chromatographed over silica gel using 5:1 hexane/ether as eluant to give adduct **47** as a white solid (2.2 g, 88%). Mp 61-62 °C (Found: C, 73.8; H, 10.5; N, 3.34. $C_{25}H_{43}NO_3$ requires C, 74.03; H, 10.69; N, 3.45%); $\nu_{max.}$ (KBr) Around 3500 (Broad), 2842, 2584, 1596, 1525, 1467, 1428, 1391, 1373, 1288, 1233, 1153, 1127, 1095, 1033, 1001, 959, 948, 924, 850, 798, 723, 673, 641, 567, and 518 cm^{-1}; δ_H ($CDCl_3$, -30 °C) 0.87 (3H, m), 1.23 (22H, m), 1.54-1.64 (2H, m), 2.00 (1H, m), 2.26-2.92 (6H, m), 3.27-3.32 (1H, m), 3.85 (3H, m), 4.26 (0.5H, m), 4.37 (0.5H, m), 6.67-6.83 (3H, m), 7.90 (1H, OH); δ_C ($CDCl_3$,-30 °C) 14.3, 22.8, 27.3, 27.4, 27.8, 29.5, 29.6, 29.7, 31.9, 33.1, 40.1 (0.5), 41.5 (0.5C), 54.4 (0.5C), 54.9 (0.5C), 55.5, 57.8 (0.5C), 58.9 (0.5C), 78.4, 111.6, 114.4, 121.5, 129.0 (0.5C), 129.4 (0.5C), 144.1, 146.5 ($CDCl_3$ middle carbon: 77.1). The NMR signals indicated the presence of nitrogen invertomers in a 1:1 ratio equilibrating slowly on a NMR time scale.

7.3.3 Corrosion inhibition studies

7.3.3.1 Materials preparation

The metal substrate utilized in the investigation was API 5L X60 steel with chemical composition as earlier reported [184]. Prior to corrosion studies, the metal substrate was cut into coupons of dimensions 3 cm × 3 cm × 1 cm for weight loss measurements and 1 cm × 1 cm × 1 cm for electrochemical measurements. The coupons were abraded using successive grades of silicon carbide paper (#120 - #1000), sonicated in ethanol bath for 10 min to remove the residues emanating from the grinding process, degreased with ethanol, rinsed with acetone and dried in warm air. Coupons for electrochemical studies were completely insulated leaving one side of the steel surface (Area = 1 cm^2) exposed. The prepared metal substrates were stored in desiccator prior to use. The corrosive medium was 1 M HCl prepared by diluting 37% analytical grade HCl (Sigma Aldrich) with double distilled water. The synthesized compounds BDMTI (**46**) and HMBTI (**47**) were used as test corrosion inhibitors in the concentration range of 20 – 100 ppm. Potassium iodide (KI) (Sigma- Aldrich) was added to the test inhibitors to evaluate synergistic inhibition effect at a concentration of 5 mM.

7.3.3.2 Gravimetric measurements

The gravimetric measurements were performed following the ASTM standard procedures [185]. The API 5L X60 steel samples were weighed and immersed in glass vessels containing 1 M HCl solution in the absence and presence of different concentrations of the

BDMTI and HMBTI maintained at 25 °C to 60 °C, in a thermostated water bath for 24 h. After 24 h, the corroded steel samples were withdrawn, immersed in 1 M HCl for 20 seconds to loosen the corrosion products, thoroughly washed with distilled water, rinsed with acetone, dried in a stream of warm air and reweighed to determine the weight loss. The experiments were carried out in triplicates, and only the average value of the weight losses was reported. The weight loss data were utilized to compute the corrosion rate and inhibition efficiency using equations (1) and (2) respectively.

$$C_R(\text{mmy}^{-1}) = \frac{87.6 \times \Delta W}{\rho A T} \qquad (1)$$

$$\text{IE }\% = \frac{C_{R(\text{blank})} - C_{R(\text{inh})}}{C_{R(\text{blank})}} \times 100 \qquad (2)$$

where $C_{R(\text{blank})}$ and $C_{R(\text{inh})}$ are the corrosion rates in the absence and presence of the inhibitor respectively, W is the average weight loss (mg), ρ is the density of the steel specimen (g cm^{-3}), A is the surface area of the specimen (cm^2), and T is the exposure time (h).

7.3.3.3 Electrochemical measurements

Electrochemical measurements were undertaken in a three-electrode cell using Gamry Instrument Potentiostat/Galvanostat/ZRA (Reference 600) with a Gamry framework system based on ESA410. Gamry applications include software DC105 for corrosion, EIS300 for electrochemical impedance spectroscopy (EIS) measurements and Echem Analyst 6.0 software package for data fitting. API 5L X60 samples, graphite rod and silver/silver chloride (Ag/AgCl) were used as working, counter and reference electrodes, respectively. All the measurements were taken after the working electrode was immersed for 1 h in the different test solutions at room temperature in order to attain a steady-state open-circuit potential (OCP). The frequency range from 100 kHz to 0.01 Hz with amplitude of 10 mV was used in electrochemical impedance experiments. The potentiodynamic polarization curves were recorded from cathodic potential of −250 mV to anodic potential of +250 mV at a scan rate of 0.5 mV/s with respect to free corrosion potential (E_{corr}). The linear Tafel segments of the anodic and cathodic curves were extrapolated to corrosion potential to obtain the corrosion current densities (i_{corr}) and other electrochemical parameters of interest. Linear polarization resistance (LPR) experiments were performed from −15 to +15 mV versus E_{corr} at the scan rate of 0.125 mV/s.

Inhibition efficiency from electrochemical impedance spectroscopy (EIS), potentiodynamic polarization (PDP) and linear polarization resistance (LPR) was computed using equations (3), (4) and (5) respectively.

$$IE_{EIS} = \left(1 - \frac{R_{ct}^{0}}{R_{ct}}\right) \times 100 \tag{3}$$

where and are the charge transfer resistances in the absence and presence of the inhibitors respectively.

$$IE_{PDP} = \left(1 - \frac{i_{\mathrm{corr}}}{i_{\mathrm{corr}}^{0}}\right) \times 100 \tag{4}$$

where i^{o}_{corr} and i_{corr} are the corrosion current densities in the absence and presence of inhibitor, respectively.

$$IE_{LPR} = \left(1 - \frac{R_{\mathrm{p}}^{0}}{R_{\mathrm{p}}}\right) \times 100 \tag{5}$$

where $R^{\mathrm{o}}{}_{\mathrm{p}}$ and R_{p} are the polarization resistance values in the absence and presence of the inhibitor, respectively.

7.3.4 Surface analysis

The surface analysis of the API 5L X60 steel was carried out using a JEOL JSM 6610- LV scanning electron microscope (SEM) operated at an acceleration voltage of 20 kV. Images of the specimens were recorded after 24 h exposure time in 1 M HCl without and with 60 ppm BDMTI, 60 ppm HMBTI and 60 ppm of each of the inhibitor in combination with 5 mM KI at 25 ±1 ◦C.

7.3.5 Computational details

7.3.5.1 Quantum chemical calculations

In this work, DFT based calculations were conducted by the DMol^3 module implemented in the BOVIA Materials Studio (Version 8.0) from Accelyrs Inc. (San Diego, CA, USA). These calculations employed Generalized gradient approximation functional (GGA) with double numerical basis set with polarization (DNP). The calculations were conducted in aqueous phase to simulate the effect of solvent. Highest occupied molecular orbitals (HOMO) and lowest unoccupied molecular orbitals (LUMO), which reveal the active sites of the molecules were plotted and discussed.

7.3.5.2 Monte Carlo simulation

The strength of the interaction between BDMTI and HMBTI and Fe (110) surface was computed by using atomistic simulation as implemented in the adsorption locator module of the MS software. Metropolis Monte Carlo (MC) simulations methodology using the adsorption Locator module by BIOVIA company. The MC calculation of the simulation of the interaction between the inhibitor molecules and Fe surface was carried out with a slab thickness of 5Å, a supercell of (12 × 12) and vacuum of 50Å with periodic boundary conditions to model a representative part of the interface devoid of any arbitrary boundary effects. For the whole simulation procedure, the COMPASS Force Field was used to optimize the structures for our systems. 100 water molecules (100 H_2O) were added to the simulation box to mimic the real corrosion environment.

7.4 Results and Discussion

7.4.1 Synthesis of BDMTI and HMBTI

The versatile nitrone cycloaddition reaction [178]–[180] is the best chemical template for efficient synthesis of the isoxazolidines (Scheme 7.1). 1-Bromotetrdecane **36** on treatment with excess hydroxylamine gave tetradecylhydroxylamine **37** as a major product. Nitrone **48**, derived via condensation of hydroxylamine **37** with formaldehyde, underwent cycloaddition reaction with naturally occurring safrole **1** and eugenol **10** gave cycloadducts **46** and **47**, respectively, in excellent yields. In each case, the cycloadduct was obtained regiospecifically; this regiochemical preference is well documented in the literature [186]. The cycloadducts, characterized by spectral and elemental analyses, are obtained by attaching oxygen terminal of the nitrone to the more substituted internal carbon of the alkene [187]. Note that the as-synthesized new inhibitor molecules **46** and **47** have isoxazolidine motifs, long hydrophobic tail as well as π-electron-rich aromatic groups which are potent corrosion inhibiting functionalities.

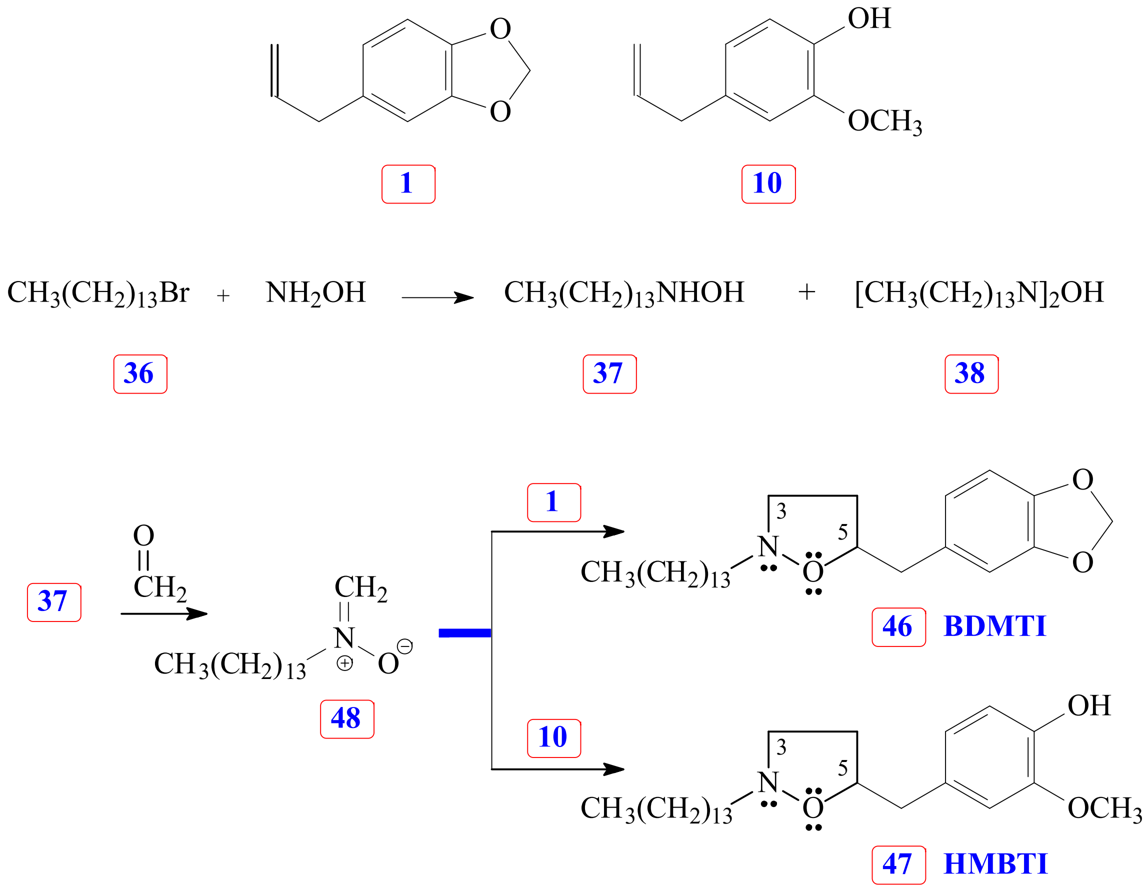

Scheme 7.1 Synthesis of inhibitor molecules **46** and **47** using nitrone cycloaddition reaction

7.4.2 Gravimetric measurements

The technique of measuring the loss in mass or thickness of metal substrate with time when exposed to corrosive environment is still a reliable method in assessing corrosion of metals. Figure 7.1 (a) and (b) depict the corrosion rate and inhibition efficiency as a function of inhibitor (BDMTI and HMBTI) concentration, respectively, at the temperatures range of 25 – 60 ^{o}C. It is clear from the figures that corrosion rate decreased in the presence of the inhibitors compared to the blank solution. This is a clear indication that both BDMTI (**46**) and HMBTI (**47**) retard the dissolution of steel sample in the acid environment. It is also observed that corrosion rate is increased when the temperature is elevated from 25 to 60 ^{o}C both in the absence and presence of the inhibitors. This shows that the metal is susceptible to faster dissolution with increasing thermal agitation of the corrosive environment. With respect to variation of inhibition efficiency with concentration, close inspection of the figure reveals that for BDMTI, inhibition efficiency increased with increase in concentration up to 60 ppm, thereafter, further increase in concentration results in a decline in inhibition efficiency. Similar observation has been reported in the literature by some researchers [188]. It was postulated that at the optimum inhibitor concentration, a maximum surface coverage was achieved and above this concentration, there may be a possibility of interaction between unadsorbed and adsorbed inhibitor molecules leading to desorption hence the decreased in IE with further increase in concentration. However, a different scenario is seen for HMBTI where inhibition efficiency increased with increase in concentration of the inhibitor. The increase in inhibition efficiency and the decrease in corrosion rates with the increase in concentration of inhibitor could be ascribed to the adsorption of the inhibitor molecules on the surface of steel and thus covered a certain area of the exposed electrode in HCl solution. By increasing the inhibitor concentration, the surface coverage was greatly increased due to the availability of more inhibitor molecules to be adsorbed on its surface. Temperature is also found to a play a significant role in the inhibitive performance of the two inhibitors. For BDMTI, it is noted that inhibition efficiency increases with increase in temperature while for HMBTI, inhibition efficiency increased with increase in temperature up to 50 °C and subsequently decline when the temperature is raised to 60 °C.

7.4.3 PDP and LPR measurements

To gain insights into the kinetics of anodic reaction (metal dissolution) and cathodic reaction (hydrogen evolution), PDP experiments were undertaken for API 5L X60 steel in 1 M HCl devoid of and in the presence of different concentrations of BDMTI and HMBTI at 25 °C. Figure 7.2 depicts the polarization curves for (a) BDMTI and (b) HMBTI respectively. It can be deduced from the plots that the nature of the polarization curves are the same in both the uninhibited and inhibited solutions. However, addition of both BDMTI and HMBTI to the corrosive medium (1 M HCl) reduces the corrosion rate of the steel specimen as evidenced in the shifting of the corrosion current density to regions of lower values in comparison to the blank indicating corrosion inhibiting ability of the compounds. Examination of Figure 7.2 also reveals that the corrosion potential (E_{corr}) in the presence of both BDMTI and HMBTI shifted to noble values relative to the blank.

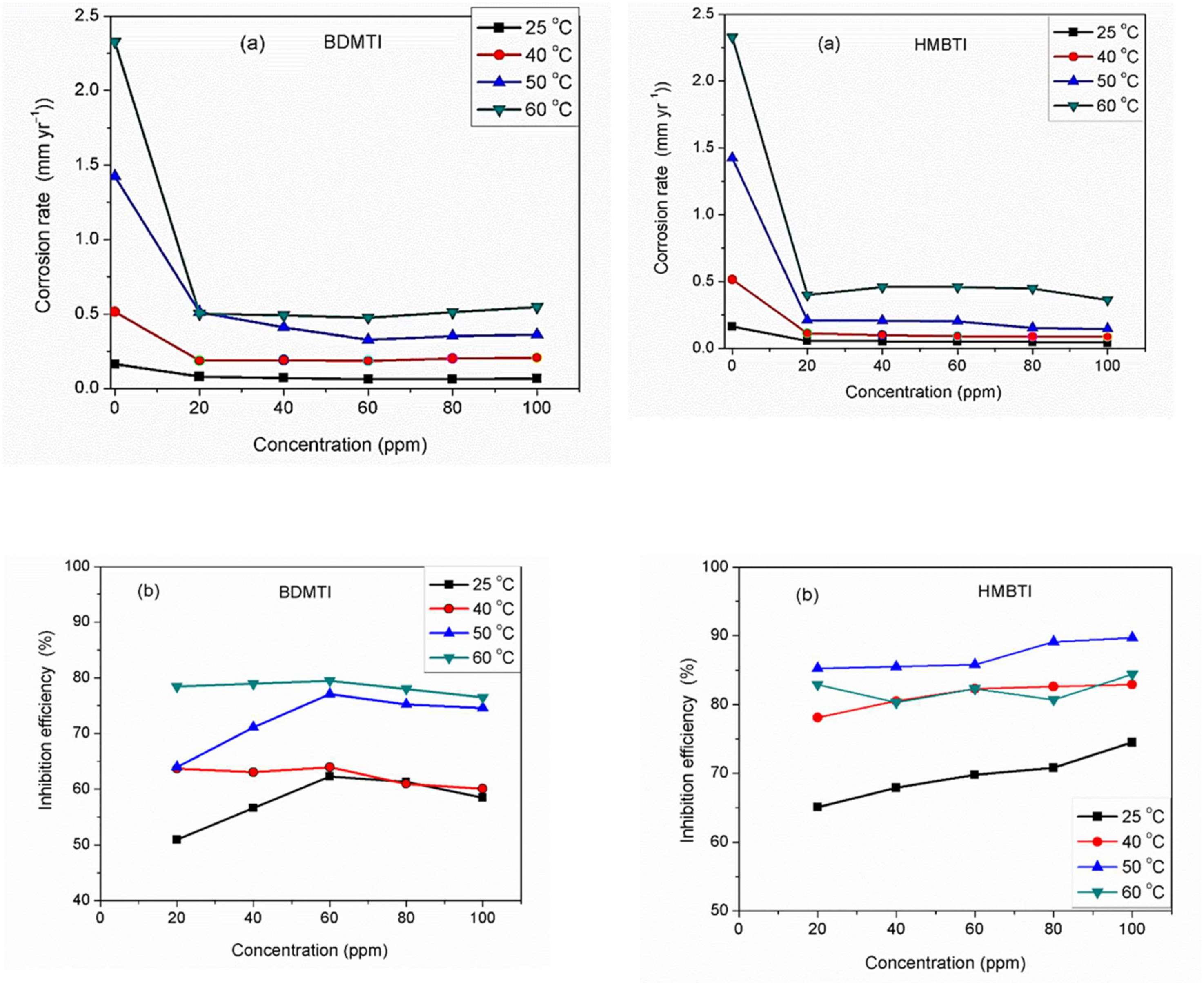

Figure 7.1 Variation of (a) corrosion rate and (b) inhibition efficiency with concentration for API 5L X60 steel without and with different concentrations of BDMTI and HMBTI in 1 M HCl solution at different temperatures from gravimetric measurements

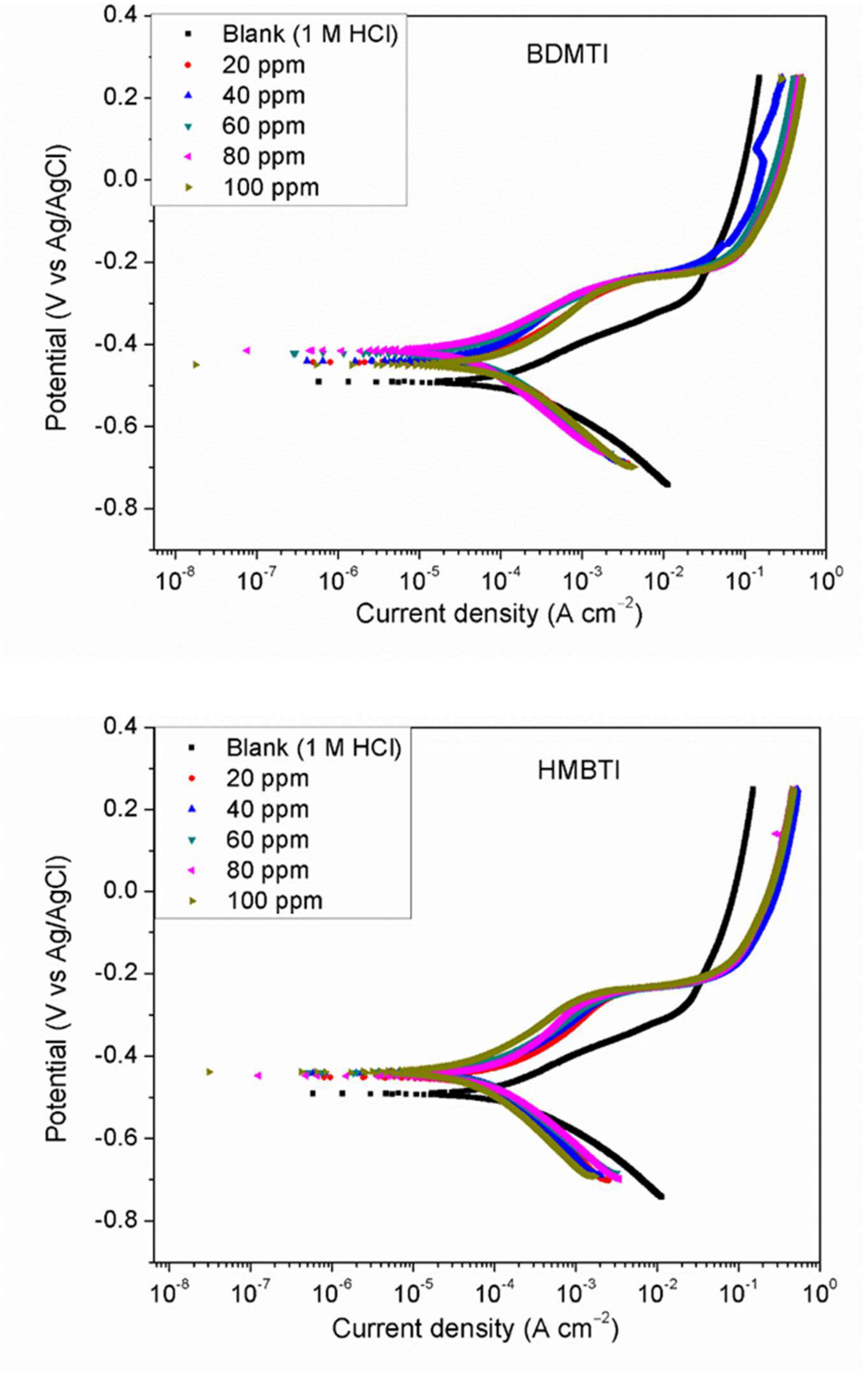

Figure 7.2 Potentiodynamic polarization plots for API 5L X60 steel without and with different concentrations of (a) BDMTI and (b) HMBTI at 25 ºC

Electrochemical parameters obtained from the analysis of the polarization curves using extrapolation method are displayed in (Table 7-1).

Table 7-1 Potentiodynamic polarization (PDP) and Linear polarization resistance (LPR) parameters for API 5L X60 steel in 1 M HCl without and with different concentrations of BDMTI and HMBTI at 25 °C

				PDP method			LPR method	
Inhibitor	Concentration (mg/L)	E_{corr} (mV/Ag/AgCl)	I_{corr} (μA cm^{-2})	β_a (mV dec^{-1})	β_c (mV dec^{-1})	IE (%)	R_p (Ω cm^2)	IE (%)
BDMTI	Blank	–491	158.0	129.5	112.6	–	189.6	–
	20	–444	102.0	146.1	153.4	35.4	310.9	39.0
	40	–440	90.7	193.9	153.8	42.6	448.2	57.7
	60	–421	52.0	114.2	131.2	67.1	497.9	61.9
	80	–445	111.0	163.5	181.2	30.4	361.3	47.5
	100	–445	127.0	151.9	236.7	19.6	291.4	34.9
HMBTI	20	–441	118	129.3	250.4	25.3	336.8	43.8
	40	–440	115	151.4	218.8	27.2	369.4	48.7
	60	–432	74.4	107.9	152.3	52.9	370.4	48.8
	80	–439	55.6	129.6	161.3	64.8	380.7	50.2
	100	–400	30.8	85.3	130.6	80.5	643.6	70.5

It is clear from the table that corrosion current density decreased while the inhibition efficiency increased with increase in concentration of BDMTI up to 60 ppm. Beyond this concentration, an upward trend in corrosion current density and a downward trend in inhibition efficiency with a further increase in BDMTI concentration is observed. As regards to HMBTI, a reduction in corrosion current density and an increase in inhibition efficiency is clearly visible from (Table 7-1). This result is in agreement with that of gravimetric measurements. Again, it is noticed from (Table 7-1) that there are notable changes in both the anodic and cathodic Tafel constants in the presence of inhibitors relative to the blank although with respect to different concentrations of the inhibitors, no definite trend is seen. This suggests that both BDMTI and HMBTI function as a mixed type corrosion inhibitors [189].

LPR method was also employed to assess the corrosion inhibition performance of BDMTI and HMBTI for API 5L X60 in 1 M HCl solution. The values of the polarization resistance (R_p) and the computed inhibition efficiency obtained from LPR measurements are also listed in (Table 7-1). From the table, R_p is observed to increase in inhibited solution compared to the blank indicating that BDMTI and HMBTI inhibited corrosion of steel in the acid medium. The trend of inhibition efficiency as a function of the inhibitors concentration noted for gravimetric and potentiodynamic polarization measurements is the same for LPR measurements. For BDMTI, the optimum inhibition efficiency (61.9%) was realized at 60 ppm and above this concentration, the IE declined to the lowest value of 34.9% at 100 ppm. For HMBTI, the IE increased with increasing concentration to reach an optimum value of 70.5% at 100 ppm concentration.

7.4.4 EIS measurements

Figure 7.3 depicts impedance plots for API 5L X60 immersed for 1 h in 1 M HCl without and with different concentrations of BDMTI in (a) Nyquist, (b) Bode modulus and (c) phase angle representations. Similar plots for HMBTI are presented in Figure 7.4.

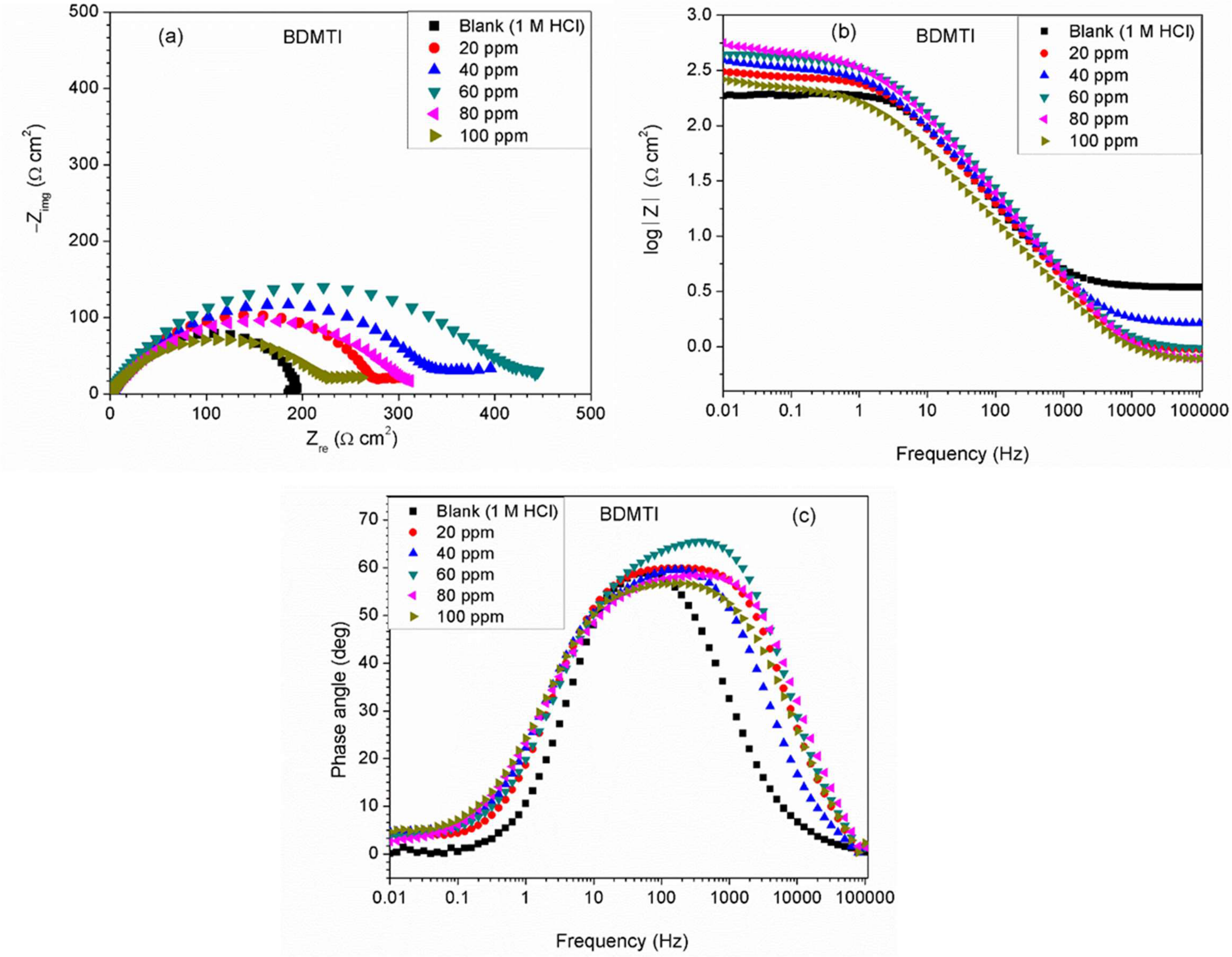

Figure 7.3 Impedance plots for API 5L X60 steel in 1 M HCl in the absence and presence of different concentrations of BDMTI exemplified as (a) Nyquist and (b) Bode modulus and (c) phase angle plots at 25 °C

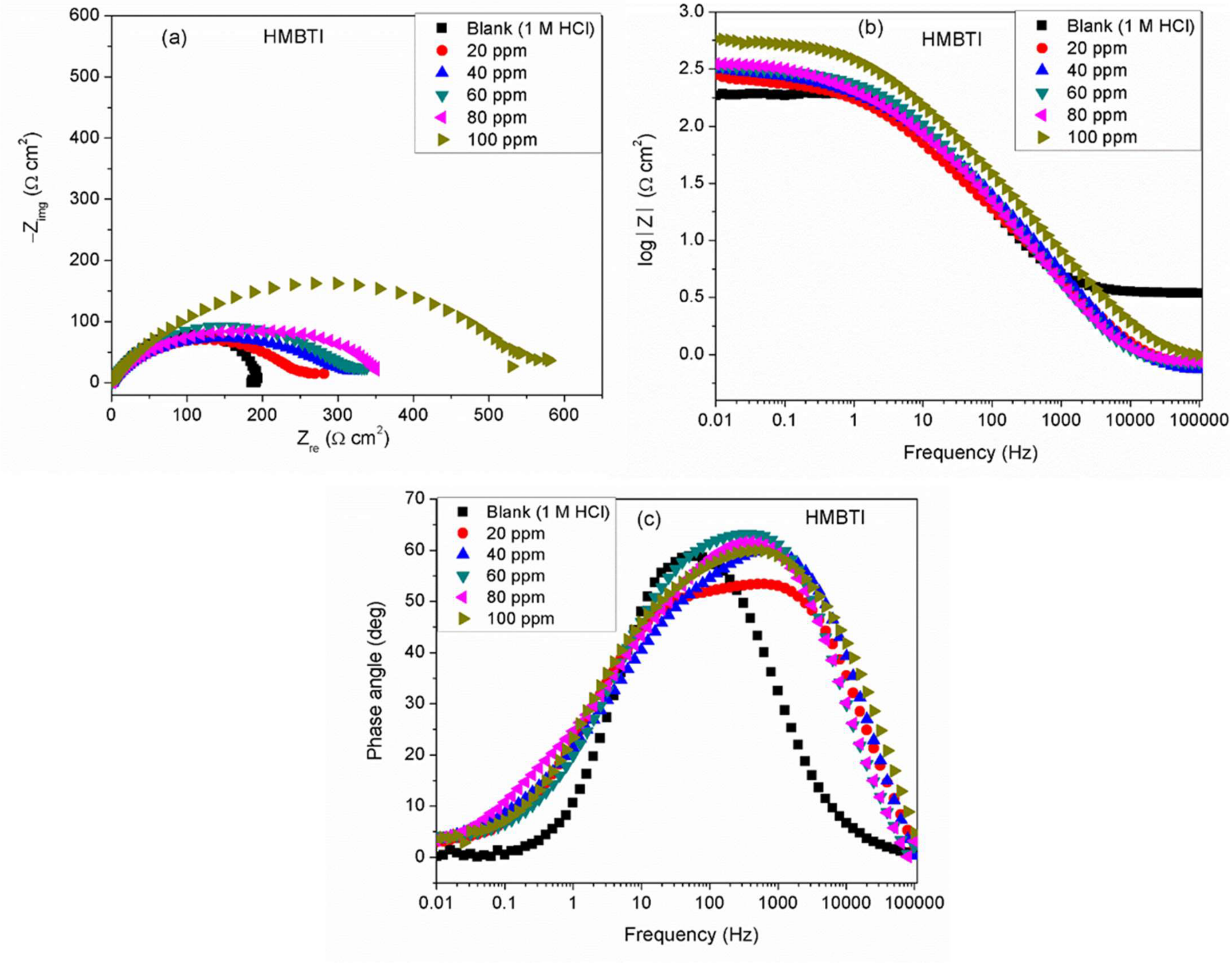

Figure 7.4 Impedance plots for API 5L X60 steel in 1 M HCl in the absence and presence of different concentrations of HMBTI exemplified as (a) Nyquist and (b) Bode modulus and (c) phase angle plots at 25 °C.

As can be clearly seen, the Nyquist plot in each case is composed of one depressed capacitive semicircle corresponding to one time constant in the Bode plot. The shape of the Nyquist plot is the same both in the absence and presence of the inhibitors indicating no change in the mechanism of the corrosion process. However, the diameter of the semicircle changes with addition of the inhibitors to the corrosive environment becoming larger as the concentration of the inhibitor increases. The two studied inhibitors displayed different kinds of behavior with respect to the growth of the Nyquist semicircles with increment in concentration. For BDMTI, the semicircle increased with increase in concentration up to 60 ppm and thereafter diminished with further increase in concentration; whereas HMBTI showed a progressive increase in the Nyquist semicircle with concentration up to 100 ppm. The depressed nature of the semicircle is a characteristic of solid electrode that show frequency dispersion which is often associated with diverse physical phenomena including surface roughness and inhomogeneities of solid electrode in the course of corrosion process [190]. The Bode modulus displayed a single time constant which is consistent with the Nyquist spectra. The value of absolute Bode modulus is seen to shift to higher values in the low frequency region with increase in the concentration of the inhibitors, again pointing to effective corrosion inhibition by higher inhibitor concentrations than lower concentrations especially for HMBTI. The phase angles in all cases are moving towards 80° and thus eliminate possible diffusion control process [191]. In modeling of corrosion systems, constant phase elements (CPE) are used in place of ideal capacitors to account for the non-homogeneity in the system [192]. The impedance of a CPE is given by:

$$Z_{CPE} = Y_o^{-1}\left(j\omega\right)^{-n} \qquad (6)$$

where is the CPE constant and ***n*** the CPE exponent; □ □ which is an imaginary number and ω is the angular frequency in rad/s. The impedance data was analyzed using an equivalent circuit that models the physical phenomena taking place at the steel – solution interface. Figure 7.5 depicts the equivalent circuit employed to simulate the experimental impedance data for the corrosion of API 5L X60 in 1 M HCl in the absence and presence of the inhibitors. The equivalent circuit consists of the solution resistance (R_s), charge transfer resistance (R_{ct}) and constant phase element (CPE). An excellent fit was obtained with this equivalent circuit as could seen from the goodness of fit values (Table 7-2). Electrochemical impedance parameters generated from the fitting results are listed in Table 7-2. From Table 7-2, it is clearly seen that the charge transfer resistance exhibits an increasing trend with increasing BDMTI concentration up to 60 ppm and beyond this concentration, it decreases, while for HMBTI, it increases with increase in concentration within the range of concentration studied. The CPE exponent, n is a measure of surface inhomogeneity, and it is observed to decrease in the presence of the inhibitors compared to the blank. Similar observation has been reported by Oguzie *et al.* and other workers [193], [194] which was attributed to an increase in heterogeneity resulting from the adsorption of the inhibitors on the metal steel surface.

The values of double layer capacitance (C_{dl}) were computed using the equation [195]:

$$C_{dl} = Y_0(\omega_{\max})^{n-1} \tag{7}$$

where $\omega_{max} = 2\pi f_{max}$, f_{max} is the frequency at which the imaginary component of the impedance is maximum. The C_{dl} values are observed to decrease in the presence of the inhibitors relative to the blank. In general, organic compounds have a much lower dielectric constant and a larger volume than water molecule [196]. The decrease in C_{dl} values might be attributed to the gradual replacement of water molecules by the adsorption of the organic molecules at the steel/solution interface [197]. The thickness of the protective film (δ) is related to C_{dl} according to the expression of the layer capacitance presented in the Helmholtz model [198],

$$C_{dl} = \frac{\varepsilon\varepsilon_0 A}{\delta} \tag{8}$$

where ε is the dielectric constant of the medium, ε_0 is the vacuum permittivity, A is the area of the electrode and δ is the thickness of the protecting layer.

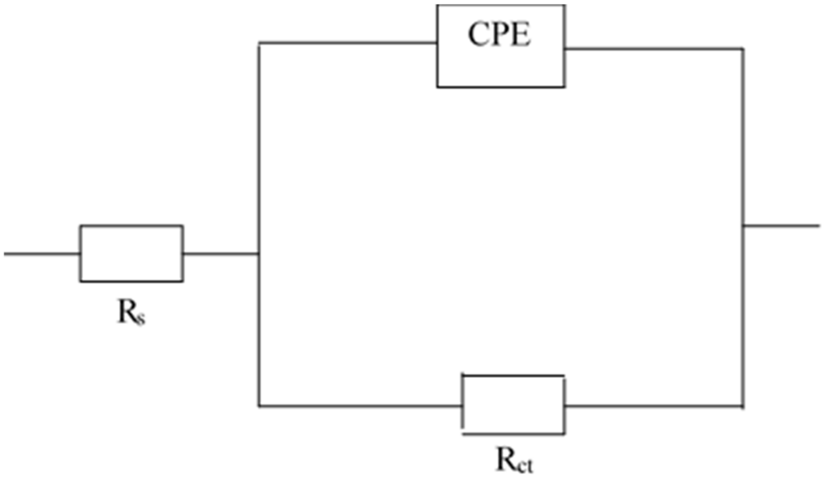

Figure 7.5 Equivalent circuit diagrams used to fit impedance data in the absence and presence of BDMTI and HMBTI

Table 7-2 Electrochemical impedance spectroscopy parameters for API 5L X60 steel in 1 M HCl without and with different concentrations of BDMTI and HMBTI at 25 °C

Inhibitor	Concentration (mg/L)	R_s (Ω cm^2)	R_{ct} (Ω cm^2)	Y_o ($\mu\Omega s^n$ cm^{-2})	n	C_{dl} (μF cm^{-2})	$\chi^2 \times 10^{-3}$	IE (%)
	Blank	3.44	192.9	784.7	0.82	377.2	1.00	–
BDMTI	20	0.85	291.0	388.7	0.75	184.3	2.76	33.7
	40	1.51	353.3	276.4	0.74	147.6	2.68	45.4
	60	0.89	417.6	241.0	0.78	131.5	3.99	53.8
	80	0.69	307.7	403.0	0.72	208.9	3.46	37.3
	100	0.69	237.6	488.9	0.71	241.0	2.51	18.8
HMBTI	20	0.58	275.8	500.0	0.69	198.2	11.6	30.1
	40	0.76	303.1	343.3	0.76	177.3	5.74	36.4
	60	0.72	324.4	389.1	0.75	246.4	3.25	40.5
	80	0.81	547.9	299.8	0.70	150.6	3.15	64.8
	100	0.76	597.4	213.0	0.81	157.3	2.53	67.7

7.4.5 Effect of iodide ions

The corrosion rate and inhibition efficiency from weight loss measurements for API 5L X60 steel in 1 M HCl without and containing 60 ppm BDMTI, 60 ppm HMBTI, 5 mM KI, 60 ppm BDMTI + 5 mM KI and 60 ppm HMBTI + 5 mM KI at 25 and 60 °C are shown in Figure 7.6 (a) and (b) respectively.

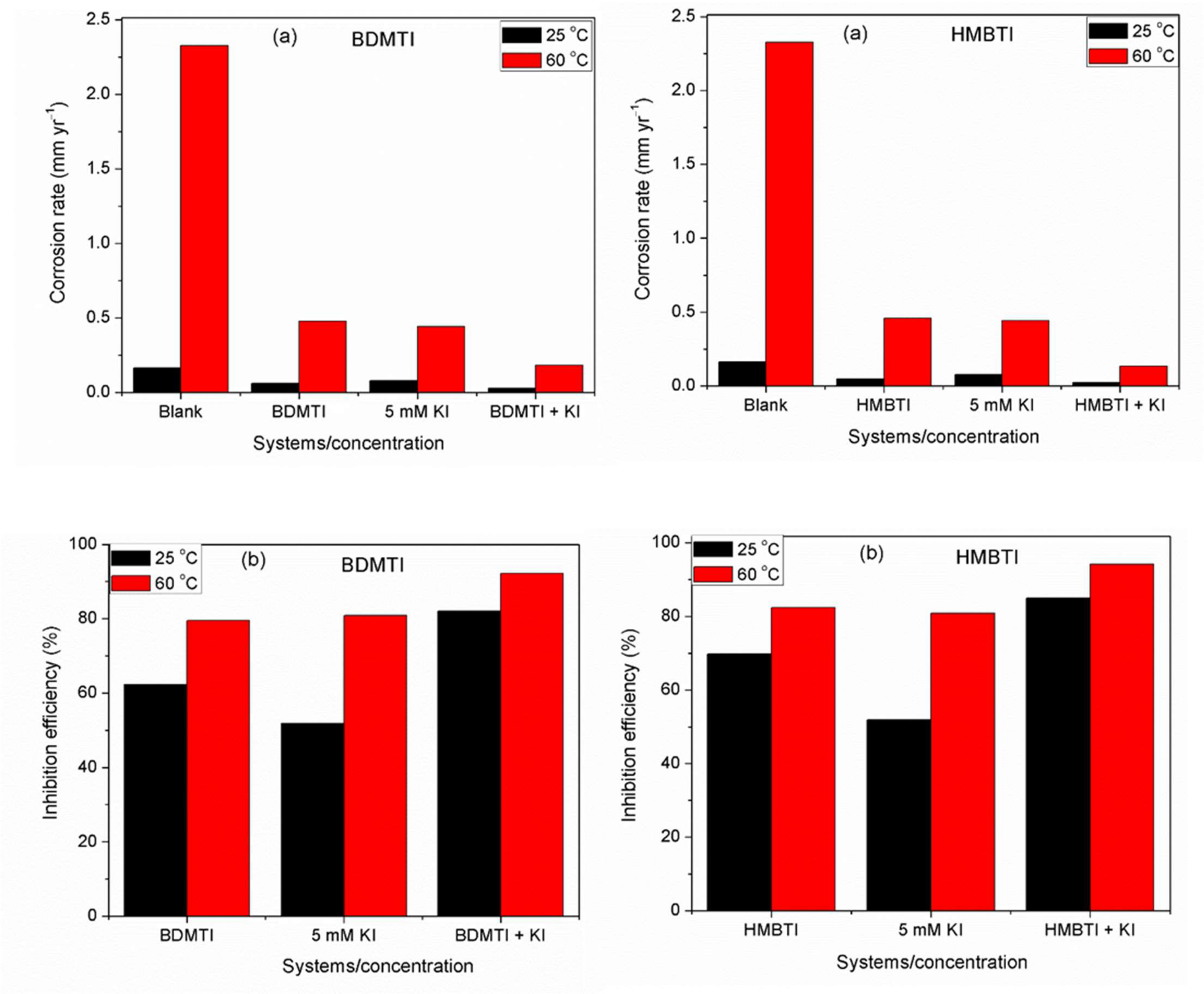

Figure 7.6 Plots showing (a) corrosion rate and (b) inhibition efficiency for API 5L X60 steel in 1 M HCl without and with KI, BDMTI, HMBTI, BDMTI + KI and HMBTI + KI at 25 and 60 ºC from gravimetric measurements

.

Inspection of the figure reveals that corrosion rate decreased when the two inhibitors and KI were added to the corrosive medium indicating that the corrosion of the steel was slowed down in the presence of the additives. Further reduction in corrosion rate is recorded in the presence of inhibitors – KI mixtures. Also, corrosion rate is observed to increase with increase in temperature from 25 to 60 ºC in the absence and presence of the additives. The inhibition efficiencies in the presence of BDMTI, HMBTI and KI alone are 62.3, 69.8 and 51.9 %, respectively at 25 ºC. The values obtained at 60 ºC were 79.5, 82.3 and 80.9% respectively. In the presence of BDMTI + KI, the IE values were 82.1 and 92.2% at 25 and 60 ºC, respectively while for HMBTI 84.9 and 94.2% inhibition efficiency were recorded at 25 and 60 ºC, respectively. These data clearly show that IE increases with increase in temperature. The increased inhibition efficiency of BDMTI and HMBTI in the presence of iodide ions shows the possible existence of synergism between the two inhibitors and iodide ions. However, in order to determine the existence of synergistic effect between BDMTI and HMBTI and iodide ions, the synergistic parameter (S_1) given by the expression in equation (9) was computed [199]–[201]:

$$S_1 = \frac{1-\theta_{1+2}}{1-\theta'_{1+2}} \qquad (9)$$

where $\theta_{1+2} = (\theta_1 + \theta_2) - (\theta_1\theta_2)$, θ_1 is the surface coverage (θ) of BDMTI and HMBTI, θ_2 is the surface coverage (θ) of KI and θ'_{1+2} is the combined surface coverage (θ) of BDMTI/ HMBTI and KI. S_1 greater than unity points to existence of synergism between the selected inhibitors combination, whereas S_1 less than unity indicates antagonistic effect which may lead to competitive adsorption, and no interaction between the two inhibitors prevails when S_1 is equal to unity. The synergistic parameter obtained for BDMTI were 1.01 and 0.50 at

25 and 60 °C, respectively, whereas the ones obtained for HMBTI at the same temperatures were 0.96 and 0.5, respectively. From these results, it does appear that there was no interaction between the inhibitors and KI at 25 °C since the synergistic parameter is almost or close to unity in case of BDMTI and HMBTI, respectively. At 60 °C, the synergistic parameter for both inhibitors is less than unity meaning that antagonistic rather than synergistic behavior between the inhibitors and KI prevails. The addition of iodide ions simply enhances the stability of both BDMTI and HMBTI adsorbed on the steel surface by co-adsorption mechanism suggested by some researchers [193], [202], [203]. The co-adsorption effect, which may be cooperative or competitive, is competitive in this case where the anion (I^-) and the inhibitors (BDMTI and HMBTI) are adsorbed on different sites on the metal surface.

7.4.6 Adsorption isotherm

The extent of corrosion inhibition is a function of mode of adsorption of the inhibitor as well as the surface conditions [204]. If it is assumed that the part of metal surface covered by inhibitor is immune to corrosion, and the area not covered are prone to corrosion, that is, the blocking effect of the adsorbed species is solely responsible for corrosion inhibition effect; then the degree of surface coverage (θ) is indispensable in the construction of adsorption isotherm. In the present work, θ values were estimated from the expression: $\theta = IE/100$ (assuming a direct relationship between surface coverage and inhibition efficiency) for different inhibitor concentrations from the weight loss measurement at different temperatures. The values obtained were theoretically fitted into different adsorption isotherm models and the correlation coefficient (R^2) value was used to select the best fit isotherm. Langmuir isotherm was found to be the best fit adsorption isotherm model to describe the adsorption of both BDMTI and HMBTI onto the steel surface. Langmuir isotherm is characterized by the following expression:

$$\frac{C_{inh}}{\theta} = \frac{1}{K_{ads}} + C_{inh} \tag{10}$$

where C_{inh} is the inhibitor concentration and K_{ads} is the equilibrium constant of the adsorption – desorption process. Figure 7.7 presents the plot of C_{inh}/θ against C_{inh} using θ values obtained for gravimetric technique at various temperatures. In all cases, linear plots were obtained and the R^2 values are close to one (Table 7-3) suggesting that the adsorption of BDMTI and HMBTI molecules onto the API 5L X60 steel surface obeys Langmuir isotherm.

Table 7-3 Langmuir adsorption parameters for API 5L X60 steel in 1 M HCl containing BDMTI and HMBTI from weight loss measurements at different temperatures

Inhibitor	Temperature (°C)	ΔG^{o}_{ads} (kJ mol^{-1})	K_{ads} (L mg^{-1})	slope	R^2
BDMTI	25	–37.01	3.07	1.66	0.988
	40	–32.13	0.23	1.69	0.998
	50	–32.91	0.21	1.27	0.997
	60	–36.49	0.53	1.32	0.999
HMBTI	25	–30.54	0.23	1.29	0.984
	40	–33.77	0.43	1.18	0.999
	50	–34.54	0.39	1.09	0.999
	60	–37.29	0.71	1.19	0.998

Although the plots are linear with good correlation coefficient values, the slopes are more than unity indicating a deviation from ideal Langmuir adsorption equation [205]. This suggests that there is an interaction between adsorbed species of the inhibitor molecules on the metal surface. Langmuir equation had been derived on the assumption that no interaction exist among adsorbed inhibitor molecules. This is not true as many reports in the literature have shown that large molecules such as polymers [206], [207] and organic molecules having polar groups [208] can interact by mutual repulsion or attraction.

From the values of K_{ads}, the standard free energy of adsorption for both BDMTI and HMBTI at different temperatures were obtained as follows [199]:

$$\Delta G^0_{ads} = -RT\ln\left(1\times10^6 K_{ads}\right) \qquad (11)$$

where R is the universal constant, T is the absolute temperature and 1×10^6 is the concentration of water molecules expressed in mg L^{-1} or ppm. The computed values of $\Delta G^{\mathrm{o}}_{\mathrm{ads}}$ listed in (Table 7-3) are in the range –30.54 and –37.29 kJ/mol. These values are less negative than –40 kJ/mol and more negative than – 20 kJ/mol. In the literature, the value of $\Delta G^{\mathrm{o}}_{\mathrm{ads}}$ equal to – 20 kJ/mol or less is taken to indicate physisorption involving electrostatic interaction between charged molecules, whereas that in the order of –40 kJ/mol or more is interpreted as chemisorption involving charge sharing or transfer from the inhibitors to the metal surface to form a kind of co-ordinate bond [199]. From the values of $\Delta G^{\mathrm{o}}_{\mathrm{ads}}$ obtained in this present work, it can be deduced that adsorption mechanism of both BDMTI and HMBTI on API 5L X60 steel surface may involve two types of interactions namely physisorption and chemisorption. As pointed out by Lozano et al. [204] as a consequence of strong adsorption of water molecules on the steel surface, it may be assumed that adsorption occurs first due to the physical forces. The replacement of the adsorbed water molecules is accompanied by a chemical interaction between the adsorbate (inhibitors) and the metal surface, which depicts chemisorption.

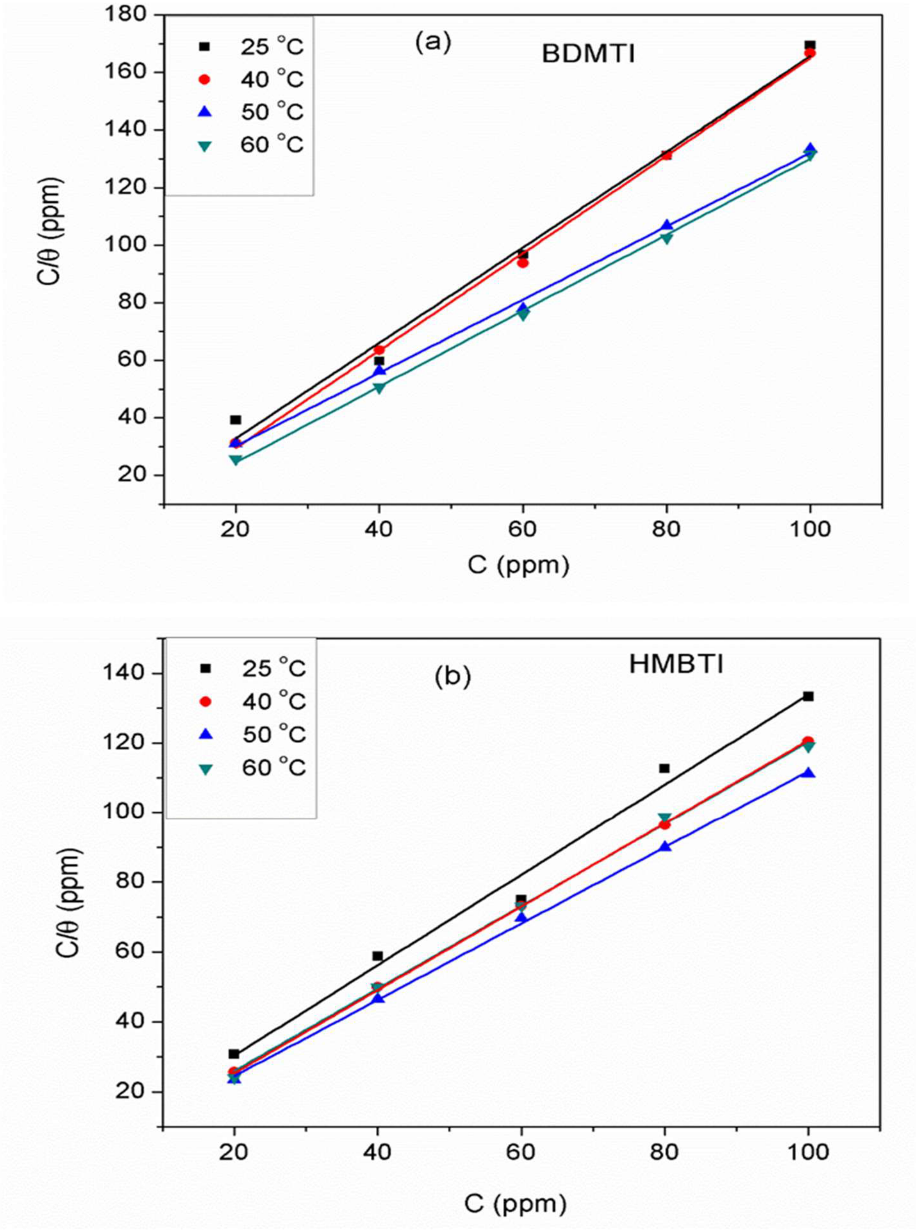

Figure 7.7 Langmuir adsorption isotherm for (a) BDMTI and (b) HMBTI on API 5L X60 steel in 1 M HCl at different temperatures

7.4.7 Effect of temperature

The influence of temperature on the corrosion inhibitive behavior of the two tested inhibitors were investigated by weight loss measurements in the temperature range 25 – 60 ºC. Results obtained as depicted in Figure 7.1 indicates that corrosion rate increased with increase in temperature in the absence and presence of the inhibitors. On the other hand, inhibition efficiency of the two inhibitors behave differently as temperature was increased. For BDMTI, *IE* increased with increase in temperature up to 50 ºC, and thereafter declined as the temperature was raised to 60 ºC. With respect to HMBTI, *IE* is noted to increase with increasing temperature. Increase in inhibition efficiency with increase in temperature is often ascribed to chemisorption of the inhibitor molecules on the metal surface. The apparent decrease in IE as temperature was raised from 50 to 60 ºC for BDMTI could be related to change of adsorption mode from chemisorption to physisorption caused by desorption of adsorbed inhibitor as a result of increased solution agitation due to higher rate of hydrogen gas evolution [192].

The apparent activation energy (E_a) for the corrosion process without and with BDMTI and HMBTI was computed from the Arrhenius equation:

$$Log\ C_R = \log A - \left(\frac{E_a}{2.303RT} \right) \qquad (12)$$

where C_R is the corrosion rate, E_a is the apparent activation energy, R is the molar gas constant, T is the absolute temperature, and A is the frequency factor. The Arrhenius plot of log C_R against reciprocal of absolute temperature ($1/T$) depicted in Figure 7.8 gives a straight line with slope of - $E_a/2.303R$ from which the activation energy was computed and listed in (Table 7-4). The enthalpy of activation (ΔH^*) and the entropy of activation (ΔS^*) for the corrosion of API 5L X60 in 1 M HCl were obtained from the transition state theory equation:

$$\log\left(\frac{C_R}{T}\right)=\left[\left(\log\left(\frac{R}{Nh}\right)+\left(\frac{\Delta S^*}{2.303R}\right)\right)\right]-\frac{\Delta H^*}{2.303RT} \qquad (13)$$

where h (□ỳ□□□□□□* □□! ÆŒŒ*≥) is the Planck's constant, N (□ỳ□□□□□* □□ÂÆ≠Ø! þ) is the Avogadro's number, R and T retain the earlier meanings. The plot of log (C_R/T) against $1/T$ is shown to be linear in Figure 7.9 from which ΔH^* and ΔS^* values were deduced from the slope and intercept of the plots respectively and also listed in (Table 7-4).

Table 7-4

Activation parameters for API 5L X60 steel in 1 M HCl in the absence and presence of different concentrations of BDMTI and HMBTI.

Inhibitor	Concentration (ppm)	E_a (kJ mol^{-1})	ΔH^* (kJ mol^{-1})	$-\Delta S^*$ (J mol^{-1} K^{-1})
	Blank	63.39	60.23	57.82
BDMTI	20	46.02	44.01	117.89
	40	46.85	44.38	117.47
	60	47.84	57.71	115.19
	80	49.02	45.37	111.54
	100	48.89	46.15	111.83
HMBTI	20	44.22	42.21	127.69
	40	49.26	46.61	113.93
	60	51.09	48.43	108.60
	80	49.02	46.37	115.85
	100	48.08	45.35	119.88

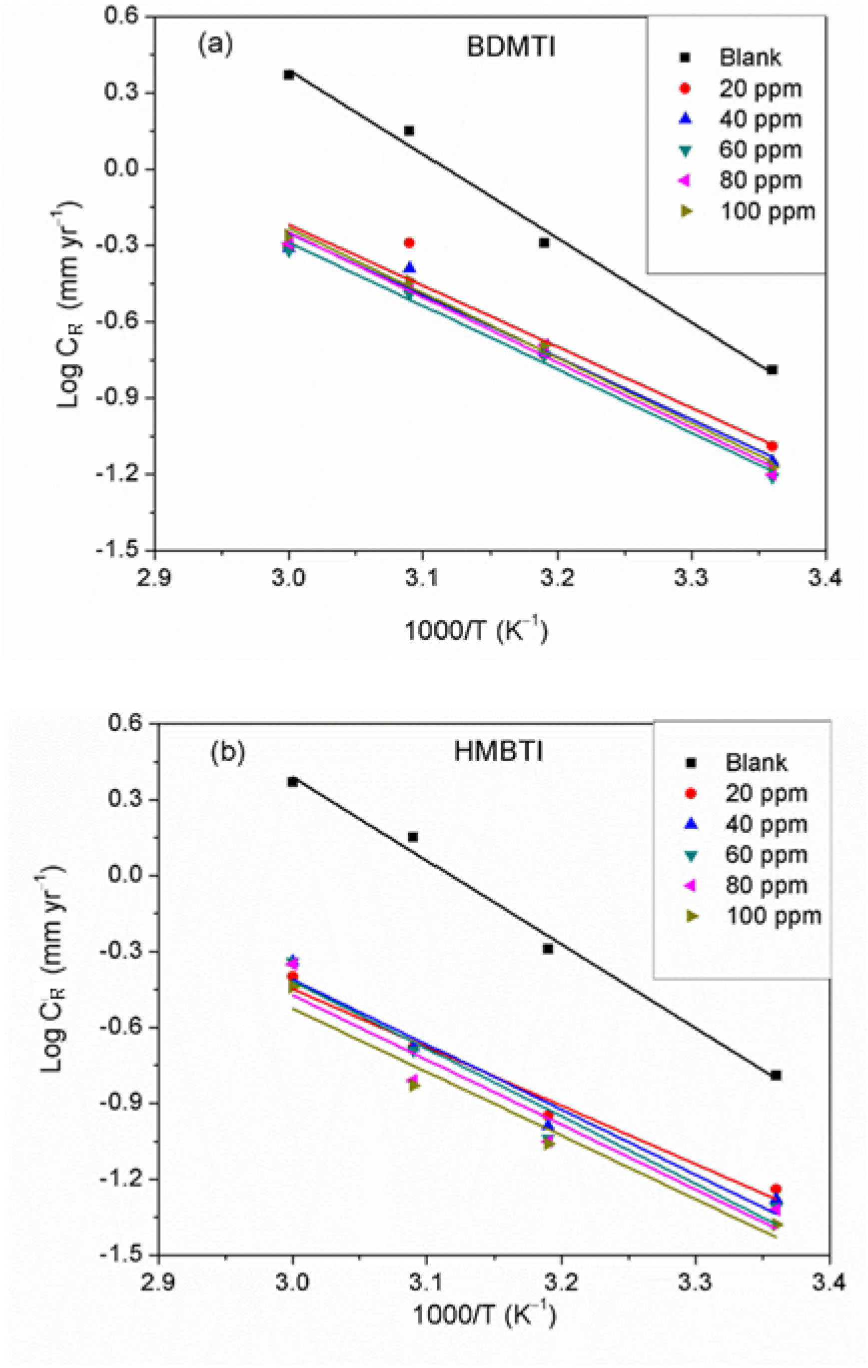

Figure 7.8 Arrhenius plot of Log C_R versus 1/T for API 5L X60 steel in 1M HCl in the absence and presence of different concentrations of (a) BDMTI and (b) HMBTI

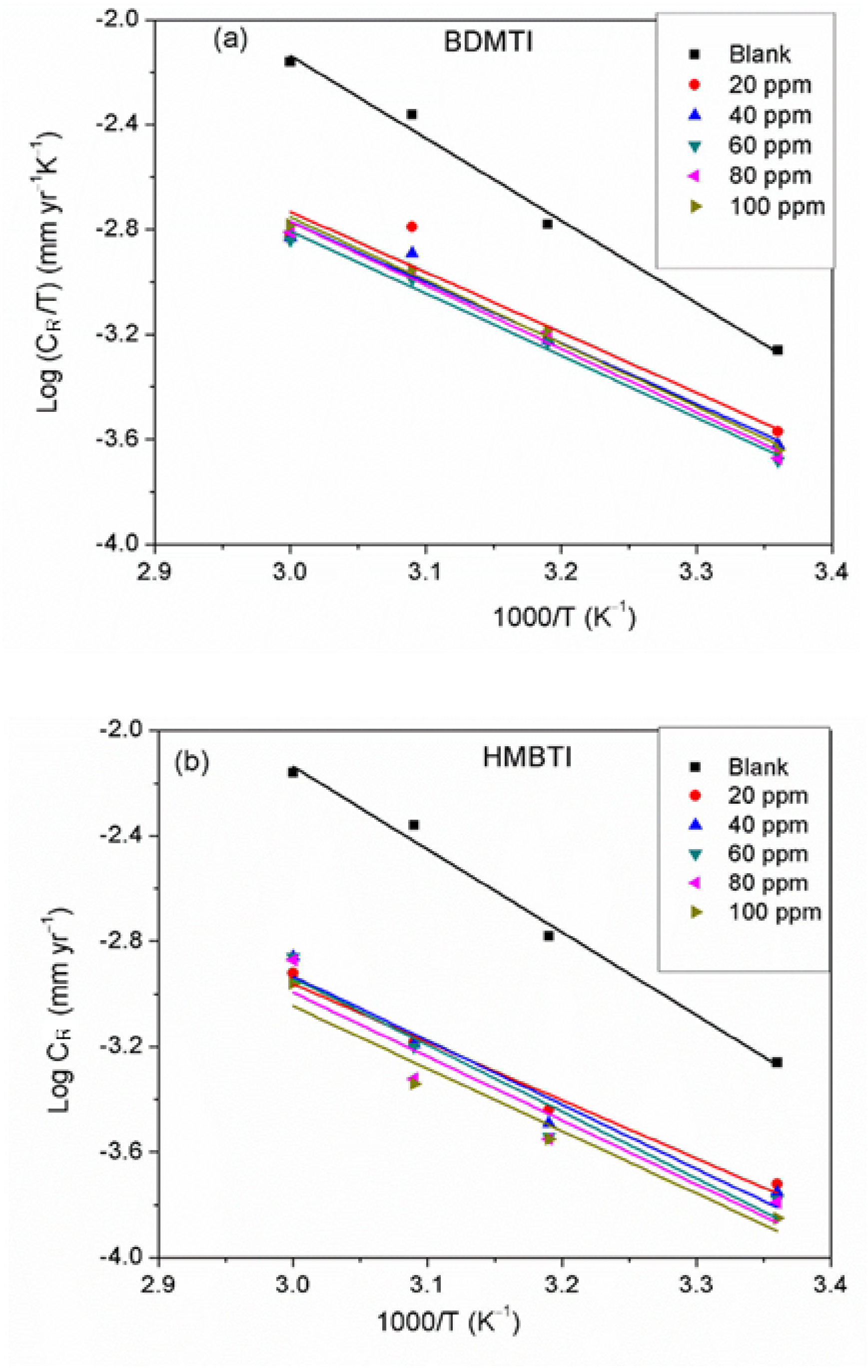

Figure 7.9 Transition state plot of Log C_R/T versus 1/T for API 5L X60 steel in 1M HCl in the absence and presence of different concentrations of (a) BDMTI and (b) HMBTI

The data in (Table 7-4) show that the values of E_a in the solution containing different concentrations of BDMTI and HMBTI are lower than those of the uninhibited solutions. It has been reported [205], [209], [210] that lower ɔ value in the presence of inhibitors relative to the blank is ascribed to chemical adsorption while the reverse is interpreted to mean physisorption mechanism. The variation of ɔ values in the inhibited solution with that of the uninhibited solution is consistent with the variation of inhibition efficiency with temperature. The activation entropy in all cases are negative, that is, in the absence and presence of the two tested inhibitors, and it is seen to be more negative in the presence of BDMTI and HMBTI. In the literature, this has been interpreted to mean that the activated complex in the rate determining step represents an association rather than dissociation step, meaning that during the adsorption process, a decrease in the degree of disorderliness takes place on moving from reactants to the activated complex. Hence, orderliness is stepped up as reactants are transformed to activated complex [211]. The enthalpy of activation values in all cases are positive, very close and exhibiting the same trend as E_a. In the literature, the negative sign of ΔH^* has been unequivocally associated with an exothermic adsorption process than can be either physisorption or chemisorption or combination of both [212], whereas the positive sign is linked to endothermic adsorption process which is attributed to chemisorptions. The positive sign of the enthalpy of activation as obtained in the present study reflects the endothermic nature of the steel dissolution process. This assumption is in agreement with the observed increase in inhibition efficiency with temperature indicating the chemisorption of the tested inhibitors on the metal surface.

7.4.8 Surfaces analysis

Figure 7.10 depicts the alteration observed in polished API 5L X60 steel surface morphology after 24 h immersion in 1 M HCl in absence and presence of 60 ppm BDMTI, 60 ppm HMBTI, and this concentration of the two tested inhibitors in combination of 5 mM KI. Surface micrographs of the steel specimens were obtained by SEM. As can be seen from Figure 7.10 b, the specimen treated with uninhibited 1 M HCl solution was highly corroded, and the surface became rough and porous. It is pertinent to conclude that the steel surface was highly damaged in absence of inhibitors due to fast and aggressive corrosion reaction. In the presence of both BDMTI and HMBTI (Figure 7.10 c and d), the API 5L X60 steel surface was much less damaged. A relatively smooth morphology of steel surface can be observed which shows the slowing down of the corrosion attack and the formation of a protective inhibitor film on the substrate surface. A smoother surface of API 5L X60 can be observed in Figure 7.10 e and f with BDMTI and HMBTI in combination with 5 mM KI, respectively. This illustrates a less damage surface, and can be linked to the co-adsorption of iodide ions and BDMTI and HMBTI molecules on the steel surface hence enhanced corrosion inhibition effect.

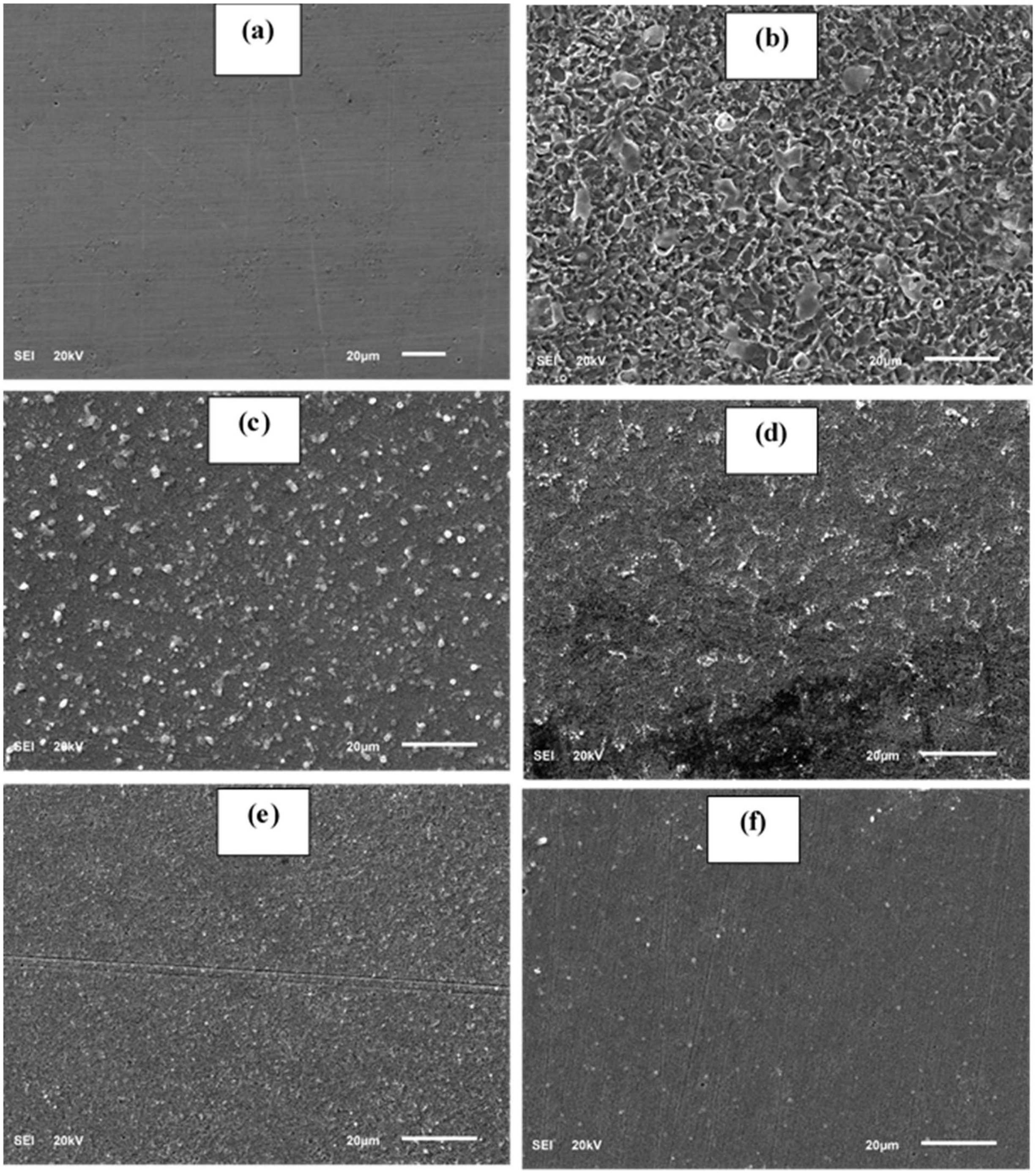

Figure 7.10 SEM images for API 5L X60 steel (a) in polished state (b) exposed to 1 M HCl solution (c) exposed to 1 M HCl solution containing 60 ppm DBMTI, (d) exposed to 1 M HCl solution containing 60 ppm HMBTI, (e) exposed to 1 M HCl solution containing 60 ppm DBMTI + 5 mM KI and (f) exposed to 1 M HCl solution containing 60 ppm HMBTI + KI at 25 °C for 24 h.

7.4.9 Quantum chemical calculations

Generally, HOMO and LUMO orbitals show the regions of molecule which can donate or accept electron, respectively. Molecule with large HOMO orbital can easily donate electron to unoccupied *d*-orbital of a metal atom. Conversely, molecules with large LUMO orbital can easily accept electrons from a *d*-orbital metal atom. The optimized structure, HOMO and LUMO diagrams of BDMTI and HMBTI molecules using DFT model chemistry in aqueous phase are illustrated in Figures. 8.11 and 8.12, respectively. In the figures, it is observed that the HOMO orbital for BDMTI are localized at 1,3-benzodioxole and isoxazolidine rings, whereas the HOMO of HMBTI is only localize on the isoxazolidine ring. These are the regions donating electron to unoccupied *d*-orbital of metal. On the other hand, LUMO orbitals for BDMTI are found on 1,3-benzodioxole, whereas those of HMBTI are localized on the 4-hydroxy-3-methoxybenzyl group. These regions can accept electron from metal surface. Thus, the HOMO and LUMO orbital analyses indicate that the isoxazolidine ring, benzodioxole ring, $C_6H_5(OCH_3)$ OH groups play an important role as active sites for the interaction of the two corrosion inhibitors with steel surface.

Optimized Structure

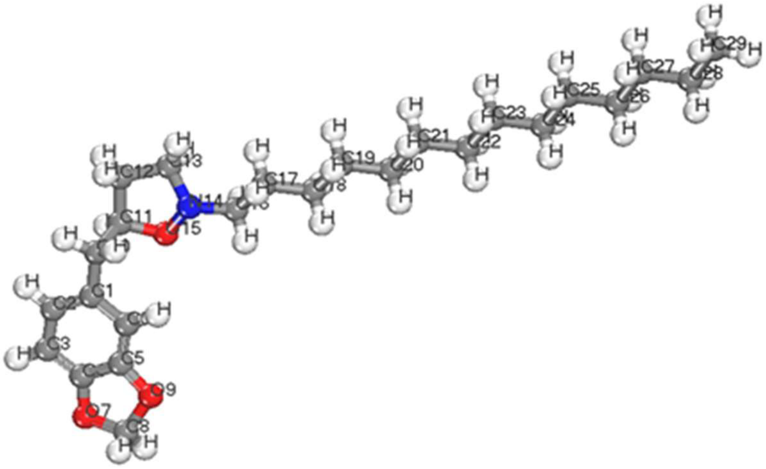

HOMO orbitals

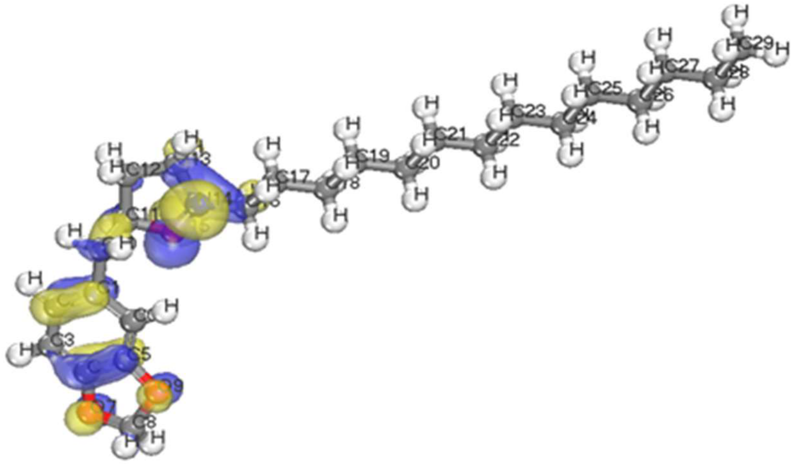

LUMO orbitals

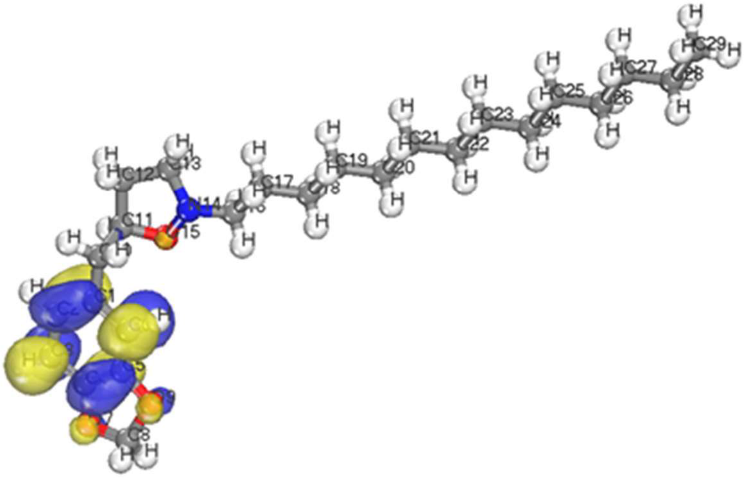

Figure 7.11 Optimized structure, HOMO and LUMO orbitals distribution of BDMTI

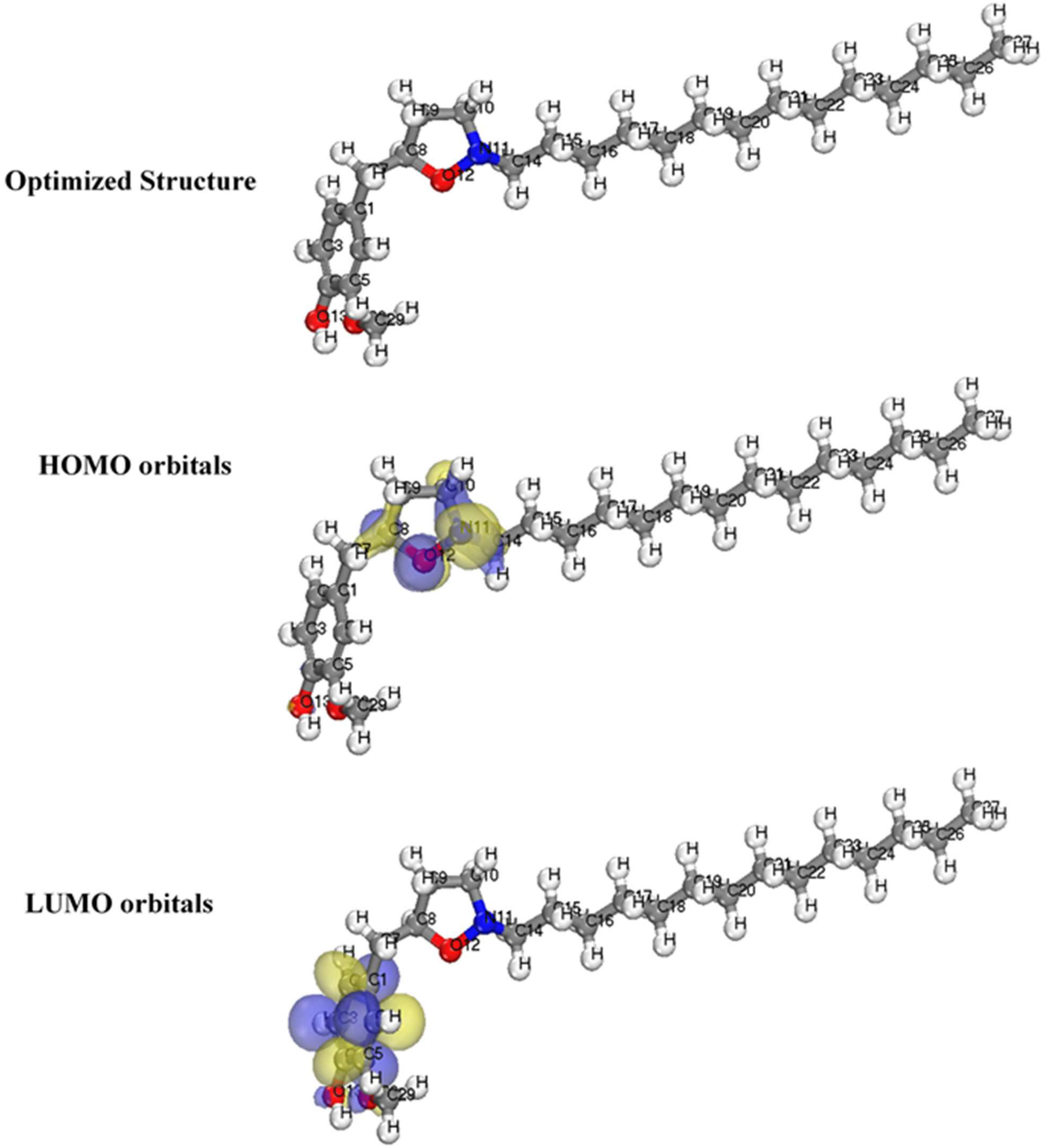

Figure 7.12 Optimized structure, HOMO and LUMO orbitals distribution of HMBTI

7.4.10 Monte Carlo simulations

Metropolis Monte Carlo simulations using simulated annealing procedure were further carried out to quantify the adsorption of BDMTI and HMBTI on steel surface. Figure 7.13 shows (a) snapshot of the stable equilibrium configuration of BDMTI adsorption on Fe (110) surface and (b) snapshot of the stable equilibrium configuration of HMBTI adsorption on Fe (110) surface. The simulation was carried out in the presence of water (100 H_2O). Table 7-5 shows the output of the results obtained using Monte Carlo simulations. As can be seen in Figures 8.13a and 8.13b, both molecules are adsorbed in a parallel orientation to the metal surface in order to maximize contact. It has been reported that the higher the negative adsorption energies, the stronger the interaction of inhibitor molecules with metal surfaces [213]–[215]. Results from Table 7-5, indicate that the order of adsorption energy is HMBTI > BDMTI. This shows that interaction of HMBTI with steel is expected to inhibit steel corrosion in acidic aqueous solution more than BDMTI. The theoretical results are in good agreement with the experiment.

Table 7-5

Parameters derived from Monte Carlo simulation of BDMTI and HMBTI adsorption on Fe (110)/100H_2O interface (kcal/mol).

Systems	Adsorption energy	Inhibition Efficiency (%)
Fe (110)- BDMTI/ 100H_20	-266.26	61.32
Fe (110)-HMBTI/100H_2O	-269.81	70.75

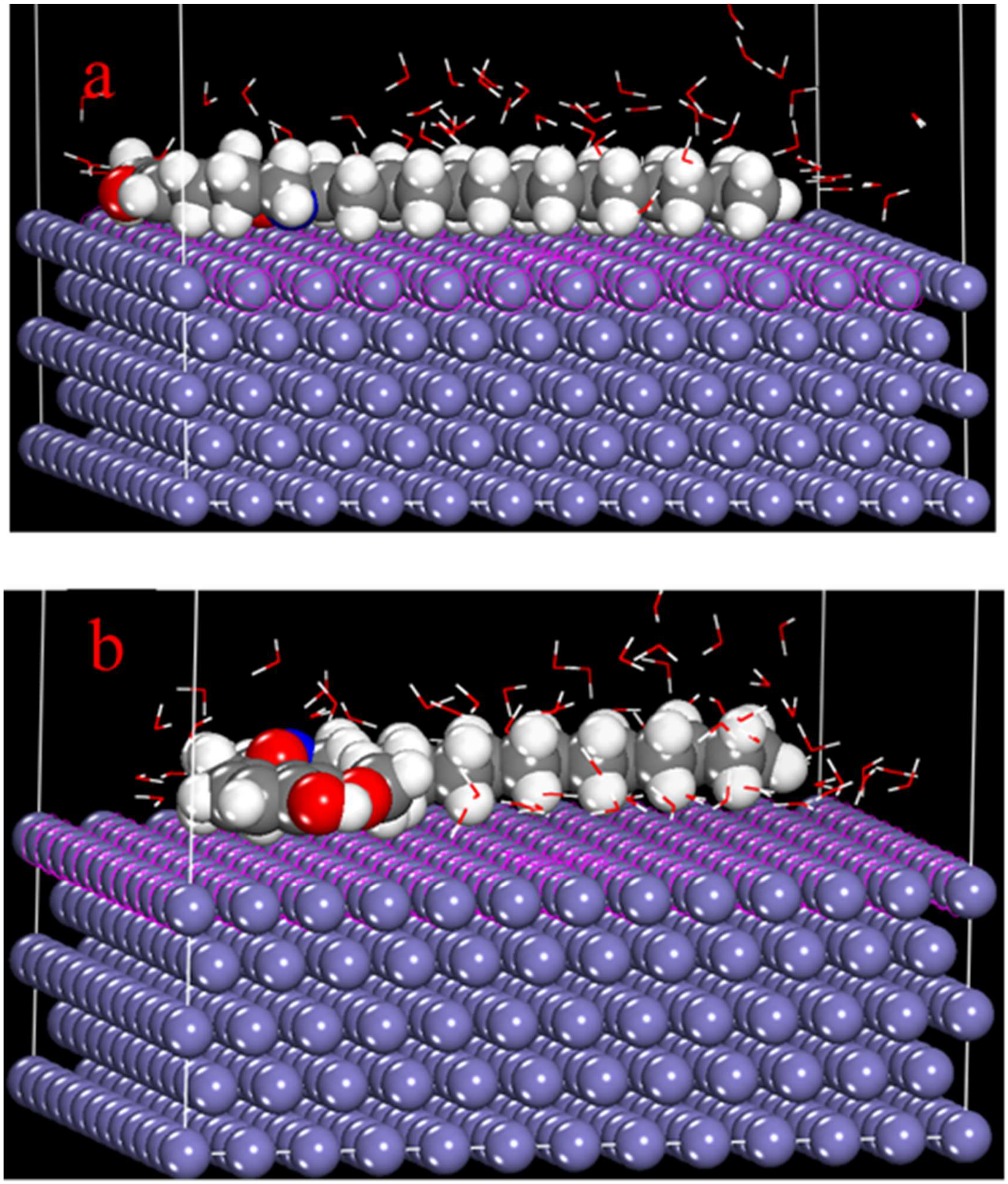

Figure 7.13 Stable equilibrium configuration of (a) BDMTI and (b) HMBTI adsorption on Fe (110)/100H_2O interface using Monte Carlo simulation methodology.

7.5 Conclusions

In the present investigation, two isoxazolidine derivatives namely 5-(benzo[d][1,3]dioxol-5-ylmethyl)-2-tetradecyl isoxazolidine (BDMTI) and 5-((4-hydroxy-3-methoxybenzyl)-2-tetradecyl isoxazolidine (HMBTI) were synthesized and characterized using FTIR, C-NMR, H-NMR, and elemental analyzer. The corrosion inhibition effect of the synthesized compounds for API 5L X60 steel in 1 M HCl solution was evaluated using weight loss and electrochemical techniques complemented with surface analysis of the corroded steel samples immersed in uninhibited and inhibited solutions with SEM. Theoretical studies were also undertaken to evaluate the adsorption/binding of the inhibitor molecules onto the steel surface. From the results obtained, the following conclusions could be drawn:

(1) Two new isoxazolidines having hydrophobic alkyl chain and π-electron-rich aromatic rings of naturally occurring safrole and eugenol have been synthesized using single-step nitrone cycloaddition reactions.

(2) The two synthesized compounds act as corrosion inhibitor for API 5L X60 in 1 M HCl, but with HMBTI showing superior performance.

(3) Corrosion inhibition performance is found to depend on the concentration of the inhibitors and temperature.

(4) Addition of small amount of iodide ions improves the inhibition efficiency of the two inhibitors due to co-adsorption of the iodide ions and the inhibitors on the steel surface.

(5) The co-adsorption of the inhibitors and iodide ions was found to be competitive in nature as confirmed from synergistic parameter (S_1) which was less than unity especially at higher temperature.

(6) Results of potentiodynamic polarization studies revealed that each of the two inhibitors functions as a mixed type corrosion inhibitor.

(7) Corrosion inhibition occurs by virtue of adsorption of the inhibitor molecules on the steel surface which was found to accord with Langmuir adsorption isotherm model.

(8) Results from the experimental and theoretical considerations are in good agreement confirming that HMBTI is a better corrosion inhibitor than BDMTI.

CHAPTER 8

ATTEMPTED ELABORATION OF BLOCK POLYMERIZATION OF EPOXIDE

8.1 ABSTRACT

Formation of copolymers having block of polyethylene glycol (PEG) **49** in the middle. Using potassium naphthalenide **50**, PEG was converted into its alkoxide at both ends of the polymer which was then subjected to undergo random polymerization with allyl glycidyl ether **7;** safrole oxide **2;** and both allyl glycidyl ether **7**, and safrole oxide **2** in presence of $^{i}Bu_3Al$ to get block copolymers **51**, **52** and **53**.

8.2 Experimental

8.2.1 Materials

Allyl glycidyl ether (99%) **7** distilled from CaH_2 , poly(ethylene glycol) (PEG) (Mn = 10,000 g mol^{-1}) dried under vacuum at 45 ºC for 4 hour, anhydrous THF distilled under sodium and stored under molecular sieves 4B, naphthalene potassium purchased from Aldrich Chemical. Potassium naphthalenide (0.4 M in THF) [216] was prepared in Schlenk flask and closed by rubber septum, safrole oxide **2** Section 3.3.3.

8.2.2 Synthesis of poly(allyl glycidyl ether)-block-poly(ethylene glycol)- block poly(allyl glycidyl ether)

PEG (0.50 g, 0.05 mmol) was added to a 50 mL flame-dried Schlenk flask with a glass-coated stirbar, dried under vacuum at 60 ␣ for 2 h then cooled to 40 ␣. Dry THF (~ 10 mL) was added via cannula under dry Ar. Potassium naphthalenide was added via cannula until getting persistence of light green color Figure 8.1. Allyl glycidyl ether **7** (0.57 g, 5.0 mmol) was added by syringe under Ar. The reaction was allowed to polymerize for 3 days. The reaction was quenched by methanol, then the solvent was removed, and the polymer was purified by a short silica plug using methanol/CH_2Cl_2 10% to elute the block copolymer.

8.2.3 Synthesis of poly allyl(glycidyl ether)-block poly(ethylene glycol)-block poly allyl(glycidyl ether) in presence of $^iBu_3Al$

The polymerization described in the Section 8.2.2 was repeated except that after allyl glacydyl ether was added. The reaction mixture was cooled to R.T., then triisobutylaluminium solution (25 wt. % in toluene) was added (1.0 mL in trial 1, and 0.5 mL in trial 2). The polymerization was stopped after 24 h by adding 4:1 MeOH/H_2O (10 mL). After removal of the solvents, the residual mixture was dissolved in CH_2Cl_2 (50 mL) and filtered over celite 545. Then, it was dried under (Na_2SO_4). The solvent was removed, and the polymer was purified by a short silica plug using methanol/DCM 10% to elute the block copolymer.

8.2.4 Synthesis of poly(safrole oxide-co-allyl glycidyl ether)-block poly(ethylene glycol)-block poly(safrole oxide-co-allyl glycidyl ether) in presence of $^{i}Bu_3Al$

PEG (0.58 g, 0.06 mmol) was added to a 50 mL flame-dried Schlenk flask with a glass-coated stirbar, dried under vacuum at 65 ⌣ for 2 h, then cooled to 45 ⌣. Dry THF (~ 15 mL) was added via cannula under dry Ar. Potassium naphthalenide was added via cannula until getting persistence of light green color. Allyl glycidyl ether **7** (0.90 g, 7.9 mmol) and safrole oxide (0.34 g, 1.9 mmol) were added by syringe under Ar. The reaction mixture was cooled to R.T., then triisobutylaluminium solution (25 wt. % in toluene) (1.0 Ml) was added. The polymerization was stopped after 4 days by adding 4:1 MeOH/H_2O (25 mL). After removal of the solvents, the residual mixture was dissolved in CH_2Cl_2 (50 mL) and filtered over celite 545. Then, it was dried under (Na_2SO_4). The solvent was removed, and the polymer was purified by a short silica plug using methanol/DCM 10% to elute the block copolymer.

8.2.5 Synthesis of poly(safrole oxide)-block poly(ethylene glycol)l-block poly(safrole oxide) in presence of $^{i}Bu_3Al$

PEG (0.50 g, 0.05 mmol) was added to a 50 mL flame-dried Schlenk flask with a glass-coated stirbar, dried under vacuum at 65 ⌣ for 3 h, then cooled to 40 ⌣. Dry THF (~ 15 mL) was added via cannula under dry Ar. Potassium naphthalenide was added via cannula until getting persistence of light green color. Safrole oxide (0.73 g, 4.1 mmol) was added by syringe under Ar. The reaction mixture was cooled to R.T. Then triisobutylaluminium solution (25 wt. % in toluene) (1.0 mL) was added. The polymerization was stopped after 20 h by adding 4:1 MeOH/H_2O (10 mL). After removal of the solvents, the residual mixture was dissolved in CH_2Cl_2 (50 mL) and filtered over celite 545. Then, it was dried under (Na_2SO_4). The solvent was removed, and the polymer was purified by a short silica plug using methanol/DCM 10% to elute the block copolymer.

Figure 8.1 Persistence of light green color whene PEG was converted into its alkoxide at both ends

8.3 Results and discussions

Block polymerization of allyl glycidyl ether **7** with PEG via potassium naphthalenide and potassium naphthalenide / ${}^{i}Bu_3Al$ are described in Scheme 8.1. The ${}^{1}H$ NMR spectra of these polymerization are shown in Figure 8.2a and 8.2b respectively. There are minor differences in the ^1H spectrum between the two spectra especially at 4.3-4.4 ppm and 5.8-6.0 ppm. This extra peaks appears in Figure 8.2a are related to an isomerization reaction of the allyl groups or fraction of allyl group happened to (Z)-prop-1-enyl group Scheme 8.2 [217], [63]. It was reported that polymerization reaction is related to temperature given by [63]:

¨Æө w̑ □□ỳ□□w □□Ẅ□□K4 □, ≠ Ø! þ ≥ þ □

In contrast, the reaction could be carried out at room temperature Scheme 8.1 by using $^iBu_3Al$, so the isomerization shown in Figure 8.2 b will be reduced. However, in case of $^iBu_3Al$, the result was two different contributions of AGE block polymer formed with 69% weight yield.

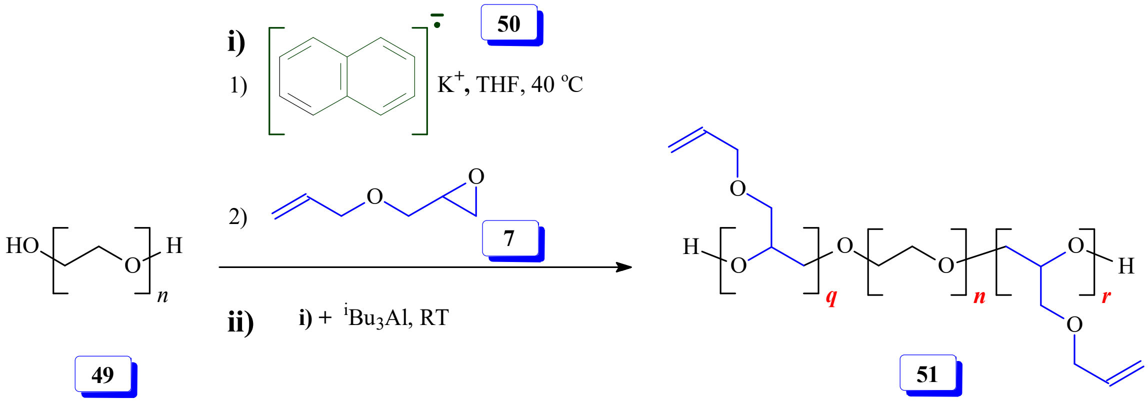

Scheme 8.1 Block polymerization of PEG **49** and AGE **7**

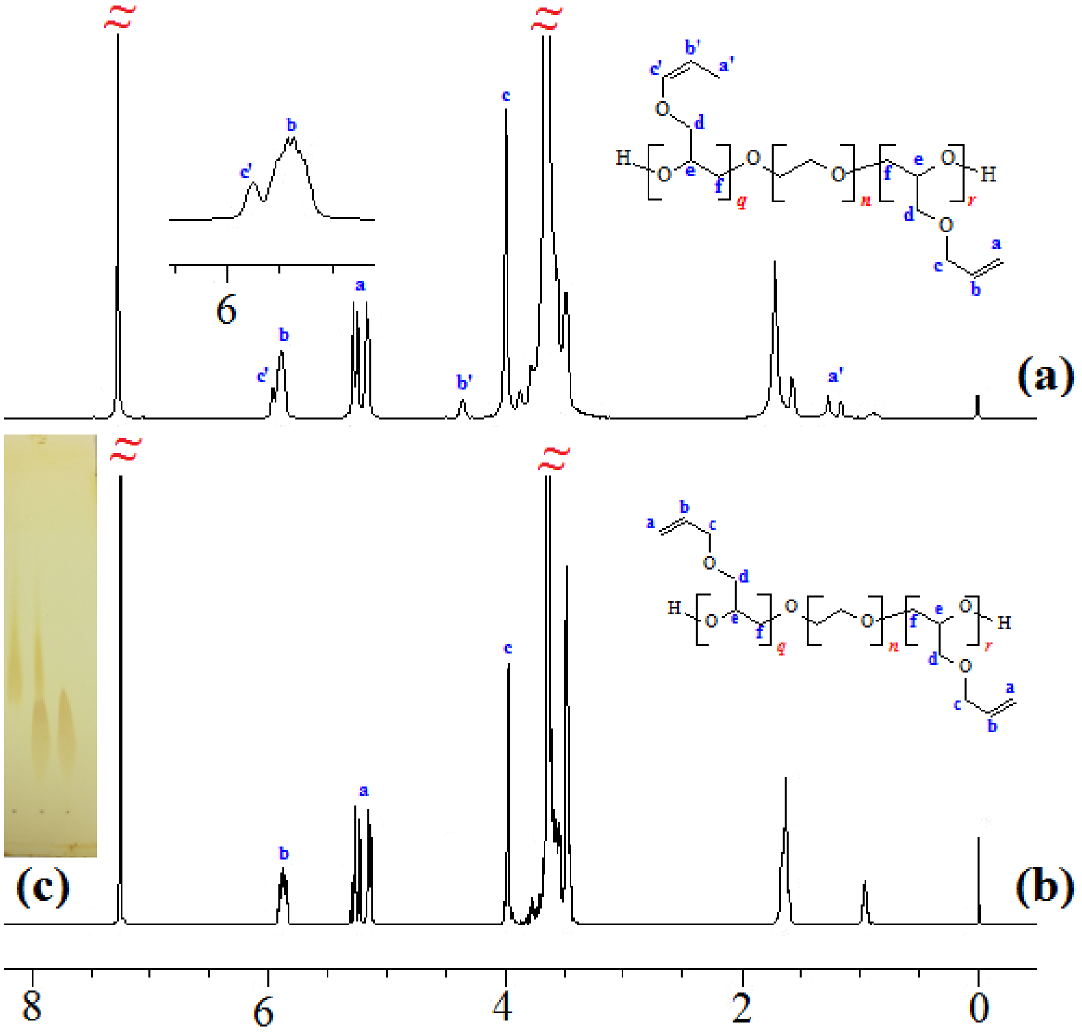

Figure 8.2 ^{1}H NMR spectra in $CDCl_3$ of PAGE-block-PEG-block PAGE 51 using (a) initiator **50**, and (b) initiator **50** in presence of $^iBu_3Al$; and TLC of PEG (on the left), PEG + polymer **51**, and polymer **51**

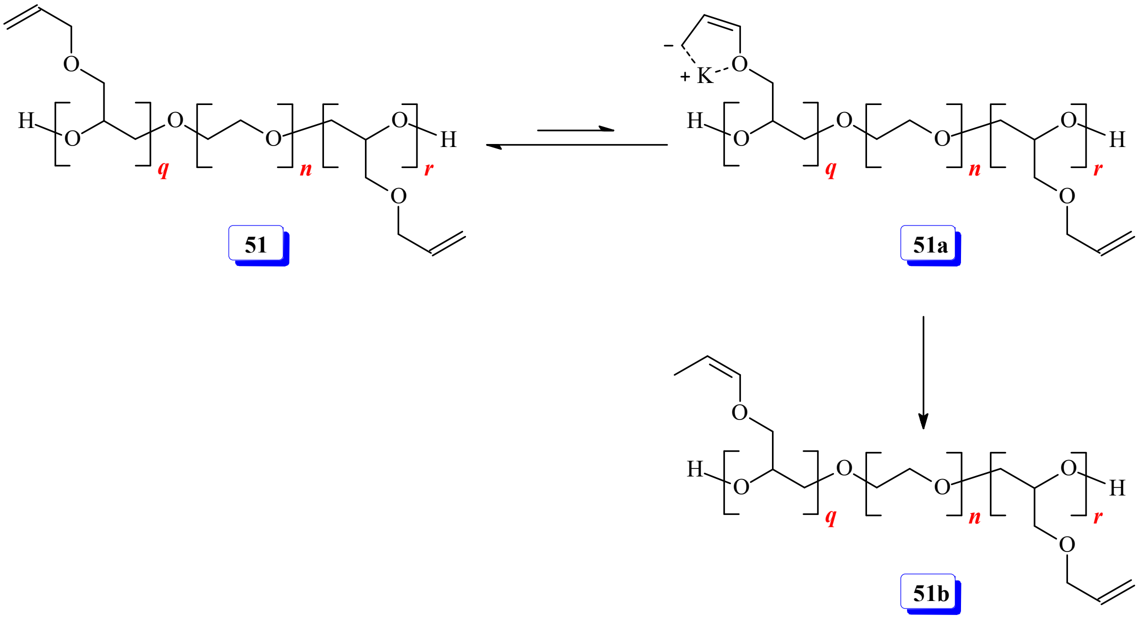

Scheme 8.2 Proposed isomerization of **51** to **51b**

The attempts to obtain block copolymers of PEG and safrole oxide **2** using only potassium naphthalenide did not succeed because a side reaction or extensive chain transfer happened as described previously in Section 3.3.4. However, the addition of $^{i}Bu_3Al$ with safrole oxide **2** Scheme 8.3 at room temperature gave the block copolymer Figure 8.3 in addition to a homopolymer of safrole oxide. This results is due to a side reaction or chain transfer happened at room temperature as mentioned in the literature where increase in the reaction temperature decreases the molar mass [218] because of chain transfer reaction. Furthermore, there is no point to conduct the reaction at lower temperature because of the very low solubility of PEG macroinitiator.

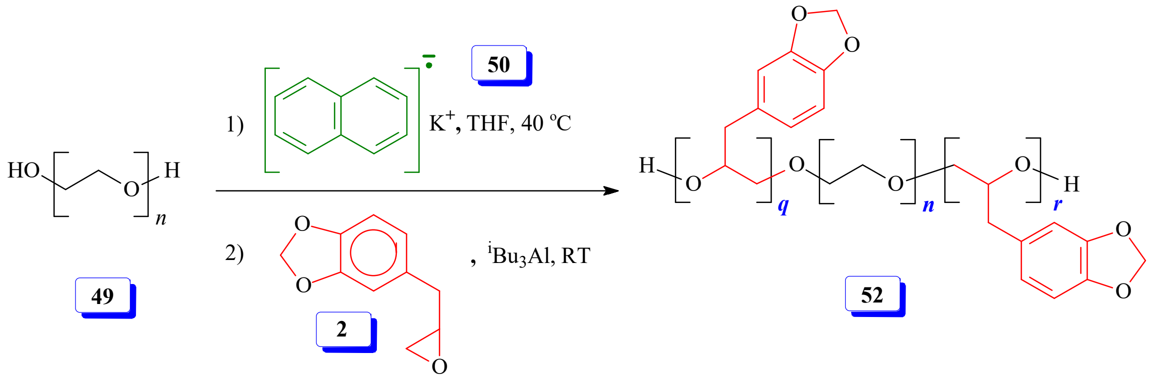

Scheme 8.3 Block polymerization of PEG **49** and SO **2**

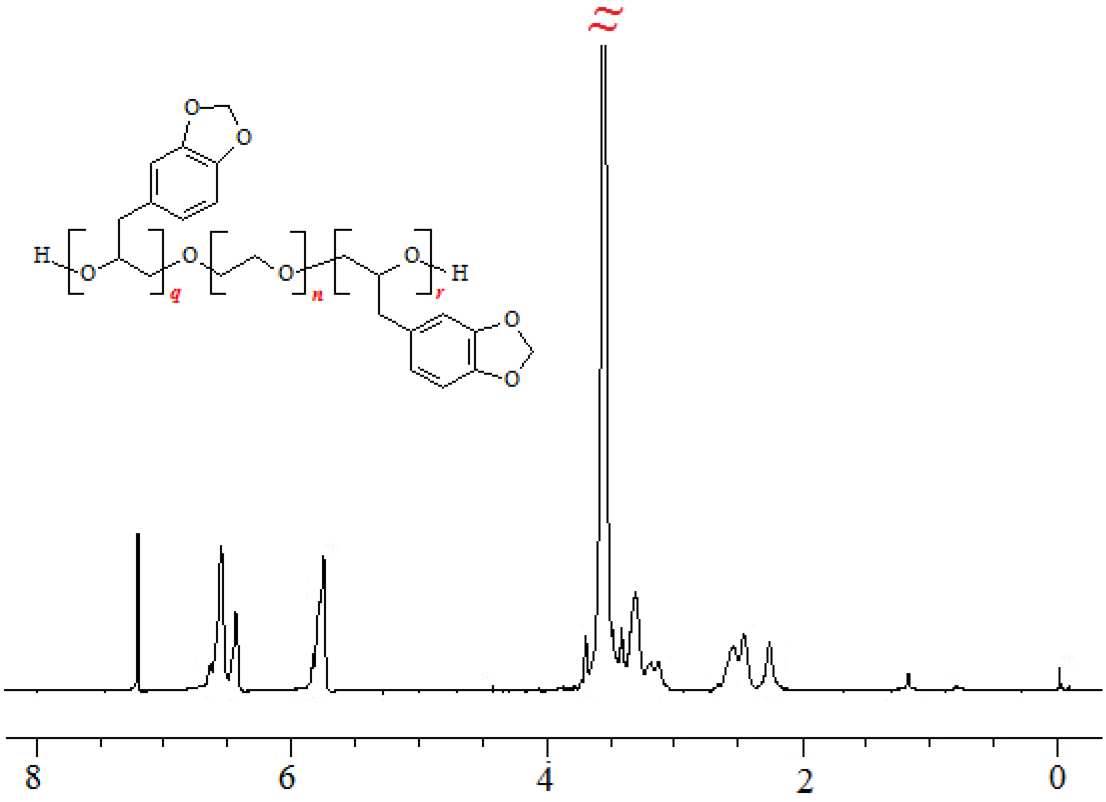

Figure 8.3 ^{1}**H** NMR spectra in $CDCl_3$ of SO-block-PEG-block SO **52**

Semiblock polymer having polyethylene glycol **49** in the middle block with copolymer of allyl glycidyl ether **7** and safrole oxide **2** was run as mention below Scheme 8.4. By using potassium naphthalenide **50**, PEG was converted into its alkoxide at both ends of the polymer, which was then subjected to undergo random polymerization with AGE **7** and safrole oxide **2** in presence of $^{i}Bu_3Al$. However, the experimental results were a mixture of semiblock polymers with different contribution of each component. Figure 8.4 shows one of this simiblock polymer.

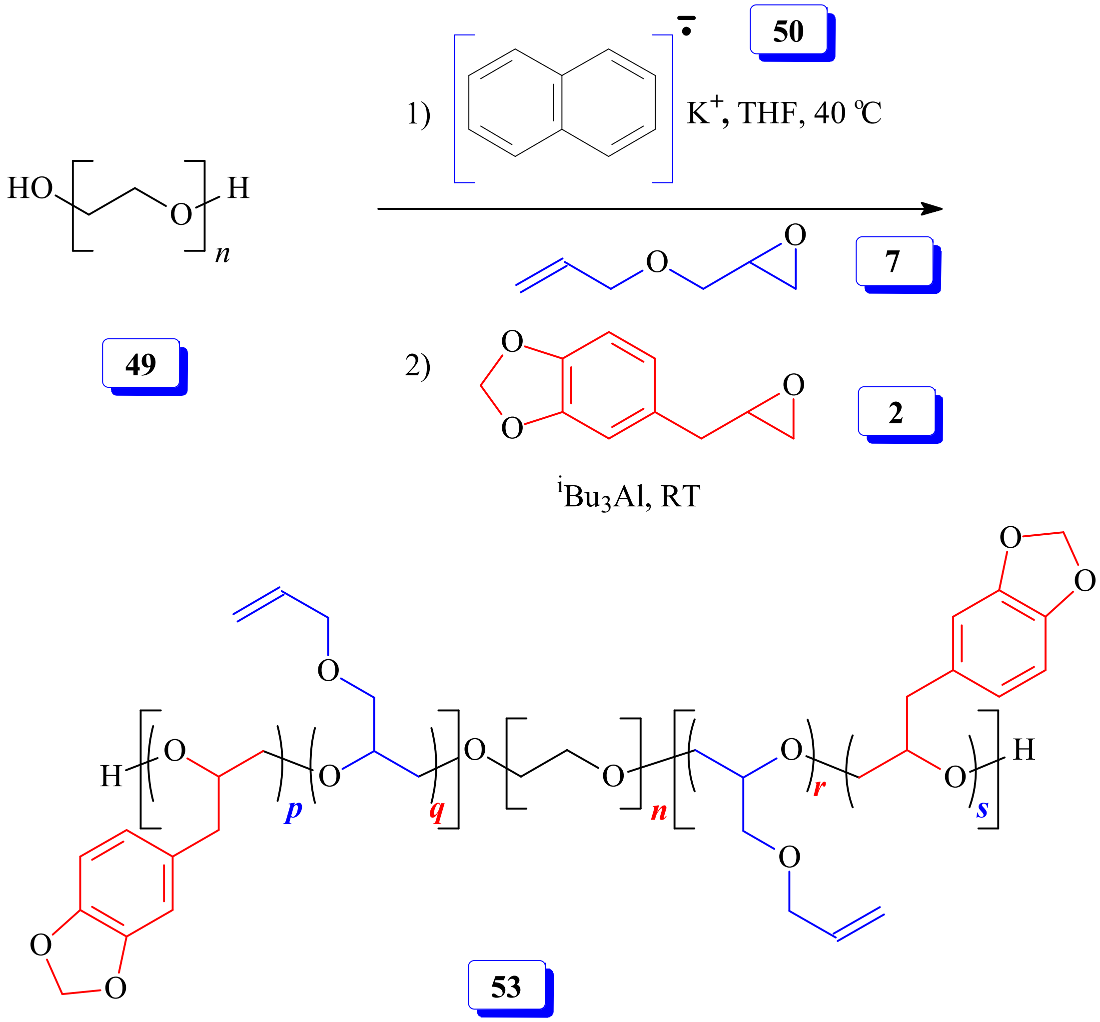

Scheme 8.4 Block polymerization of PEG **49**, AGE **7** and SO **2**

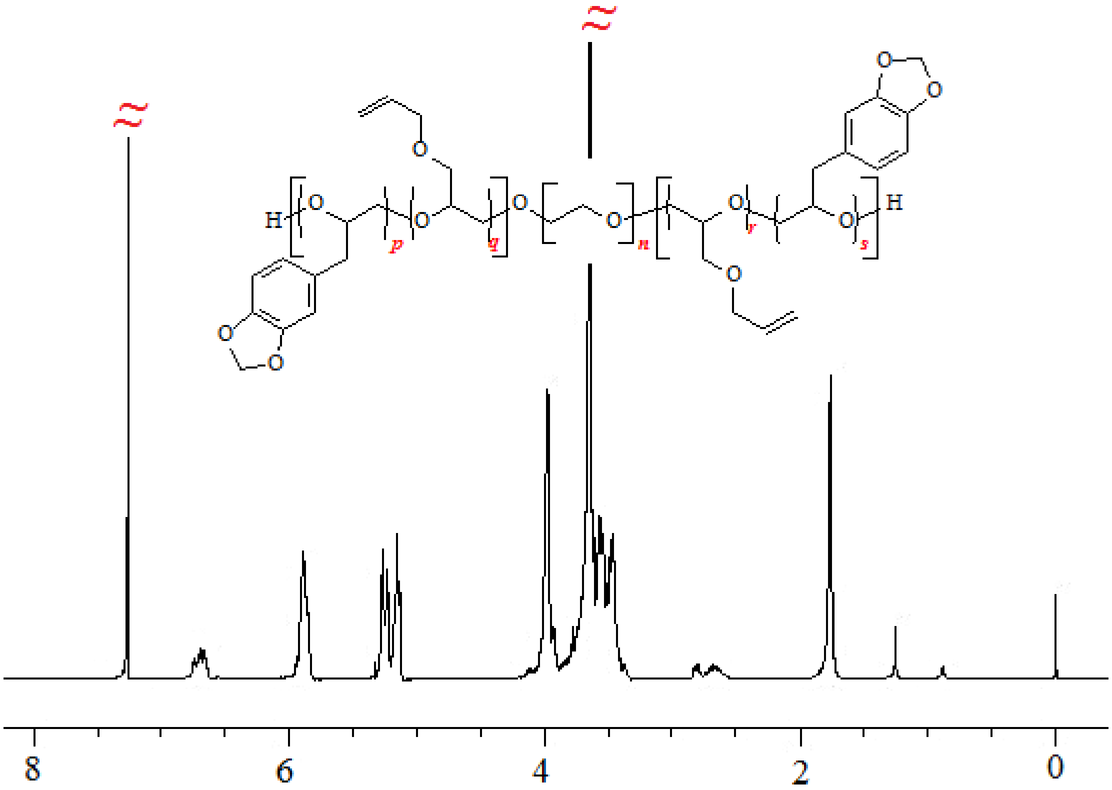

Figure 8.4 ^{1}H NMR spectra in $CDCl_3$ of (SO-co-PAGE)-block-PEG-block-(SO-co-PAGE) **53**

Appendices

HF-5a_H1

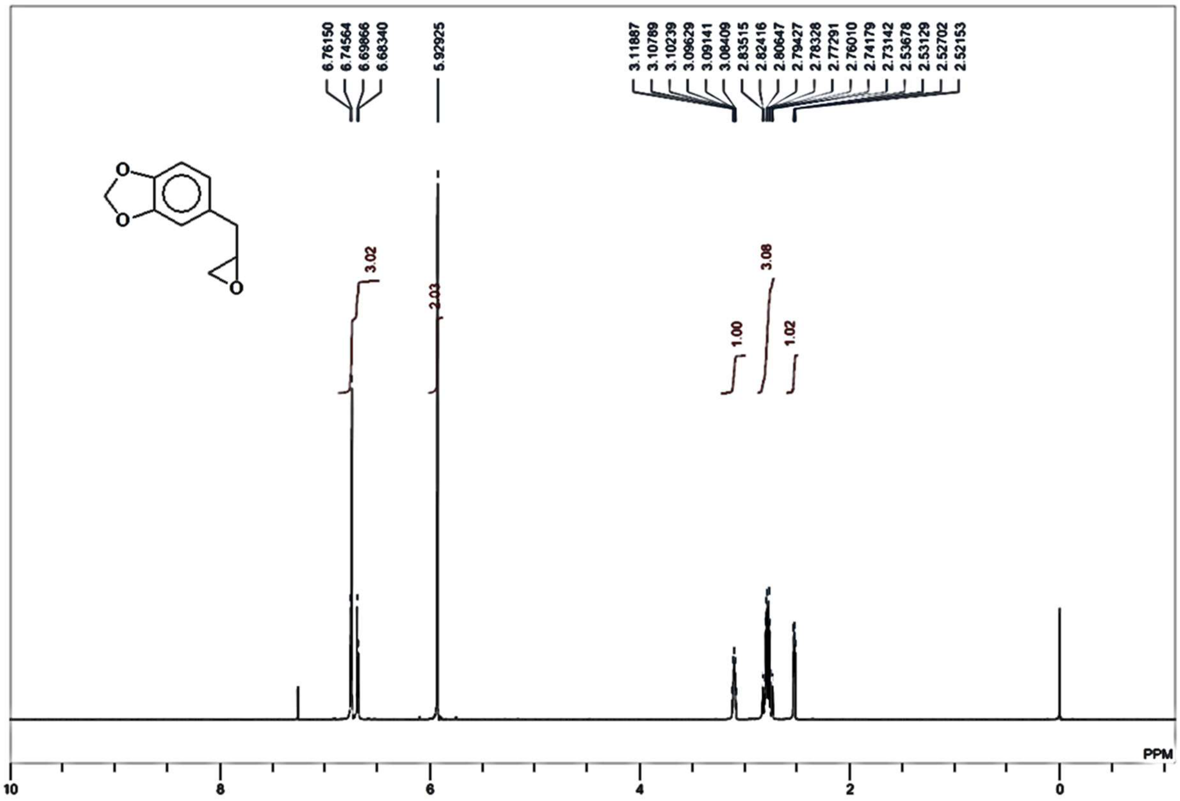

HF-4e_C13

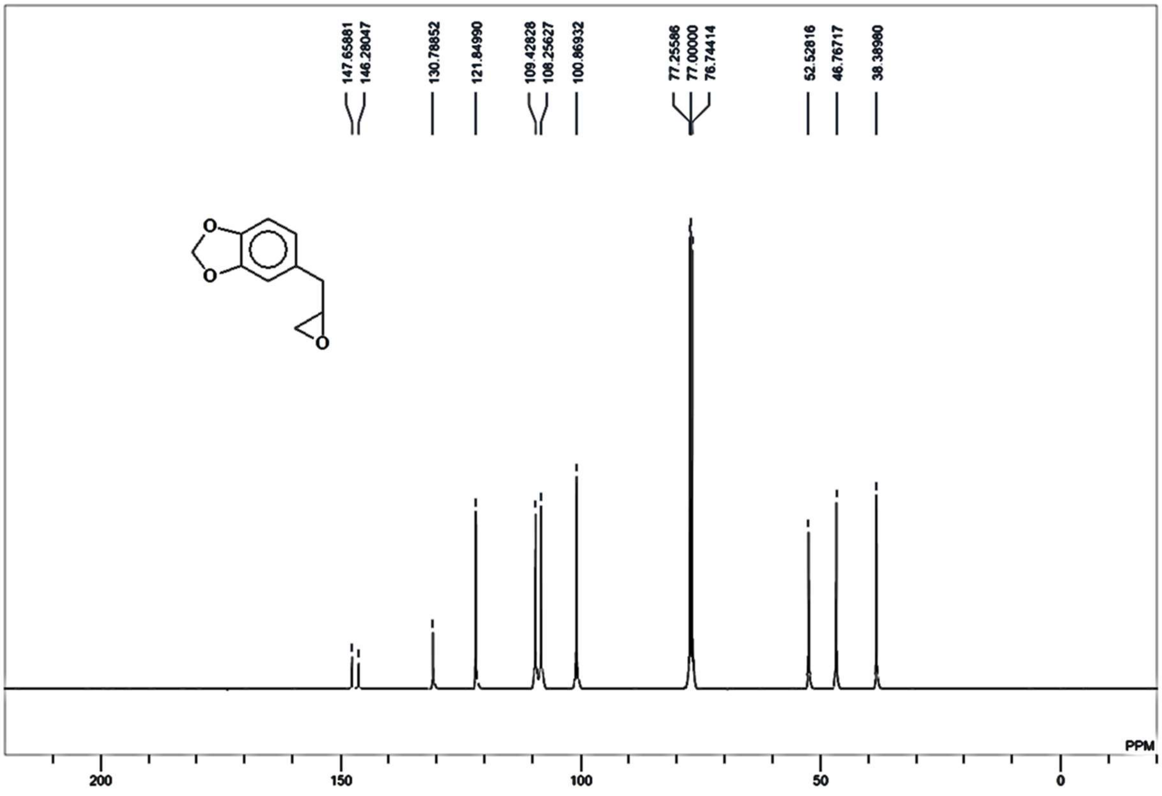

HF_131_Aug_2016_H1

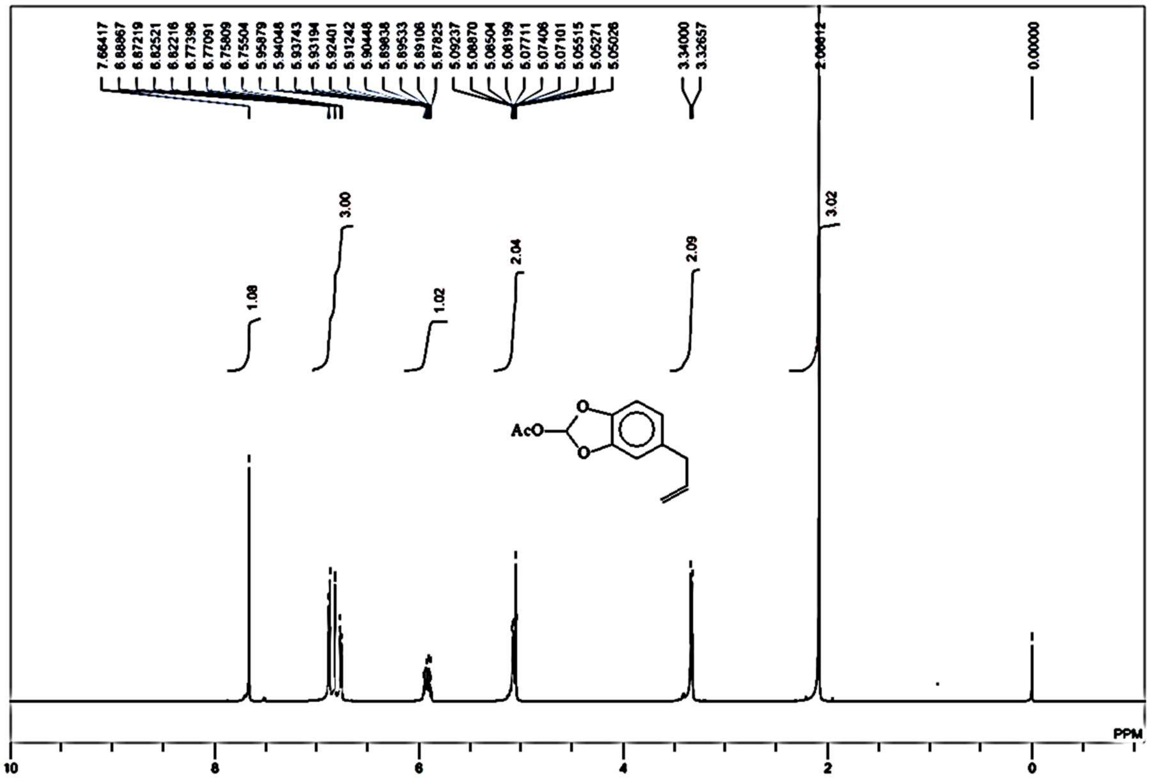

HF_131_Final_C13

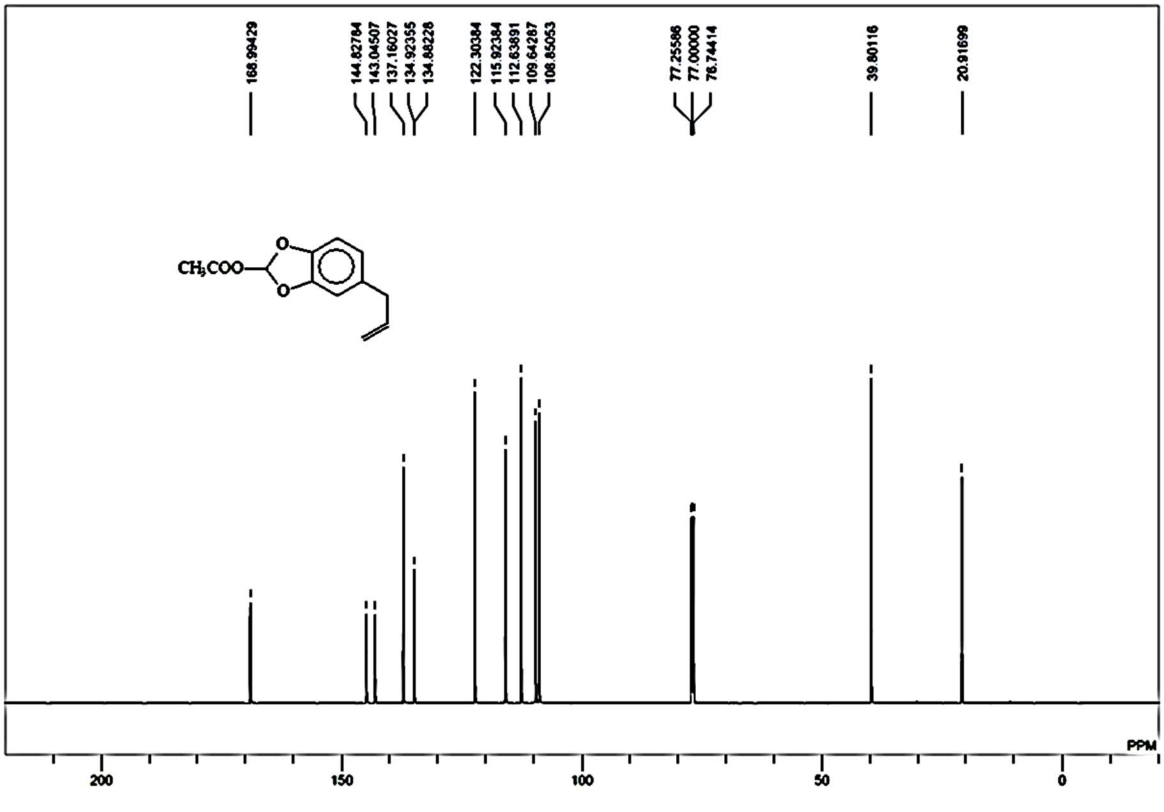

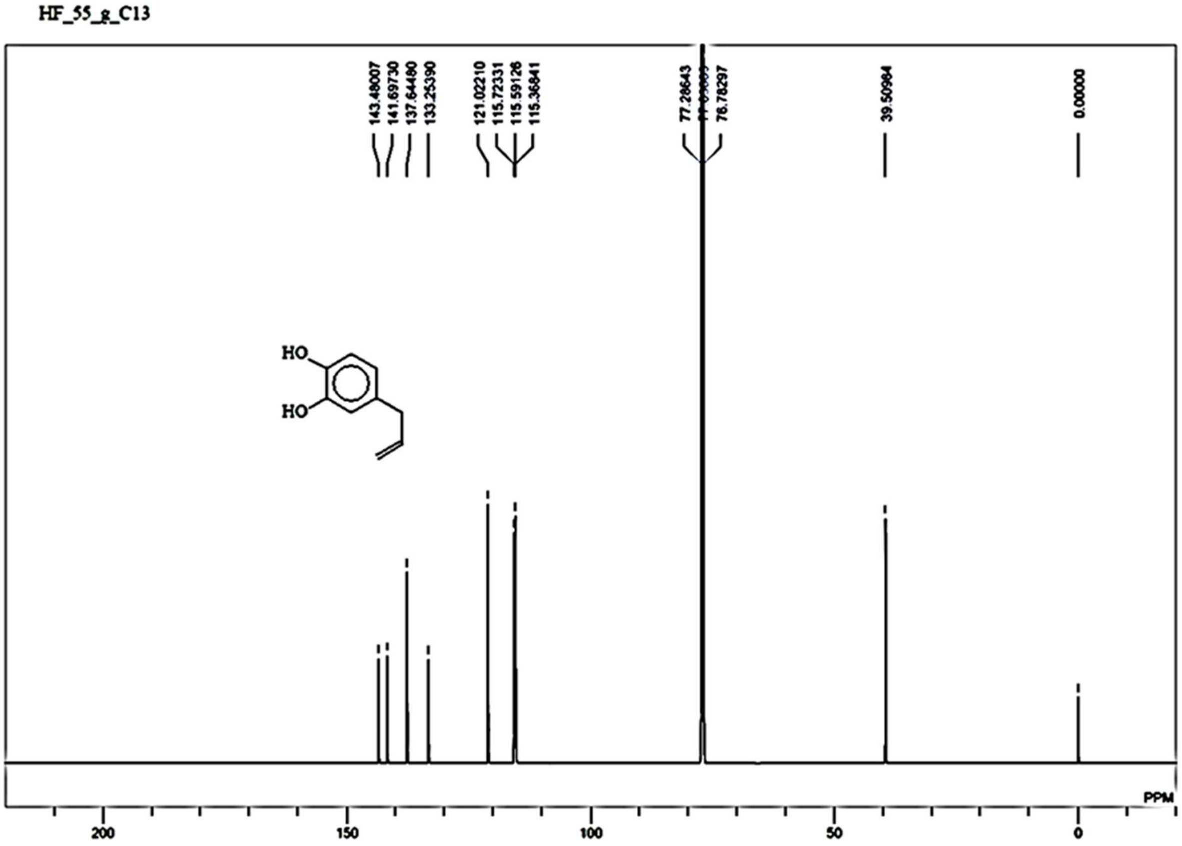
HF_55_g_C13
143.48007
141.69730
137.64480
133.25390
121.02210
115.72331
115.59126
115.36841
77.28643
76.78297
39.50984
0.00000
HO
HO
PPM
200
150
100
50
0

HF_63_2ed_fra_H1.als

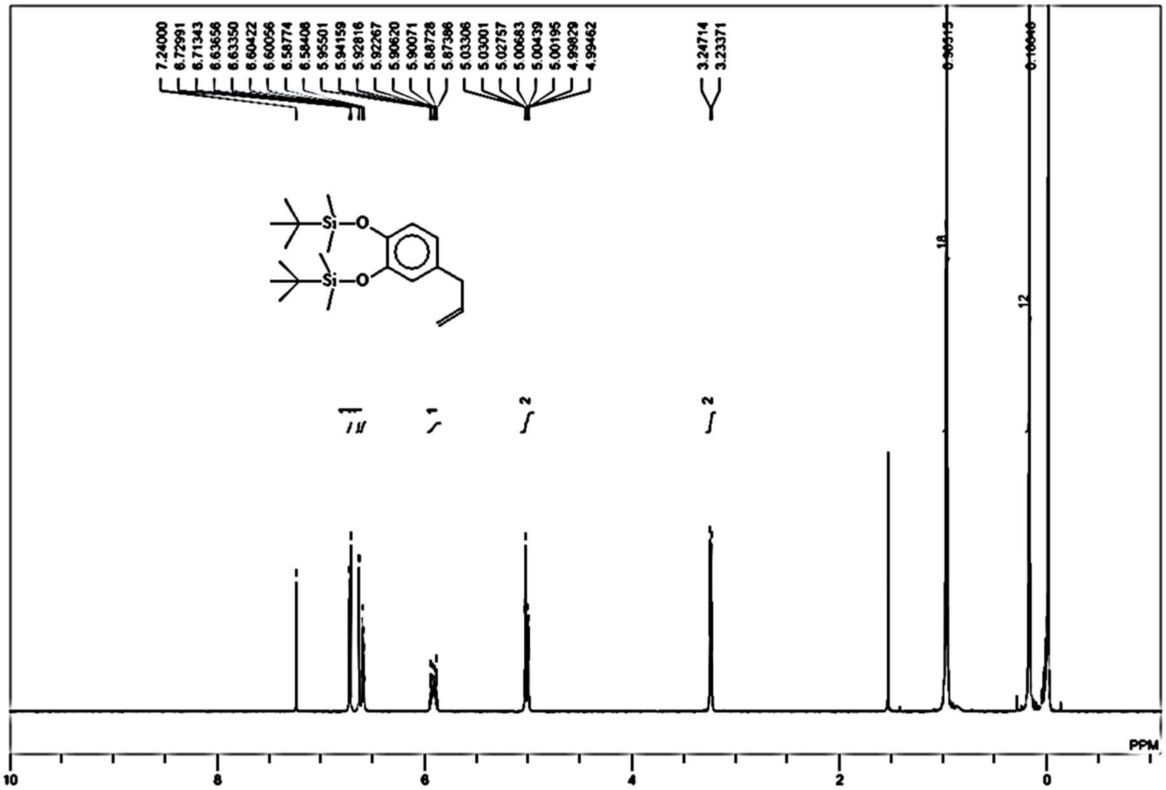

HF_63_I_frac_3_C13

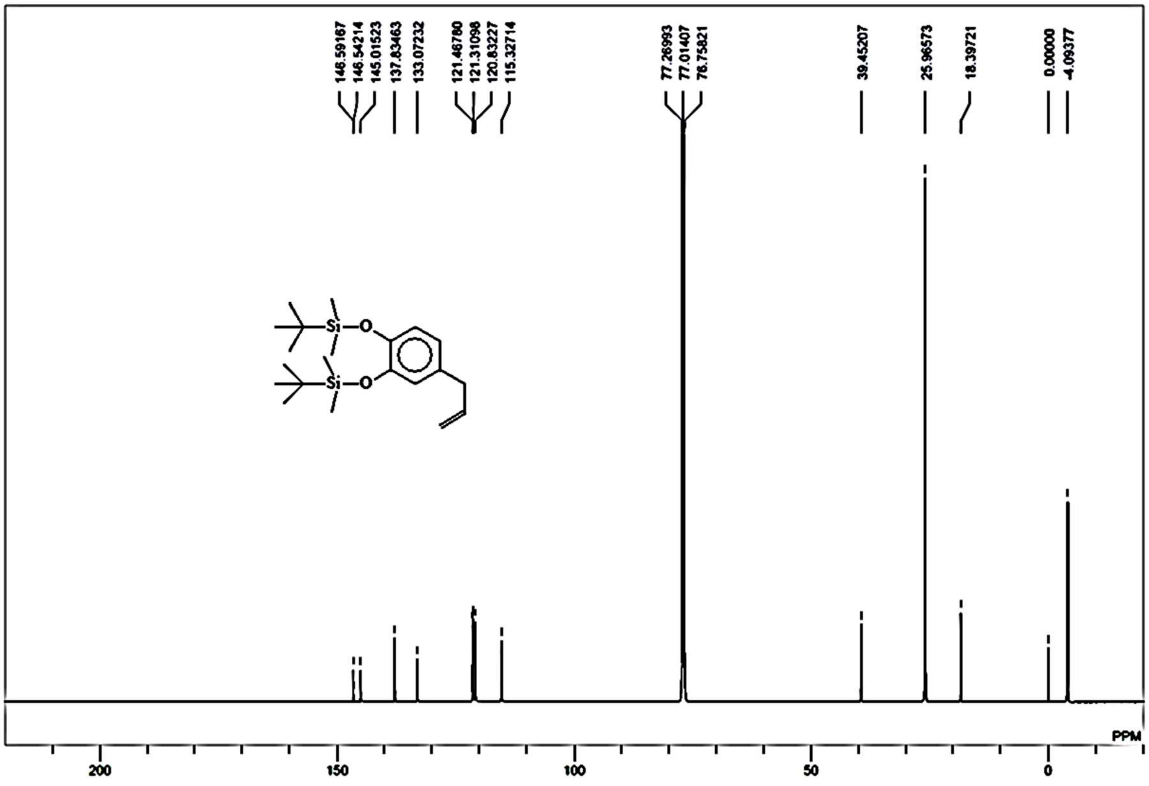

HF_104_2ed+3ed_frac_H1

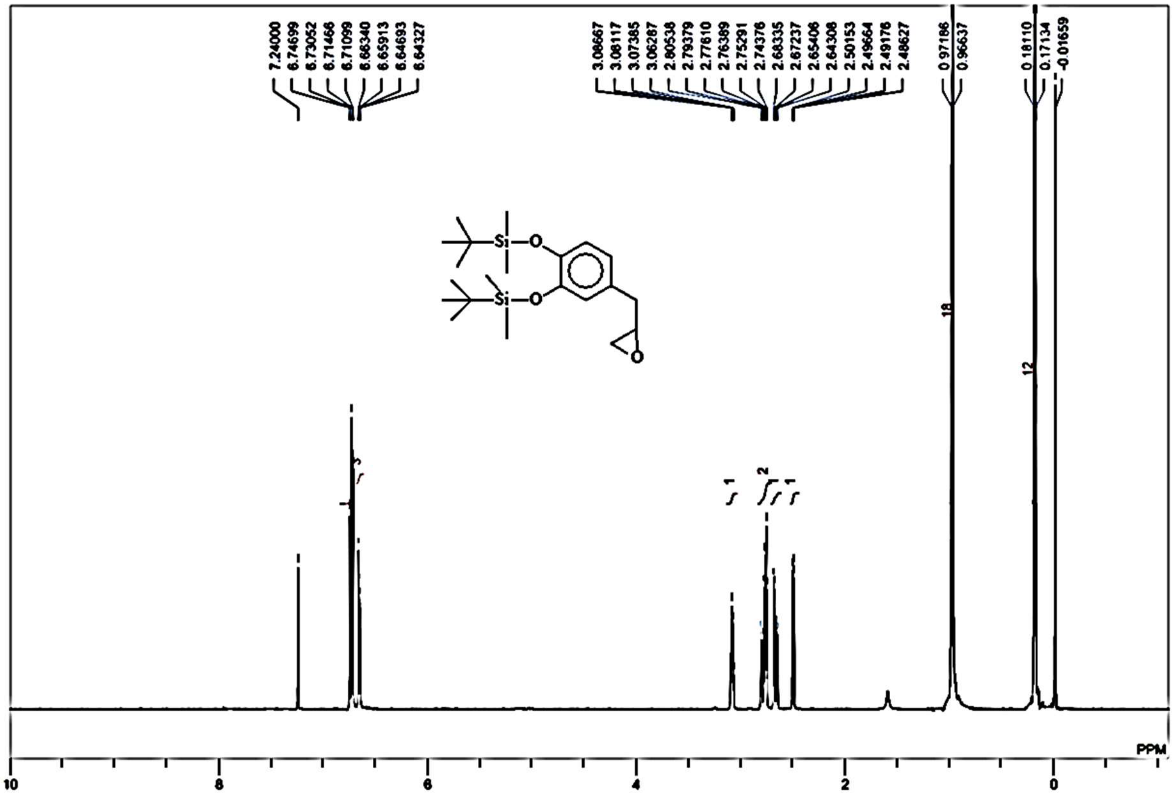

HF_104_2ed+3ed_frac_C13

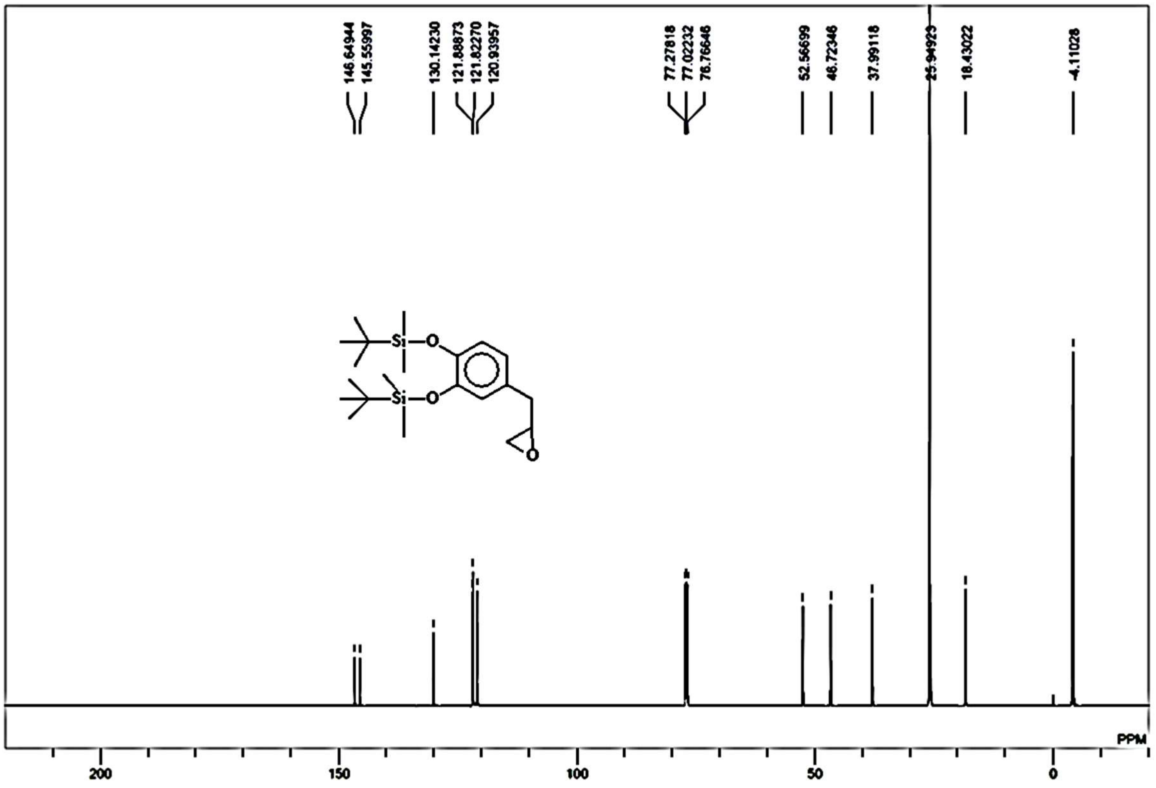

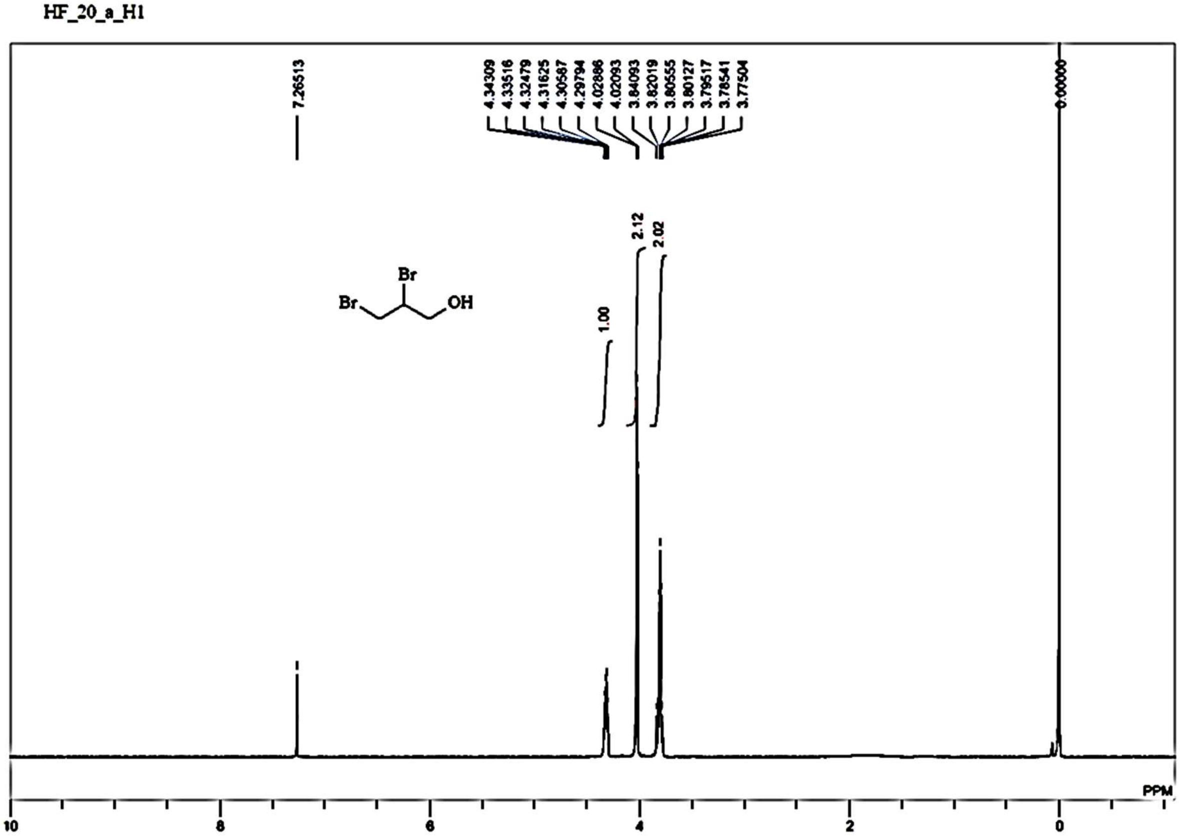
HF_20_a_H1
7.26513
4.34309
4.33516
4.32479
4.31625
4.30587
4.29794
4.02886
4.02093
3.84093
3.82019
3.80555
3.80127
3.79517
3.78541
3.77504
0.00000
Br
Br
OH
1.00
2.12
2.02
PPM
10
8
6
4
2
0

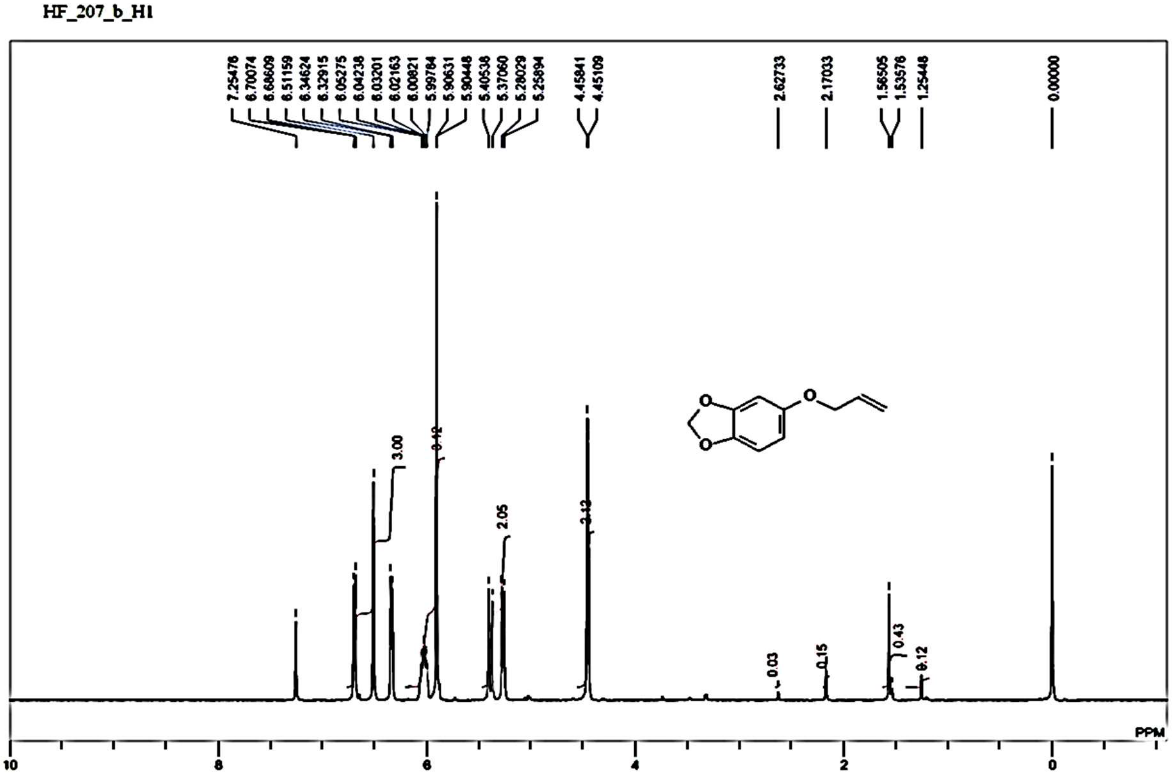
HF_207_b_H1
7.25476
6.70074
6.68609
6.51159
6.34624
6.32915
6.05275
6.04238
6.03201
6.02163
6.00821
5.99784
5.90631
5.90448
5.40538
5.37060
5.28029
5.25894
4.45841
4.45109
2.62733
2.17033
1.56505
1.53576
1.25448
0.00000
O
O
O
3.00
0.12
2.05
2.12
0.03
0.15
0.43
0.12
PPM
10
8
6
4
2
0

HF_25_b_H1

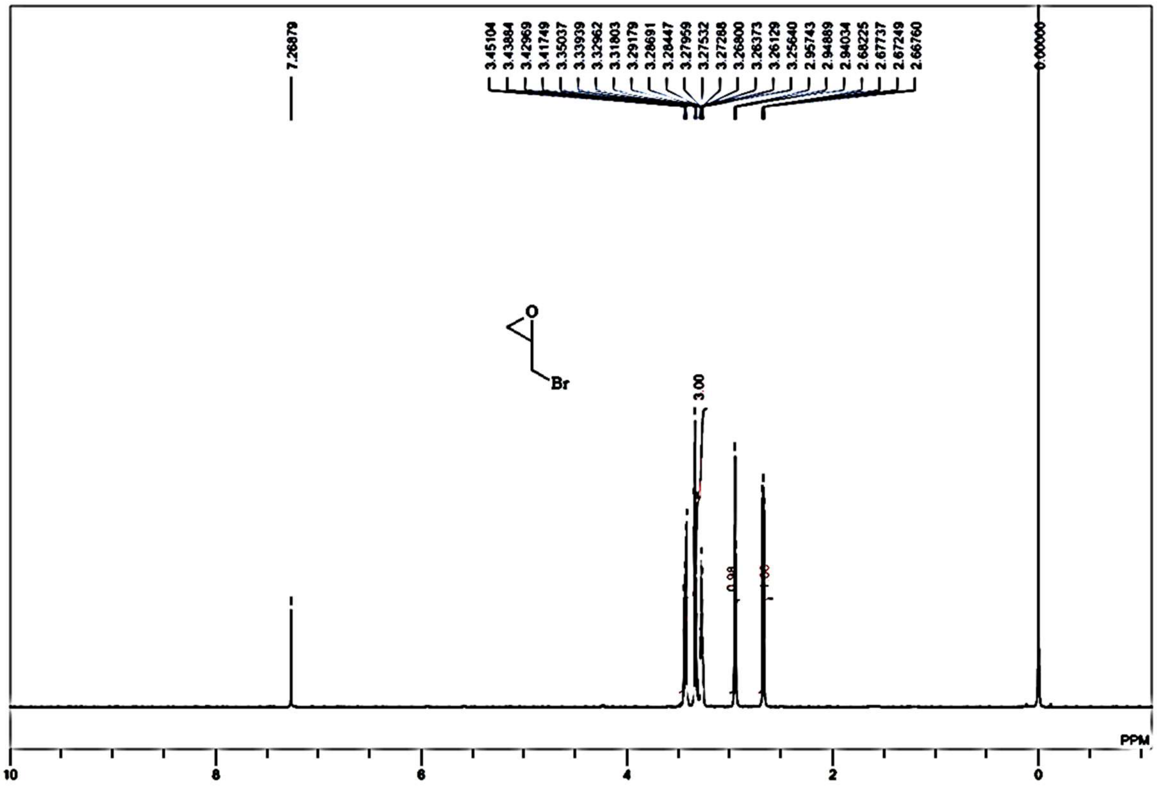

HF_25_b_C13

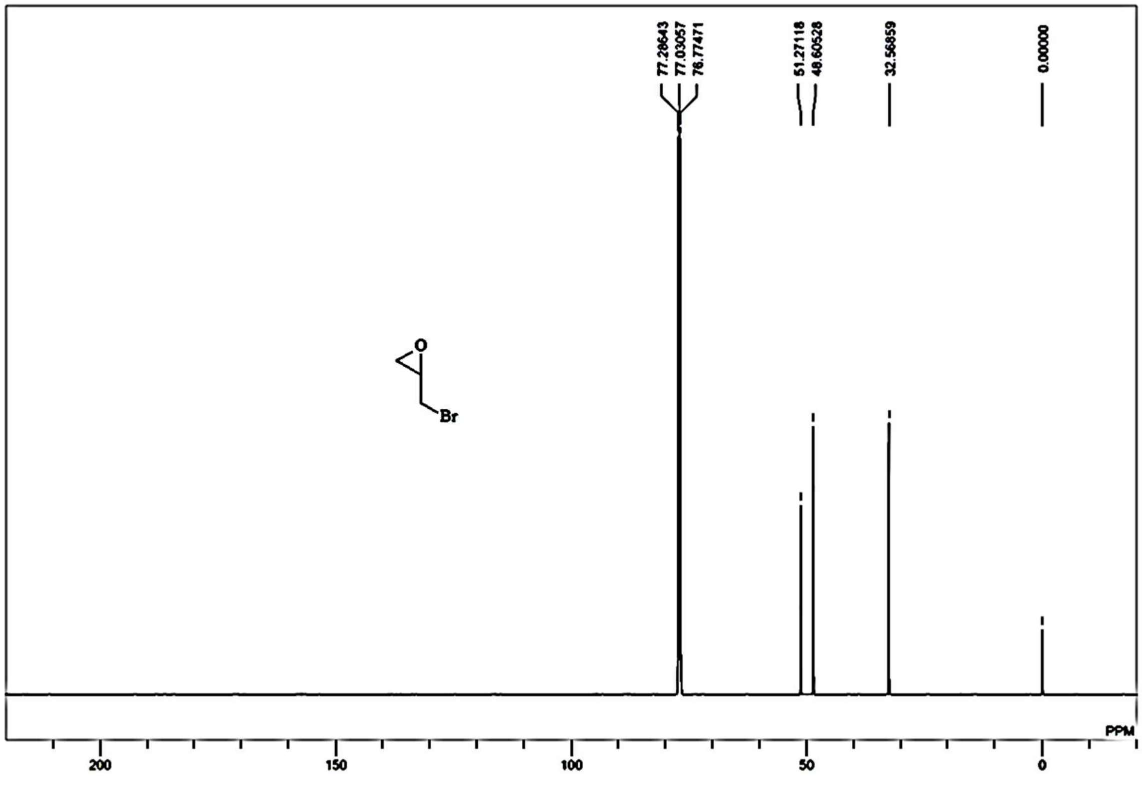

HF_88_1st+4th_frac_H1

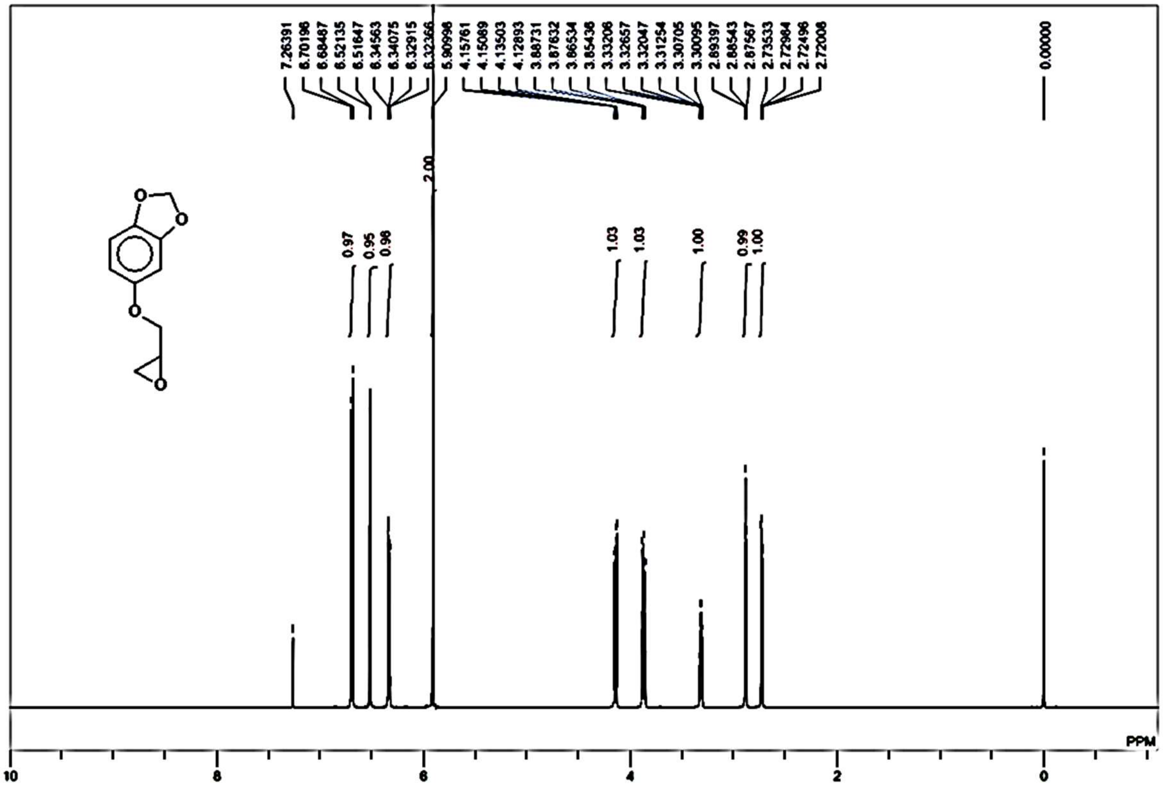

HF_40_d_C13

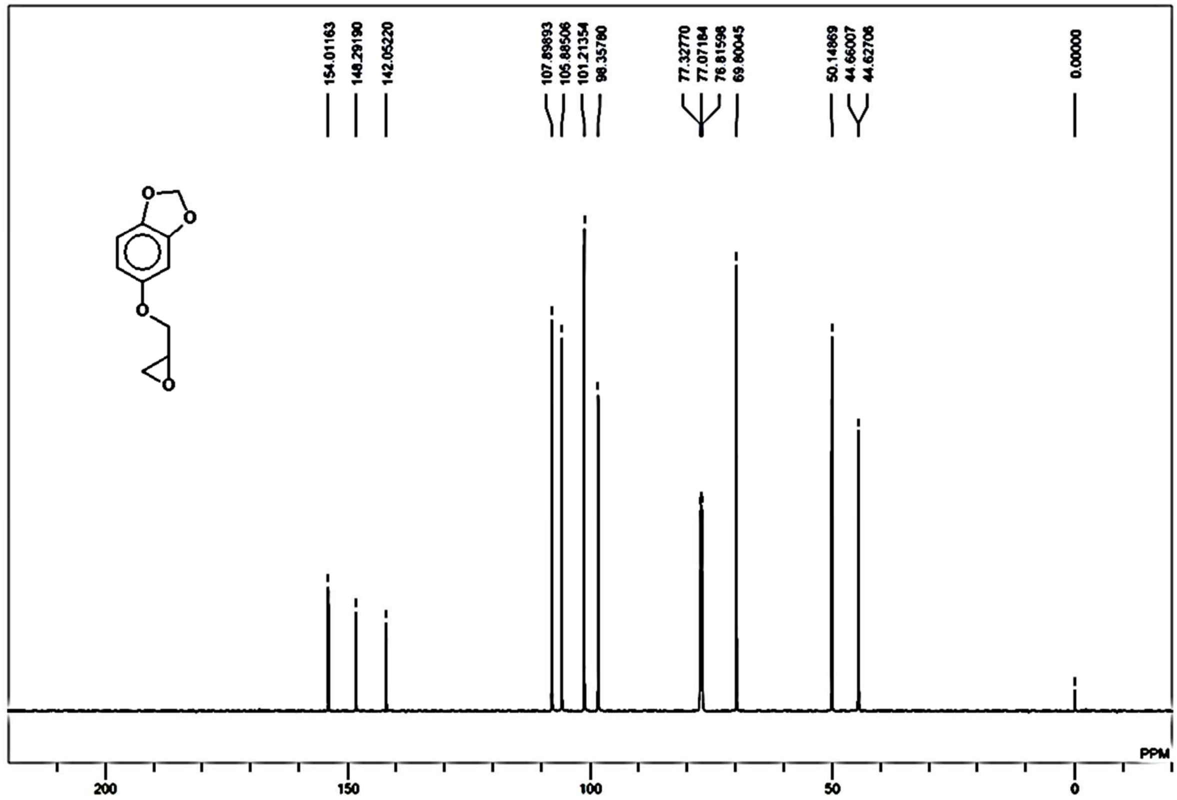

HF_19_g_H1

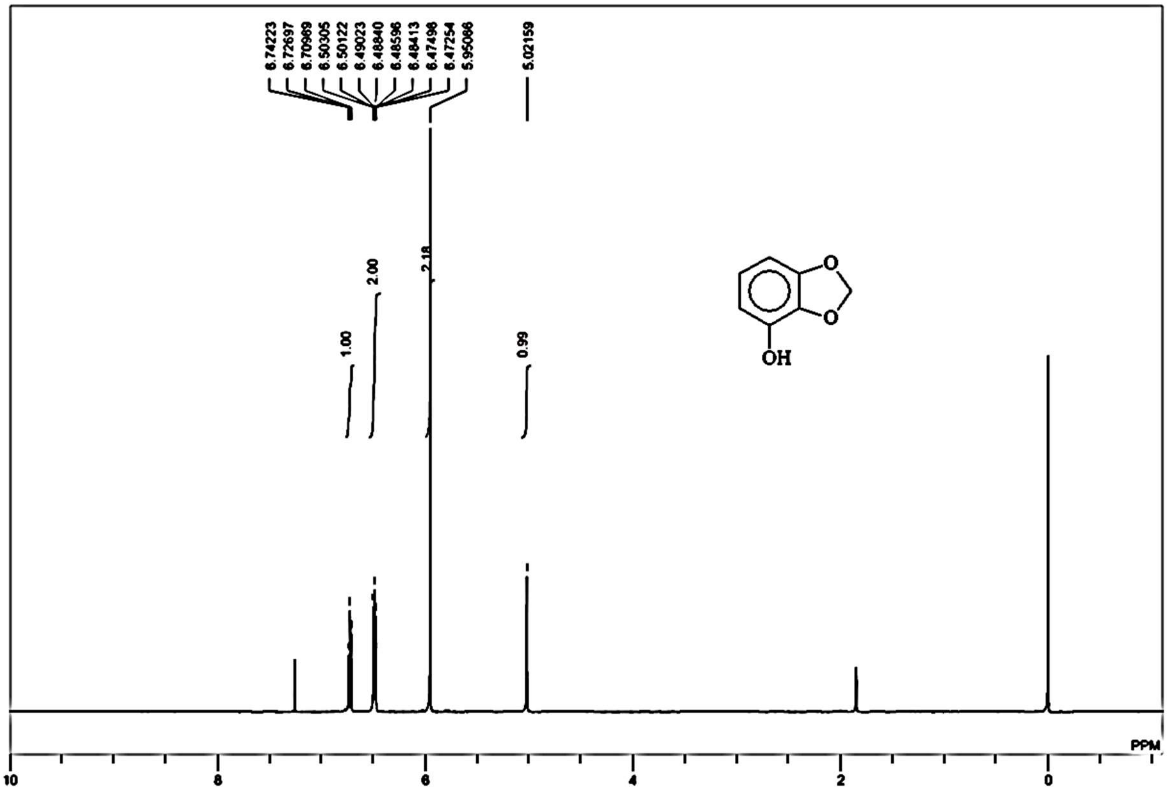

HF_23_final_C13

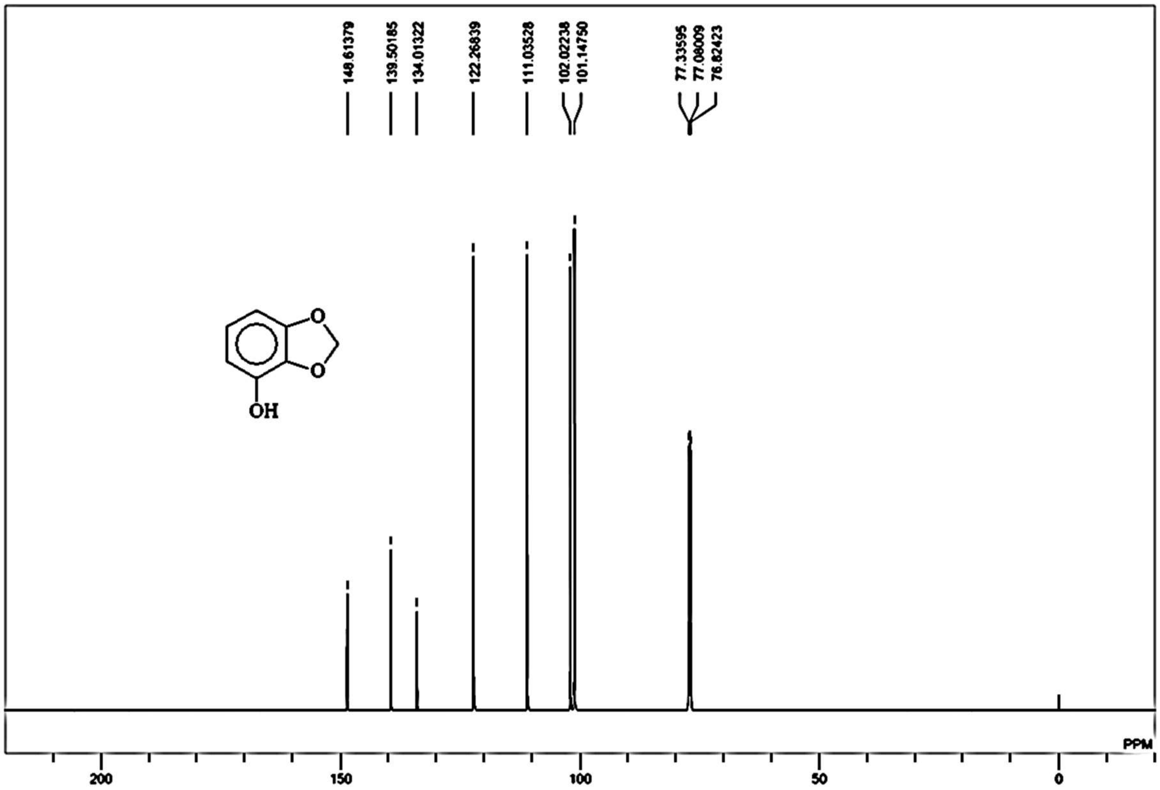

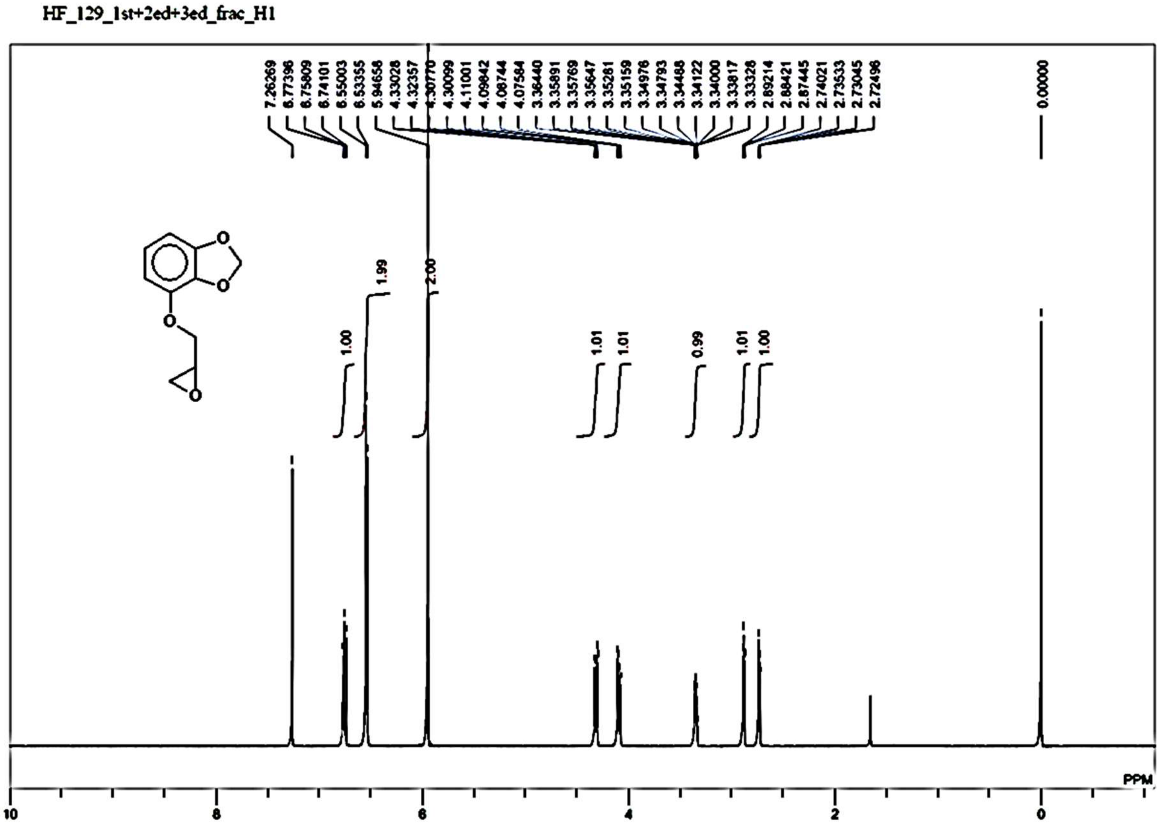
HF_129_1st+2ed+3ed_frac_H1
7.26269
6.77396
6.75809
6.74101
6.55003
6.53355
5.94658
4.33028
4.32357
4.30770
4.30099
4.11001
4.09842
4.08744
4.07584
3.36440
3.35891
3.35769
3.35647
3.35281
3.35159
3.34976
3.34793
3.34488
3.34122
3.34000
3.33817
3.33328
2.89214
2.88421
2.87445
2.74021
2.73533
2.73045
2.72496
0.00000
O
O
O
O
1.00
1.99
2.00
1.01
1.01
0.99
1.01
1.00
PPM
10
8
6
4
2
0

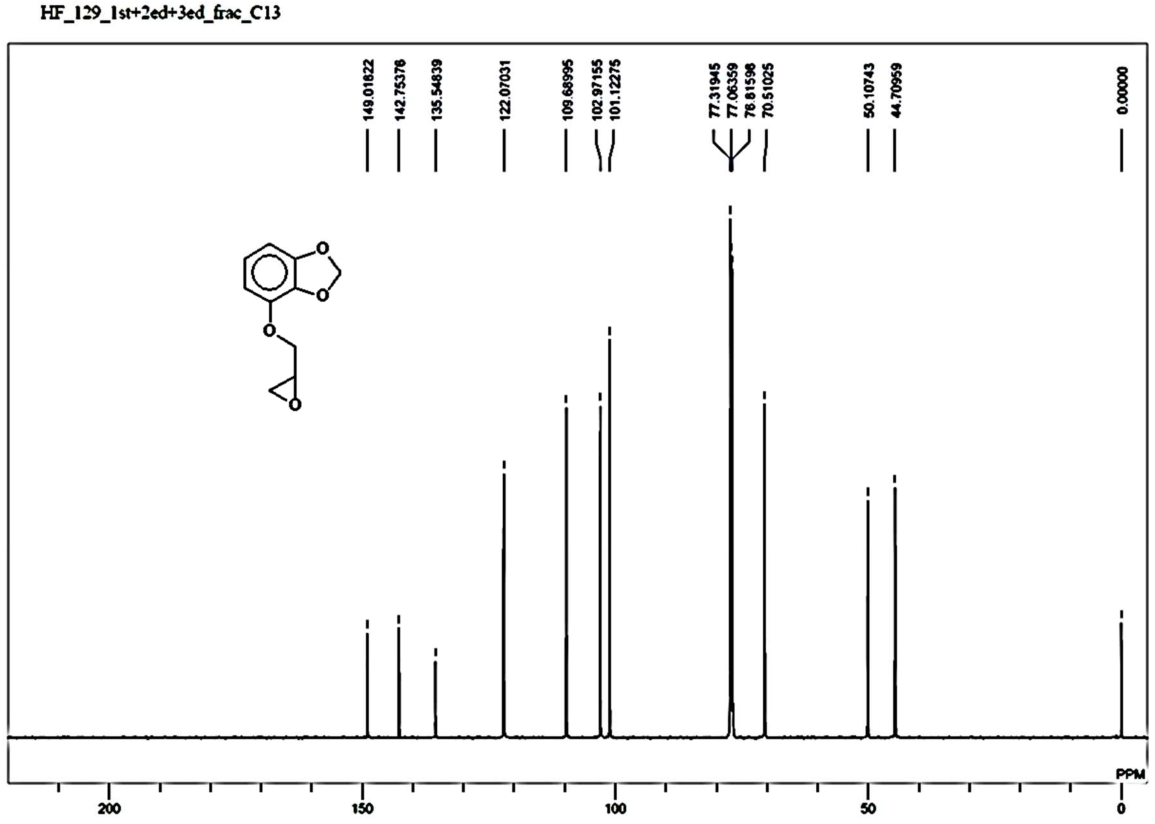
HF_129_1st+2ed+3ed_frac_C13
149.01822
142.75376
135.54839
122.07031
109.68995
102.97155
101.12275
77.31945
77.06359
76.81598
70.51025
50.10743
44.70959
0.00000
O
O
O
O
PPM
200
150
100
50
0

HF_206_b_-30oC_H1

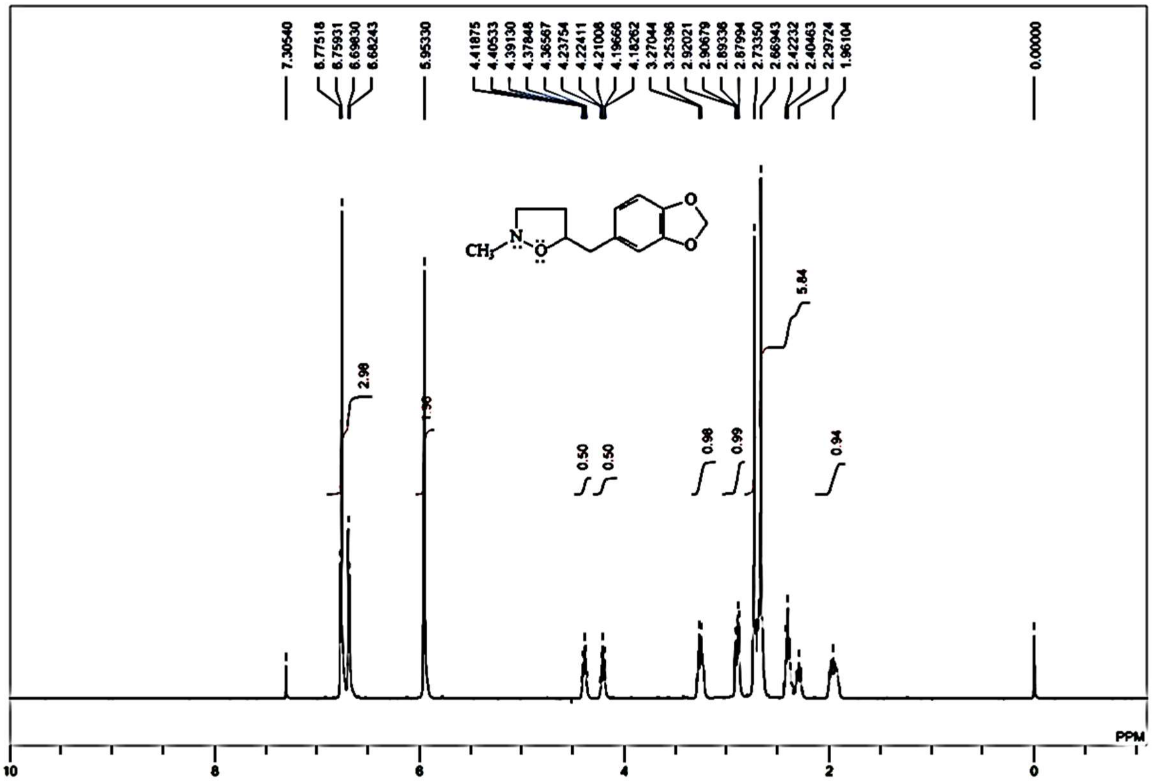

HF_206_b_-30oC_C13

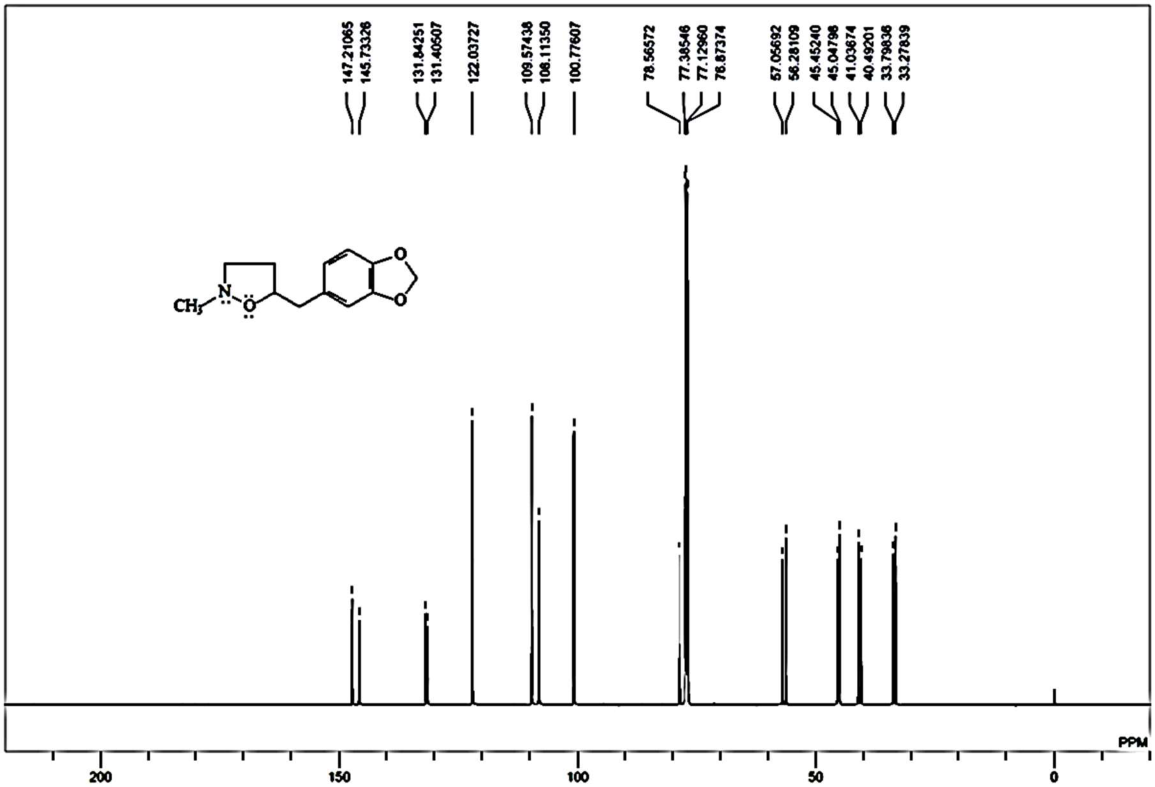

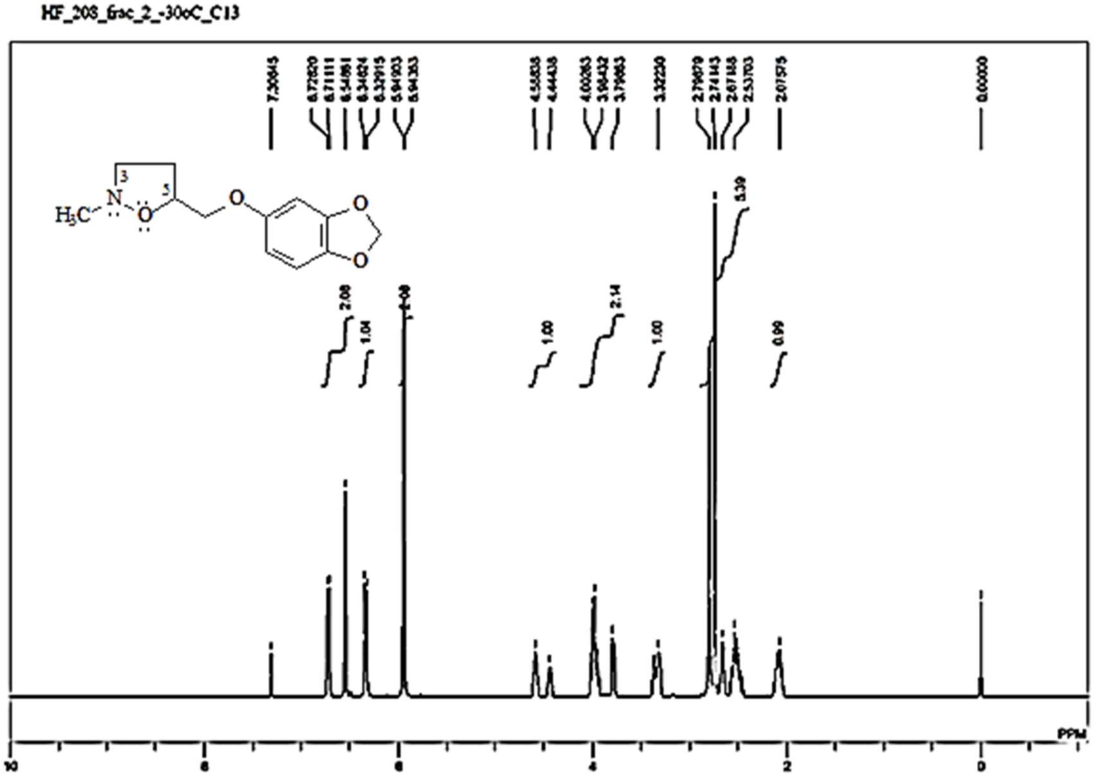
HF_208_frac_2_-30oC_C13
7.30045
6.72820
6.71111
6.54881
6.34624
6.32915
5.94933
5.94353
4.55835
4.44436
4.00263
3.98432
3.79883
3.32230
2.79879
2.74143
2.67188
2.53703
2.07575
0.00000
3
5
H_3C
N
O
O
O
O
2.08
1.04
2.08
1.00
2.14
1.00
5.39
0.99
PPM
10
8
6
4
2
0

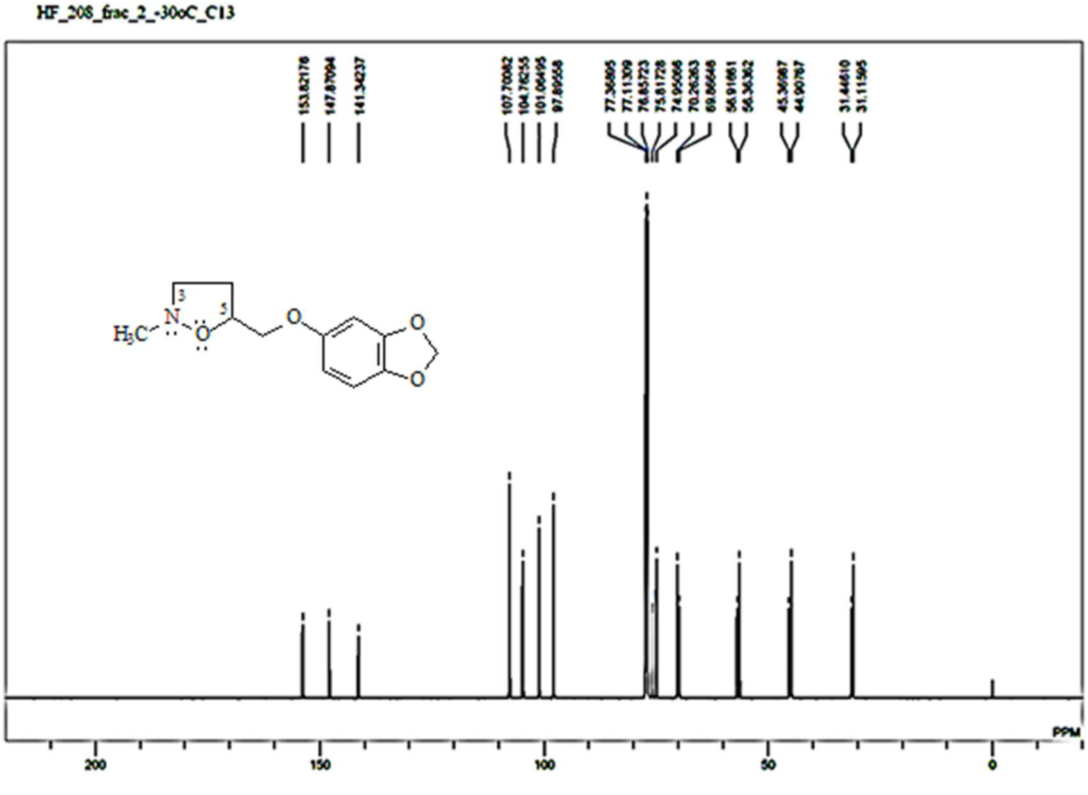
HF_208_frac_2_-30oC_C13
153.82176
147.87094
141.34237
107.70082
104.78255
101.06495
97.89558
77.36895
77.11309
76.85723
75.81728
74.95068
70.26283
69.86646
56.91861
56.36362
45.36987
44.90767
31.44610
31.11595
3
5
H_3C
N
O
O
O
O
PPM
200
150
100
50
0

HF_209_frac_2_-30oC_H1

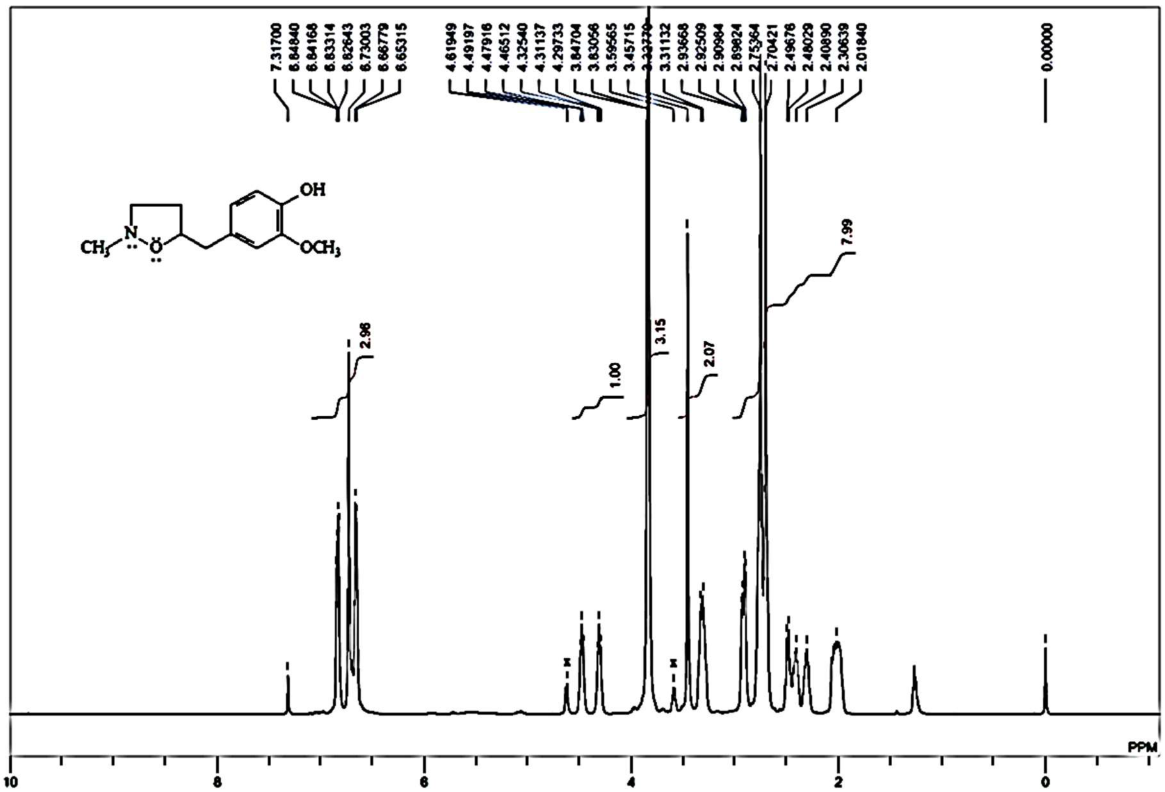

HF_209_frac_2_-30oC_C13

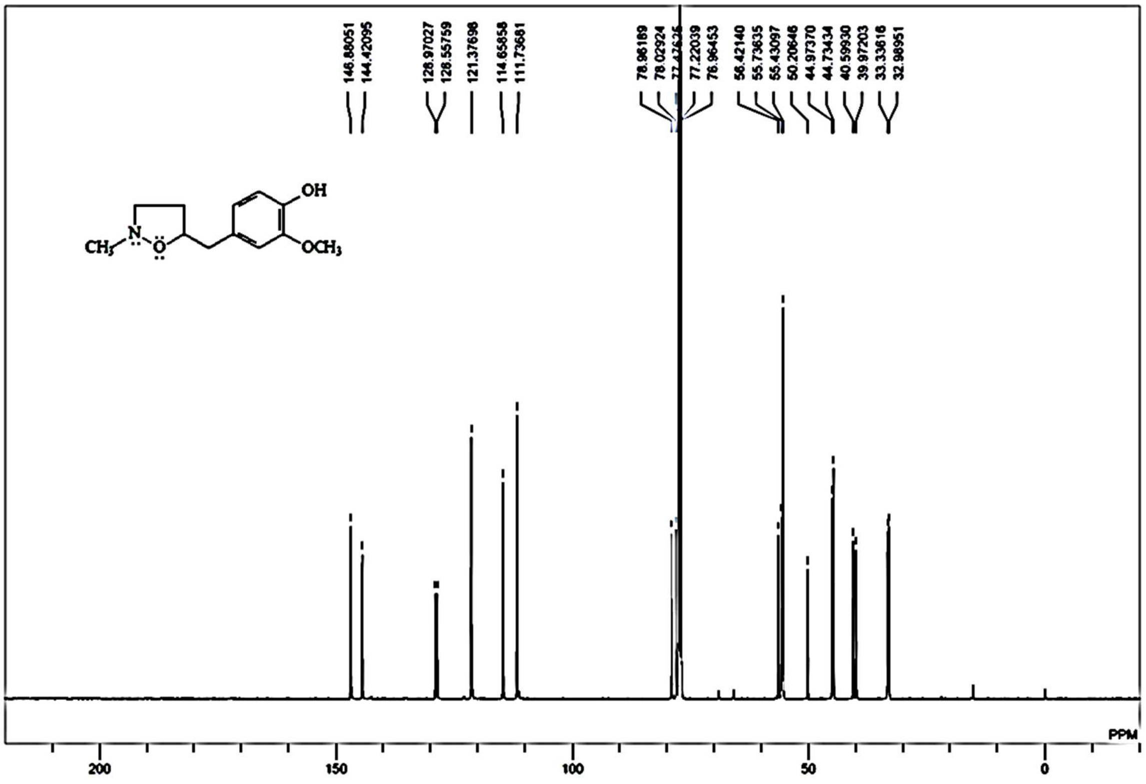

HF_211_b_-30oC_H1

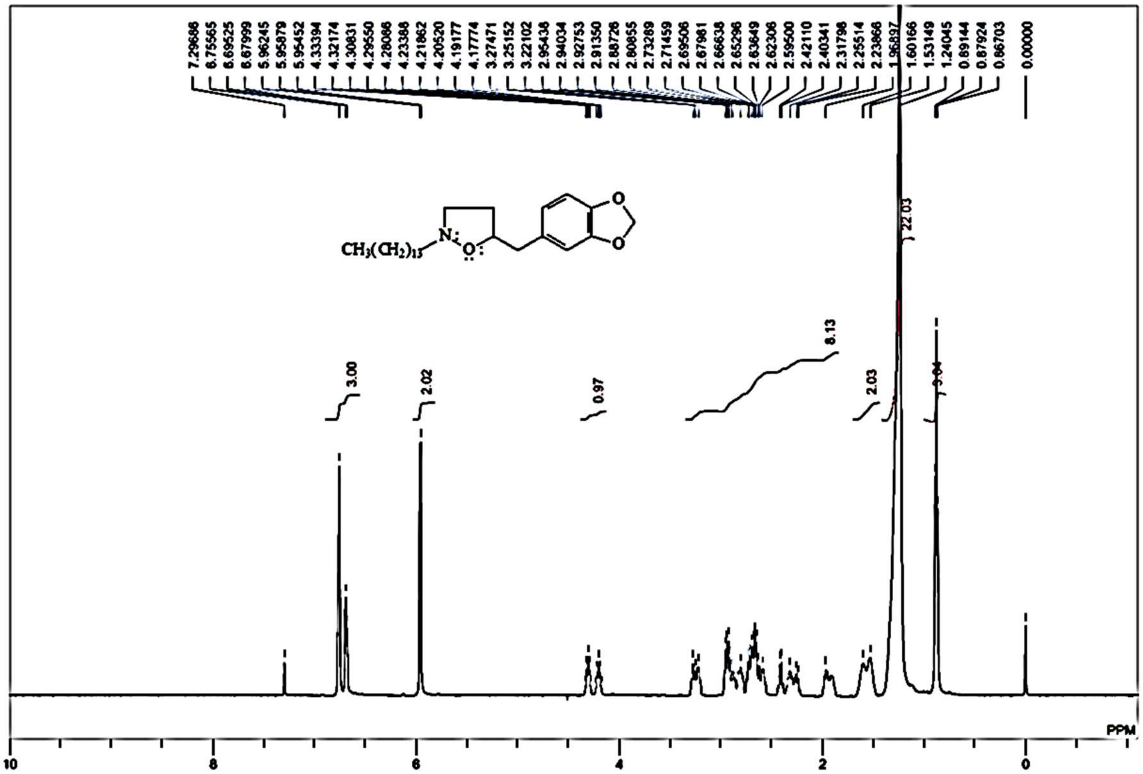

HF_211_b_-30oC_C13

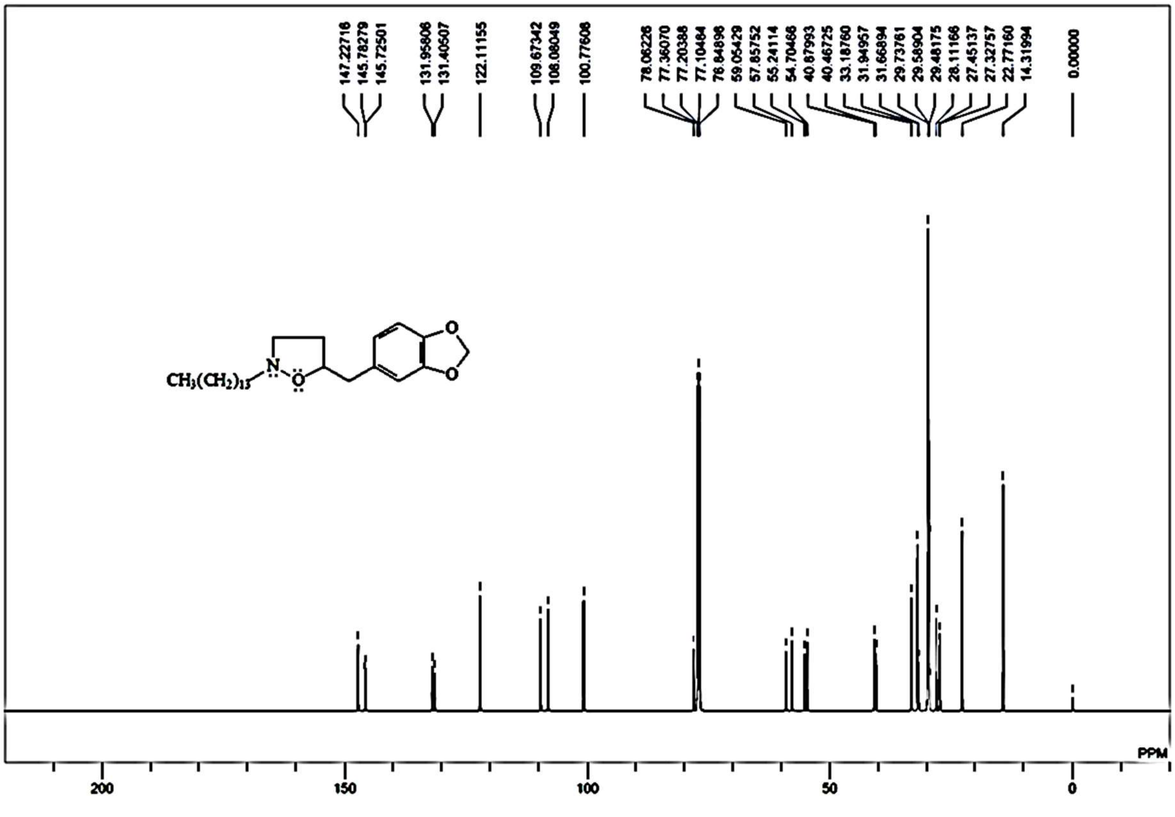

HF_213_Frac_B_-30oC_H1

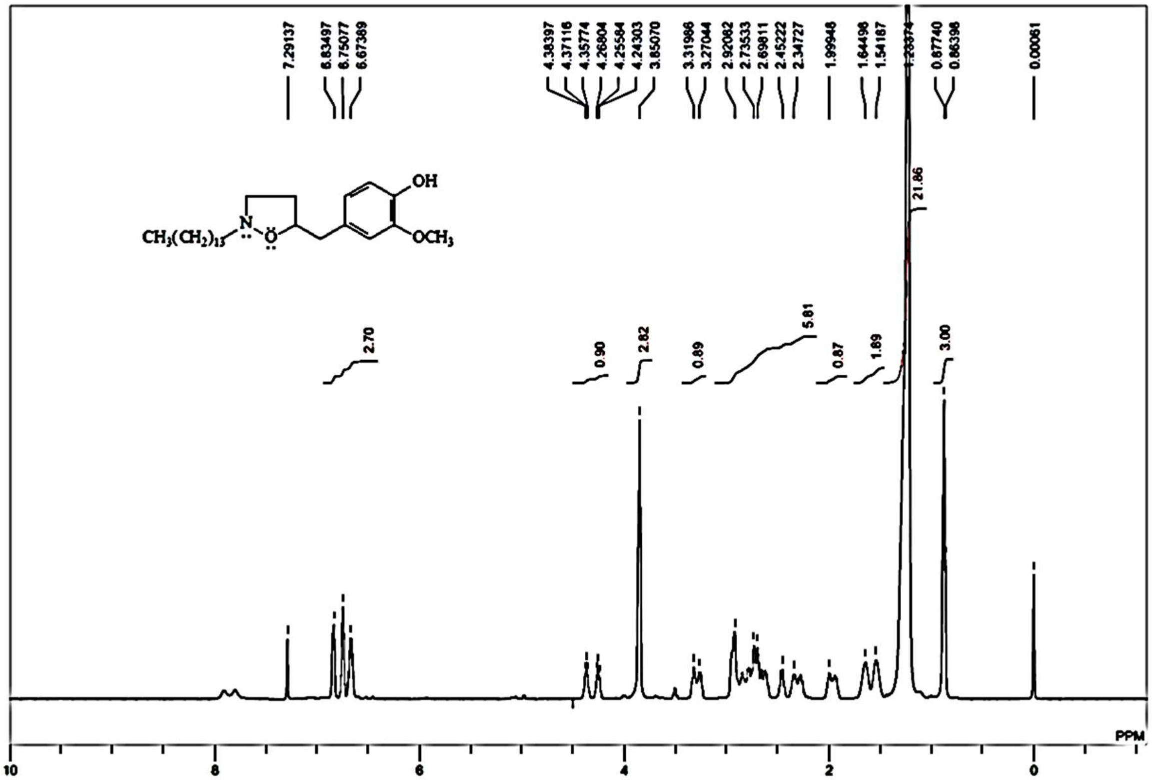

HF_213_Frac_B_-30oC_C13

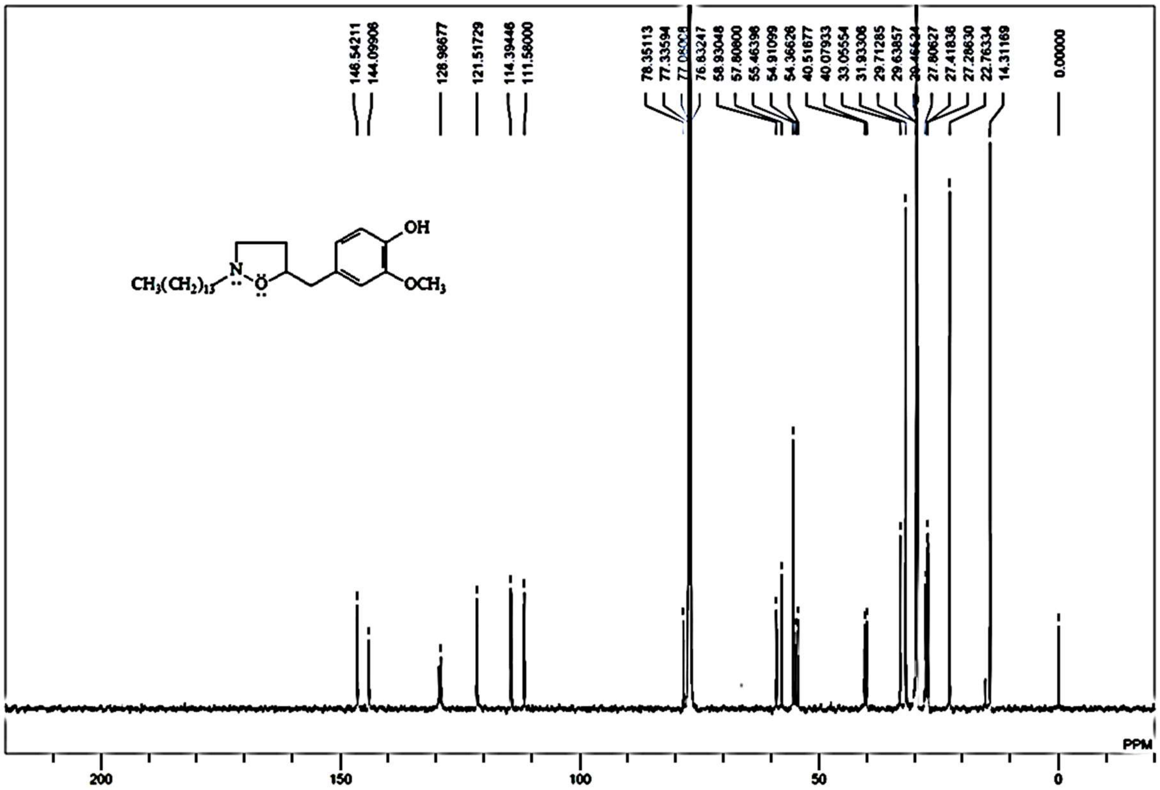

References

[1] J. Huang and S. R. Turner, "Recent advances in alternating copolymers: The synthesis, modification, and applications of precision polymers," *Polym. (United Kingdom)*, vol. 116, pp. 572–586, 2017.

[2] J. F. Lutz, "Aperiodic copolymers," *ACS Macro Lett.*, vol. 3, no. 10, pp. 1020–1023, 2014.

[3] D. A. Mortimer, "Synthetic polyelectrolytes—A review," *Polym. Int.*, vol. 25, no. 1, pp. 29–41, 1991.

[4] A. Pizzi and K. L. Mittal, *Handbook of Adhesive Technology*. 2003.

[5] D. E. Packham, "2. Theories of Fundamental Adhesion," *Handb. Adhes. Technol.*, vol. 13, no. 8, pp. 11–38, 2011.

[6] J. J. Bikerman, "Causes of Poor Adhesion: Weak Boundary Layers," *Ind. Eng. Chem.*, vol. 59, no. 9, pp. 40–44, 1967.

[7] S. Cao, J. D. Wang, H. S. Chen, and D. R. Chen, "Progress of marine biofouling and antifouling technologies," *Chinese Sci. Bull.*, vol. 56, no. 7, pp. 598–612, 2011.

[8] D. M. Yebra, S. Kiil, and K. Dam-Johansen, "Antifouling technology - Past, present and future steps towards efficient and environmentally friendly antifouling coatings," *Prog. Org. Coatings*, vol. 50, no. 2, pp. 75–104, 2004.

[9] L. D. Chambers, K. R. Stokes, F. C. Walsh, and R. J. K. Wood, "Modern approaches to marine antifouling coatings," *Surf. Coatings Technol.*, vol. 201, no. 6, pp. 3642–

3652, 2006.

[10] C. Yan and W. Zhang, *Chapter 12 – Coacervation Processes*. Elsevier Inc., 2014.

[11] Z. Xiao, W. Liu, G. Zhu, R. Zhou, and Y. Niu, "A review of the preparation and application of flavour and essential oils microcapsules based on complex coacervation technology," *J. Sci. Food Agric.*, vol. 94, no. 8, pp. 1482–1494, 2014.

[12] D. S. Hwang, J. H. Waite, and M. Tirrell, "Promotion of osteoblast proliferation on complex coacervation-based hyaluronic acid – recombinant mussel adhesive protein coatings on titanium," *Biomaterials*, vol. 31, no. 6, pp. 1080–1084, 2010.

[13] D. S. Hwang *et al.*, "Viscosity and interfacial properties in a mussel-inspired adhesive coacervate," *Soft Matter*, vol. 6, no. 14, pp. 3232–3236, 2010.

[14] S. Kaur, G. M. Weerasekare, and R. J. Stewart, "Multiphase Adhesive Coacervates Inspired by the Sandcastle Worm," *ACS Appl. Mater. Interfaces*, vol. 3, no. 4, pp. 941–944, Apr. 2011.

[15] R. L. Townsin, "The Ship Hull Fouling Penalty," *Biofouling*, vol. 19, no. sup1, pp. 9–15, 2003.

[16] P. E. Kolenbrander, "Oral Microbial Communities: Biofilms, Interactions, and Genetic Systems," *Annu. Rev. Microbiol.*, vol. 54, no. 1, pp. 413–437, Oct. 2000.

[17] W. Yang, N. Cicek, and J. Ilg, "State-of-the-art of membrane bioreactors: Worldwide research and commercial applications in North America," *J. Memb. Sci.*, vol. 270, no. 1–2, pp. 201–211, Feb. 2006.

[18] J. S. Vrouwenvelder, C. Hinrichs, W. G. J. Van der Meer, M. C. M. Van Loosdrecht, and J. C. Kruithof, “Pressure drop increase by biofilm accumulation in spiral wound RO and NF membrane systems: role of substrate concentration, flow velocity, substrate load and flow direction.,” *Biofouling*, vol. 25, no. 6, pp. 543–555, 2009.

[19] C. Werner, M. F. Maitz, and C. Sperling, “Current strategies towards hemocompatible coatings,” *J. Mater. Chem.*, vol. 17, no. 32, p. 3376, 2007.

[20] R. E. Kania *et al.*, “Biofilms on tracheoesophageal voice prostheses: a confocal laser scanning microscopy demonstration of mixed bacterial and yeast biofilms.,” *Biofouling*, vol. 26, no. 5, pp. 519–526, 2010.

[21] M. P. Schultz, “Effects of coating roughness and biofouling on ship resistance and powering,” *Biofouling*, vol. 23, no. 5, pp. 331–341, 2007.

[22] I. Omae, “Organotin antifouling paints and their alternatives,” *Appl. Organomet. Chem.*, vol. 17, no. 2, pp. 81–105, 2003.

[23] K. V. Thomas and S. Brooks, “The environmental fate and effects of antifouling paint biocides,” *Biofouling*, vol. 26, no. 1, pp. 73–88, 2010.

[24] L. Hoipkemeier-Wilson *et al.*, “Antifouling Potential of Lubricious, Micro-engineered, PDMS Elastomers against Zoospores of the Green Fouling Alga Ulva (Enteromorpha),” *Biofouling*, vol. 20, no. 1, pp. 53–63, Feb. 2004.

[25] C. S. Gudipati, J. A. Finlay, J. A. Callow, M. E. Callow, and K. L. Wooley, “The antifouling and fouling-release perfomance of hyperbranched fluoropolymer (HBFP)-poly(ethylene glycol) (PEG) composite coatings evaluated by adsorption of

biomacromolecules and the green fouling alga ulva," *Langmuir*, vol. 21, no. 7, pp. 3044–3053, 2005.

[26] Z. Hu *et al.*, "Photochemically cross-linked perfluoropolyether-based elastomers: Synthesis, physical characterization, and biofouling evaluation," *Macromolecules*, vol. 42, no. 18, pp. 6999–7007, 2009.

[27] N. S. Lee, J. a. Callow, M. E. Callow, J. a. Finlay, and W. P. Weber, "Preparation and physical properties of films prepared by crosslinking 1,9-bis(glycidyloxypropyl)pentasiloxanes with α,ω-bis(3-aminopropyl)polydimethylsiloxane and their settlement and release properties," *J. Appl. Polym. Sci.*, vol. 102, no. 1, pp. 751–757, 2006.

[28] C. M. Grozea *et al.*, "Water-Stable Diblock Polystyrene-block-poly(2-vinyl pyridine) and Diblock Polystyrene-block-poly(methyl methacrylate) Cylindrical Patterned Surfaces Inhibit Settlement of Zoospores of the Green Alga Ulva," *Biomacromolecules*, vol. 10, no. 4, pp. 1004–1012, Apr. 2009.

[29] Y. Chang, S. Chen, Z. Zhang, and S. Jiang, "Highly Protein-Resistant Coatings from Well-Defined Diblock Copolymers Containing Sulfobetaines," *Langmuir*, vol. 22, no. 5, pp. 2222–2226, Feb. 2006.

[30] Z. Zhang, T. Chao, S. Chen, and S. Jiang, "Superlow Fouling Sulfobetaine and Carboxybetaine Polymers on Glass Slides," *Langmuir*, vol. 22, no. 24, pp. 10072–10077, Nov. 2006.

[31] S. Krishnan *et al.*, "Anti-Biofouling Properties of Comblike Block Copolymers with

Amphiphilic Side Chains," *Langmuir*, vol. 22, no. 11, pp. 5075–5086, May 2006.

[32] S. Krishnan *et al.*, "Comparison of the Fouling Release Properties of Hydrophobic Fluorinated and Hydrophilic PEGylated Block Copolymer Surfaces: Attachment Strength of the Diatom Navicula and the Green Alga Ulva," *Biomacromolecules*, vol. 7, no. 5, pp. 1449–1462, May 2006.

[33] C. J. Weinman *et al.*, "ABC Triblock Surface Active Block Copolymer with Grafted Ethoxylated Fluoroalkyl Amphiphilic Side Chains for Marine Antifouling/Fouling-Release Applications," *Langmuir*, vol. 25, no. 20, pp. 12266–12274, Oct. 2009.

[34] C. J. Weinman *et al.*, "Protein adsorption resistance of anti-biofouling block copolymers containing amphiphilic side chains," *Soft Matter*, vol. 6, no. 14, pp. 3237–3243, 2010.

[35] J. A. Finlay *et al.*, "Settlement of Ulva Zoospores on Patterned Fluorinated and PEGylated Monolayer Surfaces," *Langmuir*, vol. 24, no. 2, pp. 503–510, Jan. 2008.

[36] R. Dong, S. Krishnan, B. A. Baird, M. Lindau, and C. K. Ober, "Patterned Biofunctional Poly(acrylic acid) Brushes on Silicon Surfaces," *Biomacromolecules*, vol. 8, no. 10, pp. 3082–3092, Oct. 2007.

[37] A. A. Aimetti, A. J. Machen, and K. S. Anseth, "Poly(ethylene glycol) hydrogels formed by thiol-ene photopolymerization for enzyme-responsive protein delivery," *Biomaterials*, vol. 30, no. 30, pp. 6048–6054, Oct. 2009.

[38] M. C. Cushing and K. S. Anseth, "Hydrogel Cell Cultures," *Science (80-.).*, vol. 316, no. 5828, pp. 1133–1134, May 2007.

[39] R. Langer and D. A. Tirrell, “Designing materials for biology and medicine,” *Nature*, vol. 428, no. 6982, pp. 487–492, Apr. 2004.

[40] P. C. Nicolson and J. Vogt, “Soft contact lens polymers: an evolution,” *Biomaterials*, vol. 22, no. 24, pp. 3273–3283, Dec. 2001.

[41] L. Yu and J. Ding, “Injectable hydrogels as unique biomedical materials,” *Chem. Soc. Rev.*, vol. 37, no. 8, pp. 1473–1481, 2008.

[42] M. Malkoch *et al.*, “Synthesis of well-defined hydrogel networks using Click chemistry,” *Chem. Commun.*, no. 26, p. 2774, 2006.

[43] J. Kopeček and J. Yang, “Hydrogels as smart biomaterials,” *Polym. Int.*, vol. 56, no. 9, pp. 1078–1098, Sep. 2007.

[44] S. Lin-Gibson, R. L. Jones, N. R. Washburn, and F. Horkay, “Structure-property relationships of photopolymerizable poly(ethylene glycol) dimethacrylate hydrogels,” *Macromolecules*, vol. 38, no. 7, pp. 2897–2902, 2005.

[45] M. P. Lutolf and J. A. Hubbell, “Synthesis and physicochemical characterization of end-linked poly(ethylene glycol)-co-peptide hydrogels formed by Michael-type addition,” *Biomacromolecules*, vol. 4, no. 3, pp. 713–722, 2003.

[46] Y. He and T. P. Lodge, “Thermoreversible ion gels with tunable melting temperatures from triblock and pentablock copolymers,” *Macromolecules*, vol. 41, no. 1, pp. 167–174, 2008.

[47] T. Vermonden, N. A. M. Besseling, M. J. Van Steenbergen, and W. E. Hennink, “Rheological studies of thermosensitive triblock copolymer hydrogels,” *Langmuir*,

vol. 22, no. 24, pp. 10180–10184, 2006.

[48] K. Yasuda *et al.*, "Biomechanical properties of high-toughness double network hydrogels," *Biomaterials*, vol. 26, no. 21, pp. 4468–4475, Jul. 2005.

[49] J. P. Gong, Y. Katsuyama, T. Kurokawa, and Y. Osada, "Double-Network Hydrogels with Extremely High Mechanical Strength," *Adv. Mater.*, vol. 15, no. 14, pp. 1155–1158, Jul. 2003.

[50] Q. Wang *et al.*, "High-water-content mouldable hydrogels by mixing clay and a dendritic molecular binder," *Nature*, vol. 463, no. 7279, pp. 339–343, Jan. 2010.

[51] K. Hales and D. J. Pochan, "Using polyelectrolyte block copolymers to tune nanostructure assembly," *Current Opinion in Colloid and Interface Science*, vol. 11, no. 6. pp. 330–336, Dec-2006.

[52] M. A. Cohen Stuart, B. Hofs, I. K. Voets, and A. De Keizer, "Assembly of polyelectrolyte-containing block copolymers in aqueous media," *Current Opinion in Colloid and Interface Science*, vol. 10, no. 1–2. pp. 30–36, Aug-2005.

[53] C. Tsitsilianis, "Responsive Reversible Hydrogels from associative 'smart' macromolecules," *Soft Matter*, vol. 6, no. 11, pp. 2372–2388, May 2010.

[54] I. K. Voets, A. De Keizer, M. A. Cohen Stuart, J. Justynska, and H. Schlaad, "Irreversible Structural Transitions in Mixed Micelles of Oppositely Charged Diblock Copolymers in Aqueous Solution," *Macromolecules*, vol. 40, no. 6, pp. 2158–2164, Mar. 2007.

[55] M. Lemmers, J. Sprakel, I. K. Voets, J. Van Der Gucht, and M. A. Cohen Stuart,

"Multiresponsive reversible gels based on chargedriven assembly," *Angew. Chemie - Int. Ed.*, vol. 49, no. 4, pp. 708–711, Jan. 2010.

[56] M. D. Dimitriou *et al.*, "A general approach to controlling the surface composition of poly(ethylene oxide)-based block copolymers for antifouling coatings," *Langmuir*, vol. 27, no. 22, pp. 13762–13772, 2011.

[57] T. Kang *et al.*, "Formation, Removal, and Reformation of Surface Coatings on Various Metal Oxide Surfaces Inspired by Mussel Adhesives," *ACS Appl. Mater. Interfaces*, vol. 7, no. 44, pp. 24656–24662, 2015.

[58] C. X. Wang *et al.*, "Catechol-based layer-by-layer assembly of composite coatings: a versatile platform to hierarchical nano-materials," *Soft Matter*, vol. 11, no. 31, pp. 6173–6178, 2015.

[59] H. Lee, N. F. Scherer, and P. B. Messersmith, "Single-molecule mechanics of mussel adhesion," *Proc. Natl. Acad. Sci.*, vol. 103, no. 35, pp. 12999–13003, 2006.

[60] B. K. Ahn, D. W. Lee, J. N. Israelachvili, and J. H. Waite, "Surface-initiated self-healing of polymers in aqueous media.," *Nat. Mater.*, vol. 13, no. 9, pp. 867–72, Sep. 2014.

[61] L. Li, B. Yan, J. Yang, L. Chen, and H. Zeng, "Novel mussel-inspired injectable self-healing hydrogel with anti-biofouling property," *Adv. Mater.*, vol. 27, no. 7, pp. 1294–1299, Feb. 2015.

[62] K. M. Mattson *et al.*, "A facile synthesis of catechol-functionalized poly(ethylene oxide) block and random copolymers," *J. Polym. Sci. Part A Polym. Chem.*, vol. 53,

no. 23, pp. 2685–2692, Dec. 2015.

[63] B. F. Lee *et al.*, “Poly(allyl glycidyl ether)-A versatile and functional polyether platform,” *J. Polym. Sci. Part A Polym. Chem.*, vol. 49, no. 20, pp. 4498–4504, Oct. 2011.

[64] K. P. Barteau, M. Wolffs, N. A. Lynd, G. H. Fredrickson, E. J. Kramer, and C. J. Hawker, “Allyl glycidyl ether-based polymer electrolytes for room temperature lithium batteries,” *Macromolecules*, vol. 46, no. 22, pp. 8988–8994, 2013.

[65] S. Liu, F. Zhang, Y. Zhang, and J. Xu, “Synthesis of novel glycidol copolymers with pendant alkene and hydroxyl groups,” *Chinese J. Chem.*, vol. 31, no. 10, pp. 1315–1320, Oct. 2013.

[66] J. Su, F. Chen, V. L. Cryns, and P. B. Messersmith, “Catechol polymers for pH-responsive, targeted drug delivery to cancer cells,” *J. Am. Chem. Soc.*, vol. 133, no. 31, pp. 11850–11853, Aug. 2011.

[67] J. Heo *et al.*, “Improved performance of protected catecholic polysiloxanes for bioinspired wet adhesion to surface oxides,” *J. Am. Chem. Soc.*, vol. 134, no. 49, pp. 20139–20145, Dec. 2012.

[68] V. S. Wilms *et al.*, “Catechol-initiated polyethers: Multifunctional hydrophilic ligands for pegylation and functionalization of metal oxide nanoparticles,” *Biomacromolecules*, vol. 14, no. 1, pp. 193–9, Jan. 2013.

[69] M. Hrubý, Č. Koňák, and K. Ulbrich, “Poly(allyl glycidyl ether)-block-poly(ethylene oxide): A novel promising polymeric intermediate for the preparation

of micellar drug delivery systems," *J. Appl. Polym. Sci.*, vol. 95, no. 2, pp. 201–211, Jan. 2005.

[70] B. Obermeier and H. Frey, "Poly(ethylene glycol-co-allyl glycidyl ether)s: A PEG-based modular synthetic platform for multiple bioconjugation," *Bioconjug. Chem.*, vol. 22, no. 3, pp. 436–444, Mar. 2011.

[71] B. Li *et al.*, "A novel amphiphilic copolymer poly(ethylene oxide-co-allyl glycidyl ether)-graft-poly(ε-caprolactone): synthesis, self-assembly, and protein encapsulation behavior," *Polym. Chem.*, vol. 3, no. 9, p. 2421, Jul. 2012.

[72] J. Herzberger, K. Fischer, D. Leibig, M. Bros, R. Thiermann, and H. Frey, "Oxidation-Responsive and 'clickable' Poly(ethylene glycol) via Copolymerization of 2-(Methylthio)ethyl Glycidyl Ether," *J. Am. Chem. Soc.*, vol. 138, no. 29, pp. 9212–9223, 2016.

[73] J. Herzberger, D. Leibig, J. C. Liermann, and H. Frey, "Conventional Oxyanionic versus Monomer-Activated Anionic Copolymerization of Ethylene Oxide with Glycidyl Ethers: Striking Differences in Reactivity Ratios," *ACS Macro Lett.*, vol. 5, no. 11, pp. 1206–1211, 2016.

[74] D. V Krogstad *et al.*, "Effects of polymer and salt concentration on the structure and properties of triblock copolymer coacervate hydrogels," *Macromolecules*, vol. 46, no. 4, pp. 1512–1518, 2013.

[75] H. Cui, X. Zhuang, C. He, Y. Wei, and X. Chen, "High performance and reversible ionic polypeptide hydrogel based on charge-driven assembly for biomedical

applications," *Acta Biomater.*, vol. 11, no. 1, pp. 183–190, 2015.

[76] Q. Zhao *et al.*, "Underwater contact adhesion and microarchitecture in polyelectrolyte complexes actuated by solvent exchange," *Nat. Mater.*, vol. 15, no. 4, pp. 407–412, 2016.

[77] P. Kord Forooshani and B. P. Lee, "Recent approaches in designing bioadhesive materials inspired by mussel adhesive protein," *Journal of Polymer Science, Part A: Polymer Chemistry*, vol. 55, no. 1. pp. 9–33, 01-Jan-2017.

[78] S. Seo *et al.*, "Microphase Behavior and Enhanced Wet-Cohesion of Synthetic Copolyampholytes Inspired by a Mussel Foot Protein," *J. Am. Chem. Soc.*, vol. 137, no. 29, pp. 9214–9217, 2015.

[79] P. Lim, H. Shin, B. Moon, and S. H. Choi, "Small angle neutron scattering study on complex coacervate core micelles formed by oppositely charged poly(ethylene oxide-b-allyl glycidyl ether) block copolymer in water," *Polymer Bulletin*, vol. 73, no. 9, Springer Berlin Heidelberg, pp. 1–9, 28-Sep-2016.

[80] T. Kang *et al.*, "Mussel-inspired anchoring of polymer loops that provide superior surface lubrication and antifouling properties," *ACS Nano*, vol. 10, no. 1, pp. 930–937, 2016.

[81] S. A. Mian, L. M. Yang, L. C. Saha, E. Ahmed, M. Ajmal, and E. Ganz, "A fundamental understanding of catechol and water adsorption on a hydrophilic silica surface: Exploring the underwater adhesion mechanism of mussels on an atomic scale," *Langmuir*, vol. 30, no. 23, pp. 6906–6914, Jun. 2014.

[82] B. J. Sparks, E. F. T. Hoff, L. P. Hayes, and D. L. Patton, “Mussel-inspired thiol-ene polymer networks: Influencing network properties and adhesion with catechol functionality,” *Chem. Mater.*, vol. 24, no. 18, pp. 3633–3642, Sep. 2012.

[83] L. Zhang, V. Lipik, and A. Miserez, “Complex coacervates of oppositely charged co-polypeptides inspired by the sandcastle worm glue,” *J. Mater. Chem. B*, vol. 4, no. 8, pp. 1544–1556, Feb. 2016.

[84] J. Zhou *et al.*, “Adhesion properties of catechol-based biodegradable amino acid-based poly(ester urea) copolymers inspired from mussel proteins,” *Biomacromolecules*, vol. 16, no. 1, pp. 266–274, Jan. 2015.

[85] A. Li, M. Jia, Y. Mu, W. Jiang, and X. Wan, “Humid bonding with a water-soluble adhesive inspired by mussels and sandcastle worms,” *Macromol. Chem. Phys.*, vol. 216, no. 4, pp. 450–459, Feb. 2015.

[86] P. G. M. Wuts and T. W. Greene, *Greene’s Protective Groups in Organic Synthesis*. Hoboken, NJ, USA: John Wiley & Sons, Inc., 2006.

[87] A. A. Padmapriya, G. Just, and N. G. Lewis, “A New Method for the Esterification of Sulphonic Acids,” *Synth. Commun.*, vol. 15, no. 12, pp. 1057–1062, Oct. 1985.

[88] Y. NITTA and Y. ARAKAWA, “Reaction of carboxylic acid esters with p-toluenesulfonic acid.,” *Chem. Pharm. Bull. (Tokyo).*, vol. 33, no. 4, pp. 1380–1386, Apr. 1985.

[89] N. Vignola, S. Dahmen, D. Enders, and S. Br??se, “Efficient synthesis of sulfonic, phosphoric, and phosphinic esters employing alkylating polymer-bound reagents,”

J. Comb. Chem., vol. 5, no. 2, pp. 138–144, 2003.

[90] J. Comyn, “The relationship between joint durability and water diffusion,” in *vol. 2*, _ AJ, Kinloch, Ed. Barking, UK: Appl. Sci. Publ., 1981, pp. 279–313.

[91] B. P. Lee, P. B. Messersmith, J. N. Israelachvili, and J. H. Waite, “Mussel-Inspired Adhesives and Coatings,” *Annu. Rev. Mater. Res.*, vol. 41, no. 1, pp. 99–132, Aug. 2011.

[92] A. V. Pocius, *Adhesion and adhesives technology*. Hanser/Gardner Publ., 1997.

[93] T. H. Anderson, J. Yu, A. Estrada, M. U. Hammer, J. H. Waite, and J. N. Israelachvili, “The contribution of DOPA to substrate-peptide adhesion and internal cohesion of mussel-inspired synthetic peptide films,” *Adv. Funct. Mater.*, vol. 20, no. 23, pp. 4196–4205, Dec. 2010.

[94] H. Zhao, C. Sun, R. J. Stewart, and J. H. Waite, “Cement proteins of the tube-building polychaete Phragmatopoma californica,” *J. Biol. Chem.*, vol. 280, no. 52, pp. 42938–42944, Dec. 2005.

[95] H. Shao and R. J. Stewart, “Biomimetic underwater adhesives with environmentally triggered setting mechanisms,” *Adv. Mater.*, vol. 22, no. 6, pp. 729–733, Feb. 2010.

[96] D. R. Miller, S. Das, K. Y. Huang, S. Han, J. N. Israelachvili, and J. H. Waite, “Mussel Coating Protein-Derived Complex Coacervates Mitigate Frictional Surface Damage,” *ACS Biomater. Sci. Eng.*, vol. 1, no. 11, pp. 1121–1128, 2015.

[97] H. Yamamoto, “Adhesive studies of synthetic polypeptides: A model for marine adhesive proteins,” *J. Adhes. Sci. Technol.*, vol. 1, no. 1, pp. 177–183, Jan. 1987.

[98] H. Yamamoto, S. Yamauchi, and S. Ohara, “Synthesis and adhesive studies of marine adhesive proteins of the chilean mussel aulacomya ater,” *Biomimetics*, vol. 1, pp. 219–238, 1992.

[99] H. Tatehata, A. Mochizuki, T. Kawashima, S. Yamashita, and H. Yamamoto, “Model polypeptide of mussel adhesive protein. I. Synthesis and adhesive studies of sequential polypeptides (X-Tyr-Lys)n and (Y-Lys)n,” *J. Appl. Polym. Sci.*, vol. 76, no. 6, pp. 929–937, May 2000.

[100] M. Yu and T. Deming, “Synthetic polypeptide mimics of marine adhesives,” *Macromolecules*, vol. 31, no. 15, pp. 4739–4745, 1998.

[101] M. Yu, J. Hwang, and T. J. Deming, “Role of 1-3,4-dihydroxyphenylalanine in mussel adhesive proteins,” *J. Am. Chem. Soc.*, vol. 121, no. 24, pp. 5825–5826, 1999.

[102] M. Yin, Y. Yuan, C. Liu, and J. Wang, “Development of mussel adhesive polypeptide mimics coating for in-situ inducing re-endothelialization of intravascular stent devices,” *Biomaterials*, vol. 30, no. 14, pp. 2764–2773, May 2009.

[103] H. Lee, B. P. Lee, and P. B. Messersmith, “A reversible wet/dry adhesive inspired by mussels and geckos,” *Nature*, vol. 448, no. 7151, pp. 338–341, Jul. 2007.

[104] B. P. Lee, K. Huang, F. N. Nunalee, K. R. Shull, and P. B. Messersmith, “Synthesis of 3,4-dihydroxyphenylalanine (DOPA) containing monomers and their co-polymerization with PEG-diacrylate to form hydrogels,” *J. Biomater. Sci. Polym.*

Ed., vol. 15, no. 4, pp. 449–464, 2004.

[105] W. H. Daly and S. Moulay, "Synthesis of Poly (Vinylcatechols)," *J. Polym. Sci. Symp.*, vol. 74, no. 74, pp. 227–242, Mar. 1986.

[106] Z. Yang and R. Pelton, "The synthesis of poly(3,4-dihydroxystyrene) and poly[(sodium 4-styrenesulfonate)-co-(3,4-dihydroxystyrene)]," *Macromol. Rapid Commun.*, vol. 19, no. 5, pp. 241–246, May 1998.

[107] G. Westwood, T. N. Horton, and J. J. Wilker, "Simplified polymer mimics of cross-linking adhesive proteins," *Macromolecules*, vol. 40, no. 11, pp. 3960–3964, 2007.

[108] A. Charlot *et al.*, "All-in-one strategy for the fabrication of antimicrobial biomimetic films on stainless steel," *J. Mater. Chem.*, vol. 19, no. 24, p. 4117, Jun. 2009.

[109] X. D. Pan, Z. Qin, Y. Y. Yan, and P. Sadhukhan, "Elastomers with chain-end mussel-mimetic modification for nanocomposites: Strong modifications to reinforcement and viscoelastic properties," *Polymer (Guildf).*, vol. 51, no. 15, pp. 3453–3461, 2010.

[110] H. Shao, K. N. Bachus, and R. J. Stewart, "A water-borne adhesive modeled after the sandcastle glue of P. californica," *Macromol. Biosci.*, vol. 9, no. 5, pp. 464–471, May 2009.

[111] R. Ko, P. A. Cadieux, J. L. Dalsin, B. P. Lee, C. N. Elwood, and H. Razvi, "First Prize: Novel Uropathogen-Resistant Coatings Inspired by Marine Mussels," *J. Endourol.*, vol. 22, no. 6, pp. 1153–1160, Jun. 2008.

[112] B. Dong *et al.*, "Inhibition of Bacterial Attachment by Mussel-Inspired Coatings on

Urinary Stents and Catheter Materials," *Proc. Biointerface*, p. 2009, San Mateo, CA, 2009.

[113] J. Yu, W. Wei, E. Danner, R. K. Ashley, J. N. Israelachvili, and J. H. Waite, "Mussel protein adhesion depends on interprotein thiol-mediated redox modulation," *Nat. Chem. Biol.*, vol. 7, no. 9, pp. 588–590, Jul. 2011.

[114] X. X. Qin, K. J. Coyne, and J. H. Waite, "Tough tendons. Mussel byssus has collagen with silk-like domains," *J. Biol. Chem.*, vol. 272, no. 51, pp. 32623–32627, Dec. 1997.

[115] P. Kraft and W. Eichenberger, "Conception, Characterization and Correlation of New Marine Odorants," *European J. Org. Chem.*, vol. 2003, no. 19, pp. 3735–3743, Oct. 2003.

[116] J. C. Bailar, W. C. Fernelius, and H. A. Skinner, "Lead Tetiucetate," *Inorg. Synth.*, vol. 1, pp. 47–49, 1939.

[117] L. C. Shen, S. Y. Chiang, I. T. Ho, K. Y. Wu, and W. S. Chung, "Synthesis and Characterization of Adducts Formed in the Reactions of Safrole 2′,3′-Oxide with 2′-Deoxyadenosine, Adenine, and Calf Thymus DNA," *European J. Org. Chem.*, vol. 2012, no. 4, pp. 792–800, Feb. 2012.

[118] C. Billouard, S. Carlotti, P. Desbois, and A. Deffieux, "'Controlled' high-speed anionic polymerization of propylene oxide initiated by alkali metal alkoxide/trialkylaluminum systems," *Macromolecules*, vol. 37, no. 11, pp. 4038–4043, 2004.

[119] K. Sakakibara, K. Nakano, and K. Nozaki, “Regioregular polymerization of fluorine-containing epoxides,” *Macromolecules*, vol. 40, no. 17, pp. 6136–6142, 2007.

[120] A. L. Brocas, G. Cendejas, S. Caillol, A. Deffieux, and S. Carlotti, “Controlled synthesis of polyepichlorohydrin with pendant cyclic carbonate functions for isocyanate-free polyurethane networks,” *J. Polym. Sci. Part A Polym. Chem.*, vol. 49, no. 12, pp. 2677–2684, Jun. 2011.

[121] K. C. Nicolaou, J. Wang, Y. Tang, and L. Botta, “Total Synthesis of Sporolide B and 9- epi -Sporolide B,” *J. Am. Chem. Soc.*, no. 8, p. 100722100209035, 2010.

[122] M. Lee, W. Zhang, and B. C. Noll, “Total Synthesis of Sporolide B,” *Angew. Chemie Int. Ed.*, vol. 48, no. 19, pp. 3449–3453, Apr. 2009.

[123] S. Strych and D. Trauner, “Biomimetic Synthesis of Santalin A,B and Santarubin A,B, the Major Colorants of Red Sandalwood,” *Angew. Chemie Int. Ed.*, vol. 52, no. 36, pp. 9509–9512, Sep. 2013.

[124] K. J. Winstanley *et al.*, “Anion binding by catechols—an NMR, optical and electrochemical study,” *Org. Biomol. Chem.*, vol. 4, no. 9, pp. 1760–1767, Apr. 2006.

[125] L. M. Campos *et al.*, “Development of thermal and photochemical strategies for thiol-ene click polymer functionalization,” *Macromolecules*, vol. 41, no. 19, pp. 7063–7070, 2008.

[126] S. Boileau, “In comprehensive polymer science, chain polymerization,” in *Vol. 3,*

Part 1, 1989, pp. 467–487.

[127] S. D. Gagnon, “In Encyclopedia of Polymer Science and Engineering,” in *Vol. 6*, R. P. Quirk, Ed. Wiley-Interscience: New York, 1985, pp. 273–307.

[128] R. P. Quirk and G. M. Lizarraga, “Anionic synthesis of well-defined, poly[(styrene)-block-(propylene oxide)] block copolymers,” *Macromol. Chem. Phys.*, vol. 201, no. 13, pp. 1395–1404, Aug. 2000.

[129] K. Sakakibara, K. Nakano, and K. Nozaki, “Regio-controlled ring-opening polymerization of perfluoroalkyl-substituted epoxides,” *Chem. Commun.*, vol. 57, no. 31, p. 3334, Aug. 2006.

[130] G. Boireau, D. Abenhaim, and E. Henry-Basch, “The ate complexes of aluminium. Reactivity and stereoselectivity with respect to epoxides and carbonyl compounds. Catalytic activation by salts of transition metals,” *Tetrahedron*, vol. 36, no. 20–21, pp. 3061–3070, Jan. 1980.

[131] J. J. Eisch, Z. R. Liu, and M. Singh, “Organometallic compounds of Group III. 48. High regioselectivity in the alternative, reductive cleavages of terminal epoxides with aluminum reagents,” *J. Org. Chem.*, vol. 57, no. 5, pp. 1618–1621, Feb. 1992.

[132] W. Braune and J. Okuda, “An efficient method for controlled propylene oxide polymerization: The significance of bimetallic activation in aluminum Lewis acids,” *Angew. Chemie - Int. Ed.*, vol. 42, no. 1, pp. 64–68, Jan. 2003.

[133] C. J. Harlan, A. R. Barron, and S. G. Bott, “Three-Coordinate Aluminum Is Not a Prerequisite for Catalytic Activity in the Zirconocene—Alumoxane Polymerization

of Ethylene," *J. Am. Chem. Soc.*, vol. 117, no. 24, pp. 6465–6474, Jun. 1995.

[134] T. Hagiwara, Y. Terasaki, H. Hamana, T. Narita, J. Umezawa, and K. Furuhashi, "Polymerization of 3,3,3¯trifluoro¯1,2¯epoxypropane with organozinc compounds and alkali metal alkoxides," *Die Makromol. Chemie, Rapid Commun.*, vol. 13, no. 8, pp. 363–370, Aug. 1992.

[135] K. Maruoka and T. Ooi, "The synthetic utility of the hypercoordination of boron and aluminum.," *Chem. - A Eur. J.*, vol. 5, no. 3, pp. 829–833, Mar. 1999.

[136] B. Antelmann *et al.*, "Molecular design of single site catalyst precursors for the ring-opening polymerization of cyclic ethers and esters. 2. Can ring-opening polymerization of propylene oxide occur by a cis-migratory mechanism?," *Macromolecules*, vol. 34, no. 10, pp. 3159–3175, 2001.

[137] M. H. Chisholm and D. Navarro-Llobet, "NMR assignments of regioregular poly(propylene oxide) at the triad and tetrad level," *Macromolecules*, vol. 35, no. 6, pp. 2389–2392, 2002.

[138] X. Wu *et al.*, "Direct sensing of fluoride in aqueous solutions using a boronic acid based sensor," *Chem. Commun.*, vol. 50, no. 90, pp. 13987–13989, Sep. 2014.

[139] J. Y. Kim, D. S. Choi, and M. Y. Jung, "Antiphoto-oxidative Activity of Sesamol in Methylene Blue- and Chlorophyll-Sensitized Photo-oxidation of Oil," *J. Agric. Food Chem.*, vol. 51, no. 11, pp. 3460–3465, May 2003.

[140] O. Toshiko, "Sesamol and sesaminol as antioxidants," *New Food Ind.*, vol. 33, pp. 1–5, 1991.

[141] J. P. Wynn, A. Kendrick, and C. Ratledge, “Sesamol as an inhibitor of growth and lipid metabolism in Mucor circinelloides via its action on malic enzyme,” *Lipids*, vol. 32, no. 6, pp. 605–610, Jun. 1997.

[142] J. J. Li, D. S. Johnson, D. R. Sliskovic, and B. D. Roth, *Contemporary drug synthesis*. John Wiley & Sons, Inc . Hoboken, New Jersey, 2004.

[143] P. Lahorkar, K. Ramitha, V. Bansal, and D. Anantha Narayana, “A comparative evaluation of medicated oils prepared using ayurvedic and modified processes,” *Indian J. Pharm. Sci.*, vol. 71, no. 6, p. 656, 2009.

[144] V. R. M. Chandrasekaran, D.-Z. Hsu, and M.-Y. Liu, “Beneficial Effect of Sesame Oil on Heavy Metal Toxicity,” *J. Parenter. Enter. Nutr.*, vol. 38, no. 2, pp. 179–185, Feb. 2014.

[145] S. D. Nelson, J. G. Omichinski, L. Iyer, W. P. P. Gordon, E. J. Soderlund, and E. Dybing, “Activation mechanism of Tris(2,3-dibromopropyl)phosphate to the potent mutagen, 2-bromoacrolein,” *Biochem. Biophys. Res. Commun.*, vol. 121, no. 1, pp. 213–219, May 1984.

[146] G. Brunetto, S. Gori, R. Fiaschi, and E. Napolitano, “Crystallization-induced asymmetric transformations. Enantiomerically pure (-)-(R)- and (+)-(S)-2,3-dibromopropan-1-ol and epibromohydrins. A study of dynamic resolution via the formation of diastereoisomeric esters,” *Helv. Chim. Acta*, vol. 85, no. 11, pp. 3785–3791, Nov. 2002.

[147] G. Braun, “Epichlorohydrin and Epibromohydrin,” *Org. Synth.*, vol. 16, p. 30, Apr.

2003.

[148] M. YOSHINO, M. SHIBATA, T. IKEDA, and Y. NANBA, “Hydrolysis of Epichlorohydrin with Sodium Hydroxide,” *J. Japan Oil Chem. Soc.*, vol. 13, no. 11, pp. 582–585, Nov. 1964.

[149] V. Brizzi, M. Francioli, M. Brufani, L. Filocamo, G. Bruni, and P. Massarelli, “Synthesis, binding affinity and selectivity of new β1- and β2-adrenoceptor blockers,” *Farmaco*, vol. 54, no. 11–12, pp. 713–720, Nov. 1999.

[150] E. Elzein *et al.*, “Novel inhibitors of fatty acid oxidation as potential metabolic modulators,” *Bioorganic Med. Chem. Lett.*, vol. 14, no. 4, pp. 973–977, Feb. 2004.

[151] S. Wagner *et al.*, “Synthesis and first in vivo evaluation of new selective high affinity β1-adrenoceptor radioligands for SPECT based on ICI 89,406,” *Bioorg. Med. Chem.*, vol. 12, no. 15, pp. 4117–4132, Aug. 2004.

[152] H. Morinaga, Y. Ujihara, N. Yuto, D. Nagai, and T. Endo, “Controlled polymerization of epoxides: Metal-free ring-opening polymerization of glycidyl phenyl ether initiated by tetra-n-butylammonium fluoride in the presence of protic compounds,” *J. Polym. Sci. Part A Polym. Chem.*, vol. 49, no. 24, pp. 5210–5216, Dec. 2011.

[153] H. Morinaga, B. Ochiai, and T. Endo, “Metal-Free Ring-Opening Polymerization of Glycidyl Phenyl Ether by Tetrabutylammonium Fluoride,” *Macromolecules*, vol. 40, pp. 6014–6016, 2007.

[154] H. Morinaga, Y. Ujihara, T. Yamanaka, D. Nagai, and T. Endo, “Metal-free ring-

opening polymerization of glycidyl phenyl ether initiated by tetra-n-butylammonium acetate and its application to the hydroxyl-terminated telechelic polymer," *J. Polym. Sci. Part A Polym. Chem.*, vol. 49, no. 18, pp. 4092–4097, Sep. 2011.

[155] I. C. Eromosele and D. C. Pepper, "Anionic polymerization of butyl cyanoacrylate by tetrabutylammonium salts, 2. Propagation rate constants," *Die Makromol. Chemie*, vol. 190, no. 12, pp. 3095–3103, Dec. 1989.

[156] K. C. Nicolaou, J. Wang, Y. Tang, and L. Botta, "Total synthesis of sporolide B and 9-epi-sporolide B," *J. Am. Chem. Soc.*, vol. 132, no. 32, pp. 11350–11363, 2010.

[157] W.-V. Staff, *Ullmann's Fine Chemicals, 3 Volume Set.* Wiley, 2014.

[158] N.-H. L. Lindsay Burns Barbier, Hoau-Yan Wang and A. Blasko, "Preparation of methylenedioxyisoquinolines as analgesics that bind filamin a, From U.S. Pat. Appl. Publ. US 20100280061 A1 Nov 04, 2010," 2010.

[159] J. S. Du *et al.*, "The Structural Fate of Individual Multicomponent Metal-Oxide Nanoparticles in Polymer Nanoreactors," *Angew. Chemie - Int. Ed.*, vol. 56, no. 26, pp. 7625–7629, 2017.

[160] B. H. McDonagh *et al.*, "L -DOPA-Coated Manganese Oxide Nanoparticles as Dual MRI Contrast Agents and Drug-Delivery Vehicles," *Small*, vol. 12, no. 3, pp. 301–306, 2016.

[161] H. Cai *et al.*, "Facile Hydrothermal Synthesis and Surface Functionalization of Polyethyleneimine-Coated Iron Oxide Nanoparticles for Biomedical Applications,"

ACS Appl. Mater. Interfaces, vol. 5, no. 5, pp. 1722–1731, 2013.

[162] M. J. Baek *et al.*, “Water-soluble MnO nanocolloid for a molecular T 1 MR imaging: A facile one-pot synthesis, in vivo T 1 MR images, and account for relaxivities,” *ACS Appl. Mater. Interfaces*, vol. 2, no. 10, pp. 2949–2955, 2010.

[163] M. Létourneau *et al.*, “MnO-labeled cells: Positive contrast enhancement in MRI,” *J. Phys. Chem. B*, vol. 116, no. 44, pp. 13228–13238, 2012.

[164] P. Caravan, “Resonance Imaging (MRI) Contrast Agents : Design and Mechanism of Action,” vol. 42, no. 7, 2009.

[165] T. D. Schladt *et al.*, “Highly soluble multifunctional MnO nanoparticles for simultaneous optical and MRI imaging and cancer treatment using photodynamic therapy,” *J. Mater. Chem.*, vol. 20, no. 38, p. 8297, 2010.

[166] L. Gutiérrez *et al.*, “Synthesis methods to prepare single- and multi-core iron oxide nanoparticles for biomedical applications,” *Dalt. Trans.*, vol. 44, no. 7, pp. 2943–2952, 2015.

[167] T. D. Schladt, T. Graf, and W. Tremel, “Synthesis and characterization of monodisperse manganese oxide nanoparticles-evaluation of the nucleation and growth mechanism,” *Chem. Mater.*, vol. 21, no. 14, pp. 3183–3190, 2009.

[168] D. Liu, Y. B. Qiu, Y. Tomoe, K. Bando, and X. P. Guo, “Interaction of inhibitors with corrosion scale formed on N80 steel in CO2-saturated NaCl solution,” *Mater. Corros.*, vol. 62, no. 12, pp. 1153–1158, Dec. 2011.

[169] S. Öztürk, A. YIldIrIm, M. Çetin, and M. TavaslI, “Synthesis of quaternary, long-

chain N-alkyl amides and their corrosion inhibition in acidic media," *J. Surfactants Deterg.*, vol. 17, no. 3, pp. 471–481, 2014.

[170] R. Rihan, R. Shawabkeh, and N. Al-Bakr, "The Effect of Two Amine-Based Corrosion Inhibitors in Improving the Corrosion Resistance of Carbon Steel in Sea Water," *J. Mater. Eng. Perform.*, vol. 23, no. 3, pp. 693–699, Mar. 2014.

[171] E. Barmatov, T. Hughes, and M. Nagl, "Performance of Organic Corrosion Inhibitors on Carbon Steels and High Alloys in 4M Hydrochloric Acid," *NACE Int.*, May 2015.

[172] Y. P. Khodyrev, E. S. Batyeva, E. K. Badeeva, E. V. Platova, L. Tiwari, and O. G. Sinyashin, "The inhibition action of ammonium salts of O,O'-dialkyldithiophosphoric acid on carbon dioxide corrosion of mild steel," *Corros. Sci.*, vol. 53, no. 3, pp. 976–983, Mar. 2011.

[173] I. Ibeawuchi, "Review Applications to Prevent Corrosion Reducing Gas Pipe Line," *Int. J. Chem.*, vol. 1, pp. 94–101, 2013.

[174] M. Finšgar and J. Jackson, "Application of corrosion inhibitors for steels in acidic media for the oil and gas industry: A review," *Corros. Sci.*, vol. 86, pp. 17–41, Sep. 2014.

[175] L. Popoola, A. Grema, G. Latinwo, B. Gutti, and A. Balogun, "Corrosion problems during oil and gas production and its mitigation," *Int. J. Ind. Chem.*, vol. 4, no. 1, p. 35, 2013.

[176] D. I. Horsup, J. C. Clark, B. P. Binks, P. D. I. Fletcher, and J. T. Hicks, "The Fate

of Oilfield Corrosion Inhibitors in Multiphase Systems," *CORROSION*, vol. 66, no. 3, pp. 36001-36001–14, Mar. 2010.

[177] V. S. (Vedula S. . Sastri, *Corrosion inhibitors : principles and applications*. Wiley, 1998.

[178] J. J. Tufariello, *"1, 3-Dipolar Cycloaddition Chemistry,"* 2nd ed. Wiley and Sons, New York, 1984.

[179] P. N. Confalone and E. M. Huie, "The [3 + 2] Nitrone-Olefin Cycloaddition Reaction," *Org. React.*, vol. 36, pp. 1–173, Aug. 1988.

[180] S. A. Ali and M. I. M. Wazeer, "The regiochemistry and stereochemistry of 1,3-dipolar cycloaddition of a cyclic nitrone," *J. Chem. Soc. Perkin Trans. 1*, vol. 0, no. 3, p. 597, Jan. 1988.

[181] H. Iida and C. Kibayashi, "Synthesis of Natural Products via 1,3-Dipolar Cycloadditions of Nitrones," *Yuki Gosei, Kagaku Kyokaishi=Journal Synth. Org. Chem. Japan*, vol. 41, pp. 652–666, 1983.

[182] Sk.A.Ali, M.T.Saeed, and S.U.Rahman, "The isoxazolidines: a new class of corrosion inhibitors of mild steel in acidic medium," *Corros. Sci.*, vol. 45, no. 2, pp. 253–266, Feb. 2003.

[183] S.A.Ali, A.M.El-Shareef, R.F.Al-Ghamdi, and M.T.Saeed, "The isoxazolidines: the effects of steric factor and hydrophobic chain length on the corrosion inhibition of mild steel in acidic medium," *Corros. Sci.*, vol. 47, no. 11, pp. 2659–2678, Nov. 2005.

[184] "ASTM- G 01-03, ASTM Book of Standards, vol 3.02. (2003) West Conshohocken: ASTM."

[185] Saviour A.Umoren, "Polypropylene glycol: A novel corrosion inhibitor for × 60 pipeline steel in 15% HCl solution," *J. Mol. Liq.*, vol. 219, pp. 946–958, Jul. 2016.

[186] M. I. M. Wazeer and S. A. Ali, "NMR Study of Nitrogen Inversion process in some Isoxazolidines," *Canad. J. Appl. Spectry.*, vol. 40, pp. 53–60, 1995.

[187] S. A. Ali, S. M. Azhar Hashmi, M. N. Siddiqui, and M. I. M. Wazeer, "Regiochemistry of mercury(II) oxide oxidation of unsymmetrical N,N-disubstituted hydroxylamines," *Tetrahedron*, vol. 52, no. 47, pp. 14917–14928, 1996.

[188] M. K. Pavithra, T. V Venkatesha, K. Vathsala, and K. O. Nayana, "Synergistic effect of halide ions on improving corrosion inhibition behaviour of benzisothiozole-3-piperizine hydrochloride on mild steel in 0.5M H2SO4 medium," *Corros. Sci.*, vol. 52, no. 11, pp. 3811–3819, 2010.

[189] C. B. P. Kumar, K. N. Mohana, and H. B. Muralidhara, "Electrochemical and thermodynamic studies to evaluate the inhibition effect of synthesized piperidine derivatives on the corrosion of mild steel in acidic medium," *Ionics (Kiel).*, vol. 21, no. 1, pp. 263–281, Jan. 2015.

[190] A. A. Farag, A. S. Ismail, and M. A. Migahed, "Inhibition of carbon steel corrosion in acidic solution using some newly polyester derivatives," *J. Mol. Liq.*, vol. 211, no. Supplement C, pp. 915–923, 2015.

[191] M. M. Solomon, H. Gerengi, and S. A. Umoren, "Carboxymethyl Cellulose/Silver Nanoparticles Composite: Synthesis, Characterization and Application as a Benign Corrosion Inhibitor for St37 Steel in 15% H_2SO_4 Medium," *ACS Appl. Mater. Interfaces*, vol. 9, no. 7, pp. 6376–6389, Feb. 2017.

[192] B. S. Sanatkumar, J. Nayak, and A. N. Shetty, "Influence of 2-(4-chlorophenyl)-2-oxoethyl benzoate on the hydrogen evolution and corrosion inhibition of 18 Ni 250 grade weld aged maraging steel in 1.0 M sulfuric acid medium," *Int. J. Hydrogen Energy*, vol. 37, pp. 9431–9442, 2012.

[193] E. E. Oguzie, Y. Li, and F. H. Wang, "Corrosion inhibition and adsorption behavior of methionine on mild steel in sulfuric acid and synergistic effect of iodide ion," *J. Colloid Interface Sci.*, vol. 310, pp. 90–98, 2007.

[194] S. A. Umoren, M. M. Solomon, U. M. Eduok, I. B. Obot, and A. U. Israel, "Inhibition of mild steel corrosion in H 2 SO 4 solution by coconut coir dust extract obtained from different solvent systems and synergistic effect of iodide ions: Ethanol and acetone extracts," *J. Environ. Chem. Eng.*, vol. 2, pp. 1048–1060, 2014.

[195] S. Tu, X. Jiang, L. Zhou, M. Duan, H. Wang, and X. Jiang, "Synthesis of N-alkyl-4-(4-hydroxybut-2-ynyl) pyridinium bromides and their corrosion inhibition activities on X70 steel in 5M HCl," *Corros. Sci.*, vol. 65, pp. 13–25, 2012.

[196] S. A. Umoren and A. Madhankumar, "Effect of addition of CeO2 nanoparticles to pectin as inhibitor of X60 steel corrosion in HCl medium," *J. Mol. Liq.*, vol. 224, pp. 72–82, 2016.

[197] M. Lagren Ee, B. Mernari, M. Bouanis, M. Traisnel, and F. Bentiss, “Study of the mechanism and inhibiting efficiency of 3,5-bis(4-methylthiophenyl)- 4H-1,2,4-triazole on mild steel corrosion in acidic media,” *Corros. Sci.*, vol. 44, pp. 573–588, 2002.

[198] M. A. Chidiebere, E. E. Oguzie, L. Liu, Y. Li, and F. Wang, “Corrosion Inhibition of Q235 Mild Steel in 0.5 M H_2SO_4 Solution by Phytic Acid and Synergistic Iodide Additives,” *Ind. Eng. Chem. Res.*, vol. 53, no. 18, pp. 7670–7679, May 2014.

[199] P. Roy, A. Pal, and D. Sukul, “Origin of the synergistic effect between polysaccharide and thiourea towards adsorption and corrosion inhibition for mild steel in sulphuric acid,” *RSC Adv.*, vol. 4, no. 21, p. 10607, Feb. 2014.

[200] C. Jeyaprabha, S. Sathiyanarayanan, and G. Venkatachari, “Effect of cerium ions on corrosion inhibition of PANI for iron in 0.5M H2SO4,” *Appl. Surf. Sci.*, vol. 253, no. 2, pp. 432–438, 2006.

[201] M. Mobin, S. Zehra, and R. Aslam, “L -Phenylalanine methyl ester hydrochloride as a green corrosion inhibitor for mild steel in hydrochloric acid solution and the effect of surfactant additive,” *RSC Adv.*, vol. 6, no. 7, pp. 5890–5902, Jan. 2016.

[202] T. Murakawa, T. Kato, S. Nagaura, and N. Hackerman, “A contribution to the understanding of the synergistic effect of anions for the corrosion inhibition of Fe by amines,” *Corros. Sci.*, vol. 8, pp. 483–489, 1968.

[203] S. M. A. Shibli and V. S. Saji, “Co-inhibition characteristics of sodium tungstate with potassium iodate on mild steel corrosion,” *Corros. Sci.*, vol. 47, no. 9, pp.

2213–2224, 2005.

[204] I. Lozano, E. Mazario, C. O. Olivares-Xometl, N. V Likhanova, and P. Herrasti, “Corrosion behaviour of API 5LX52 steel in HCl and H2SO4 media in the presence of 1,3-dibencilimidazolio acetate and 1,3-dibencilimidazolio dodecanoate ionic liquids as inhibitors,” *Mater. Chem. Phys.*, vol. 147, no. 1, pp. 191–197, 2014.

[205] M. M. Solomon, S. A. Umoren, I. I. Udosoro, and A. P. Udoh, “Inhibitive and adsorption behaviour of carboxymethyl cellulose on mild steel corrosion in sulphuric acid solution,” *Corros. Sci.*, vol. 52, no. 4, pp. 1317–1325, 2010.

[206] S. A. Umoren, M. J. Banera, T. Alonso-Garcia, C. A. Gervasi, and M. V Mirífico, “Inhibition of mild steel corrosion in HCl solution using chitosan,” *Cellulose*, vol. 20, no. 5, pp. 2529–2545, Oct. 2013.

[207] S. A. Umoren, “Synergistic inhibition effect of polyethylene glycol–polyvinyl pyrrolidone blends for mild steel corrosion in sulphuric acid medium,” *J. Appl. Polym. Sci.*, vol. 119, no. 4, pp. 2072–2084, 2011.

[208] Z. Tao, W. He, S. Wang, S. Zhang, and G. Zhou, “A study of differential polarization curves and thermodynamic properties for mild steel in acidic solution with nitrophenyltriazole derivative,” *Corros. Sci.*, vol. 60, no. Supplement C, pp. 205–213, 2012.

[209] D. Thirumoolan, V. A. Katkar, G. Gunasekaran, T. Kanai, and K. A. Basha, “Hyperbranched poly(cyanurateamine): A new corrosion inhibitor for mild steel in hydrochloric acid medium,” *Prog. Org. Coatings*, vol. 77, no. 8, pp. 1253–1263,

2014.

[210] M. Mobin and M. A. Khan, "SYNERGISTIC INFLUENCE OF POLYVINYL ALCOHOL AND SURFACTANTS ON THE CORROSION INHIBITION OF MILD STEEL IN 0.1 M H2SO4," *Chem. Eng. Commun.*, vol. 200, no. 9, pp. 1149–1169, 2013.

[211] M. Shabani-Nooshabadi and M.-S. Ghandchi, "Introducing the Santolina chamaecyparissus Extract as a Suitable Green Inhibitor for 304 Stainless Steel Corrosion in Strong Acidic Medium," *Metall. Mater. Trans. A*, vol. 46, no. 11, pp. 5139–5148, Nov. 2015.

[212] H. Ashassi-Sorkhabi and M. Es'haghi, "Corrosion inhibition of mild steel in acidic media by [BMIm]Br Ionic liquid," *Mater. Chem. Phys.*, vol. 114, no. 1, pp. 267–271, 2009.

[213] A. Madhan Kumar, R. Suresh Babu, I. B. Obot, and Z. M. Gasem, "Fabrication of nitrogen doped graphene oxide coatings: experimental and theoretical approach for surface protection," *RSC Adv.*, vol. 5, no. 25, pp. 19264–19272, 2015.

[214] I. B. Obot, E. E. Ebenso, and M. M. Kabanda, "Metronidazole as environmentally safe corrosion inhibitor for mild steel in 0.5M HCl: Experimental and theoretical investigation," *J. Environ. Chem. Eng.*, vol. 1, no. 3, pp. 431–439, 2013.

[215] I. B. Obot, S. A. Umoren, Z. M. Gasem, R. Suleiman, and B. El Ali, "Theoretical prediction and electrochemical evaluation of vinylimidazole and allylimidazole as corrosion inhibitors for mild steel in 1M HCl," *J. Ind. Eng. Chem.*, vol. 21, no.

Supplement C, pp. 1328–1339, 2015.

[216] B. A. Merrill, Merrill, and B. A., “Potassium Naphthalenide,” in *Encyclopedia of Reagents for Organic Synthesis*, Chichester, UK: John Wiley & Sons, Ltd, 2001.

[217] G.-E. Yu, F. Heatley, C. Booth, and T. G. Blease, “Anionic polymerization of propylene oxide: Isomerization of allyl ether to propenyl ether end groups,” *J. Polym. Sci. Part A Polym. Chem.*, vol. 32, no. 6, pp. 1131–1135, Apr. 1994.

[218] A. Labbé, S. Carlotti, C. Billouard, P. Desbois, and A. Deffieux, “Controlled High-Speed Anionic Polymerization of Propylene Oxide Initiated by Onium Salts in the Presence of Triisobutylaluminum,” *Macromolecules*, vol. 40, no. 22, pp. 7842–7847, 2007.

Vitae

Name	Mouheddin Tahseen Alhaffar
Nationality	Syrian
Date of Birth	25-June-1982.
Email	mouheddin@gmail.com.
Address	KFUPM, P.O.Box: 241, Dhahran, 31261, Saudi Arabia
Alternative Email	mouhee@gmail.com

Academic Background

PhD	**Chemistry**, King Fahd University of Petroleum & Minerals	2012-2017
Dissertation:	Synthesis of Bio-inspired Block Polyelectrolytes for the Formation of Coacervates	
MSc.	**Chemistry**, King Fahd University of Petroleum & Minerals	2006-2010
Thesis:	Rhodium-Catalyzed Hydroformylation-Cyclization of Allylbenzene Derivatives	
BSc.	**Applied Chemistry,** University of Damascus	1999-2004
Project:	kinetic study for the oxidation of cyclo-hexanol and cyclo-hexanon with molecular oxygen in presence of several catalysts	

Professional Membership

- Saudi Chapter of American Chemical Society (SCACS)
- Syrian Chemical Society (SCS)

List of Publications

- Isoxazolidine derivatives as corrosion inhibitors for low carbon steel in HCl solution: experimental, theoretical and effect of KI studies.

  Mouheddin T. Alhaffar, Saviour A. Umoren , Ime. B. Obot, Shaikh A. Ali

  RSC Adv. 8 (**2018**) 1764–1777.

- Immobilization of Two Polyelectrolytes Leading to A Novel Hydrogel for High-performance Hg^{2+} Removal to ppb and Sub-ppb Levels

  Mohammad A.J. Mazumder, **Mouheddin T. Alhaffar**, Shaikh A. Ali

  Chemical Engineering Journal 334 (**2018**) 1440–1454.

- Hierarchical ZnO/zeolite nanostructures: synthesis, growth mechanism and hydrogen detection

  Ahsanulhaq Qurashi, **Mouheddin Alhaffar** and Zain H. Yamani

  RSC Adv. 5 (**2015**) 22570–22577.

- Ultranox626 as a selective ligand in rhodium-catalyzed hydroformylation–acetalization of allylbenzene derivatives

  Mouheddin Alhaffar, Rami Suleiman, S. M. Shakil Hussain, Bassam El Ali

  Reaction Kinetics, Mechanisms and Catalysis 104 2 (**2011**) 323-336.

- Rhodium-catalyzed one pot hydroformylation-cyclization of allylbenzene derivatives: simple and efficient roule to 5,6-dihydronaphthalenes

  Mouheddin Alhaffar, Rami Suleiman and Bassam El Ali

  Catalysis Communication 11 (**2010**) 778-782.